



<https://theses.gla.ac.uk/>

Theses Digitisation:

<https://www.gla.ac.uk/myglasgow/research/enlighten/theses/digitisation/>

This is a digitised version of the original print thesis.

Copyright and moral rights for this work are retained by the author

A copy can be downloaded for personal non-commercial research or study, without prior permission or charge

This work cannot be reproduced or quoted extensively from without first obtaining permission in writing from the author

The content must not be changed in any way or sold commercially in any format or medium without the formal permission of the author

When referring to this work, full bibliographic details including the author, title, awarding institution and date of the thesis must be given

Enlighten: Theses

<https://theses.gla.ac.uk/>
research-enlighten@glasgow.ac.uk

SUMMARY.

The present understanding of the way in which thermal history affects the structure and mechanical properties of thermoplastics is reviewed. This research expands upon previous work by examining the effects of moulding cooling rate on the structure and transient mechanical properties of polypropylene.

A technique is first developed for measuring the cooling rate and crystallisation temperature during compression moulding polypropylene sheets. The results obtained for the dependence of crystallisation temperature on cooling rate are predicted with good agreement by an extension of the Avrami equation, which is normally used to describe the process of isothermal crystallisation.

Measurements of density and the rate of crystallisation and optical microscopy, indicate that a change in crystallisation kinetics occurs in polypropylene at a crystallisation temperature of about 120.5°C ., which results from a cooling rate of $10^{\circ}\text{C}/\text{min}$. in the polypropylene used in this research.

At crystallisation temperatures above this point of change in kinetics a sharp increase in the tendency to internal cracking and subsequent strain whitening is observed following tensile testing. A comparison of the effects of moulding cooling rate with ageing and annealing on the material's modulus prior to this state of cracking suggests that the state of relaxation of the non-crystalline phase is relatively more important than the content and perfection of the crystalline phase.

The deformation mode within thick tensile test pieces is compared with that in sections of material which are thinner than their constituent spherulites. The comparatively ductile behaviour of such thin films is explained in terms

ProQuest Number: 10646177

All rights reserved

INFORMATION TO ALL USERS

The quality of this reproduction is dependent upon the quality of the copy submitted.

In the unlikely event that the author did not send a complete manuscript and there are missing pages, these will be noted. Also, if material had to be removed, a note will indicate the deletion.



ProQuest 10646177

Published by ProQuest LLC (2017). Copyright of the Dissertation is held by the Author.

All rights reserved.

This work is protected against unauthorized copying under Title 17, United States Code
Microform Edition © ProQuest LLC.

ProQuest LLC.
789 East Eisenhower Parkway
P.O. Box 1346
Ann Arbor, MI 48106 – 1346

of the effect of film thickness on the development of structural complex stressing and the reorientation rates of the units of structure.

Using a technique for measuring the amount of light transmitted through the plastic during tensile testing, the process of opacity is traced as starting at about 2% strain in all samples and reaching a maximum rate of change during the yielding of the specimen. The beginning of opacity is interpreted as the point at which the crystalline phase is either reorientated or disrupted and a point between this and the yield point is constructed as a measure of the onset of permanent cracking. Faster moulding cooling rates are shown in this way to improve the material's resistance to the onset of cracking in the range of cooling rates faster than about 100°C/min.

Stress relaxation tests show that whilst some small differences in the relaxation rate exist between samples of varying thermal history in the strain range below about 2%, these differences diminish and become negligible in the strain range above 2% and prior to the commencement of gross cracking. These results are considered to extend the dynamic relaxation results previously reported.

From considerations of the results of the deformation mode in thick and thin sectioned material, it is concluded that the moulding cooling rate will influence the modulus and ductility of thin sections of material to a much larger extent than the relatively thick sections used in the tensile tests carried out in this work.

A STUDY OF THE EFFECT OF
THERMAL HISTORY ON THE INTERNAL STRUCTURE
AND MECHANICAL PROPERTIES OF POLYPROPYLENE

by

Brian Procter, BSc.

Thesis submitted to the University of Glasgow for
the degree of Doctor of Philosophy

Engineering Laboratories,
The University,
Glasgow, W.2.

September, 1967.

ACKNOWLEDGEMENTS

The author is grateful to the University of Glasgow for the provision of services and equipment necessary for the performance of this research, and wishes to express his thanks to Dr. P. Hancock for advice, encouragement and discussion during the course of this work.

Thanks are also due to ICI (Hyde Division) who supplied the material used in the research, ICI (Welwyn Garden City) for technical advice, and to the staff of the Engineering Workshop of the University who made much of the equipment.

CONTENTS

	Page
CHAPTER 1.	
1. <u>INTRODUCTION</u>	1
1.1 The General Structure of Crystalline Polymers	3
1.2 The Effects of Thermal History on Morphology	10
1.3 Previous Studies of the Effects of Thermal History on Mechanical Behaviour	16
1.4 Relating Mechanical Properties to Structure	23
1.5 Conclusions	31
1.6 Material used in this Research	33
CHAPTER 2.	
2. <u>DEVELOPMENT OF APPARATUS FOR RECORDING COOLING RATE AND CRYSTALLISATION TEMPERATURE DURING MOULDING POLYPROPYLENE SHEETS.</u>	34
2.1 Standard Compression Moulding Procedure	34
2.2 Experimental Moulding Apparatus	35
2.21 Technique and Apparatus	35
2.22 Calibration and errors in the Temperature Measuring System	38
2.23 Moulding Procedure	39
2.24 Evaluation of Apparatus	40
2.3 Choice of Melt Conditions	43
2.31 Theoretical Aspects	43
2.32 Procedure for finding true melt conditions	45
2.4 Results for Crystallisation Temperature versus Cooling Rate	48
2.41 A Strict Definition of Cooling Rate	48
2.42 Assessment of Errors in T_c and cooling rate	49
2.5 Theoretical Prediction of the Crystallisation Temperature	51
2.51 Introduction to the Theoretical Concept	51
2.52 The value of the Avrami Exponent n and the crystallisation rate constant k_s for polypropylene	52

	Page
2.53 The Temperature Dependence of log k_s	54
2.54 Theory and results derived from typical kinetic data	57
2.55 Discussion of Theoretical Results	61
2.56 A note on the effect of pressure on the crystallisation temperature	62
2.6 Conclusions	65

CHAPTER 3.

3. <u>THE EFFECT OF MOULDING CONDITIONS ON THE STRUCTURE OF POLYPROPYLENE</u>	67
3.1 The Structure of polypropylene spherulites	67
3.2 Microscopy of Samples with varying T_c	70
3.21 Spherulite Size	70
3.22 Spherulite Type	72
3.3 Density as a Measure of Crystallinity	74
3.4 Measurement of Density	75
3.41 Experimental Procedure and Errors	75
3.42 Results	76
3.43 Existing Theoretical Predictions of crystallinity as varied by age and T_c	77
3.5 Discussion	80
3.6 Conclusions	83

CHAPTER 4.

4. <u>TENSILE TESTING OF SAMPLES WITH VARIED THERMAL HISTORY</u>	84
4.1 Thermal History of Samples Tested	84
4.2 Tensile Test Piece	85
4.3 Apparatus and Procedure	87
4.31 Constant Temperature Test Cabinet	87
4.32 Strain Measurement	88
4.33 Experimental Errors	91
4.34 Test Procedure	93

	Page
4.4 Results	94
4.5 Discussion	96
4.51 Strain to Yield	96
4.52 Modulus	98
4.6 Conclusions	102
 CHAPTER 5.	
5. <u>OBSERVATIONS ON THE COURSE OF DEFORMATION OF POLYPROPYLENE UNDER VARIOUS STRESS SYSTEMS</u>	103
5.1 Microscopy of tensile test pieces from chapter 4.	103
5.11 Strain Whitening	103
5.12 Microscopy of Tensile Test Pieces	103
5.13 Discussion	106
5.2 Uniaxial Extension of Microtomed Films	111
5.21 Introduction	111
5.22 Apparatus and Procedure	113
5.23 Results	114
5.24 Note on Failure in Improperly Moulded Material	115
5.3 Extension under imposed non-axial conditions	117
5.31 Biaxial tension on microtomed films	117
5.32 Testing notched specimens	118
5.4 Discussion on sections 5.2 and 5.3	120
5.5 Transmitted light measurements during tensile testing	124
5.51 Apparatus	125
5.52 Results	126
5.53 Discussion	129
5.6 Conclusions	132
 CHAPTER 6.	
6. <u>RELAXATION TESTS</u>	135
6.1 Introduction	135
6.11 Scope of tests	135
6.12 Choice of strain-rate to attain prescribed strain	135
6.13 Material samples tested	136
6.14 Annealing Procedure	137

	Page
6.2 Apparatus, Procedure and Errors	138
6.21 Apparatus and Experimental Errors	138
6.22 Experimental Procedure	141
6.3 Results	142
6.4 Discussion	144
6.5 Conclusions	149
CHAPTER 7.	
7. <u>CONCLUSIONS.</u>	150
APPENDIX I	158
APPENDIX II	160
APPENDIX III	162
APPENDIX IV	163
APPENDIX V	164
REFERENCES	

1. INTRODUCTION.

Plastics, because of their resistance to corrosion and mouldability, are finding increasing usage in load bearing and impact withstanding applications such as piping, containers, and casings.

Crystalline polymers are a class of thermoplastics (plastics which may be heat-softened many times without chemical change) with mechanical properties that make them useful in numerous applications of the above type. Their mechanical behaviour is, however, complicated by being time dependent at room temperature and by being strongly dependent on temperature and detailed structure.

This research is a study of how thermal history affects the structure and mechanical properties of polypropylene at approximately room temperature.

Polypropylene is one of the polyolefin group of crystalline polymers which has already established itself as an engineering design material and has certain advantages over similar plastics which may be listed as follows;

- a) a relatively high melting point,
- b) resistance to environmental stress cracking,
- c) low density and relatively cheap cost,
- d) a very favourable combination of relatively high modulus with great ductility.

A comparison with similar properties of other thermoplastics has been given by Kresser ⁽¹⁾.

Its convenience as a research material is also governed by the fact that its structure is readily visible in the optical microscope.

The structure of the material is, however, quite complex and in the following pages a survey of the important

structural features common to this class of plastics .
which determine their practical usefulness, will be
given. Sections 1.2 and 1.3 survey the effects of thermal
history on structure and mechanical properties respectively,
with particular reference to polypropylene, and section 1.4
surveys the problem of relating mechanical properties to
structure.

1.1. The General Structure of Crystalline Polymers

Most physical properties of crystalline polymers depend strongly on their detailed morphology which may be varied basically by the structure of the molecule, the sample's thermal history, and mechanical treatment during moulding

A summary of the most important variables may be made as follows:

- i) Variables in the hands of the polymer producer
 - a) the degree of polymerisation i.e. molecular weight or length of molecular chain,
 - b) the distribution of molecular weight or polydispersity, commonly measured as the ratio of the weight to number average molecular weights M_w/M_n ,
 - c) the crystallisable fraction of the polymer,
 - d) the stereoregularity within individual molecules,
 - e) copolymerisation with other polymers,
 - f) additives such as antioxidants, and nucleating agents.
- ii) Variables in the hands of the fabricator
 - a) the melt condition,
 - b) flow during moulding,
 - c) the rate of cooling of the polymer after or during moulding,
 - d) the pressure of the mould.
- iii) Variables in the hands of the design engineer
 - a) working temperature,
 - b) working environment,
 - c) state of stress and of strain,
 - d) duration of stress or strain.

The polypropylene (hence forward abbreviated to PP) molecule shown in Fig. 1.1 comprises a carbon chain with a methyl group (CH_3) attached at every other carbon atom.

Since every other carbon atom in a PP molecule possesses an asymmetric centre, the stereoregularity of the molecule as a whole and the distribution of stereoregularity govern the configuration adopted by the molecular chain. Isotactic molecules in which the methyl group tacks on to the chain, consistently by the same bond permit the molecule to arrange itself into a compact helical chain which can pack very closely with similar neighbouring chains to form part of a crystalline array. Atactic molecules in which the methyl group tacks on at irregular bond sites have a random configuration and are incapable of close packing and crystalline order. It is further possible for mixed stereoregularity within a single molecule to occur which leads to structures of intermediate order.

The length of such molecular chains chiefly affects long time mechanical properties by controlling the amount of cooperative movements within the structure through chain entanglement and 'connectivity' between crystalline units. The dependence of PP's mechanical properties on molecular weight (MW) and stereoregularity have been reported by several authors ⁽²⁾⁽³⁾⁽⁴⁾⁽⁵⁾.

Keller ⁽⁶⁾ led the way to the present understanding of crystalline structure in polymers when in 1957 he showed that single crystals of polyethylene (hereafter abbreviated to PE) grown in solution, comprised flat lozenge shaped plates or crystallites typically about 100 Å thick and several hundred Å in lateral dimensions. His discovery that the molecular chains within these

crystals were perpendicular to their faces, despite a molecular chain length of many thousands of Å, led to the postulation of a folded chain morphology as shown in Fig. 1.2.

The packing of the parallel molecular stems within the body of these crystals has since been characterised for many polymers and the results are listed in a recent review⁽⁷⁾ on polymer morphology by Geil.

In the case of polypropylene the more usual crystal modification is monoclinic⁽⁸⁾ and is shown in Fig. 1.3.

An apparently hexagonal modification⁽⁹⁾ is also seen much less frequently and appears to be favoured by rapid cooling.

Detailed theories have been proposed to predict the rate of chain folding during crystallisation and are summarised by Price⁽¹⁰⁾. The major effect of an increase in crystallisation temperature is to increase the fold period such that thicker crystals result. Inevitably, it must be concluded that the most equilibrium configuration of the long chain molecules is ^{for them} to align themselves fully throughout their length into extended chain crystals. Such crystals have recently been observed⁽¹¹⁾ in polyethylene which had been bulk crystallised; their occurrence is enhanced by crystallisation at elevated temperatures under high pressures.

Crystallisation in the bulk yields a much more complex structure comprising spherically symmetric crystalline aggregates of radiating fibrils, known as 'spherulites'. Shown in Fig. 1.4 are two-dimensional spherulites of PP grown between glass slides at 125°C in the laboratory. A process of small-angle branching is characteristic of this growth⁽¹²⁾ and enables the fibrils to fill the spherulitic volume whilst retaining

a degree of preferential crystallographic orientation along a radius. Historically this growth habit has been recognised for many years ⁽¹³⁾, and has been recently shown ⁽¹⁴⁾ to be typical of many multi-component systems having preferentially crystallisable species in a relatively viscous melt.

In spherulites it has been possible to determine the orientation of the crystallographic axes by optical means ⁽¹⁵⁾ and by microbeam X-ray techniques ⁽¹⁶⁾. Observations have indicated that the molecular chain axis (c-axis) is, on average, tangentially orientated (perpendicular to the radius) in many polymers. The consequent optical anisotropy of the radiating fibril leads to the appearance of a dark Maltese Cross (seen faintly in Fig. 1.4) when spherulites are observed between crossed polarised light, the arms of the cross being parallel to the vibrational directions of the polarised light. A concentric banded appearance may also be observed under similar lighting conditions for some polymers, including PP ⁽¹⁷⁾ under certain conditions of crystallisation, and this has been shown ⁽¹⁵⁾ to be due to the regular twisting of radial fibrils forming a helical type of structure along the radius.

In the case of PP different results for the orientation of the molecular axis with respect to the spherulite radius (values are quoted as 90° and $\sim 10^\circ$ ⁽¹⁸⁾, 68° to 70° ⁽⁹⁾, or 65° to 71° ⁽¹⁹⁾) have delayed a strictly defined morphology of this polymer's most typical spherulitic growth habit, see section 3.1. It seems probable, however, that helical twisting may be a feature common to all spherulite fibrils ⁽²⁰⁾, but it is only discernible when the effect is reinforced by cooperative twisting in neighbouring fibrils.

Electron microscopy has shown that the radiating fibrils comprise thickly packed lamellae. For a

detailed survey of spherulitic morphology in polymers the reader is referred to Geil⁽⁷⁾ (Chapter IV).

Palmer and Cobbold⁽²¹⁾ have succeeded in separating lamellate structure from bulk crystallised polyethylene by an acid attack technique which preferentially attacks disordered regions. They confirm that the molecular chain axis is approximately normal to the layer surface of the lamellar debris. The folded chain concept developed for single crystals grown in solution, has therefore been invoked to explain the lamellate structure in spherulites, and the normal model assumed for spherulitic morphology is shown in Fig. 1.5.

It should be emphasised that the above model is probably an over simplification of the true spherulitic morphology. Peterlin and Meinel⁽²²⁾ have found that the weight loss following acid attack treatments of PE single crystals are not explicable on the grounds of a simple minimum energy chain folded surface, of the type proposed by Basset, Frank and Keller⁽²³⁾, but one comprising more voluminous folding.

Less favourable crystallisation conditions in the bulk may well lead to a compromise lamellate structure in which there is greater 'connectivity' between lamellae due to shared molecules.* Acid attack treatments on bulk crystallised PP have shown that whereas a lamellate appearance may be resolved⁽²⁴⁾, the occurrence of tie 'molecules' would appear to be more prevalent in this polymer than in PE, due to the greater difficulty of separating these lamellae.⁽²⁵⁾ This concept is further supported in the case of PP by the difficulty with which poor single crystals can be grown⁽²⁶⁾⁽²⁷⁾ from the most favourable conditions, compared with PE. Rånby et al⁽²⁶⁾ attribute this difficulty to the properties of the PP

* usually called tie molecules.

molecular chain. These chains are much more restricted in their packing together to form a crystalline lattice, since the chain can take on RH or LH helices which are not identical. Therefore, when a PP chain folds back to crystallise it has to select the proper site on the lattice surface according to how the chain adopts a new helical twist after looping. It may therefore be true to say that the chain folded structure is not typical of PP under normal commercial crystallisation conditions, and there is also good reason to believe that under such crystallisation conditions a significant amount of intermediately ordered material is formed, see section 1.2. Further recent morphological studies by Padden and Keith ⁽¹⁸⁾, see section 3.1, have thrown some light on the complexity of the most typical PP spherulite.

The same authors ⁽²⁸⁾ ⁽²²⁾ have considered in great detail how the fibrillar growth habit develops, using PP extensively as a model, by the segregation of 'impurity' species at the growth front, comprising lower molecular weight chains (rejection by fractionation), and non-crystallisable molecules (rejection by incompatibility). During growth, therefore, less crystallisable material is pushed into regions between lamellae and ahead of the growth front. Secondary crystallisation, controlled chiefly by diffusion, may then proceed in inter-lamellar regions as far as steric hindrance and the impediment of neighbouring lamellae allows. Due to MW fractionation it also seems likely that lower MW material will be pushed to the outer circumference of the spherulite. In extreme cases of dilution with non crystallisable species this can lead to spherulites which do not meet one another. Despite the importance of inter-spherulitic bonding in determining mechanical properties, see section 1.3, little is known about the state of morphological 'connectivity' in these regions.

In order to explain the overall toughness of crystalline polymers it has long been appreciated (29) (30) that a significant amount of 'connectivity' must exist between the crystalline layers, otherwise it would have been possible for deformation to occur largely in amorphous regions without a great deal of contribution from crystalline lamellae, other than in the role of a 'solid' filler. Since this time some striking examples of bundled tie molecules between lamellae^{and spherulites} have been observed in bulk crystallised PE (31), and have been reported to occur between mechanically separated lamellae of bulk crystallised PP (32).

It may be considered in the light of these observations, that crystalline lamellae behave as relatively stiff cross-linking platforms which give skeletal reinforcement to relatively flexible regions, whilst at the same time being arranged as spherulitic aggregates.

1.2. The Effects of Thermal History on Morphology

The detailed effects of thermal history on the bulk morphology of crystalline polymers are as yet limited by the incomplete understanding of their basic structure.

Increasing the crystallisation temperature increases the ratio of spherulitic growth rate to nucleation rate so that fewer and larger spherulites grow. Whilst this is a generally appreciated fact no correlations of spherulite size against crystallisation temperature in PP have been found by the author. More commonly measurements are made of nucleation and growth rate. (33)

The melt condition is also important in controlling the content of retained crystalline embryos which act as heterogeneous nuclei during crystallisation (34) and can to a large extent affect the number and size of spherulites (35) (36). It has been proposed (37) that the PP molecule is particularly inflexible in the melt and that this could lead to a relatively high degree of melt order compared with other polyolefins (38). It is, therefore, not surprising to find that the melting point of PP is somewhat ill defined, values being quoted in the literature varying from 149°C for low MW material (39) up to 189°C for well annealed samples (40). A second order transition at a temperature 30°C higher than this normal range of melt temperatures has also been reported. (41) Hence the melt condition has considerable effect on the subsequent nucleation density and hence spherulite size in this polymer. More favourable crystallisation conditions which accompany a raised temperature or duration of crystallisation lead to an increased percentage of the crystalline content. This may be attributed to -

- i) a longer time allowed for completion of crystallisation.

- ii) an increase in the average thickness of lamellae ⁽⁴²⁾⁽²⁴⁾ at the expense of density-deficient surface layers ⁽⁴³⁾.
- iii) to an improvement in perfection of the crystalline state arising from more efficient segregation of 'impurity' species. Keith ⁽⁴⁴⁾ also suggests that there are a greater number of dislocations within PE crystals grown at a faster rate.

It is, however, apparent from the data of Hock ⁽²⁴⁾ for bulk crystallised PP, shown in table 1.1., that there is little change in the absolute degree of crystallinity, compared with lamellar thickness, following extremes of crystallisation conditions in this polymer. X-ray studies following annealing treatments on PP have also shown ⁽⁴⁵⁾⁽⁴⁶⁾ that the reordering of molecules that occurs during annealing, involves more of an increase in the size and perfection of crystalline areas rather than their quantity, whilst dynamic mechanical tests on PP ⁽⁴⁷⁾ have indicated that the state of this perfection is inferior to that resulting from an isothermal crystallisation which produces the same overall density.

TABLE 1.1

Property	Quench cooled in ice water	Isothermal Crystallisation Temperature °C.		
		125	145	161
a) lamellar height Å	80	105	158	210
b) inter lamellar thickness Å	40	48	68	95
ratio a/b	2.0	2.1	1.9	1.8
crystallinity by X-ray diffraction %	55	62	64	68
melting temperature °C.	173	173	174	176

Numerous reports have been made (45)(48-53) of a state of intermediately ordered material between the purely crystalline and amorphous states in PP, the occurrence of which is enhanced by increasing the cooling rate from the melt and by extension of a sample either by extruding (52) or cold drawing (45). It is suggested that this state is either a smectic configuration (48) due to RH and LH helices being randomly placed with respect to each other to give a pseudo-hexagonal structure, or a para-crystalline configuration (50)(45) in which the crystal lattice is considered to be deformed or disordered.

Material of intermediate order in PP, as induced by rapid quenching, has been found (53) to be essentially removed by heating for half an hour at 85°C. On the other hand, where its presence was induced by cold drawing, it has been found (45) that for half-hour heat treatments its presence starts to diminish following a 70°C annealing and reaches half conversion following a 110°C annealing.

Wyckoff (45) gives the following mechanism for the increase of crystallite size following annealing. At low annealing temperatures ($T_A \lesssim 110^\circ\text{C}$) the initial small increase in crystallite size might be at the expense of material of intermediate order, but at higher annealing temperatures ($T_A \gtrsim 130^\circ\text{C}$) the large increase observed must be due to a conversion of small crystallites, having an unstable fold period at the annealing temperature, to larger crystallites.

The ability for inter-lamellar links to form in PE as found by Keith, Padden and Vadimsky (31) would appear to depend on the average length of the chain molecules and the distance separating the lamellae. The relationship

they find for the ability for a tie molecule of PE of molecular weight M_w to bridge a distance d , $d \cong 20 M_w^{1/2} \text{ \AA}$, if applied to PP* under the crystallisation conditions in table 1.1, would predict the possibility of a great many inter-lamellar links. This desirable situation, aided by the selective folding required of the PP molecule during crystallisation, as already mentioned, fits in with Hock's (25) conclusion that crystalline lamellae in PP have morphological individuality but are parts of a coherent system in which the amorphous component is not conspicuous.

Ageing at room temperature has been considered by Keith and Padden (22) to involve slow diffusion-controlled crystallisation in inter-lamellar regions. Sasaguri, Hoshino and Stein (54) find that birefringence changes upon ageing of PP suggest an increase in tangentially orientated crystalline molecules which have a considerable restricting effect on crystallite mobility.

The effect of 'impurity' concentration and the crystallisation temperature on the spherulite compactness and coarseness respectively have been examined by Keith and Padden (28). They find that the most important parameter determining these texture effects is the quantity $\delta = D/G$, where D is the diffusion coefficient for impurity in the melt, and G is the radial growth rate of a spherulite. The bulk of their results show that as crystallisation temperature and hence δ is decreased, the cross section of fibers have dimensions reasonably comparable with an estimated value of δ , and that the incidence of non-crystallographic branching of fibrils is increased. This latter result they attribute to δ becoming more comparable with the sizes of disordered regions on lamellate surfaces. A strict application of this useful concept is, however, hampered by the detailed knowledge required of the diffusion

* In PP this relationship becomes $d \cong 10M_w^{1/2} \text{ \AA}$.

rates of the impurity species.

Prolonged heat treatments of PP of the order of days at 130°C produce cracking at both spherulite boundaries (55) and radial cracking (55)(56).

The former crack location has been attributed to thermal decomposition of the molecules in the vicinity of the spherulite boundary, whilst the radial cracking has been attributed to tangential stresses set up within the spherulite (particularly near its boundary) by internal density changes accompanying an increase in crystallinity. Kavafian (57) finds a similar embrittlement of spherulite boundaries in PE.

At higher crystallisation temperatures ($T_c \approx 130^\circ\text{C}$), however, the most likely cause of interspherulite weakness is not due to degradation but due to the enhanced diffusion conditions during crystallisation which might permit non-crystallisable species to become lodged between spherulites (58), rather than the physical separation of spherulites by voids. Samples of bulk crystallised PP at $T_c \geq 125^\circ\text{C}$ were found by Hock (25) to separate into spherulites in the earlier stages of an acid attack examination, supporting the concept of a more 'porous' acid accessible structure in these regions. During crystallisation of PP films between glass slides at $T_c = 125^\circ\text{C}$, Barish (59) observed some very occasional minor voiding between spherulites after about 4 mins., which he attributes to spherulite contraction during crystallisation (cf. Fig. 1.4 crystallised at 125°C for 1½ hours in which there is gross voiding between some spherulites and some radial cracking near one boundary of a ^{large} spherulite.) Whether or not such a voided condition would be present in a moulded product following the same crystallisation temperature conditions would depend on

a) the effect of adhesion to the glass slides and the effect of differential thermal contraction during cooling, in inducing cracking in the observations made above,

and

b) the effect of moulding pressure in preventing gross voiding following secondary and tertiary crystallisation (60)(61).

From this survey it is seen that improvement in crystallisation conditions affects the size of spherulites and of the crystalline regions within them, the degree of crystallinity in PP is varied to a lesser extent. More extreme heat treatments affect the ^{size and} perfection of crystalline regions and the type of bonding between spherulites. Ageing at room temperatures enables secondary crystallisation to proceed in inter-lamellar regions. It is also concluded that the non-crystalline component may exist partly as lattice defects within the lamellae, and partly as inter-lamellar layers rather than as isolated amorphous regions.

1.3 Previous Studies of the Effects of Thermal History on Mechanical Behaviour.

The importance of thermal history in determining the mechanical properties of PP was illustrated most dramatically by Keith and Padden ⁽¹⁷⁾ who found that following a very thorough prolonged crystallisation at a high crystallisation temperature, individual spherulites could be separated by hand.

This thermal treatment represents an extreme which is not generally encountered under commercial moulding conditions, but illustrates a general tendency to weakness at specific regions in thermoplastics which may be related to their structure. In this context it has been found that PP shows a tendency to earlier and more pronounced weakness at spherulite boundaries ⁽⁵⁹⁾⁽⁶³⁾ than other thermoplastics such as nylon ⁽⁶⁴⁾, polychlorotrifluoroethylene ⁽⁶⁵⁾, and polyethylene ⁽⁶⁶⁾ in which cracking is shared between spherulite boundaries and across spherulites. In some cases ⁽⁶⁵⁾⁽⁶⁶⁾ cracking within spherulites is identifiable as taking a route between the radiating fibrils. Discrete heat treatments such as those used in the above observations probably cause cracking due to structural contraction during secondary crystallisation, rather than thermal degradation, as outlined in section 1.2.

Where crystallisation conditions are such that spherulites of PP are separated by an amorphous phase Barish ⁽⁵⁹⁾ has shown that a very large increase in ductility and fall in yield stress results. Under more conventional moulding cycles in PE, however, McCrum and Morris ⁽⁶⁷⁾ have shown that inter-spherulite slip is unlikely, and the same condition might be expected for PP when conventionally moulded.

Following normal moulding cooling rates and in the absence of inter-spherulitic cracking mechanical properties generally depend on the degree of crystallinity, increases in crystallinity producing a tendency to become less ductile but increasing the modulus.

For a non-linear stress-strain curve the modulus may be measured as either a tangent to the curve (tangent modulus) or as the ratio of stress to strain (secant modulus) at any chosen point. For time dependent materials both the time (or strain rate) and strain at which the modulus is measured has to be stated. A relaxation test in which a strain is applied at zero time and held constant thereafter gives a relaxation modulus which is defined as the relaxation stress divided by the applied strain; again both the strain and time at which the modulus is measured should be stated. A strict comparison of modulus values quoted in the literature is made difficult by the fact that frequently either the type of modulus quoted or the strain and time at which it was measured are not specified.

In PP increase in crystallinity where it has been induced by either changes in crystallisation conditions⁽⁶⁷⁾ age of specimen⁽⁶⁸⁾, or by annealing treatments⁽⁴⁶⁾ show the expected 'normal' tendency towards loss in ductility and increase in modulus.

However, Wyckoff⁽⁴⁵⁾, testing cold-drawn PP samples at a strain rate of 100 %/minute following a series of annealing treatments, has shown that these tendencies in mechanical properties may be reversed as the annealing treatment becomes more thorough; the turning point for his results appears following annealing for 30 mins. at $T_A \gtrsim 100^\circ\text{C}$. This is attributed to a gross melting and reorganisation of the structure at $T_A \gtrsim 100^\circ\text{C}$.⁽⁴⁵⁾ resulting

in a release of prestress and molecular entanglements in the amorphous region, thereby weakening the overall structure.

Turley and Keskkula⁽⁴⁶⁾, however, showed a 'normal' trend in mechanical properties following annealing compression moulded PP samples more thoroughly than Wyckoff's treatment; they used 60 mins. at $T_A \approx 160^\circ\text{C.}$, but tested their samples at a lower strain-rate of about $10^\circ/\text{o}/\text{min.}$

These inconsistent mechanical properties are difficult to reconcile purely by the explanation given by Wyckoff, and it would therefore appear that the point of reversal in the 'normal' trend for modulus must depend at least in the case of PP, on the strain-rate as well as the annealing treatment; a more thorough annealing treatment and increase in strain rate both producing a tendency to crack and hence weaken the overall modulus where this is measured beyond the threshold of cracking. A similar dependence for the strength of annealed PP samples on the test strain-rate has been reported elsewhere⁽⁷⁰⁾, and Barish⁽⁵⁹⁾ has demonstrated, for example, that increase in strain-rate produces a tendency to brittle failure between spherulites of PP. Hall⁽⁸⁰⁾ has however shown that PP's strain to/^{yield} is almost completely insensitive to strain-rate, and small scale cracking in crystalline polymers may be accepted as part of their normal visco-elastic response⁽¹⁰⁴⁾, such that an increase in ductility is still possible where samples undergo microscopic cracking.

Results reported for PE⁽⁷¹⁾ using a strain-rate of $25^\circ/\text{o}/\text{min.}$, show an increase in tensile modulus and decrease in yield strain following the annealing of a quench cooled specimen.

Generally, because spherulite size is an easily observed measure of cooling rate during moulding, many polymers' mechanical properties are related to this feature⁽⁷²⁾ rather than the detailed changes which also occur in the finer morphology. A relationship between

spherulite size and mechanical properties quite apart from more detailed morphological changes, does appear valid where the thickness of the test piece is of the same order as the spherulite diameter⁽⁷³⁾, and under such conditions it has been shown that a non-spherulitic structure, induced by more rapid cooling, heralds a fall in relaxation modulus.

It would, however, appear that in normal sections of material and at low strain-rates, spherulite size in PP would become of less importance compared with changes in the finer morphology, but at fast strain-rates both spherulite size and fine morphology, particularly at spherulite boundaries, may influence mechanical properties.

Other than the strain-rate effects already mentioned, there is little catalogued information on the effect of thermal history on the time dependence of thermoplastics in general, and PP in particular. One of the most complete examinations bearing on this subject has been published as a series of articles entitled 'Creep in Thermoplastics' by Turner^(74 - 77). In this work annealed and quench-cooled PP samples gave results which appeared on a plot of isochronous log (stress) versus log (strain) as parallel lines, at least up to about 1⁰/₀ strain; thereby showing that the shape of the stress-strain response of these polymers which is a measure of their non-linearity is independent of the internal state of the material. It is suggested⁽⁷⁴⁾ that the properties of polymers of intermediate thermal history may be obtained by interpolating between these two extremes of treatment.

Prolonged creep tests plotted as log (strain) versus log (time) show⁽⁷⁴⁾⁽⁷⁵⁾ a sharp decrease in creep rate which Turner interprets as an interaction of the crystallites with the rubbery amorphous region, and calls this a pseudo-equilibrium zone by analogy with the equilibrium zone in cross-linked rubbers in which strain ceases. However,

since no true 'equilibrium' behaviour exhibits after prolonged tests (on PE) it must be assumed that instead of the crystalline lamellae arresting further deformation (cf. cross-links in vulcanised rubber) they proceed to deform themselves as outlined in section 1.4. As far as predicting long term mechanical behaviour (i.e. an isochronous stress-strain curve at long times) it would appear safe, at present, to extrapolate these 'linearised' creep curves over considerable time spans, provided the overall strains do not exceed values of the order 1⁰%. The type of structural change occurring during ageing has been shown by birefringence tests ⁽⁵⁴⁾ to restrict the mobility of the crystalline phase. A similar effect has been found by Flocke ⁽⁷⁸⁾ to occur only in the temperature range 0 - 90⁰C. It is interesting to note that this upper temperature fits in with the limit of stability of partially ordered material ⁽⁵³⁾ as already discussed. The effect of annealing and ageing on the visco-elastic response of crystalline polymers has been shown by Turner ⁽⁷⁵⁾⁽⁶⁹⁾ to be essentially different in that annealing translates the creep curve along the time axis, but ageing translates it along the strain axis. No rational explanation for this difference, which was demonstrated in PE, has yet come to light.

Dynamic mechanical tests, which measure the in-phase and out-of-phase deformational responses of polymers to an applied alternating stress, are capable of detecting transitions in the mobility of polymer chains or their segments in the temperature range below their melting point. Crystalline polymers are typified as having a number (usually three) transition maxima.

The lower temperature maxima, occurring at $\sim 220^{\circ}\text{K}$ and $\sim 280^{\circ}\text{K}$ in PP, are generally attributed ⁽⁷⁹⁾ to segmental motion of a short or longer length of chain

respectively, in the amorphous regions. The high temperature maximum occurring at $\sim 370^{\circ}\text{K}$ is interpreted as either a liberation or reorientation within ordered regions (50) or movement of lamellar surfaces or inter-lamellar regions (47).

Using this technique Flocke (78) has demonstrated a large increase in mobility of the amorphous phase with increase in atactic content of PP, as would be expected. Miller (50) and Passaglio and Martin (47) find temperature shifts in the maximum occurring at 280°K when samples of PP are prepared at decreasing cooling rates, which they respectively attribute to either a decrease in constraint on the amorphous phase, or to an improvement in segregation of atactic molecules.

From the above description of the effect of thermal history on mechanical properties it is seen that at slow rates of deformation and in the absence of inter-spherulitic voiding all the structural components take part in deformation and contribute to the overall mechanical properties. Under these conditions, crystallisation conditions which favour an increase in crystalline content increase the sample's modulus and decrease its ductility. Subsequent thermal history/^{changes} which may extend from ageing at room temperatures to annealing treatments control the modulus without greatly changing the crystalline content due to their effect on crystalline size and perfection and the state of relaxation in non crystalline regions. The effect of ageing on ductility has not been reported.

Under crystallisation or annealing conditions which produce inter-spherulite voiding, or at strain-rates which exceed the rate of relaxation of the crystalline phase, cracking may occur between or within spherulites, thereby lowering the modulus. At high strain rates, spherulite

size might also become a factor in affecting the compatibility forces between spherulites. These considerations show that there exists a complicated interplay between strain-rate and thermal history. i/

1.4. Relating Mechanical Properties to Structure

The deformation response of the spherulite is complicated because of the radiating symmetry of the spherulite, the anisotropy of the radiating unit, the efficiency of connection between spherulites and the varying time dependent response to stress of all the various elements of structure. Numerous review articles have been given on general structural interpretations of the mechanical properties of polycrystalline polymers, (11)(81-83).

A general theory relating crystal orientation and birefringence of polymers to spherulite deformation has been proposed by Sasaguri, Hoshino, and Stein (54). Using this theory they have shown that at short times and small strains the earliest deformation mode comprises a transformation of the spherulite shape to an ellipsoid, with the internal structure of the spherulite subjected to the type of transformation shown in Fig. 1.6. Deformation up to this point is largely concentrated into non-crystalline regions. At longer times, and larger strains, this is followed by a time dependent orientation of the molecular axis (c-axis) towards the extension direction which may be characterised by a compliance. Similar results for PP have been obtained by Samuels (84).

Light scattering experiments (85) also confirm that the deformation mode of PE spherulites is a two stage process in which changes in light scattering following spherulite deformation precede the birefringence changes which follow with reorientation of the crystals.

Stein (81) has listed the possible rearrangements of the crystals within the spherulites as,

- a) physical rotation of crystals,
- b) unfolding of folded chain crystals,
- c) recrystallisation
- d) dislocation migration, slip, and twisting within the crystals,
- e) formation of 'tilted chain' type crystals,
- f) crystal structure transition,
- g) deformation of the crystal lattice,
- h) change in the degree of crystallinity

Whilst a well established theory ⁽⁸⁶⁾ based on entropy changes has been developed for the elasticity of a system of randomly coiled cross-linked molecules as are found in vulcanised rubbers, a similarly satisfying theory for multiphase polymers cannot yet be evolved because of

- a) the complexity and incomplete comprehension of their structure,
- and b) the lack of a simple mathematical framework to describe a system comprising a phase whose elasticity depends on its entropy (randomness), and a phase whose elasticity is determined by the potential of its lattice.

The situation is further complicated by the knowledge that the polymeric crystalline phase must house regions of misfit i.e. dislocations ⁽⁸⁷⁾, and slip planes ⁽⁸⁸⁾ similar to metal crystals. The crystals themselves have, therefore, all the ingredients of an elastic/plastic deformation model. Electron microscopy, see Geil ⁽⁷⁾ chapter VII, has further shown that shearing of lamellae over one another is a typical deformation response. Other more complex deformation modes have been proposed ⁽⁶⁷⁾ to take into account the effect of a periodic keying of lamellae which are cooperatively twisted around each other. This sort of texture effect may explain why in PE, which frequently displays the banded appearance associated with cooperative twisting, it has been found ⁽⁶²⁾ that the radiating

fibrils themselves are drawn out into aligned molecules at fairly low strains ($\sim 5^\circ/\%$). In PP, which only rarely displays a banded appearance ⁽¹⁷⁾, deformation may be concentrated into inter-fibrillar regions up to considerably higher strains ⁽⁶²⁾ ($\sim 30^\circ/\%$) prior to the drawing out process.

A simple model in which the overall visco-elastic response of the spherulite composite is considered as a combination of two different visco-elastic mechanisms has been proposed by Matsuoka ⁽⁸⁹⁾⁽⁸²⁾. In this model, shown in Fig. 1.7a for tension in the vertical direction, the two mechanisms comprise an α stress propagation route linking essentially crystalline regions, and a β route linking a sandwiched structure of alternate crystalline and quasi-amorphous layers connected in series. This model essentially differentiates between the mechanical behaviour of the polar and equatorial regions of the spherulite, as defined by the extension direction.

The concept of this model proves useful in explaining some of the mechanical properties of these polymers. The β route would be expected to display many of the properties of a highly cross-linked rubber but with movement of the rubbery phase being hindered by the bonded lamellae.

Such a system has a typical long time modulus ⁽⁹⁰⁾ of from 10^7 dyne/cm², compared with an observed overall modulus for crystalline polymers of about 10^9 dyne/cm² in the long time range ⁽⁹¹⁾. It must be concluded that the much stiffer α stress route serves to bolster the overall modulus and that the two mechanisms act in parallel as shown in Fig. 1.7b for which,

$$E_{\text{overall}} = \frac{A_\alpha}{A_0} E_\alpha + \frac{A_\beta}{A_0} E_\beta \quad \text{---(1)}$$

where $\frac{A_\alpha}{A_0}$ and $\frac{A_\beta}{A_0}$ are the fractional areas operated on by each mechanism.

Films of uniaxially crystallised polybutene, in which the fibrillar growth habit of spherulites was made to grow predominantly in one direction, have been used by Sasaguri, Yamada and Stein ⁽⁹²⁾ to demonstrate the greater deformability and lower modulus of a β stress route which is perpendicular to the fibrils, when compared with the response of an α stress route which is parallel to the fibrils. Their results show, however, that the stiffness of the β response is only about half of the α response over the three decades of time for which measurements were made on this polymer. By substituting this ratio of moduli $E_{\alpha} = 2E_{\beta}$ into equation (1), it would then appear that for any reasonable values for A_{α}/A_0 and A_{β}/A_0 the values obtained for E_{α} and $2E_{\beta}$ are of a similar order of magnitude to the observed modulus of 10^9 dyne/cm². This deduction would mean that the response of the β visco-elastic mechanism is by no means comparable with a heavily cross-linked filled rubber system, and suggests that either a) the quasi-amorphous layers are far from being random in configuration or that the 'random' PP chain is much stiffer than a rubber chain, or/and b) the lamellae themselves in the equatorial regions participate considerably in the deformation. These respective conclusions would agree with the findings of Hock ⁽²⁵⁾ on PP and McCrum and Morris ⁽⁶⁷⁾ on PE.

Some success in relating this equivalent model method to dynamic rheo-optical properties of crystalline polymers has been reported by Takayanagi, Uemura and Minami ⁽⁹³⁾, using a similar model shown in Fig. 1.8.

In this model the overall modulus is related to the modulus of its component phases by the more complex relationship shown below.

$$E_{\text{overall}} = \left[\frac{\phi}{(1-\lambda)E_1 + \lambda E_2} + \frac{1-\phi}{E_1} \right]^{-1} \quad \text{---(2)}$$

in which E_1 and E_2 are the moduli of the crystalline regions and disordered regions respectively, λ and ϕ define the dispersion of the amorphous phase with respect to the stress direction.

Theoretically derived moduli in the chain axial direction of several crystalline polymers have been reported ⁽⁹⁴⁾ to be of the order 1.5×10^{12} dyne/cm². Empirically determined values ⁽⁹⁵⁾ agree quite well with this figure for PE (2.4×10^{12} dyne/cm²) and other polymers in which the bond angle in the carbon chain gives them a zig-zag configuration, but show PP, which has a helical molecular chain configuration, to have a lower modulus of about 4.2×10^{11} dyne/cm². Nevertheless, these values exceed the observed elastic modulus of crystalline polymers by at least a factor of 10, because in the stiffest stress route, stresses are applied principally to the weaker Van der Waal bonding forces between molecular stems of lamellae, see Fig. 1.7c.

The conventional picture of polymer crystals acting as relatively non-deformable cross-linking points in a rubber-like lattice, has been the starting point for a number of attempts to predict the modulus of crystalline polymers in terms of molecular constants etc. Beuche ⁽⁹⁶⁾ uses this model directly and produces a theory valid at small strains by which he is enabled to use the theory of equilibrium rubber elasticity applied to the inter-crystallite regions. Becker ⁽⁹⁷⁾ has combined this theory with the Mooney-Rivlin theory to extend the modulus predicted to larger deformations ($\approx 20\%$). Other theories have further modified the gaussian network treatment through either an introduction of an appropriate correction for the filler action of the crystallites ⁽¹¹¹⁾ or by taking into account the action of crystallisation in

in straining the quasi-amorphous chains whose ends are embedded in more than one growing crystal (98).

All these approaches neglect deformation of the crystalline phase and should therefore strictly only apply to short time/small strain responses of the type used in dynamic mechanical testing. In any normal type of transient test some deformation of the crystalline phase must occur which, in some cases, (111) makes agreement fail by a factor between 5 and 10. In other approaches (98), better agreement is obtained by using an adjustable parameter which unintentionally includes the deformability of the crystalline phase. Because deformation in the crystalline phase is neglected all of these derived moduli have a similar form in which the expression, equation (3), for rubber elasticity is conspicuous in one form or another.

$$G = \frac{\rho RT}{M_c} \text{-----} (3)$$

where G = shear modulus

ρ = density of the amorphous phase

R = the gas constant

T = the absolute temperature

M_c = the number average chain molecular weight between crosslinks.

For a derivation of this equation the reader is referred to Chaps. III and IV of Ref. (86)

The difficulties of extending such approaches into the realms of time dependence has inevitably led to a more empirical approach.

Mathematical models comprising arrays of Hookean springs and Newtonian dashpots are frequently used to describe the response of polymeric systems to stress, strain and time, although it is difficult to interpret their strict relationship with morphological features. The most general

- 29 -

arrangement of springs and dashpots which can represent both creep and relaxation behaviour is shown in Fig. 1.9.*

These simple models lead to solutions involving terms of the form $\exp(-t/\tau)$, see Appendix I, where t is time measured after the imposition of either a prescribed stress or strain function, and τ depends on the modulus and viscosity of the model elements. τ is called either a relaxation or retardation time according as either strain or stress is the prescribed function. To closely approximate to the visco-elastic response of polymers requires a large number of model elements which in the limit leads to a continuous relaxation or retardation spectrum.

Little morphological meaning can be assigned to the values of spring and dashpot constants in models comprising discrete numbers of elements since their values are not uniquely determined by simple visco-elastic tests. The continuous relaxation spectrum has, however, been given some morphological meaning by extensions to Rouse's (99) theory for relaxation in dilute solutions of amorphous polymers, but has to date been assigned little significance for crystalline polymers.

Whilst a combination of these elements is capable of simulating the approximate visco-elastic response of crystalline polymers it is subject to the following limitations,

- i) no single model can predict the response to stresses, strains or times which exceed the rather ill-defined bounds of linear visco-elastic behaviour. A normally accepted strain limit of about 1% (91)(100) is often proposed, but long term recovery (101) and relaxation experiments (102) suggest that non-linearity is almost always present to some degree.

* SEE APPENDIX I

- ii) The response to complex stress (or strain) histories cannot be accurately predicted by a Boltzman superposition law, ⁽¹⁰¹⁾ due to the above noted non-linearity effects.
- iii) Any long time experiments may have superimposed on their response the effects of a time-dependent change in structure.

The difficulties of incorporating non-linear effects into such models has led to empirical equations such as Findley's ⁽¹⁰³⁾ creep equation (4). Turner ⁽⁶⁹⁾ has correlated the effect of density in PE on the constants in Findley's equation, but again no morphological interpretation is capable for such results.

$$\epsilon = A \sinh B\sigma + K \sinh D\sigma \quad * \text{-----} (4)$$

From this review it can be seen that the intricacies of the deformation behaviour of the crystalline phase have made a strict relationship between structure and mechanical properties impossible at this stage.

* where A, B, K and D are constants.

1.5. Conclusions.

This survey has shown that whilst thermal history is known to affect the structure and mechanical properties of PP, amongst other crystalline polymers, its treatment on a quantitative basis is lacking. st/

One of the most important thermal history variables from the practical point of view is the rate of cooling from the melt during moulding. This can control the initial modulus and ductility of the material, depending on the use to which the plastic is to be put.

Previous workers find that moulding cooling rates are so variable within a single moulding or from a sequence of mouldings that a fairly thorough annealing treatment is given to samples in order to obtain repetitive and meaningful data for mechanical properties which may not be typical of the normally unannealed plastic. Ageing is an unavoidable history variable and yet little has been published on its effect on the transient mechanical properties of PP. Again owing to the variability of moulding conditions the annealing treatments used to obtain repetitive results for mechanical properties largely remove the effects of age as a variable in laboratory testing. Annealing treatments are seldom used in practice but may become important where PP components are welded together.

The experiments undertaken were, therefore, based on the effects of moulding cooling rate and age on the transient mechanical properties of PP. Annealing treatments were used principally to elucidate the importance of some structural features in determining mechanical properties. Where possible these properties will be related to the structure of PP as revealed by optical microscopy and density measurements.

The results of these tests should establish both useful practical data and some more systematic interpretation of the effects of moulding conditions on structure and mechanical properties.

It is not intended to apply any of the existing theories for prediction of either modulus or time dependence as varied by structure because of the considerable uncertainty as to the detailed morphology of PP and because of the inapplicability of existing theories to testing procedures which must involve participation of the crystalline phase.

1.6. Material Used in this Research.

The polypropylene homopolymer used in this research was 'Propathene' G.P.E. 33, normally used for general extrusion and blow moulding purposes.

This material was supplied in sheet form by I.C.I. (Hyde Division) as required by the moulding apparatus at hand in the laboratory, see section 2.21, and is characterised as follows:

Melt Flow Index	M _w	Normal Density g/ml	Additives	
			Antioxi- dant and thermal heat stab- iliser	Extrusion additives Nucleating agents
0.3	1-1.5x10 ⁶	0.905	0.1-0.25 ^o /*	stearate lubricant 0.2-0.4 ^o / _o none

* The strict type and quantity of such additives are trade secrets.

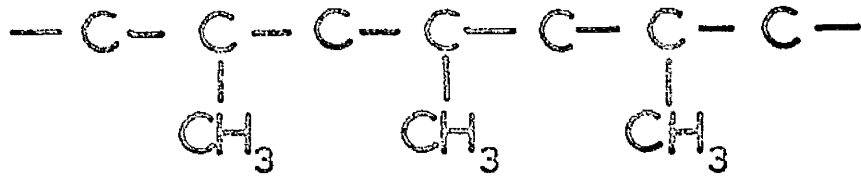


FIG 1.1

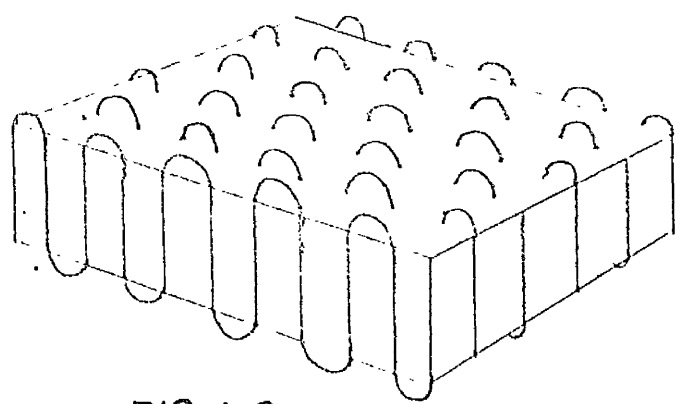


FIG 1.2

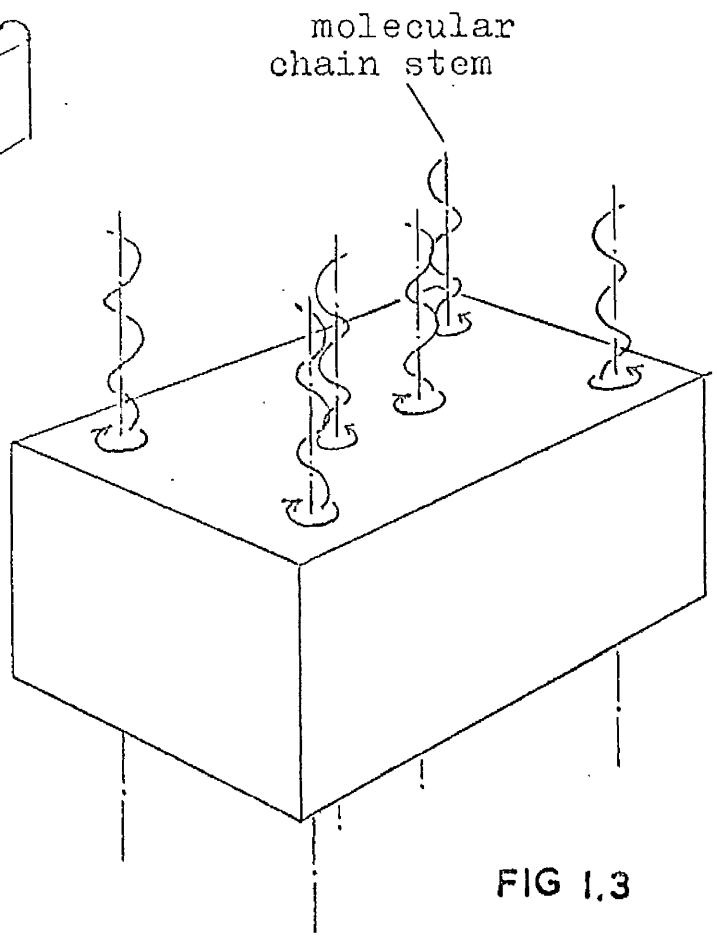


FIG 1.3

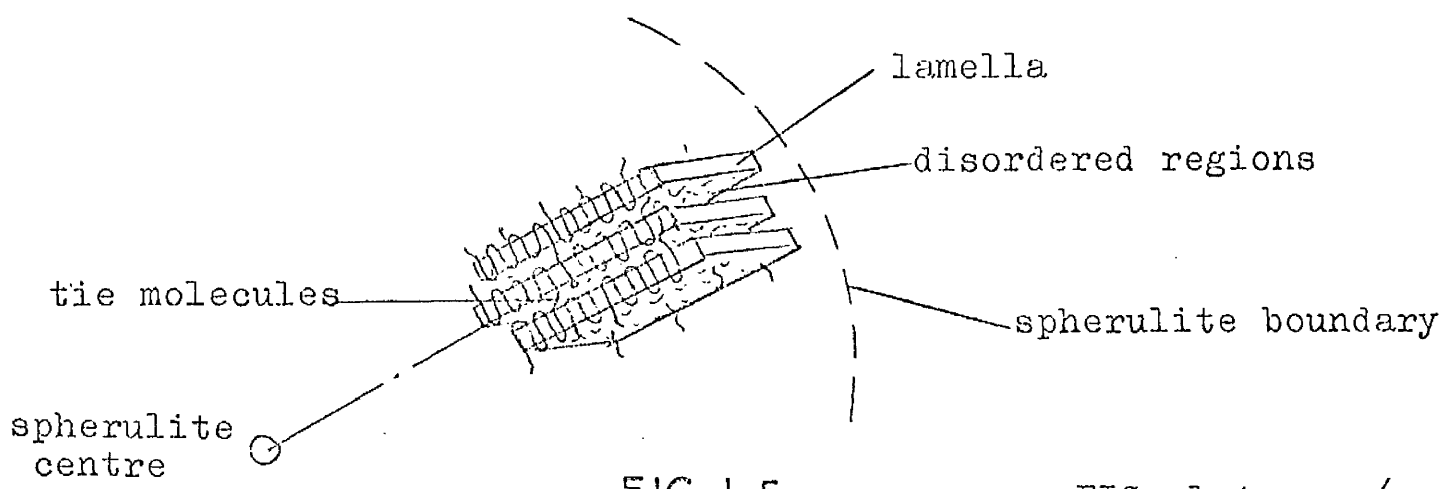


FIG 1.5

FIG. 1.4 over/

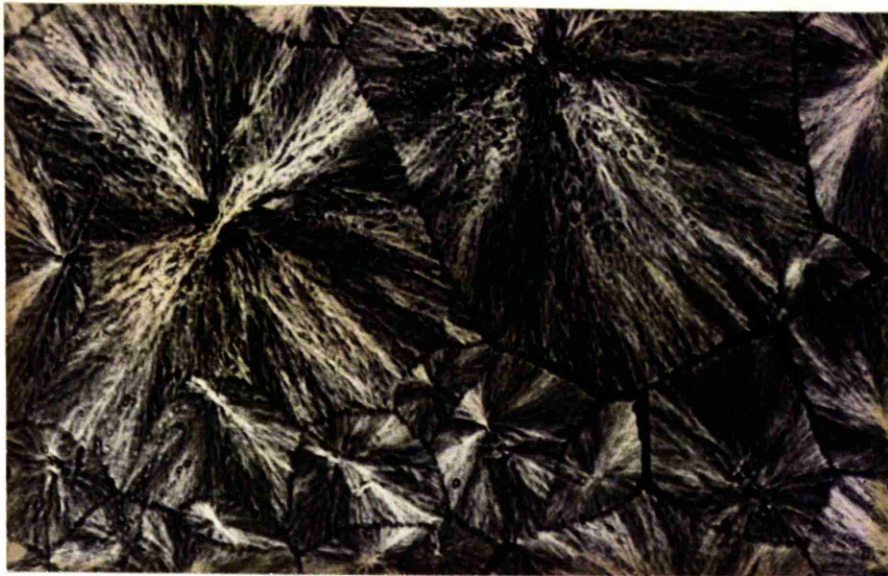


FIG. 1.4 x 400

FIG. 1.6

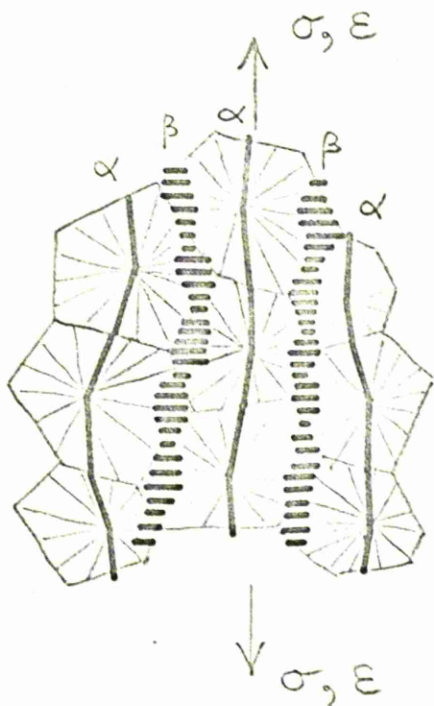
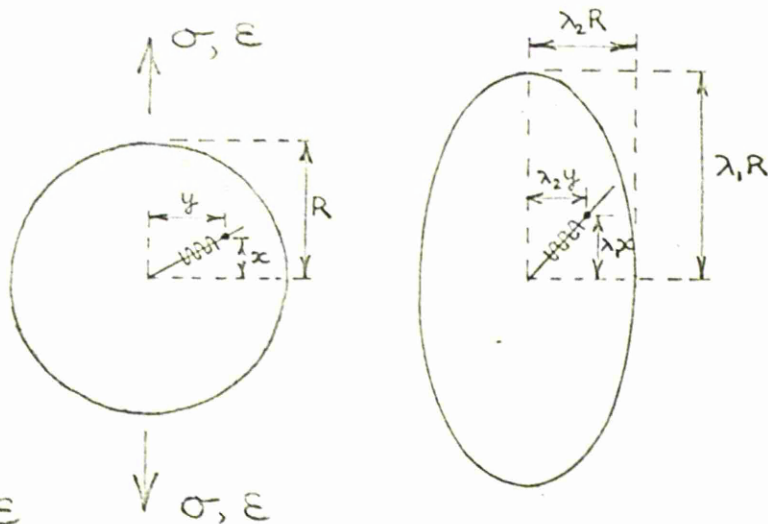


FIG. 1.7a

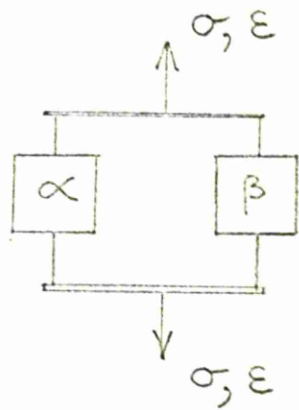


FIG. 1.7b

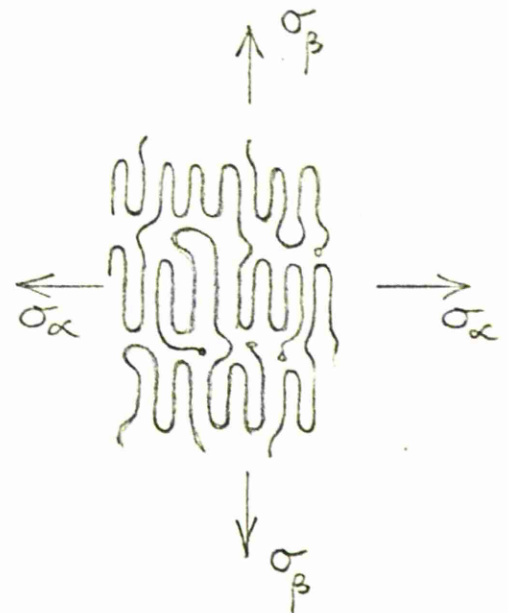
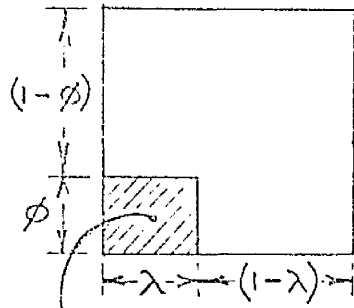
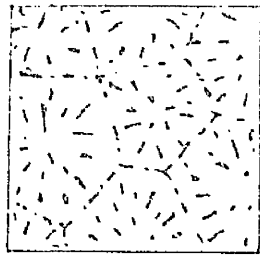
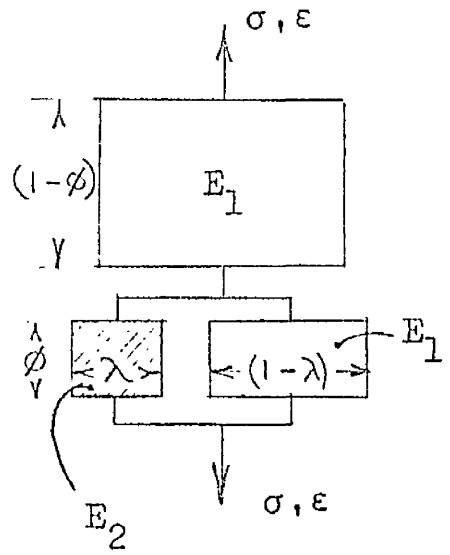


FIG. 1.7c

FIG. 1.8



amorphous phase



2. DEVELOPMENT OF APPARATUS FOR RECORDING COOLING RATE AND CRYSTALLISATION TEMPERATURE DURING MOULDING POLYPROPYLENE SHEETS.

2.1 Standard Compression Moulding Procedure.

The normal laboratory moulding procedure for producing a compression moulded sheet from polypropylene (PP) starting with granules of plastic is as follows. The granules are first made to coalesce by heating and shearing them with contra-rotating rollers into a "creped" sheet. Several of these "creped" sheets, sufficient to give the required thickness, are then trimmed to fit the moulding frame. Polished facing plates are placed either side of the plastic to give a good surface finish, and a light retaining pressure applied to the sandwiched system comprising a) plastic within a metal frame in the middle, with b) facing plates, and c) heating and cooling plattens at either side.

The plattens are brought to a temperature of about 200°C and held at this temperature for 5 minutes, whilst applying a light retaining pressure. This pressure is then built up over about 30 secs. in a series of stages or bumps to about 20 tons/in². This "breathing" process is designed to release any trapped air pockets. A further 2 mins. are spent at the platten temperature of 200°C ., to allow nominally complete melting, prior to flushing the cooling coils with an air/water mixture to bring the plastic to a handling temperature of about $30^{\circ} - 40^{\circ}\text{C}$. within about 10 mins., representing a cooling rate of approximately $15^{\circ}\text{C}/\text{min}$.

2.2 Experimental Moulding Apparatus

2.21 Technique and Apparatus for Recording Cooling Rate and Crystallisation Temperature during Moulding.

An early feasibility study was undertaken to find if the crystallisation temperature within a moulded polymer could be resolved by a thermocouple and continuous e.m.f. recorder. Iron/constantan thermocouples, chosen for the size of their e.m.f. response, were first embedded into 1in. diameter plugs of polypropylene (PP) which were moulded from granules in a laboratory mounting press. The e.m.f. from these thermocouples was displayed on a Kent Mk. III single channel continuous recorder. Tests at varying cooling rates from the melt confirmed that under suitable conditions the e.m.f. response gave a clear indication of the process of crystallisation.

The shape of the e.m.f. versus time trace showed that the exothermic process of crystallisation takes place over a temperature range of the order of 12°C ., a temperature range comparable with DTA results⁽⁶⁸⁾. During this period of resolvable crystallisation, a maximum in the exotherm exists, appearing as a plateau or inflection in the curve. The point at which this occurs corresponds to a peak in the exothermic curve of a DTA experiment and is the result of a maximum in the rate of crystallisation within the polymer. This point of maximum crystallisation rate was chosen as, and is hereafter defined as, the crystallisation temperature (T_c) for the moulded polymer.

For this crystallisation point to be clearly indicated the polymer had to be in intimate contact with the thermocouple. Due to the low thermal conductivity of polymeric materials, temperature gradients between the surface and

interior make it difficult to mould thick sections straight from granules without trapping air pockets. The design of a steel frame which would admit properly sheathed thermocouples into a moulded sheet made it necessary to have a frame thickness of 0.2 ins. Because of the necessity of prior shearing of the polymer nibs into "creped" sheets to obtain a homogeneous moulded sheet of plastic of this thickness, it was decided to eliminate the compacting problem by melting and remoulding ready-made sheets 0.25 ins. thick which were supplied by ICI (Hyde division).

PP sheets of this thickness could be remoulded down to the 0.2 ins. frame thickness, allowing for the excess material to (a) fill channels which were cut for the thermocouples, and (b) produce a slight flash of extrudate between the frame and facing sheets. The experimental arrangement is shown in Fig. 2.1.

The flash of extruded plastic acts as a seal for the retention of a pressure on the bulk of the sheet by the plattens. Fig. 2.2 shows the results of an inadequate pressure during moulding on a finished PP sheet in which gas has come out of solution from the polymer. Plastic was prevented from leaking through the thermocouple access holes by using a thicker refractory sheath inside the frame, which under pressure butted against the inside edge of the frame to make a pressure seal, see Fig. 2.3. The thicker sheath also served to support the thermocouple in the approximate centre of the sheet thickness.

A recommended temperature - pressure moulding cycle for these sheets was obtained by consultation with ICI (Plastics Division, Welwyn Garden City). This involved applying pressure during the melting cycle at the softening temperature of PP, which is at about 140°C ., and during the cooling cycle maintaining a moulding pressure of about 2 tons/in².

The lateral dimensions of the moulded sheet were chosen so that four tensile test pieces of a modified ASTM specification shape, as described in section 4.21, could be machined out. This, in conjunction with the requirement of admitting thermocouples into the sheet, determined the final moulded sheet dimensions of 8 ins. x 5 ins. x 0.2 ins. The lateral area of 40 in² of polymer meant a deadweight load of 80 tons was required to produce the recommended 2 tons/in² moulding pressure. These considerations led to the adoption of a 200 ton concrete press which, as is shown in Fig. 2.4, was easily adapted to mould thermoplastic sheets.

Two heating plattens were made to specification by Eltron Electric Elements Ltd., each comprising a 1 kilowatt heating element cast into an aluminium block measuring 11 ins. x 8 ins. x 1 in. A variac was used to control the voltage supply to the heating plattens.

Two cooling plattens of the same dimensions were each made in two parts to permit the machining of cooling channels, and were bolted together with a copper gasket and sealing paste to prevent leakage. The shape of the cooling channels was chosen to produce as uniform a cooling rate across the platten face as possible, and in operation the plattens were arranged so that a contra flow of coolant was applied at either side of the moulded sheet, as shown in Fig. 2.5. It was found that this arrangement, together with a device for distributing coolant at equal rates to both plattens, see section 2.24, produced fairly uniform cooling rates across the plastic sheet. A strict definition of the cooling rate during moulding is given in section 2.41.

Variation in the cooling rate was achieved by -

- a) inserting heat shields of sindanyo, steel, or the heating platten itself, between the cooling plattens and the plastic ;
- b) varying the rate of flow of coolant, and sometimes simultaneously adjusting the voltage to the heating plattens ;
- c) using water or compressed air as the coolant ;
- d) lowering the voltage to the heating plattens by hand .

To measure discrepancies in cooling rate and resulting T_c across each 8 ins. x 5 ins. sheet, three thermocouples were inserted into the positions shown in Fig. 2.9 which form part of a grid matrix within the frame.

2.22 Calibration and Errors in the Temperature Measuring System.

To obtain sufficient accuracy in converting from the e.m.f. of the iron/constantan thermocouples as recorded on the Kent recorder into temperatures, the thermocouple wire was calibrated and the Kent recorder's accuracy and resolution were checked.

Calibration of the thermocouple wire was carried out against an NPL calibrated ^{platinum} resistance thermometer. Three thermocouples, from the same reel of wire, were tested simultaneously using an 'ice in water' cold junction as a zero degree centigrade reference. The greatest difference between e.m.f. readings of these thermocouples was found to be equal to .01 mV. This was taken to be representative of the error which was assumed to hold for the remainder of the wire which was taken from the same reel throughout this work.

The Kent recorder was made to read the e.m.f. supplied to a Tinsley Vernier Potentiometer, which showed that over the selection of mV ranges used, the poorest agreement was

in error by .005 mV, whilst the resolution of the instrument appeared to be .001 mV.

Accumulating the errors from the thermocouple calibration and the recorder made the greatest possible error equal to ± 0.015 mV. Assuming the approximation that for Iron/constantan 1 mV corresponds to 20.0°C throughout its range, (an approximation which will slightly over-estimate the error at temperatures in the range where crystallisation takes place in PP), the temperatures recorded in this way may be in overall error by $\pm 0.3^{\circ}\text{C}$.

2.23 Moulding Procedure.

The thermocouple wires were first threaded through the frame, sheathed, and spot welded in situ; the other end of these wires was taken via an 'ice in water' cold junction to a three way switch and then connected to a mobile Kent recorder.

The as-received plastic sheet was trimmed to fit into the frame and had three channels cut into it to take the thermocouples. Facing plates of polished aluminium were placed either side of the sheet which was then inserted between the selected arrangement of cooling and heating plattens. A light retaining pressure equal to $1/10$ ton/in² (4 tons on the ram) was applied to the plastic during heating until the plastic reached 140°C at which the pressure was built up to 1.5 tons/in² (60 tons on the ram). Heating was continued until the plastic reached 240°C ., a procedure which was found to produce the required thoroughness of melting, see section 2.32.

Before starting the selected cooling procedure the ram load was raised to 80 tons and held at this value during cooling. This was adopted as a standard procedure for producing a nominal pressure on the plastic sheet of 2 tons/in².

The actual pressure on the plastic sheet is imprecise, since it depends on the surface area of extrudate which also supports the ram load. However, this pressure was taken to be virtually constant from one moulding to another.

Throughout this moulding cycle the e.m.f. from the thermocouples was tracked on the Kent continuous recorder. During the cooling cycle a chart speed was selected which would best indicate the crystallisation point according to cooling rate, and a careful tracking of the response of all three thermocouples was made. After each moulding the thermocouples and sheaths were left embedded in the plastic and the wires had to be cut and new thermocouples made up as before for the next moulding. A completed moulded sheet with thermocouples embedded ~~is~~ shown in Fig. 2.6. ✓

2.24 Evaluation of Apparatus.

Before proceeding with the main experimental programme, a few moulding runs were carried out at various cooling rates to test the performance of the apparatus.

At slow cooling rates, using compressed air for the coolant, a very uniform cooling was obtained and a variation in crystallisation temperature of not more than 0.5°C was measured across the sheet. The resultant sheet was also perfectly flat.

At the fastest cooling rates, in which the cooling blocks were immediate to the plastic and water coolant at the fastest rate was used, large discrepancies in cooling rate ($73^{\circ}\text{C}/\text{min}$ to $102^{\circ}\text{C}/\text{min}$) and resultant T_c (114.7°C to 110.3°C) were recorded. The resultant sheet was also seriously distorted to an extent which would have made 'uniaxial' tensile testing of the finished tensile piece meaningless. ✓

Microscopy of a fast-cooled sheet showed a marked

asymmetry in the distribution of spherulite size through the thickness direction of the sheet, as would result from a considerable difference in the cooling rate applied at either face of the sheet. This would induce an asymmetric density distribution through the thickness direction, which would result in the distorted shape of the sheet.

A simple device, shown in Fig. 2.7, was therefore designed to distribute coolant at equal rates to either side of the sheet. The resulting improvement in the flatness of quench-cooled sheets is shown in Fig. 2.8.

Where cooling was faster than about $40^{\circ}\text{C}/\text{min}$. a small degree of distortion in the moulding sheet was an unavoidable consequence of using faster cooling rates than are recommended for thermoplastic sheets of 0.2 ins. thickness; a normal injection moulding would typically limit cooling rates for this thickness to about $25^{\circ}\text{C}/\text{min}$.

The thickness of the sheets was, therefore, not a completely independent variable in determining the effects of cooling rate in the mould on subsequent mechanical properties for comparisons on a general basis, but was a factor predetermined by the requirement for facilitating the repeated induction of thermocouples through the moulding frame.

There is a limit, for example, to how fast the interior of a thick sheet can be cooled, which is determined by the early solidification and insulating qualities of the sheet faces. Allowance for this was made in this moulding apparatus by recording the cooling rate as it occurred within the central zone of the sheet, rather than by relating it to the cooling rate of the plattens themselves. Once, therefore, the sheet faces are machined off, the structure remaining should be typical of the recorded cooling rate applied at the plattens to a thinner section of material. This does not, however, remove the consequences of quench cooling a

thick section in relation to slight distortions, as can still be seen in Fig. 2.8.

The limit to which machining-off of faces was taken was dictated by (a) its usefulness in reducing the T_c spread in the remaining thickness of material to a level no more than is expected in the lateral direction of the sheet, and (b) the dangers of concentrating too much 'work heat' into the material during machining. These aspects are dealt with more fully in the section 4.2. which deals with the scatter in thermal history on each tensile test piece.

These preliminary experiments showed that the limit of cooling rate obtainable at the centre of the sheet with this apparatus was of the order of $150^{\circ}\text{C}/\text{min}$.

The presence of the three thermocouples was desirable in order to have a record of the distribution of thermal history applied to each sheet in the lateral direction, and enabled a fairly accurate interpolation for each tensile test piece where this was necessary. A typical record and interpolation is shown in Fig. 2.9 for one of the fastest cooled sheets.

2.3 Choice of Melt Conditions

The selection of a suitable melt treatment which will eliminate all traces of prior crystalline structure is an important consideration in any detailed study of the effects of thermal history on structure and mechanical properties in polymeric material.

2.31 Theoretical Aspects.

The most important parameters determining a polymer's morphology and degree of crystallinity are the overall nucleation rate \dot{N} , and the spherulite growth rate G . Mandelkern⁽¹⁰⁵⁾ has shown that the isothermal process of crystallisation of homopolymers in bulk can, with certain assumptions which do not affect the present discussion, be expressed by the equation,

$$\ln \left(\frac{X_{\infty} - X_t}{X_{\infty}} \right) = - \frac{\pi}{3} \cdot \frac{1}{X_w} \cdot \frac{\rho_c}{\rho_l} \cdot \dot{N} \cdot G^3 \cdot t^4 \quad (1)$$

- where, X_t = the crystallised fraction at time t ,
 X_{∞} = the equilibrium crystalline fraction,
 X_w = the mass fraction of the system which eventually becomes transformed,
 ρ_l, ρ_c = the densities of the polymeric liquid and completely crystalline polymer, respectively,
 \dot{N} = the nucleation rate,
 G = the crystallisation growth rate.

The right hand side of this equation has the form $-k_s t^n$, in which k_s is a crystallisation rate constant which embodies the nucleation rate and growth rate terms, and n is an integer.

$$k_s = \left(\frac{\pi}{3} \cdot \frac{1}{X_w} \cdot \frac{\rho_c}{\rho_l} \right) \dot{N} \cdot G^3$$

An illustration of the relative temperature dependence of the homogeneous nucleation rate and the spherulite growth rate for PP is shown in Fig. 2.10.

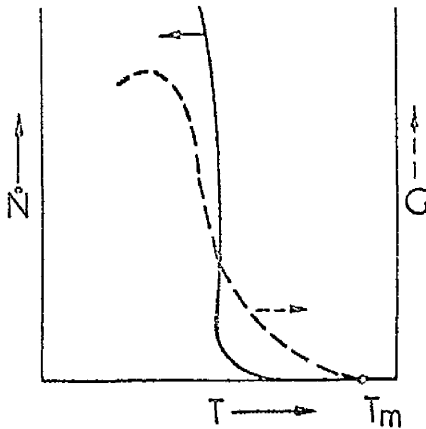


FIG. 2.10

Any unmelted crystalline embryos which remain during cooling a polymer from the melt become seeds for heterogeneous nucleation⁽³⁵⁾. The presence of an increased number of heterogeneous nuclei tends to increase the overall nucleation rate whilst the spherulite growth rate is relatively unchanged⁽⁶⁸⁾⁽³³⁾.

This has the effect of moving the nucleation rate curve further to the right of the spherulitic growth rate curve, thus increasing the crystallisation rate constant k_s at any chosen temperature.

For moulded polymer sheets to be consistent on a comparative basis it would be sufficient to produce the same melt conditions for each moulding run.

There are, however, slight variations in the heating time within the polymer sheet according to variations in the thermal mass of material between the heating plattens and the polymer, this being a requirement of the procedure for varying the cooling rate. This produces a variable melt treatment liable to leave the molten polymer with a different content of unmelted crystalline embryos, and hence produce sheets of differing nucleation rate not necessarily associated with the cooling rate and T_c . Thus any correlation of the final structural or mechanical properties against the cooling rate, T_c , or density would also represent a function of

melt conditions and prior thermal history.

In view of these considerations and the hope to utilise typical kinetic crystallisation data from the literature for predicting the T_c following various cooling rates, it was required to produce a similar melt having the minimum of heterogeneous nuclei.

2.32 Procedure for Finding True Melt Conditions.

The effect of the density of heterogeneous nuclei on the crystallisation rate provides a fairly straightforward test capable of determining^a melt condition which is sufficient to melt out all the crystalline material without proceeding to a stage of thermal or oxidation degradation, the products of which will again increase the content of heterogeneous nuclei.

This test involves systematically varying the melt conditions and either measuring the crystallisation temperature T_c following a standard cooling rate, usually on DTA apparatus⁽³⁴⁾; or calculating the crystallisation rate constant k_s , following isothermal crystallisation at a standard temperature, from either DTA⁽¹⁰⁶⁾ or dilatometry tests⁽¹⁰⁷⁾⁽¹⁰⁸⁾. The minimum value of either T_c or k_s corresponds to the optimum melting conditions. Detailed studies have been made to find these melt conditions in PP⁽³⁴⁾⁽¹⁰⁶⁻¹⁰⁸⁾, but results differ markedly, e.g. Griffith and Rånby⁽¹⁰⁹⁾ find a melt temperature of 180°C held for 20 mins. is adequate, whilst Marker et al.⁽¹⁰⁷⁾ find a melt temperature of 190°C held for 30 mins. is inadequate; it must be concluded that factors such as steric regularity, stabilizing and antioxidant additives, as well as molecular weight (MW) and polydispersity (M_w/M_n) are playing an active part⁽¹¹⁰⁾.

In choosing a melt condition for the moulding procedure in this research two factors had to be considered:

i) Melting is carried out at a moulding pressure of approximately 1.5 tons/in²(= 229 atmospheres) which will call for a more thorough melt treatment than in the literature references quoted above.

ii) The upper temperature should be limited by considerations of thermal and oxidation degradation.

Research by Davis, Tobias and Peterli⁽¹¹¹⁾ has shown that negligible thermal degradation in PP proceeds at a temperature of 250°C held for a time far in excess of normal melting times. Falkai⁽³³⁾ has found that unstabilised PP suffered negligible change in MW following heating for 30 mins. at 200°C. On the basis of these results a maximum melt temperature of 240°C was chosen for the stabilised PP sample used in this research and two moulding runs were completed to test if this produced the required melt condition. Both tests were made in the slow cooling range where compressed air coolant could be used to obtain repeatable cooling rates, their temperature - time curves in the melt are shown in Fig. 2.11. The first moulding (A) was made a typical one approximating to the minimum melt procedure encountered in the moulding programme. In the second moulding (B), the polymer was held at 250°C for 15 mins., a melt procedure far in excess of the maximum in the moulding programme. The results are shown in table 2.1 over and shown in Fig. 2.12 designated as test B. They show that the normal melt procedure used in the production of PP sheets was adequate, whilst the procedure used in sheet (B) demonstrated slight signs of contamination by degraded products.

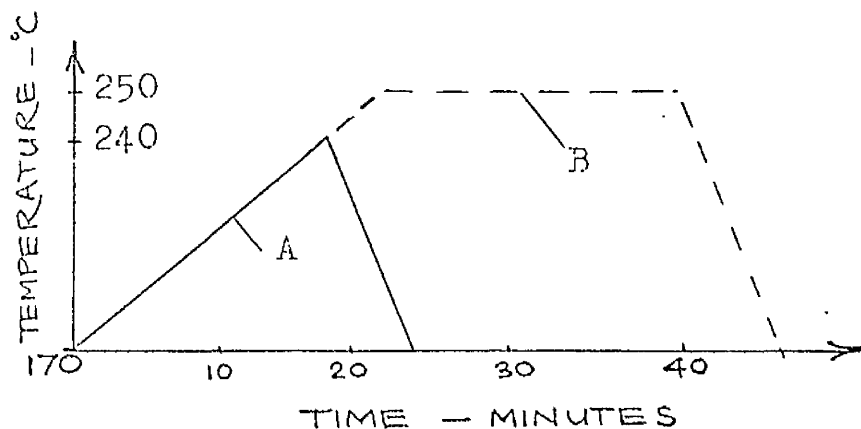


FIG. 2.11

SHEET	Average Cooling Rate °C/min.	Average T _c
A	9.3	121.0
B	10.5	121.5

Table 2.1

A further cause of abnormal crystallisation is the presence of cracks and flow lines which act as inhomogeneities and produce a type of line nucleation (112)(113) (11). Examples of this were found to occur in moulded plugs of PP where melt conditions (= 210°C for 30 secs.) were inadequate to produce coalescence between granules, see section 5.24. Since during the softening stages of the sheet, there is a flow close to the thermocouple due to the collapse of the sheet to fill the channels made for the thermocouples, it must be concluded that this source of heterogeneous nucleation is also eliminated by the standard melting procedure. This was later confirmed by microscopy of sections taken very close to thermocouples.

2.4 Results for Crystallisation Temperature versus Cooling Rate. Fig. 2.12.

2.4.1 A Strict Definition of Cooling Rate.

The cooling rate C was selected as a tangent to the temperature - time curve at the melting point T_m of the polymer at nominal moulding pressure of 2 tons/in². The approximate T_m at this pressure was arrived at by taking the T_m as found during the heating cycle (heating rate \approx 5°C/min) from the latent heat exchange point, and adjusting this value (= 168°C) as shown below to allow for the pressure of 2 tons/in² used during the cooling cycle. This adjustment was assessed from the data of Beer and Kardos⁽³⁸⁾ on the effect of pressure on the T_m of homopolymers, to be 2°C, making $T_m = 170^\circ\text{C}$ at 2 tons/in².

It is likely that the value of 168°C is below the equilibrium melting temperature, since this should be considered to be representative of the corresponding temperature for the hypothetically perfect macroscopic crystal. The assignment of T_m for a given polymer therefore requires that the fusion process be carried out very slowly so that the most perfectly ordered crystalline structures are developed. This condition did not prevail during the heating cycle of a moulding run. Since a range of T_m values are quoted for PP from 149°C for low MW material⁽³¹⁾, up to 189°C for well annealed samples⁽⁴⁰⁾, or even higher⁽⁴¹⁾, and since the value of $T_m = 170^\circ\text{C}$ is not accurate, it seemed undesirable to relate the T_c found in these experiments to a degree of supercooling (= $T_m - T_c$). It is shown in section 2.5 that the value of T_c predicted from typical crystallisation data for PP was relatively insensitive to quite large changes in the choice of T_m . An optimum heating rate for T_m

determination in PP would appear to be about $1^{\circ}\text{C}/\text{min}$.
(114) Since cooling rates in this temperature ^{range} were almost linear, cooling rates were defined as a tangent to the temperature - time curve at 170°C .

2.42 Assessment of Errors in T_c and Cooling Rate.

The errors in the measurement of temperature using iron/constantan thermocouples and the Kent recorder have already been discussed in section 2.15, where it was concluded that the maximum error in temperature measurement was $\pm 0.3^{\circ}\text{C}$.

In slow-cooled sheets, where the maximum in the rate of crystallisation produces a well defined plateau in the e.m.f. - time curve, the accuracy of determination of T_c is the same as that of the temperature measuring system. However, at faster cooling rates, greater than about $20^{\circ}\text{C}/\text{min}$., this plateau tended to become more of an inflection despite the use of faster recording speeds. This represents a significant change in the 'dwell time' during crystallisation and is discussed in section 3.5. At the fastest cooling rates possible with this apparatus, a resolution error for T_c of $\pm 0.5^{\circ}\text{C}$ made the overall error in T_c in this zone $\pm 0.8^{\circ}\text{C}$.

The effect on T_c of any slight variation in moulding pressure due to the variable area of extrudate was shown to be completely negligible in the light of the experiment in section 2.56 in which a sheet was moulded at a greatly reduced pressure.

In the fastest cooled sheets an increase in the cooling rate was observed shortly before the crystallisation point, see Fig. 2.13, ^{over}making it difficult to decide at which point to measure the cooling rate responsible for the observed T_c .

This was only seen in those sheets where cooling was achieved by passing water coolant at the maximum rate through the cooling coils, when these were separated from the polymer by the minimum thermal barrier equal to 0.25ins. of aluminium. In particular, since this irregularity in cooling rate was not found when compressed air was the coolant with the cooling coils in the same position; it was concluded that the effect was due to the initial conversion of water coolant to steam during the first 30 secs. of cooling changing to a more efficient single phase water cooling when the exit temperature fell below 100°C . Where a greater thermal barrier of metal was present between the cooling platten and the polymer, this effect could not be detected within the polymer.

In view of the indecisive cooling rate in the most rapid range, it was chosen to retain the cooling rate as defined at 170°C as that responsible for crystallisation throughout this programme.

It is suggested that these sources of error combined to produce the greater scatter in the results shown towards faster cooling rates, in Fig. 2.12.

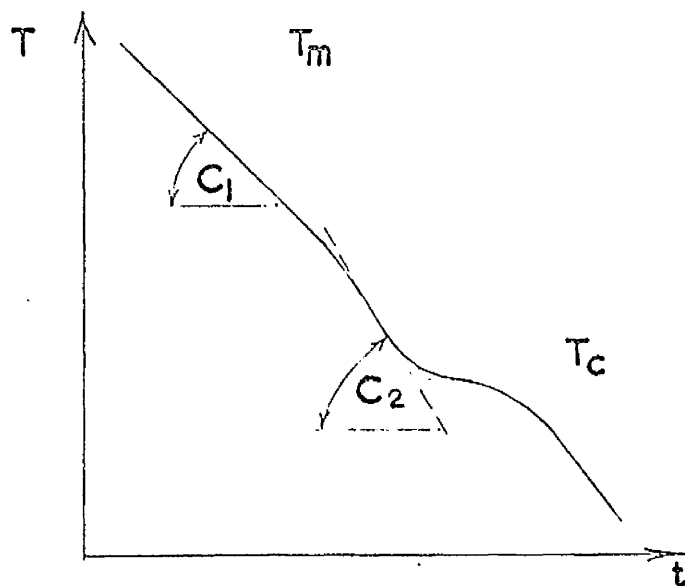


FIG. 2.13

2.5 Theoretical Prediction of the Crystallisation Temperature as a result of varying the Cooling Rate from the Melt

2.51 Introduction to the Theoretical Concept.

In general the isothermal crystallisation of bulk polymers has been found to fit the following type of relationship proposed by Avrami⁽¹¹⁵⁾ for the kinetics of phase change for a random distribution of nuclei.

$$X_t = X_\infty \left[1 - \exp (-k_s t^n) \right] \text{-----}(2)$$

where X_t = the crystallised fraction at time t ,
 X_∞ = the equilibrium crystalline fraction,
 k_s = a rate constant which depends on the nucleation rate and growth rate,
 n = a constant, the value of which depends on the type of nucleation and growth mechanism as shown in table 2.2 below.

TABLE 2.2

<u>Growth</u>	<u>Homogeneous Nucleation</u>	<u>Heterogeneous Nucleation</u>
three-dimensional	4	$3 \leq n \leq 4$
two-dimensional	3	$2 \leq n \leq 3$
one-dimensional	2	$1 \leq n \leq 2$

This equation is a more general form of equation (1) already mentioned in section 2.31, in that it can describe the progress of any of the crystallisation mechanisms in a temperature and time range where the characteristic kinetics of phase change remain the same. The assumption of an isokinetic range makes the exponent n a constant, as stated

above, independent of temperature and time, whilst k_s remains a function of temperature alone.

The prediction of T_c , as defined throughout this work, during a constant cooling rate obtains from an extrapolation of the Avrami equation (2) to a condition of monotonic change in temperature, and the calculation of the time at which a maximum occurs in the crystallisation rate. This is a valid procedure if isokinetic conditions are assumed to prevail during the temperature and time field covered during the stages of cooling prior to the T_c .

2.52 The Value of the Avrami Exponent n and the Crystallisation Rate Constant k_s for polypropylene.

Polypropylene is generally found to be a well-behaved polymer for the simple application for the Avrami equation. This can be seen from the bulk of the results for the isothermal crystallisation kinetics of PP (117) (116) (107) (33) (116) (117) which support the requirement of an isokinetic zone which spans the temperature range of 121.5°C to 156.0°C for which readings are available. A temperature-dependent change in kinetics has, however, been reported by Magill (116) to occur at about 115°C . This change, which is within the T_c range covered by these experiments, was neglected for the purposes of a prediction of T_c during constant cooling principally because of doubt as to the precise kinetics of crystallisation at these relatively low temperatures. For example, Magill plots his data with values of n equal to 2.0 and 4.0 with no apparent reduction in the scatter of values for $\log k_s$ versus T .

Recently, Hoshino et al (58) have reported that the Avrami exponent n for PP is also time dependent as a result of the onset of secondary crystallisation. They find that the primary spherulitic growth process is describable by

by an Avrami equation with $n = 3.9$. Secondary crystallisation is also describable by an Avrami equation with $n = 1.8$. According to Keith and Padden⁽²²⁾, the former is a process of growth of primary radial fibers to form spherulites, the latter is one of crystallisation of the material between radial fibers. Hoshino et al.'s work also indicates that polymer samples of different tacticity are likely to have changes in n due to the effect of tacticity on the ratio of primary to secondary growth process.

Thus, although the value of n has been shown to be substantially independent of temperature and time (where measurements are commonly for the early stages of crystallisation) the precise value of n found varies between 2.5 and 4.0 with the most commonly quoted value equal to 3; as would, according to the findings of Hoshino et al., befit the earlier stages of crystallisation. It is obvious that this variation in values reflects principally the possibility of differing amounts of inherent heterogeneous nuclei, the development of mixed crystallisation kinetics coupled with variations in sample tacticity, and also the difficulty of determining the best values of the dependent variables k_s and n because of the insensitivity of the plot of

$$\ln \left[\ln \left(\frac{X_\infty - X_t}{X_\infty} \right) \right] \quad \text{versus } \ln t$$

normally used to find n .

Aside from considerations of the type of crystallisation mechanism (i.e. the value assigned n), there is evidence that the size and distribution of molecular weight influence the rate of crystallisation i.e. k_s . It has^{generally} been found that the rate of crystallisation in PP increases with increase in molecular weight (MW) (118)(106)(34). However,

other results⁽¹¹⁰⁾ show a tendency to decrease the rate of crystallisation as MW is raised, while polydispersity (M_w/M_n) is unchanged. A decrease in crystallisation rate with increase in MW has also been found for poly-ethylene⁽⁶¹⁾. Other available data for PP⁽¹⁰⁹⁾⁽¹⁰⁷⁾ see table 2.3, shows no clear tendency for the dependence of crystallisation rate on MW. These results suggest the dominance of one or other of the effects of kinetic or thermodynamic motivation; the former of which would predict that crystallisation rate decreases as MW is increased due to the action of entanglements, whilst the latter would predict the opposite due to the effects of the number of chain ends on the concentration of crystallisable species.

The results for $\log k_s$ versus temperature available from the literature are shown in Fig. 2.14 and are tabulated with other relevant data in table 2.3.* In all cases but one,⁽¹¹⁶⁾ the data published was in a tabulated form which enabled the fitting of a 'least-squares' straight line by a standard curve fitting computer programme. A general similarity in results can be seen in Fig. 2.14. and has been commented on by Limbert and Baer⁽¹¹⁹⁾, who have also observed the surprising degree of similarity in the results of various investigations on PP even where samples used were of quite different origin.

2.53 The Temperature Dependence of $\log k_s$.

A review of crystallisation kinetics for polymers by Mandelkern⁽¹⁰⁵⁾ shows that for a surface nucleation and two dimensional growth mechanism,

$$\log k_s = \text{'constant'} - c_1 \frac{T_m}{T(T_m - T)} \quad (3)$$

* see Appendix II and beside Fig. 2.14

whilst for a three-dimensional nucleation and growth mechanism,

$$\log k_s = \text{'constant'} - c_2 \frac{T_m^2}{T(T_m - T)^2} \quad (4)$$

where c_1 and c_2 are constants, T_m is the equilibrium melting point, and T is the crystallisation temperature. The 'constant' in equations (3) and (4) has the form $(A - B/T)$ where A and B are constants. Falkai⁽³³⁾ has shown that variations in $\frac{B}{T}$ are negligible compared with variations in the second temperature dependent term in the normal crystallisation temperature range for PP.

e.g. for $122 < T_c < 145^\circ\text{C}$,
 B/T varies by a factor 1.07

$c_1 T_m / T(T_m - T)$ varies by a factor 1.8

Therefore to a first approximation the expression $(A - \frac{B}{T})$ behaves as a constant in this range of temperatures. Thus by a plot of $\log k_s$ (or $\log \dot{N}$ or $\log G$) versus $\frac{T_m}{T(T_m - T)}$ and $\frac{T_m}{T(T_m - T)^2}$, it might be expected that the better correlation and hence the dominant crystallisation mechanism would show up as a better straight line fit to experimentally determined data.

This procedure suffers the disadvantage that the resulting plots are very sensitive to the value assigned T_m . This situation is complicated by the change in apparent M.P. accompanying changes in crystallisation temperature (119)(33). Falkai has shown that the amount of supercooling based on this variable M.P. predicts a better temperature dependence for $\log G$ as in equations (3) and (4) than the assumption of a constant equilibrium T_m .

Other attempts at delineating the dominant crystallisation mechanism for PP⁽⁵⁸⁾ based on a constant value of T_m , show no clear graphical preference of fit for the alternative mechanisms.

A more detailed analysis was therefore undertaken, using the data of Falkai, to calculate a comparative value for the correlation of $\log k_s$ plotted against a base of

(i) $\frac{T_m}{T(T_m - T)}$ and (ii) $\frac{T_m}{T(T_m - T)^2}$

and to compare this with the correlation against (iii) T . The latter has the advantage of not specifying T_m .

A non-dimensional correlation coefficient was calculated to measure the goodness of fit between the experimental data and a 'least-squares' straight line fitted to the data using a standard curve fitting computer programme.

A suitable correlation coefficient is⁽¹²⁰⁾

$$r = \frac{\sum [(x - \bar{x})(y - \bar{y})]}{\sqrt{\sum (x - \bar{x})^2 \sum (y - \bar{y})^2}}$$

in which,

$(x - \bar{x})$ = the distance between the data point and the 'best fit' linear relationship in the X-direction

$(y - \bar{y})$ = the same distance in the Y-direction.

When the value of r is unity, there is a perfect linear relationship between the variables x and y ; and when zero, there is no linear relationship between the variables.

The following results for the dependence of $\log k_s$ on the various functions of temperature were obtained,

(i) $\log k_s$ as a function of $\frac{T_m}{T(T_m - T)}$ $r = 1.0000$

(ii) $\log k_s$ as a function of $\frac{T_m^2}{T(T_m - T)^2}$ $r = 1.0000$

(iii) $\log k_s$ as a function of T $r = 0.9999$

It therefore appears that both a two dimensional and three dimensional nucleation and growth mechanism is equally favoured for this data. This fact may explain the most commonly found Avrami exponent equal to 3.0 which is the only value common to both a two and three dimensional growth mechanism, see Table 2.2.

Result (iii) shows that the commonly used presentation of $\log k_s$ as being linearly dependent on T is reasonable, and this simplified type of dependence, which does not require the specification of T_m , was used in the following section 2.54

2.54. Theory and Results derived from Typical Kinetic Data.

The assumption that isokinetic conditions prevail during the temperature and time field covered during the stages of cooling prior to T_c in the Avrami equation (2) means that,

- a) the exponent n equals a constant
- b) k_s remains a function of temperature alone

$$X_t = X_{\infty} \left[1 - \exp(-k_s t^n) \right] \quad \text{_____} (2)$$

This assumption and the assumption that $\log k_s$ is well represented by a linear function of temperature (T) enables the definition of the crystallisation rate-temperature relationship by the equation

$$\log k_s = A - m(T - 110) \quad \text{_____} (5)$$

where A is the intercept at an arbitrarily chosen temperature = 110°C , and m is the gradient of the $\log k_s - T$ line, as illustrated in Fig. 2.15., over.

Assuming that the cooling rate c applied to the polymer is linear, which neglects the effect of crystallisation on latent heat exchange as shown in Fig. 2.16., the temperature-time dependence during moulding becomes

$$T = \bar{T} - ct \quad \text{-----} (6)$$

where \bar{T} is an approximate value for the equilibrium T_m .

Substituting equation (6) into (5) gives,

$$\log k_s = A - m [(\bar{T} - 110) - ct]$$

i.e. $k_s = \exp \left\{ 2.303A - 2.303m [(\bar{T} - 110) - ct] \right\}$ ----- (7)

Equation (7) represents the time dependence of k_s for the particular cooling cycle applied to the polymer.

The rate of crystallisation at any time t , from equation (2), becomes

$$\frac{dX}{dt} = X_{\infty} \exp(-k_s t^n) \left[t^n \frac{dk_s}{dt} + k_s n t^{n-1} \right] \quad \text{-----} (8a)$$

where, from equation (7)

$$\frac{dk_s}{dt} = 2.303 m c k_s \quad \text{-----} (8b)$$

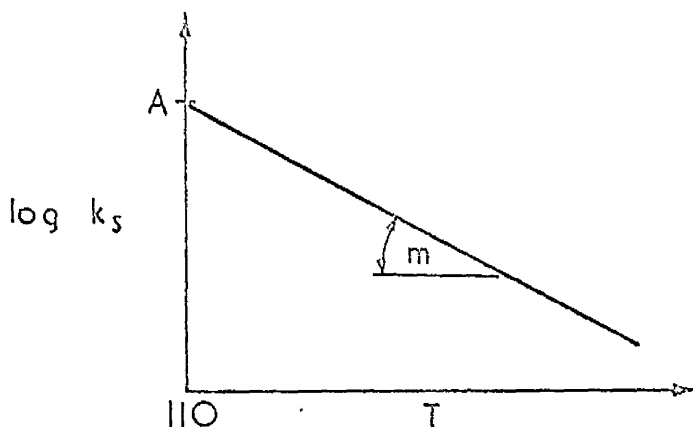


Fig. 2.15

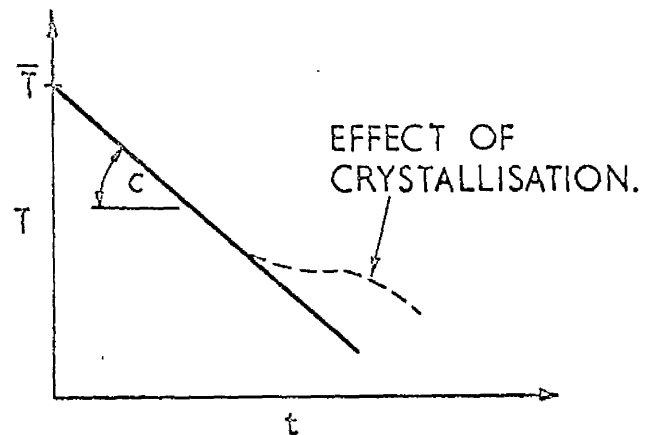


Fig. 2.16

Differentiating (8a) again gives,

$$\frac{d^2 X_t}{dt^2} = X_\infty \exp(-k_s t^n) \left[t^n \frac{d^2 k_s}{dt^2} + 2nt^{n-1} \frac{dk_s}{dt} + k_s n(n-1)t^{n-2} - 2k_s n t^{2n-1} \frac{dk_s}{dt} - t^{2n} \left(\frac{dk_s}{dt} \right)^2 - k_s^2 n^2 t^{2n-2} \right] \quad (9a)$$

where, from equation (7)

$$\frac{d^2 k_s}{dt^2} = (2.303 \text{ mc})^2 k_s \quad (9b)$$

The turning points in the value of $\frac{dX_t}{dt}$ are given when $\frac{d^2 X_t}{dt^2} = 0$,

this occurs when

- i) $X_\infty \exp(-k_s t^n) = 0$, i.e. when $t \rightarrow \infty$
- ii) $k_s = 0$, i.e. when $t \rightarrow -\infty$

(unreal solution)

iii) when $t = 0$

The values of $\left(\frac{dX_t}{dt}\right)$ at $t = 0$ and $t = \infty$ must be minimum ones by simple reasoning, and hence for X_t to be a continuous function, there should exist a third real root for the RHS. of (9a) corresponding to a maximum in the crystallisation rate.

A computer programme was written to find the second real root \bar{t} (the other real root being $t = 0$) for the equation ,

$$t^n \frac{d^2 k_s}{dt^2} + 2nt^{n-1} \frac{dk_s}{dt} + k_s n(n-1)t^{n-2} - 2k_s n t^{2n-1} \frac{dk_s}{dt} - t^{2n} \left(\frac{dk_s}{dt} \right)^2 - k_s^2 n^2 t^{2n-2} = 0$$

where $k_s = \exp \left\{ 2.303A - 2.303 n \left[(\bar{T} - 110) - ct \right] \right\}$

This requires the specification of values for the constants n , A , m , \bar{T} and c . The first three constants define the kinetics of crystallisation and values for these are shown against their respective authors in Table 2.3. The last two constants define the moulding conditions.

Having found \bar{t} , which equals the time at which $\frac{dXt}{dt}$ is a maximum, T_c is arrived at by using equation (6),

$$T_c = \bar{T} - c\bar{t} \quad \text{-----} \quad (6a)$$

A graphical representation of the dependence of the quantities $\frac{dXt}{dt}$, c , and t is shown in Fig. 2.17.

Some theoretically derived results for T_c versus cooling rate, as found for the typical kinetic data for PP are shown as full lines in Fig. 2.12. In all these curves the value taken for \bar{T} was 170°C , which was the reasonable estimate for the T_m of the experimental PP at the moulding pressure used in this programme. Since this value of \bar{T} is likely to differ from the equilibrium T_m for the PP types used in table 2.3* it became necessary to find what effect variations in \bar{T} have on the value of T_c .

The influence of the value given \bar{T} on the curve for T_c versus cooling rate was tested for the data of Marker et al. It was found that varying \bar{T} between 165°C and 185°C changed the T_c at any chosen cooling rate by a maximum of 1.6°C ., see Fig. 2.12. It was thus shown that this procedure for predicting T_c is relatively insensitive to the value chosen for the T_m of the polymer.

* see Appendix II and beside Fig. 2.12.

2.55 Discussion of Theoretical Results.

1. The shape of all the curves predicted by the foregoing theory agrees very well with the trend of the experimentally determined points. The kinetic data which predicts the best fit is that of Marker et al⁽¹⁰⁷⁾ This can be explained on the grounds that

- a) the PP type used by Marker et al is very similar to the one used in this work⁽¹²¹⁾
- b) Marker et al give results which show that their kinetic data are practically unaltered in the range of melt index (MI) 1.05 to 0.11 which covers the MI of 0.3 for this experimental material.
- c) Very similar melt conditions were used.

It should be noted that the additional kinetic results of Falkai⁽³³⁾ given in Table 2.3,* where more thorough melting conditions were used, predict a $\log k_s - T$ line, (shown as a dashed line in Fig. 2.14), very close to that of Marker et al.

The other kinetic results give poorer agreement probably because of the factors sited in section 2.52.

2. There is a general agreement between the T_c versus cooling rate results derived from kinetic data at atmospheric pressure and the experimental results which are for a nominal pressure of 2tons/in². The conclusions drawn from this result are stated and expanded in section 2.56.

3. The general agreement between theory and experiment justifies the assumptions of an isokinetic zone in which the temperature dependence of k_s is described by a straight line on a $\log k_s - T$ plot; in particular these results show

* see Appendix II

that any change of kinetics that might occur does not make the theoretical agreement on this basis any less accurate.

4. This procedure for predicting T_c does not rely on accurate data for the equilibrium T_m of the polymer, e.g. an estimate of T_m to within $\pm 5^\circ\text{C}$ is capable of predicting T_c to within $\pm 0.4^\circ\text{C}$.

2.56 A note on the Effect of Pressure on the Crystallisation Temperature.

One of the features noted from the general agreement between theory and experiment is the apparent applicability of kinetic data at a nominally atmospheric pressure to the kinetics of phase change at a nominal pressure of 2tons/in² (305 atmospheres).

Since there is a paucity of results for the dependence of T_c on cooling rate it seemed worthwhile to carry out a single test to elucidate the effect of pressure on these results. A sheet was therefore moulded using a reduced nominal pressure of $\frac{1}{2}$ ton/in² (76 atmospheres) during the cooling cycle. The results for this sheet, designated as test 'C', are shown on Fig. 2.12 with the rest of the results, and are given in Table 2.4. Again a slow cooling was chosen in order that differences would not be masked by larger experimental errors.

TABLE 2.4

<u>Nominal Pressure During Crystallisation (ATM)</u>	<u>Cooling Rate °C/min.</u>	<u>T_c °C/min</u>
305	10.5	120.5 (a)
76	10.5	119.3
1 (b)	10.5	108.5 (c)

- (a) taken from a mean curve fitted to the data at slow cooling rates.
- (b) pressure within the capsule of a DTA instrument.
- (c) read from the graph of Beck and Ledbetter.⁽⁶⁸⁾

The conclusions drawn from the applicability of the appropriate kinetic data at atmospheric pressure to the dose prediction of results for T_c at 305 atmospheres and the very small fall in T_c caused by the above change in moulding pressure are that

- a) Within the resolution of this test the kinetics of crystallisation for PP are practically unaffected by pressure on an absolute temperature scale.
- b) their dependence on the degree of supercooling ($T_m - T_c$) is ^{however} shifted in a direction and by an amount approximately equal to the effect of pressure on the equilibrium T_m .

This conclusion means that the slight fall in T_c recorded in the above test should be deducible from a knowledge of the effect of pressure on T_m for PP, and the subsequent small effect of changes in T_m on the value of T_c predicted from the typical kinetic data at atmospheric pressure.

The results of Baer and Kardos⁽³⁸⁾ show a drop in T_m of about $12^{0+} 1^{\circ}\text{C}$ for the change in pressure 305 atmospheres to 76 atmospheres for PP. Using the results for the effect of \bar{T} on T_c this change in T_m would produce a fall in T_c equal to 1°C . which compares well with the fall of 1.2°C . found for this reduced pressure moulding.

The only other results which were found giving the T_c versus cooling rate for PP at atmospheric pressure are those of Beck and Ledbetter. As can be seen in Fig. 2.12 their curve covers only a limited range of cooling rates and

has a level much lower than the results of this work. This difference is not explicable on the grounds of a pressure effect alone and it is concluded that their PP sample must have a particularly low $\log k_s - T$ curve.

2.6 Conclusions

1) This moulding programme showed that for this PP a change in cooling rate from $1.2^{\circ}\text{C}/\text{min.}$ to $140^{\circ}\text{C}/\text{min.}$ produced an overall change in crystallisation temperature of 17.3°C. It is necessary, therefore, if meaningful results are to be obtained, to use an accurate apparatus for measuring temperatures and cooling rates, such as was developed in this programme for recording the thermal history of moulded PP sheets.

2) It is possible to predict the variation of T_c with cooling rate for a crystalline polymer where a simple isokinetic application of the Avrami equation is possible, by using the appropriate data for the crystallisation rate constant and its dependence on temperature. Where accurate predictions are to be made from available kinetic data taken from other work, great care should be taken to observe the compatibility of materials, melt, and moulding conditions. The effect of moulding pressure on T_c can be calculated.

This important extension of the Avrami equation would also enable the effects of nucleating agents or melt conditions on T_c during constant cooling to be predicted where their influence on isothermal crystallisation kinetics is known.

3) Any change in crystallisation kinetics within the temperature - time field covered by these results for PP does not produce an observable change in the trend of the experimental results for T_c versus cooling rate; nor does it vitiate the agreement in trend obtained by assuming an isokinetic application of the Avrami equation covering the same temperature - time field.

It follows, therefore, that where crystallisation rate data is available in a limited temperature range a good agreement with experimental results is still obtained in

the case of PP by extrapolating into the T_c range covered by the faster cooling rates.

4) Within the resolution of this test, it appears that the sole effect of pressure on the crystallisation kinetics of PP is to shift their dependence on the degree of supercooling ($T_m - T_c$) in a direction and by an amount approximately equal to the effect of pressure on the equilibrium T_m .

5) Values calculated for the correlation of $\log k_s$ as a function of $\frac{T_m}{T_m(T_m - T)}$ and $\frac{T_m^2}{T_m(T_m - T)^2}$ fail to discern

the preferred crystallisation mechanism for one of the most complete sets of kinetic data found for PP. This is consistent with the proposal that the commonly found value of Avrami exponent equal to 3, represents the results of an observation of both primary and secondary crystallisation processes by most authors during isothermal crystallisation studies. A value of 3 was present in the kinetic results which gave the best prediction for T_c versus cooling rate for the PP used in this work.

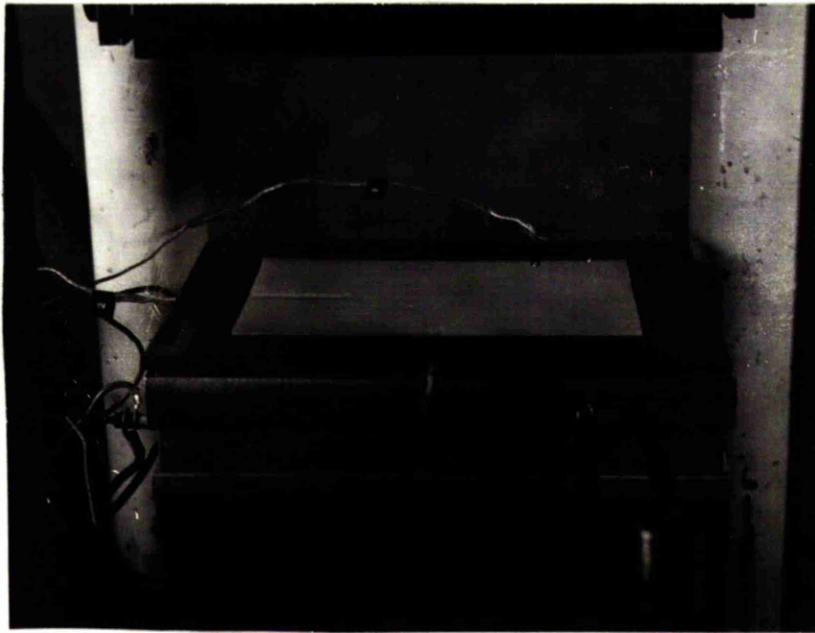


FIG. 2.1

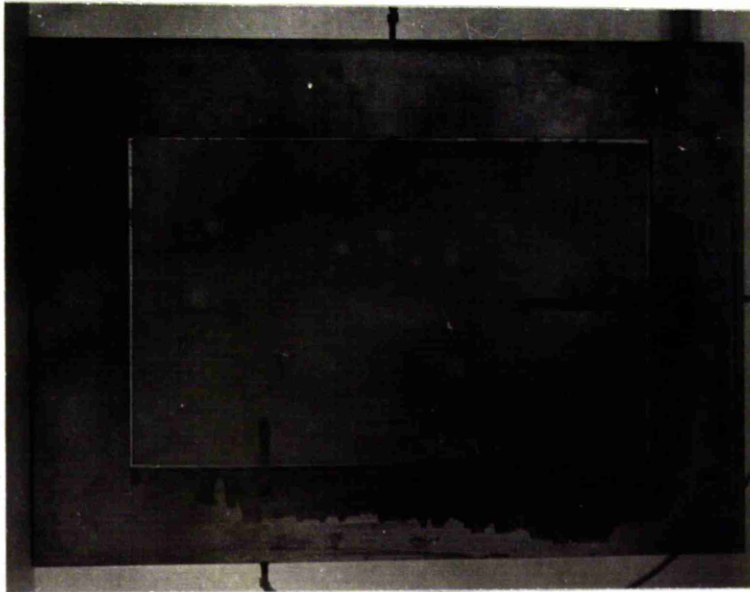
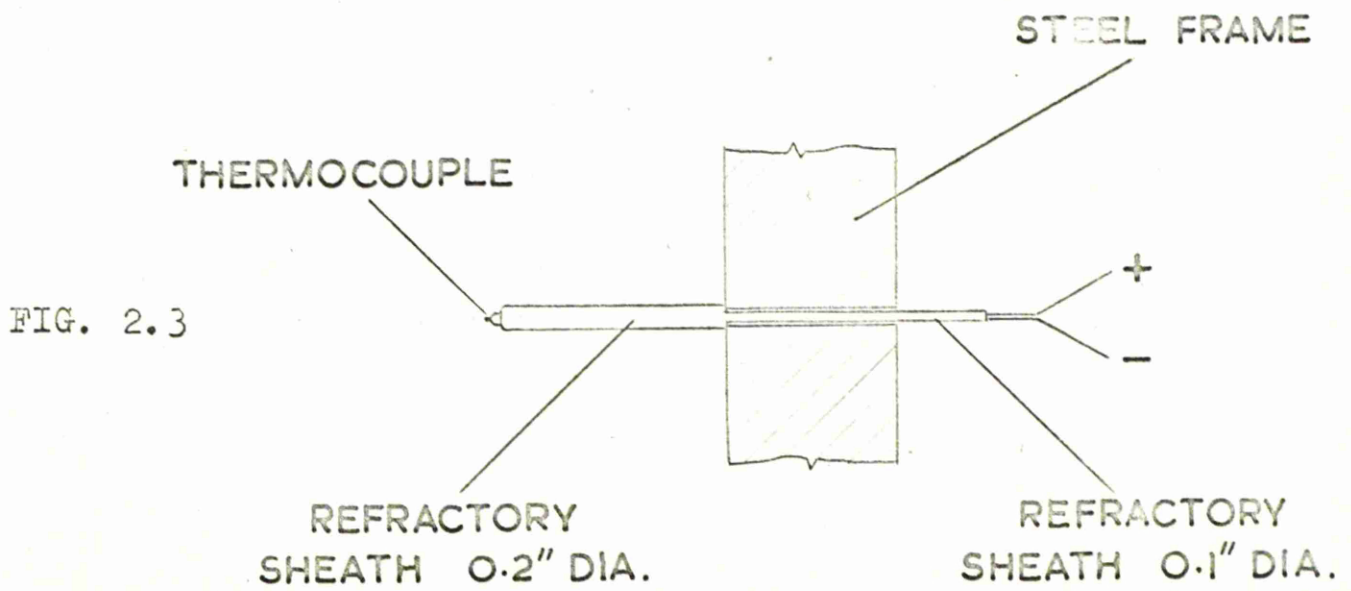


FIG. 2.2



FIGS. 2.4, 2.5

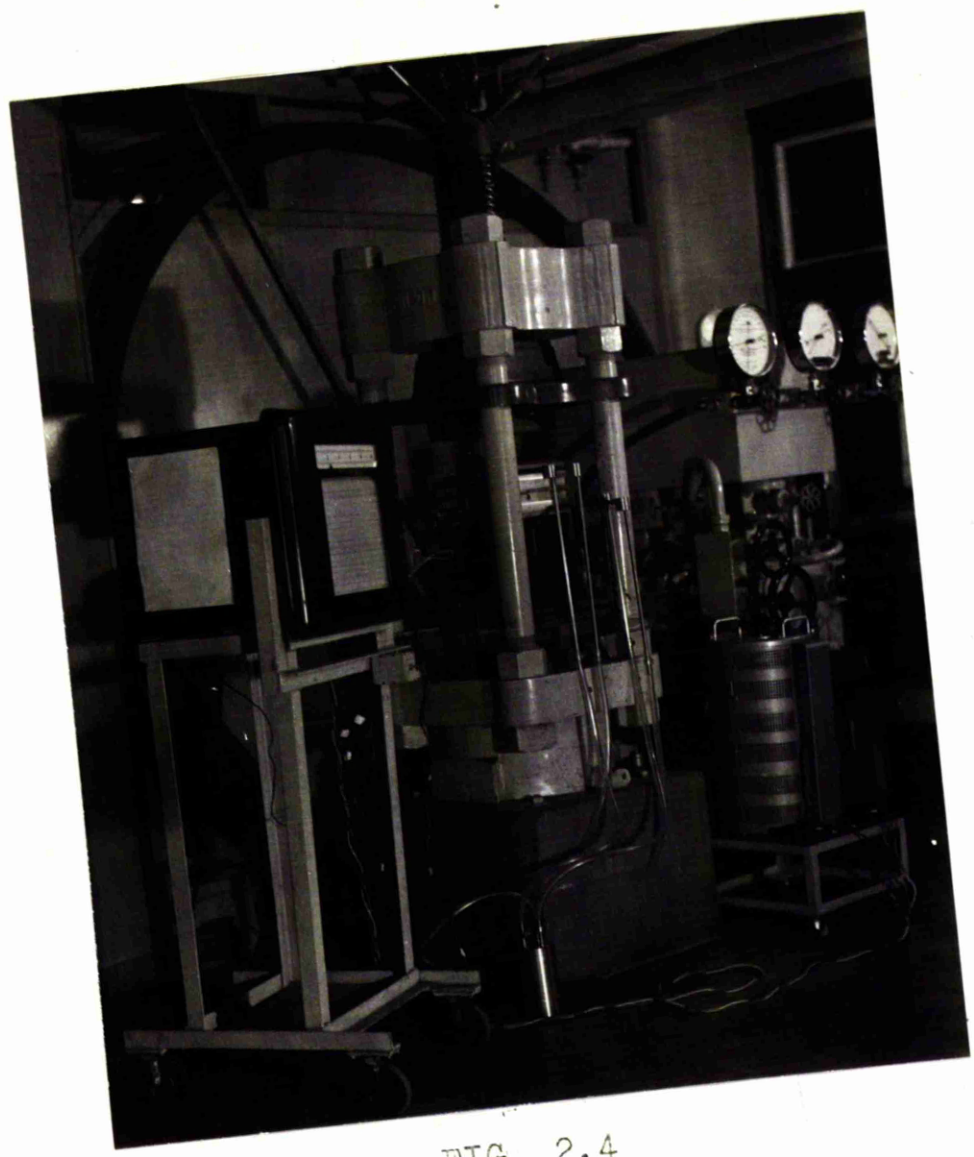


FIG. 2.4

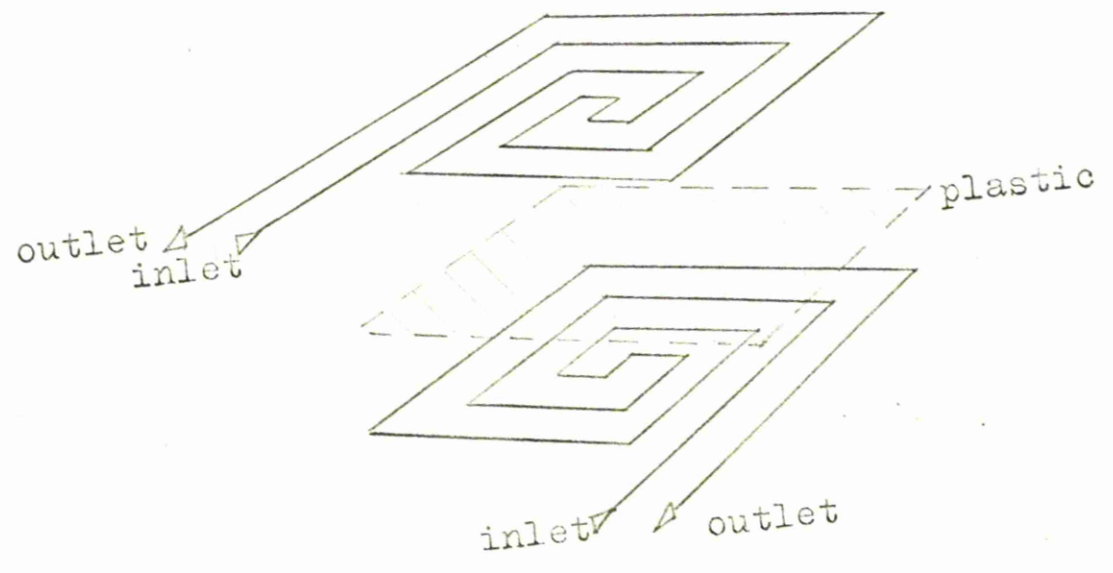


FIG. 2.5

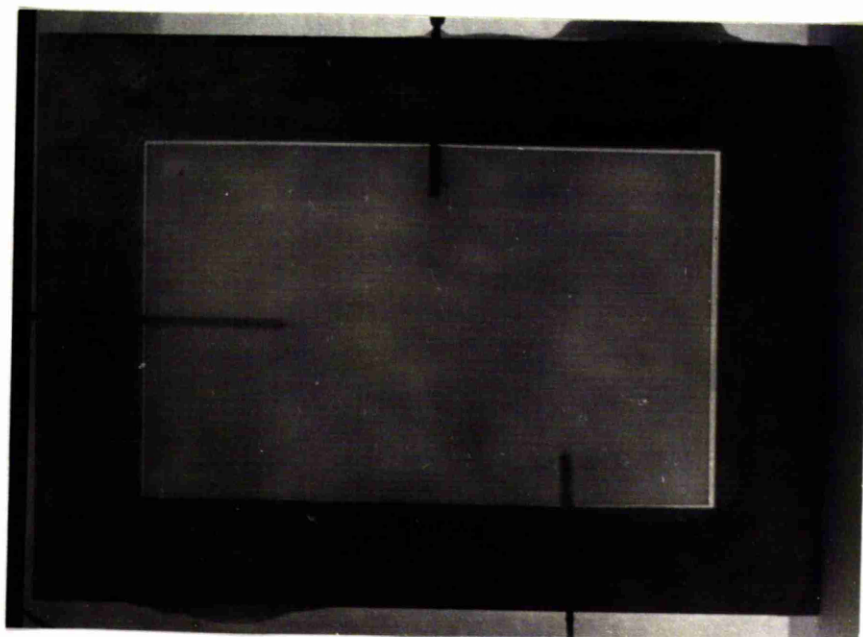


FIG. 2.6

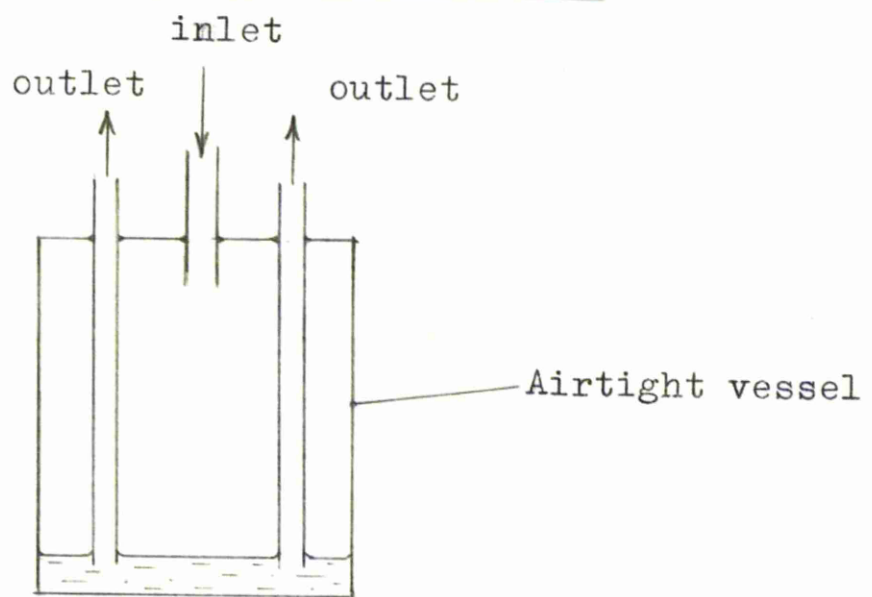
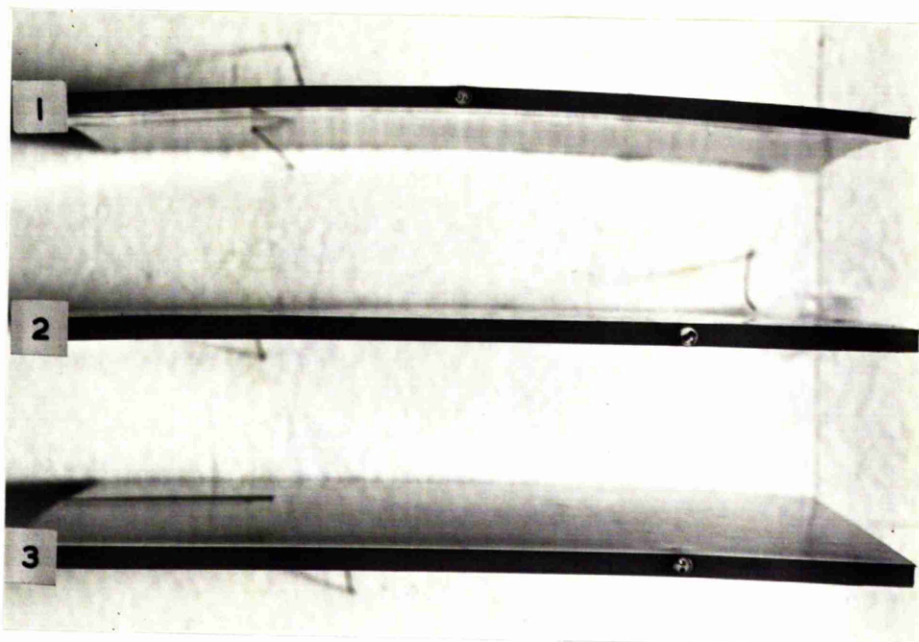


FIG. 2.7



- 1) Prior to using coolant distribution device in Fig. 2.7 $C=70^{\circ}\text{C}/\text{min}$.
- 2) After using coolant distribution device in Fig. 2.7 $C=100^{\circ}\text{C}/\text{min}$
- 3) " $C=40^{\circ}\text{C}/\text{min}$.

FIG. 2.8

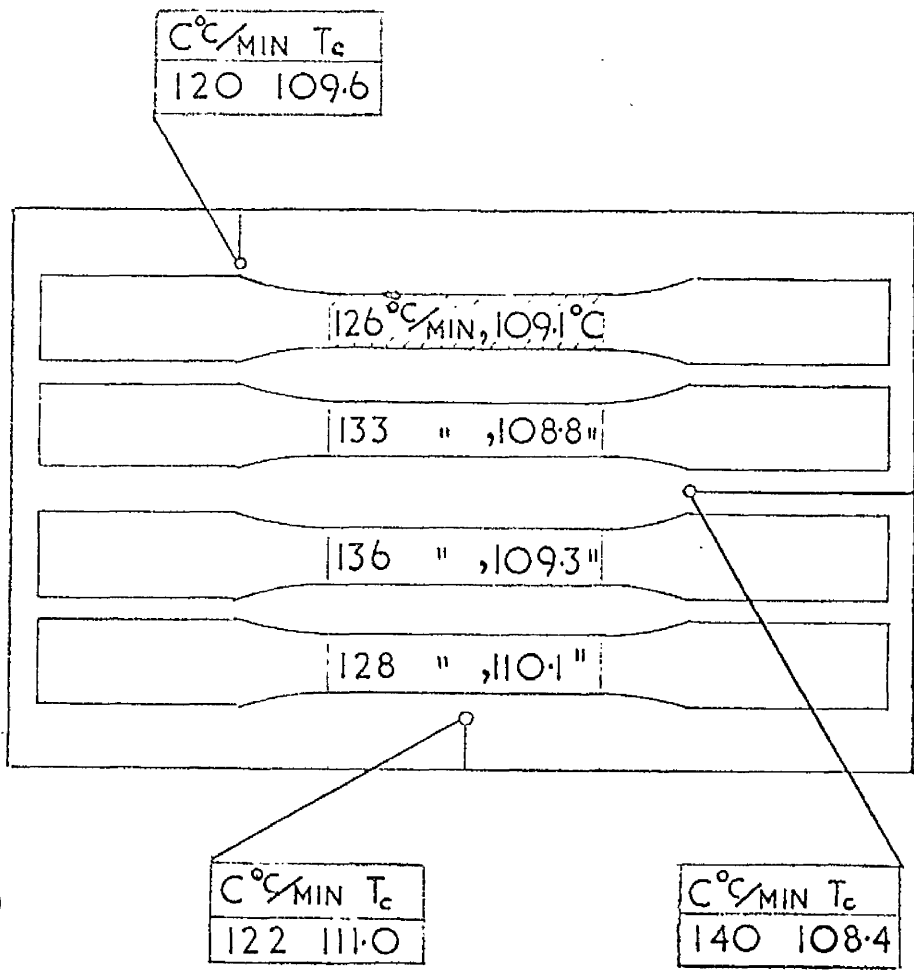


FIG 2.9

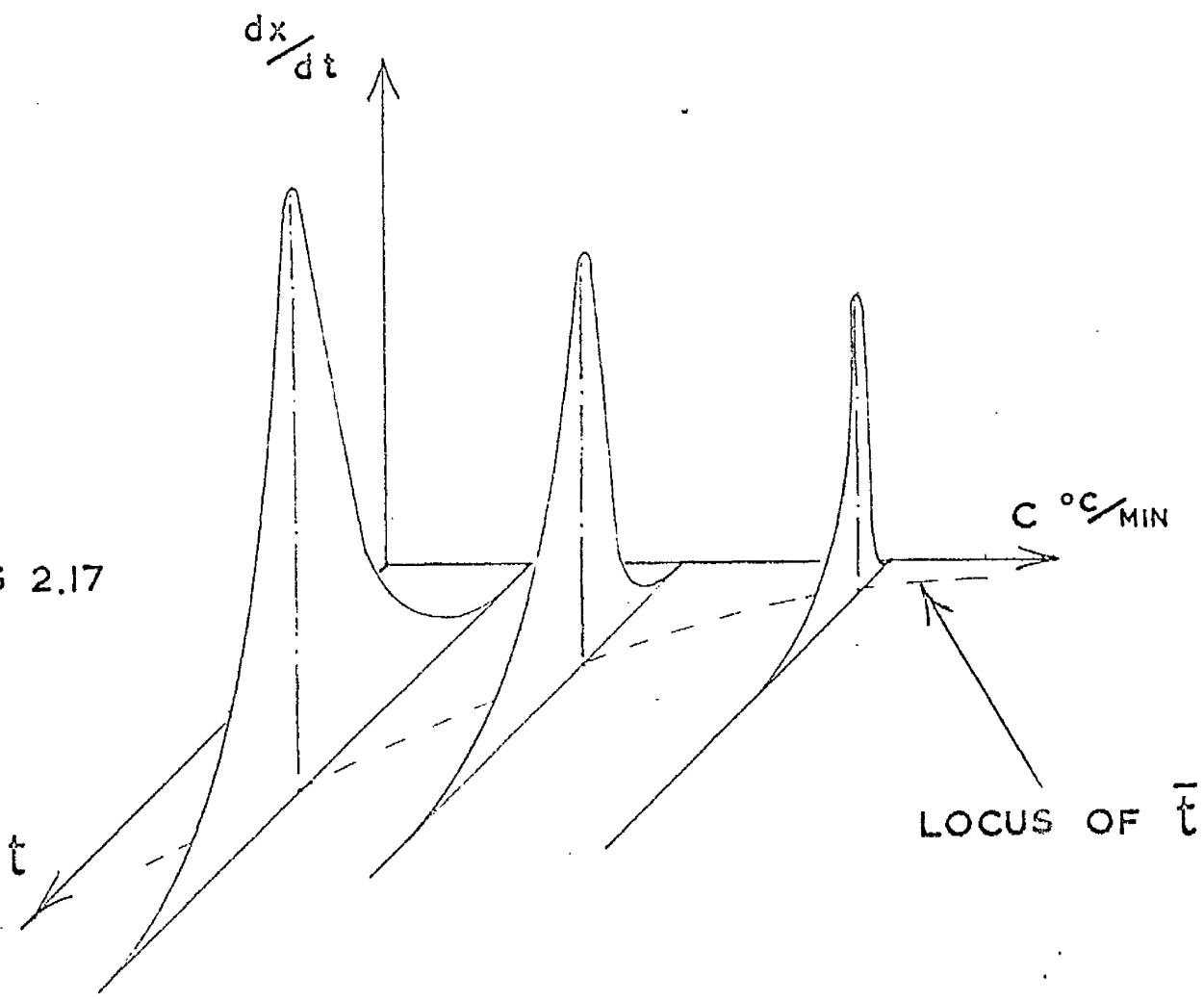


FIG 2.17

AUTHORS	CURVE	n	A	M	MOLECULAR WT.	MELT CONDITION
GRIFFITH, RANBY REF. 109	1A	3.0	6.322	.362	$M_n = 5.05 \times 10^4$	T = 190°C FOR ~20 MIN.
	1B	"	9.307	.544	$= 9.70 \times 10^4$	
	1C	"	5.614	.354	$= 3.08 \times 10^5$	
MARKER, HAY, TILLEY, EARLY, SWEETING. REF. 107	4	3.0	1.824	.305	MI = 1.05 (a)	T = 220°C FOR ~30 MIN.
	3A	3.0	2.030	.276	$M_n = 5.1 \times 10^4$	INCOMPLETE MELTING AT T = 180°C, FOR 15 MIN. MORE THOROUGH MELTING AT T = 200°C, FOR 15 MIN.
FALKAI REF. 33	3B	GRAPHICAL FIT TO TWO DATA POINTS (d)				
MAGILL REF. 116	5	3.0	4.1(b)	.36(b)	$M_w = 1.96 \times 10^5$	T = 270°C FOR 30 MIN.
	2	2.5	2.665	.271 (c)	$M_n \approx 4.13 \times 10^5$	NOT SPECIFIED
GORDON, HILLIER REF. 117						

a) other single values of k at $T=136.0^\circ\text{C}$ show very little variation with molecular weight as measured by MI. (melt index).

MI	1.05	0.45	0.11
Log k_s	-6.14	-5.86	-6.10

b) from graphical data

c) fitted to data in the temperature range 134.1 to 140.2°C.

d) single values of $\log k_s$ are given following this more thorough melt condition

T	130	140
Log k_s	-4.20	-6.96

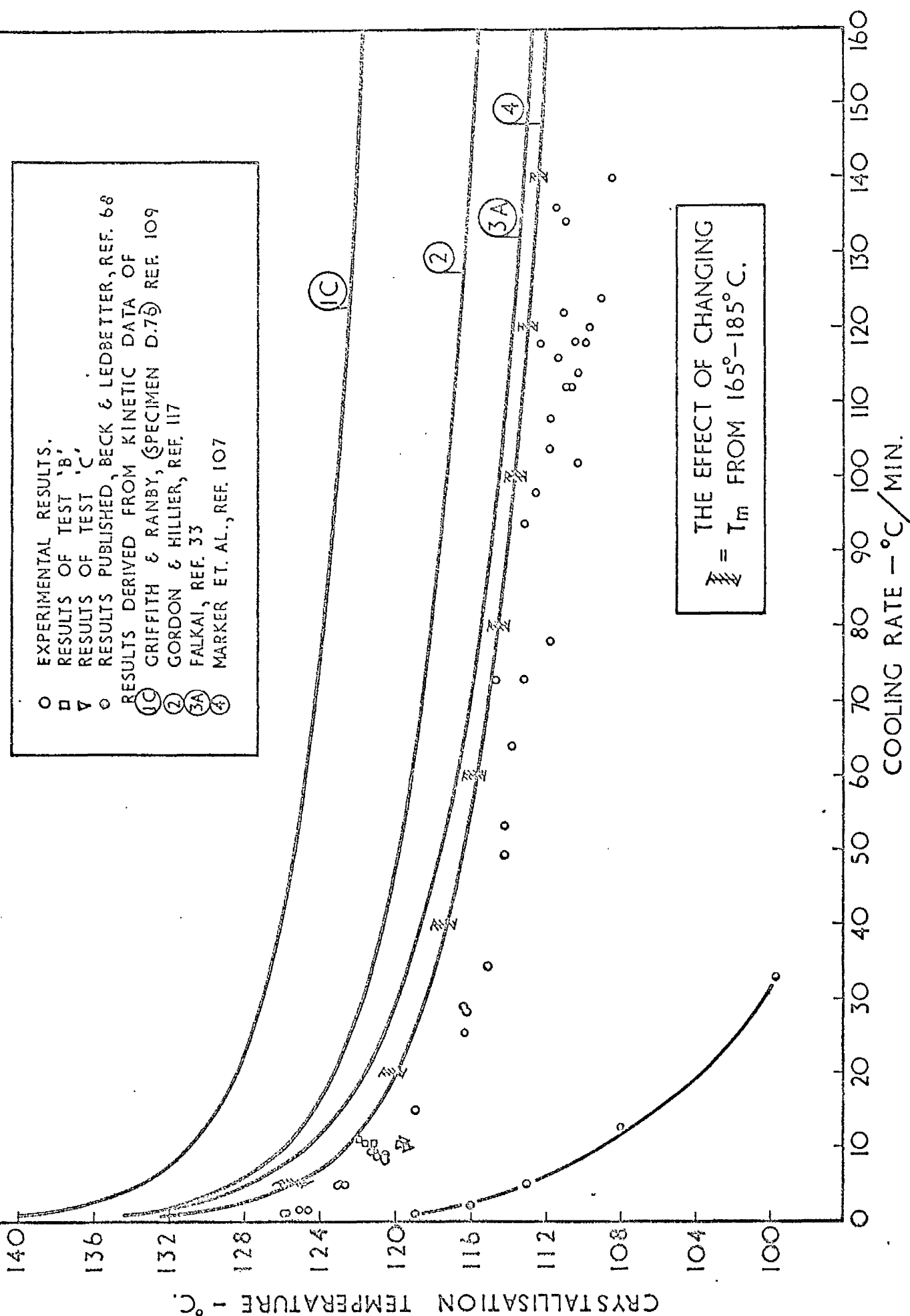


FIG. 2.12. THE EFFECT OF COOLING RATE ON CRYSTALLISATION TEMPERATURE.

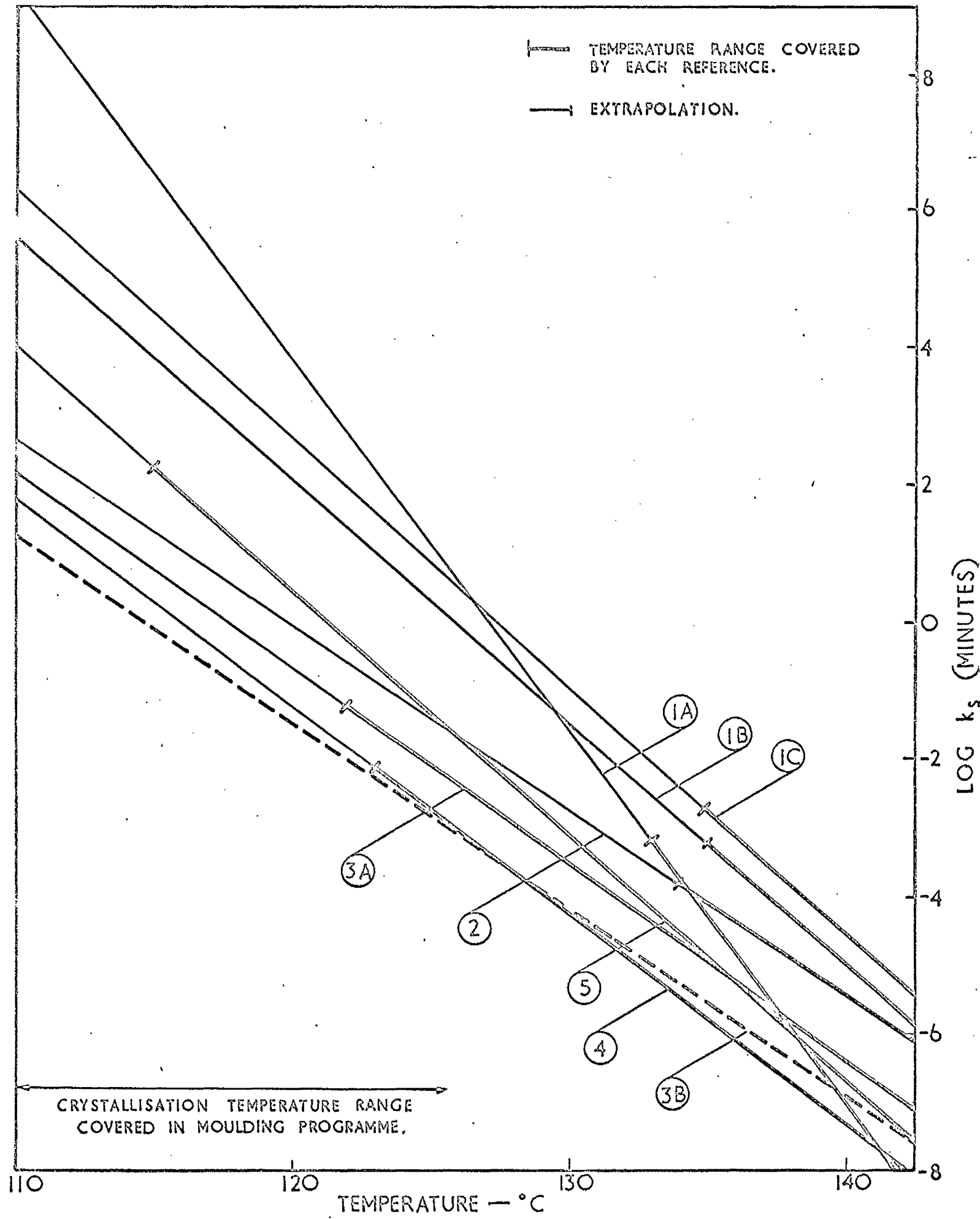


FIG.2.14. VALUES OF LOG k_s VERSUS CRYSTALLISATION TEMPERATURE, TAKEN FROM THE LITERATURE.

3. THE EFFECT OF MOULDING CONDITIONS ON THE STRUCTURE OF POLYPROPYLENE.

In chapter 2 the method of preparing compression moulded sheets of PP of known cooling rate and crystallisation temperature (T_c) was described.

This chapter describes the observations made on the spherulitic structure and density of samples taken from the above sheets.

3.1. The Structure of Polypropylene Spherulites.

Polypropylene is unusual, though not unique, in its ability to grow more than one kind of spherulite. Four distinct types have been identified and are characterised as follows:

type I, consists of monoclinic crystals, has weak positive birefringence*, grows below about 134°C , and melts at 168°C .

type II, consists of monoclinic crystals, has weak negative birefringence, grows above about 138°C , and melts at 168°C .

type III, consists of hexagonal crystals, has strong negative birefringence, appears to be able to grow sporadically throughout the normal crystallisation temperature range but is reported⁽¹⁷⁾ to be favoured by rapid cooling rates, melts at about 150°C .

type IV, consists of hexagonal crystals, has a banded appearance, grows sporadically in the range $128^{\circ} - 132^{\circ}\text{C}$, and melts at about 150°C .

* birefringence $= n_r - n_t$ where n_r and n_t are the radial and tangential refractive indices

A recently published examination by Padden and Keith⁽¹⁸⁾ of the detailed structure of the most common spherulite types I, II suggests that the radiating fibrils which can be seen in the optical microscope comprise 'fronds' which have the growth habit described below and shown in Fig. 3.1.

- a) 'radially directed leader lamellae' made up of chain folded molecules, and having the a-axis orientated radially, grow out into the melt until they impinge on similar lamellae from neighbouring spherulites,
- b) primary branched lamellae grow outward from and over the radial leader lamellae almost simultaneously and have an orientation almost at right angles to the parent lamellae, their c-axis making an angle of about 90° with that of their parent lamellae,
- c) a very few secondary lamellae having the same orientation as the radial leaders may grow on the primary branched lamellae.

This morphology means that the molecular chain (c-axis) is orientated both tangentially as in units (a) and (c), and approximately radially as in unit (b).

As was pointed out in section 1.1, a more strictly defined morphology of these structures is not possible at present because of the different values found for the angle made by the molecular chains with the radius in type I,II spherulites. No detailed knowledge of the growth habit of type III or IV spherulites is known to the author except that these appear to have a simplified morphology, similar to PE spherulites, in that they comprise purely radiating lamellae⁽¹⁷⁾⁽⁹⁾ having the molecular chain (c-axis) tangential and with the possibility of cooperative twisting along a

radius. They may easily be distinguished from the normal type I, II spherulites by their bright appearance, see Fig. 3.2. .

3.2 Microscopy of Samples with varying T_c .

Direct observation of the structure of the samples was limited to the optical microscope. For this work the equipment used was a Leitz base sledge microtome and a Vickers projection microscope.

Liquid nitrogen was used as an aid to microtoming. The lightly scored film surfaces of specimens microtomed for observation were optically occluded by oiling to a glass slide with dimethyl phthalate ($n^{20} = 1.515$), the refractive index of PP has been reported⁽¹⁷⁾ to be 1.510. The structure was then viewed through crossed polarised light.

Changes in the cooling rate through the thickness direction of these fairly thick plastic sheets inevitably complicates observations of a typical structure. Observation of spherulite size and type was therefore made only near the sheet centre which should approximate to the position of the thermocouple head which was supported by its refractory sheath in this position.

3.21 Spherulite Size

Spherulite diameters were measured on a selected range of samples in two orthogonal directions to eliminate the influence of any strain induced orientation from either moulding or microtoming. The results are given as the mean of ten measurements on each sample against respective values of T_c in table 3.1/^{over} and are shown together with the scatter in measured diameters in Fig. 3.3.

TABLE 3.1

<u>T_c</u> <u>(°C)</u>	<u>Mean</u> <u>Spherulite</u> <u>Dia. (cm) x 10²</u>
110.3	.220
113.1	.303
113.7	.326
116.1	.438
118.9	.615
120.5	.836
121.6	.979
123.0	1.071
125.7	1.172

A scatter in the measured diameters follows from (i) nucleation which is sporadic in time and space, (ii) any difference in cooling rate within the plane at which observations were made, and (iii) the measurement of spherulite dimensions at a section not through the centre of the spherulite.

3.22 Spherulite Type.

Broadly speaking microscopic observation in transmitted polarised light showed that the rate of occurrence of type III spherulites varied unsystematically with cooling rate from the melt. Whilst in a fixed area scanned by the microscope their number appeared to increase in faster cooled sheets, after the increase in number of spherulites was taken into account, the rate at which they occurred per 100 spherulites was found to vary unsystematically within the range 0.09 to 0.86.

Equation (1) relates the overall density ρ_o to the densities of the amorphous phase ρ_a and the monoclinic and the hexagonal crystalline phases, ρ_m and ρ_h respectively.

$$\rho_o = (1 - X)\rho_a + X \left[(1 - H)\rho_m + H\rho_h \right] \quad \text{---(1)}$$

where X = the crystalline fraction
and H = the fraction of the total crystalline phase which has a hexagonal structure.

$$= \frac{n \frac{\pi}{6} d^3}{WLd}$$

where n type III spherulites of diameter d are observed in a scanned area W x L.

Using typical values for

$$X = 0.6, \rho_a = 0.850, \rho_m = 0.936, \rho_h = 0.880$$

(see page 514 Ref.(7))

the maximum change in overall density resulting from the variable concentration of hexagonal crystals was found to be ± 0.0001 g/mL.

All the other spherulites seen apart from this were of type I,II. No type IV spherulites were clearly observed.

Cooling rates were apparently not sufficiently high to produce the non-spherulitic structure which has been observed in samples quenched rapidly in dry ice-acetone., see page 20 of Geil (7).

3.3 Density as a Measure of Crystallinity

Whilst density or specific volume is valuable as a simple index of local configurational structure its relationship with the content of crystalline phase in crystallisable polymers can only be inferred by a proportioning similar to equation (1), of the respective densities for two phases normally assumed to be perfectly crystalline and perfectly amorphous. The occurrence of a class of material of intermediate order, which has been identified in PP, makes any method used to determine crystalline content give a different result (122) according to whether the results interpret partially ordered material as being crystalline (density measurement) or non-crystalline (X-ray diffraction). Thus the percentage of crystallinity inferred by density measurement is often found to be higher than that measured by X-ray diffraction⁽⁵²⁾, although the density is more or less a linear function of the X-ray-determined crystallinity under normal crystallisation conditions.⁽⁴⁰⁾

Density measurements made in this work were not, therefore, converted into absolute values of percentage crystallinity.

3.4 Measurement of Density in Samples with varying Crystallisation Temperature.

3.4.1 Experimental Procedure and Errors.

Densities were measured using the density - gradient column method, in accordance with ASTM D - 1505 - 57T. Columns were built with either an alcohol and distilled water mixture or an isopropanol and diethylene glycol mixture. The latter was found to remain stable for far longer but suffered the disadvantage of being more viscous, which meant a longer time had to be allowed for a sample under test to reach an equilibrium level. So that measurements of density could be found at short times a calibration curve was plotted of the distance of a test piece above the equilibrium level for the first 48 hours of immersion.

The only other experimental drawbacks to this method for measuring the density of a moderate number of test pieces at once were the occasional attachment of one test piece to another and the occurrence of entrained air against test pieces where these had any inward cut in their identifying profile. These drawbacks were largely avoided by limiting the number of test pieces in the column at any one time and by washing them thoroughly in a sample of the column mixture before testing.

All densities were measured at $23.0 \pm 0.1^{\circ}\text{C}$ as the average of four test pieces taken from each sample. Densities measured in this way were tracked for about 60 days from the time of moulding.

The scatter in height of any one sample in the column made the accuracy of the density determination vary from ± 0.00025 g/ml in fast cooled sheets, to ± 0.00015 g/ml in slow cooled sheets. Extremes of cooling rate produced

a total change in density of only 0.006 g/ml, which meant that even with this degree of accuracy of density determination an error of approximately ± 4 % was inevitable where properties were correlated against density.

3.42 Results.

The results are shown as density versus time in hours for the experimentally available range of T_c in Fig. 3.4.

An isochronous plot of density against T_c at ages of 240 hours (10 days) and 1440 hours (60 days) is shown in Figs. 3.6 and 3.7 respectively. Results are shown with a chain line indicating the limits of scatter which are attributed to errors in measuring T_c , as described in section 2.42; and with scatter lines which indicate the spread in density from any one sample. An increase in the scatter of the results as shown in Figs. 3.6 and 3.7 towards the range of fast cooling follows from the reduced accuracy with which T_c could be determined in this range, and the increase in scatter of sample density in fast cooled sheets.

A change in the density of samples taken from different sheets is also possible due to the imprecision of moulding pressure. Pressure during crystallisation has been held ⁽⁶⁰⁾(61) to affect the quantity of void space which is likely to develop during secondary and tertiary crystallisation. Because of the standardised procedure used in moulding and the small fluctuation expected in mould pressure, this cause of scatter was neglected.

The curves obtained for density versus T_c show a significant change in density dependence on T_c for temperatures either side of $T_c \approx 120.5^\circ\text{C}$., with an abnormally large scatter in sample density at this temperature. The

plot of density versus both age and T_c which resulted from this work together with the record of T_c from the three thermocouples embedded in each sheet, enabled a fairly accurate interpolation of the density for each tensile test piece to be made where necessary. The accuracy of this determination was reduced as the cooling rates of the sheets increased.

3.43. Existing Theoretical Predictions of Crystallinity as varied by age and T_c .

Collins⁽¹²³⁾ has used a relationship of the form shown in equation (2) to fit the progress of crystallinity in PE with age up to times for which crystallinity equals the maximum allowed by structural impediments.

$$X_t = A + C_1 \log t \cdot \exp(C_2/T) \text{-----} (2)$$

where X_t = the crystallinity at time t

A, C_1, C_2 = constants

T = absolute temperature

The form of temperature dependence of this equation suggests that the process of secondary crystallisation is diffusion controlled. For a fixed temperature, therefore, a plot of density to a base of $\log t$ should appear as linear.

Some typical results from section 3.42 were plotted to a base of $\log t$ (hours) in Fig. 3.5 and confirm the applicability of the form of equation (1) to PP.

Collins did not extend his study to examine the effect on his results of the degree of initial cooling rate of the sample. From Fig. 3.5 it can be seen that the values of the rate quantity, $C_1 \exp(C_2/T)$, vary by very little and show only a slight tendency to faster diffusion rates

in the fastest cooled sheets.

In Fig. 3.5 the slopes of lines for test B^{*1} and test C^{*2} of the last chapter do, however, show respectively that the melt condition and pressure of moulding may control subsequent diffusion rates for age induced crystallisation to a larger extent than the cooling rate. The increased slope for test B is explained by the slight degree of thermal degradation which was indicated in the T_c results for this sample, see section 2.32. Thermal degradation would be expected to reduce the average chain length of the material and hence increase its self-diffusion rate.

No specific values for the slopes of the density versus log (time) lines were calculated because of the size of cumulative errors resulting from T_c and density determinations. The change in slope after a time of the order 700 hours in several of the samples may be due to the onset of structural impediments to further increase in crystallinity, but because of its irregular disposition between samples of varying cooling rates it is more likely to result from density test pieces coming into close contact with the wall of the density column.

Krigbaum and Uematsu⁽¹²⁴⁾ have developed a relationship of the form shown in equation (3) for the dependence of the equilibrium crystallinity in PP on isothermal crystallisation temperature. Their results, which cover the limited temperature range of 137°- 156°C, give good agreement with this relationship.

$$(1 - X)^{-2} = K T^{-1} \text{-----} (3)$$

where X = equilibrium or final crystallinity

K = a constant

T = absolute temperature.

*¹ this sample was thermally degraded, see p. 46

*² moulded at a reduced pressure, see p. 62

The results of section 3.42 show, however, that a continuous function of this kind is incapable of accurately predicting the final crystallinity where the temperature is below about 120.5°C ., where there are some indications of a change in crystallisation kinetics.

3.5 Discussion.

As is to be expected, both spherulite size and density increase as T_c is raised. There is, however, a marked increase in spherulite diameter at a T_c of about 120.5°C and a jump in density at the same point. Some results on PP by Beck and Ledbetter⁽⁶⁸⁾ where T_c was varied by the addition of nucleating agents, are too scattered to show any apparent discontinuity in the way density depends on T_c .

No other reference has been found to this sharp increase in density in PP. A similar discontinuity has, however, been reported⁽¹²⁵⁾ to occur in PE at $T_c = 85^\circ\text{C}$ and in polyethylene terephthalate⁽¹²⁶⁾.

The observed variation in the content of hexagonal crystals has already been shown to be incapable of producing a density change of more than .0002 g/mL. The observation that type III spherulites occurred under all moulding conditions does not agree with Putti and Sabbioni⁽¹²⁷⁾ who pinpoint a $T_c = 120^\circ\text{C}$ as being the threshold for the growth of type III spherulites in PP during constant cooling from the melt. The same authors also report that a maximum in both the overall rate of crystallisation (k_s) and spherulite growth rate (G) is attained at about this same point. Isothermal observations⁽¹⁷⁾ of G , however, do not show a maximum at this temperature.

As an indication of a possible change in crystallisation kinetics, a measurement of the 'dwell time' during crystallisation was made for a selection of crystallisation results from Chapter 2. Dwell time was defined arbitrarily as the time in minutes spent in passing from $(T_c + 1)^\circ\text{C}$. to $(T_c - 1)^\circ\text{C}$.^{*} The results are shown in Fig. 3.3. As in Magill's⁽¹¹⁶⁾ results on the induction time for crystallisation,

* and may be regarded as a measure of crystallisation rate.

a change in crystallisation kinetics is indicated to occur at a temperature of about 120°C ., by a large change in the dwell time in this region.

In answer to the question, what would the effects of a large change in crystallisation rate be on morphology, it is interesting to scan the available literature on the subject of PP morphology as varied by T_c . There seems strong reason to believe that a crystallisation temperature above 120°C is required before crystallinity and crystallite size acquires a maximum⁽¹²⁸⁾. Recent success in growing single crystals of PP⁽²⁷⁾ also confirms that prolonged crystallisation above 120°C is required to produce well defined lamellar crystals, and a tendency to the development of numerous fibrils at equally prolonged crystallisation below this temperature range. It is tempting, therefore, to conclude that the occurrence of an intermediately ordered state in PP begins to disappear where the T_c is above a temperature in this range. Although from Hock's⁽²⁵⁾ results on acid-attacked samples crystallised at $T_c \geq 125^{\circ}\text{C}$. this would not appear to make PP lamellae any easier to separate, this might be attributed to the structure of interleaved lamellae of types (a) and (b) proposed by Padden and Keith⁽¹⁸⁾.

Where intermediately ordered material has been produced by rapid cooling, it has been found⁽⁵³⁾ to be essentially removed by heating for half an hour at 85°C , and it might therefore be deduced that structure of this type is not favoured at higher temperatures than about 90°C . It is difficult to be specific about the temperature at which it will not occur as a result of crystallisation during constant cooling because of the difference in time scale allowed for completion of crystallisation between a sample being constantly cooled and one being heated for half an

hour. In this context, it is worth noting that the cooling rate during moulding was maintained down to at least 70°C and this constitutes a moderate annealing treatment in slow cooled samples.

It is concluded that the large increase in dwell time which occurs at this point in PP, and which indicates a change in crystallisation kinetics, together with the decrease in cooling rate, will enhance the more rapid development of perfectly ordered crystalline lamellae sufficiently to increase the sample density.

In Chapter 2 it was shown that test C which involved moulding at a reduced pressure produced an overall fall in T_c of about 1.2°C (table 2.4). It would appear from the dwell time for test C in Fig. 3.3 that there is an approximate translation by the same temperature shift of the dwell time curve, indicating a change in T_c with little or no change in crystallisation kinetics. The density of this sample is, nevertheless, greater than a sample having the same dwell time, which would follow from the lower degree of supercooling ($T_m - T_c$) at which this sample crystallised due to the effect of pressure on T_m .

3.6 Conclusions.

1) A discontinuity of sample density and spherulite size has been found to occur where $T_c \cong 120.5^\circ\text{C}$. It is concluded, from measurements of dwell time during crystallisation, that this is the result of a change in crystallisation kinetics for $T_c \cong 120.5^\circ\text{C}$.

2) The change in dwell time is such as to enhance the rapid development of a greater portion of ordered material at slower cooling rates. It is implied by this that there may be a significant loss of intermediately ordered material in the range of T_c above 120.5°C .

3) The changes in induction time which should also accompany more rapid crystallisation at $T_c \cong 120.5^\circ\text{C}$ do not appear to affect the continuity of the results obtained for T_c versus cooling rate in Chapter 2. Nor does this change in crystallisation kinetics appear to affect the agreement in trend between the theory developed in Chapter 2 to predict T_c versus cooling rate, which was based on the assumption of an isokinetic zone during the temperature-time field prior to crystallisation.

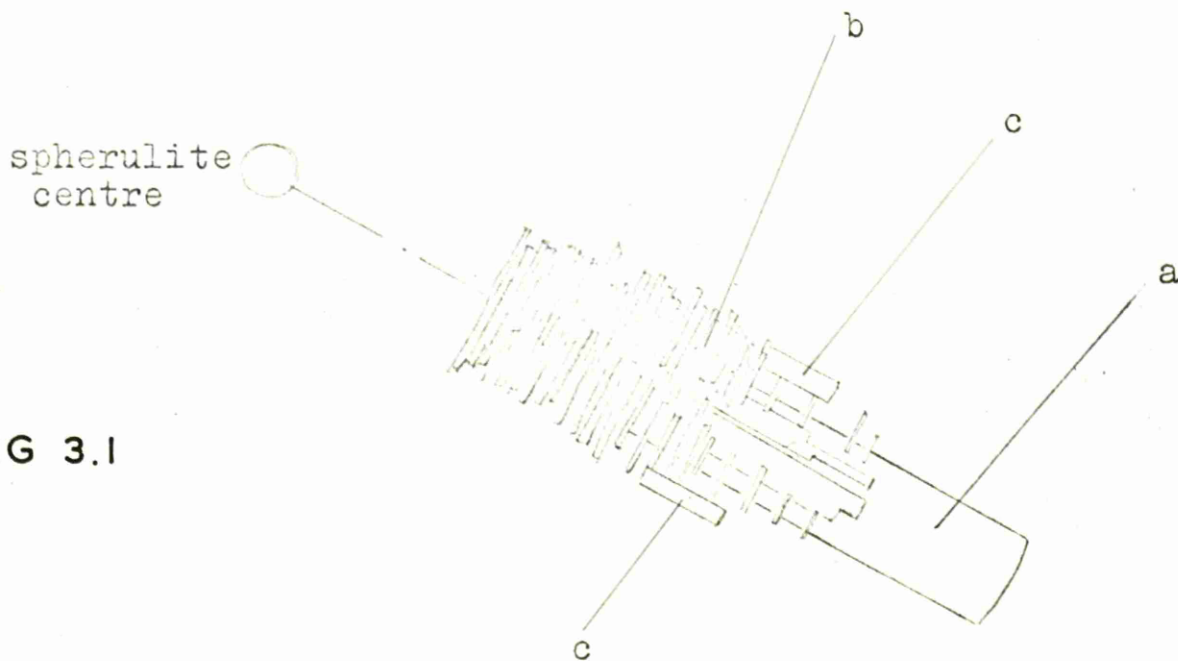


FIG 3.1

- a) " radially directed leader lamella" , c - axis perpendicular to the radius
- b) primary branched lamellae, c - axis almost parallel with the radius
- c) secondary lamellae, c - axis perpendicular to the radius.



FIG 3.2 $T_c = 125.7^\circ\text{C} \times 350$

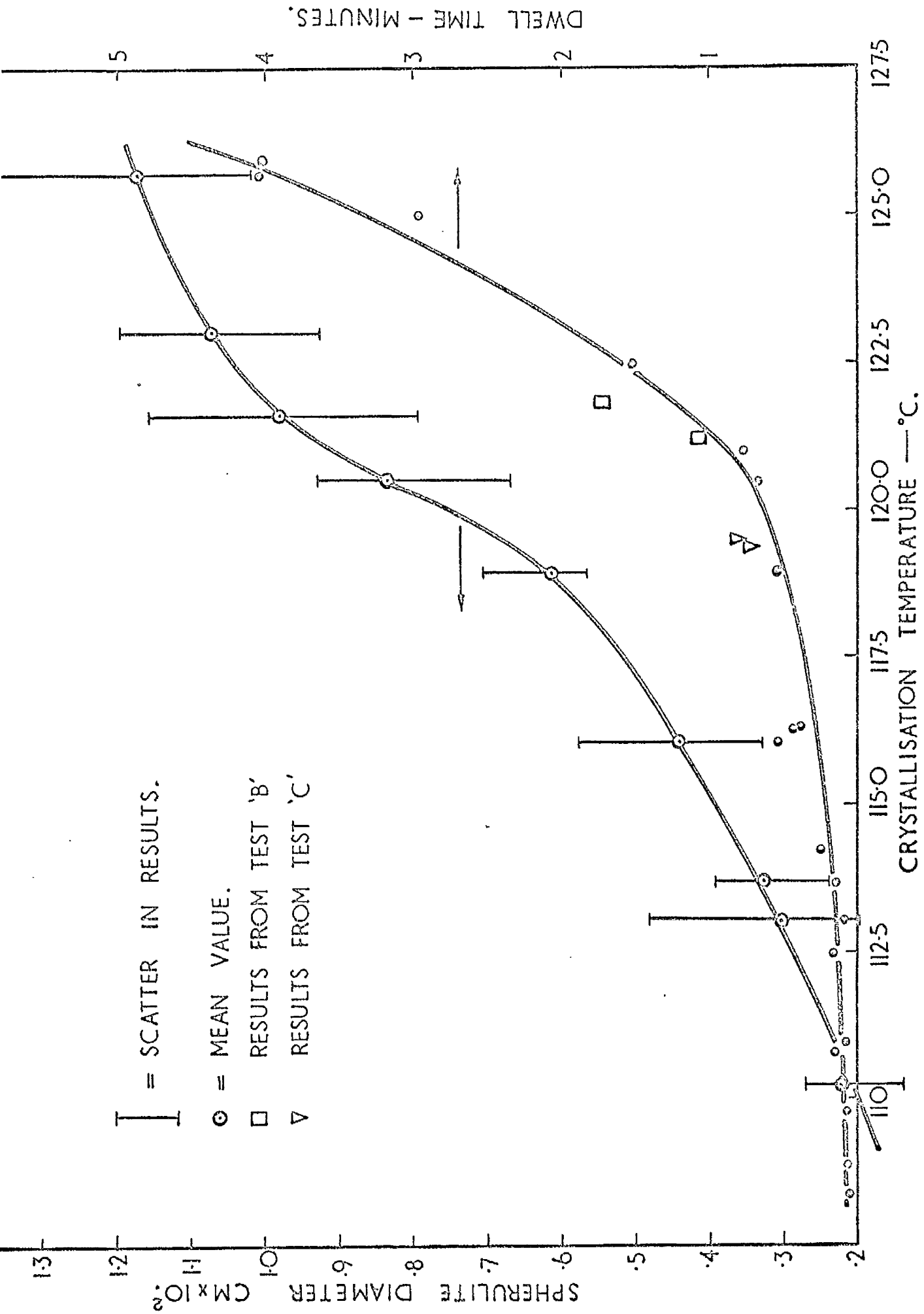


FIG. 3.3. THE EFFECT OF CRYSTALLISATION TEMPERATURE ON SPHERULITE DIAMETER AND DWELL TIME.

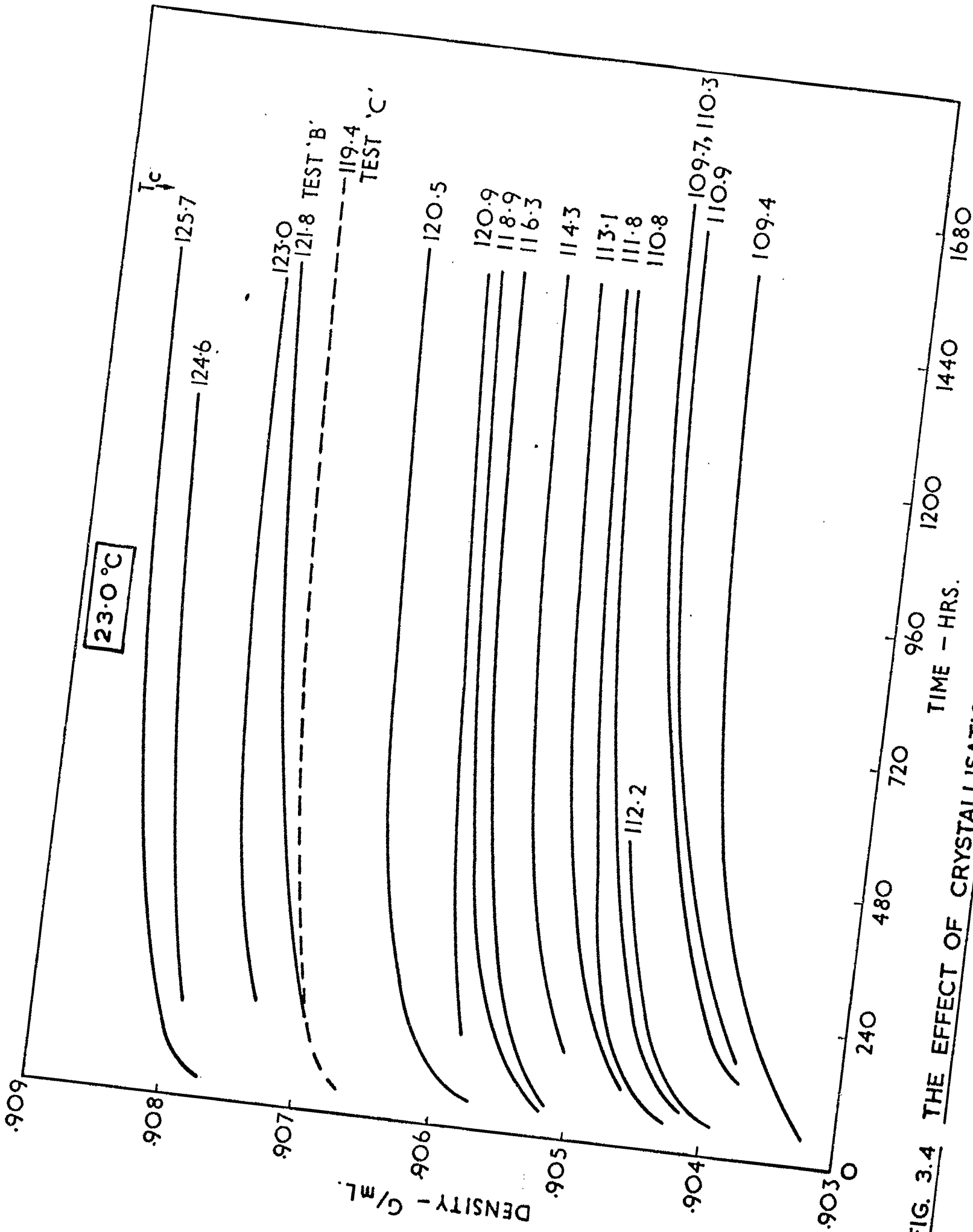


FIG. 3.4 THE EFFECT OF CRYSTALLISATION TEMPERATURE AND AGE ON DENSITY.

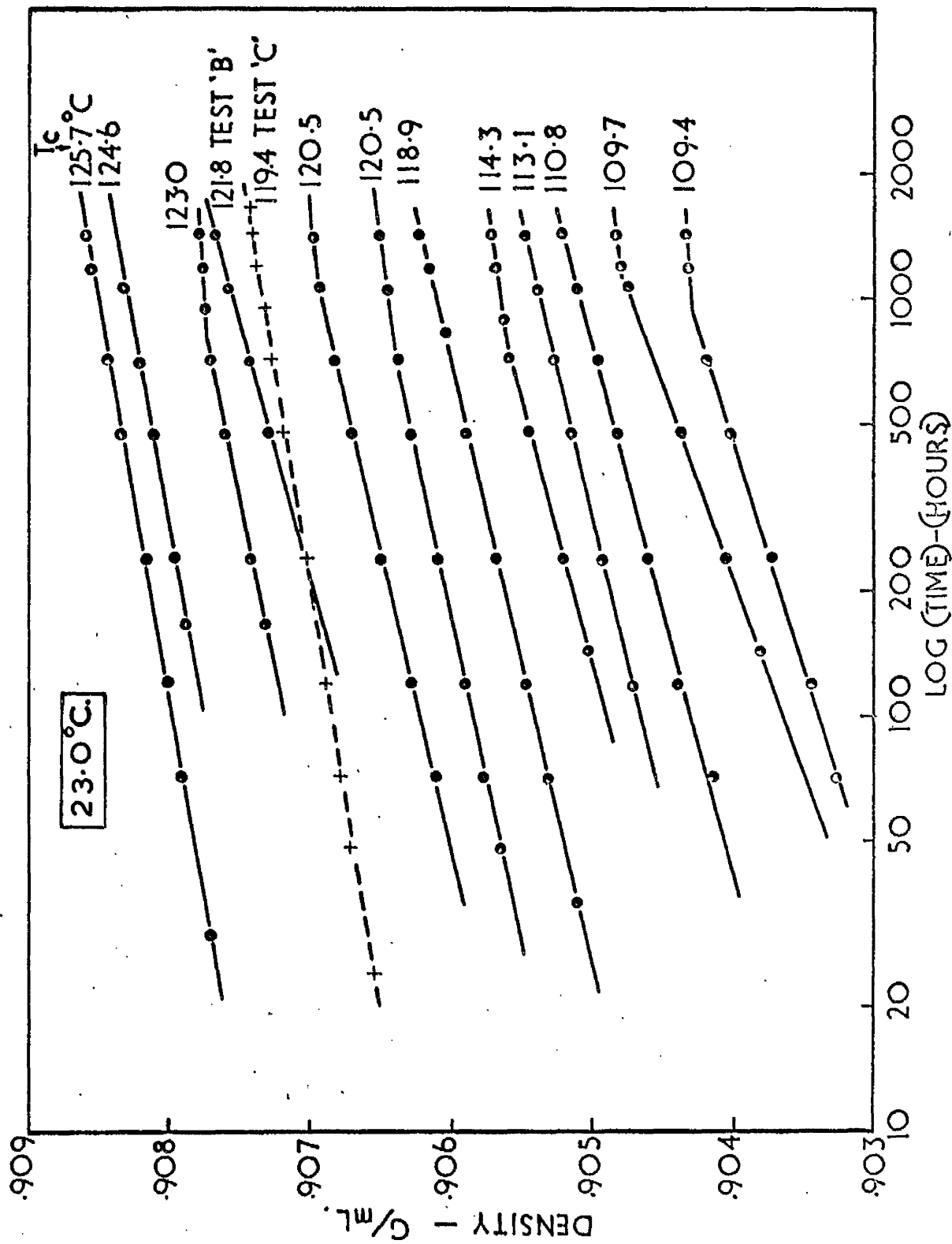


FIG. 3.5 PLOT OF DENSITY VERSUS LOG (TIME)

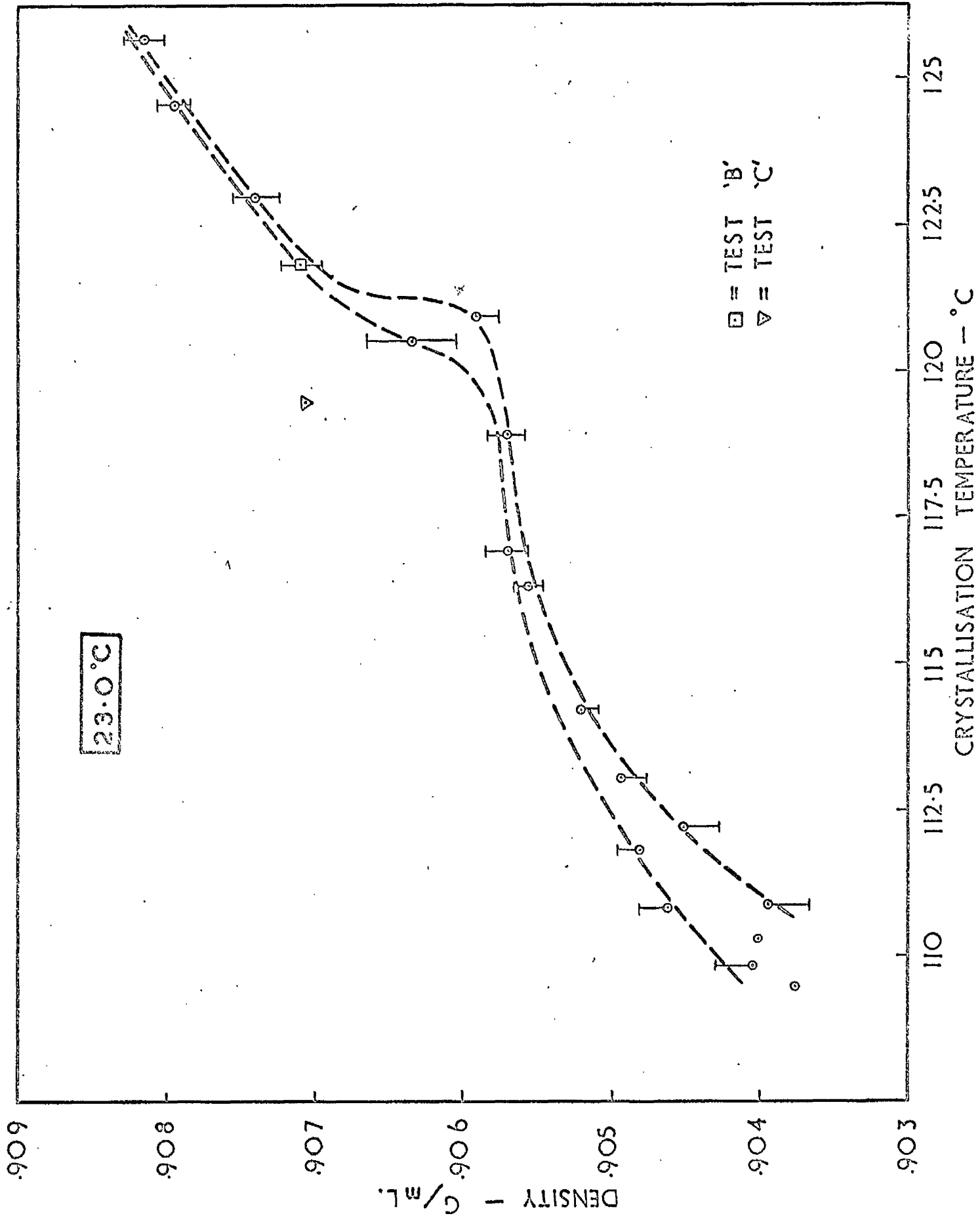


FIG. 3.6 DENSITY AT 240 HRS. VERSUS T_c

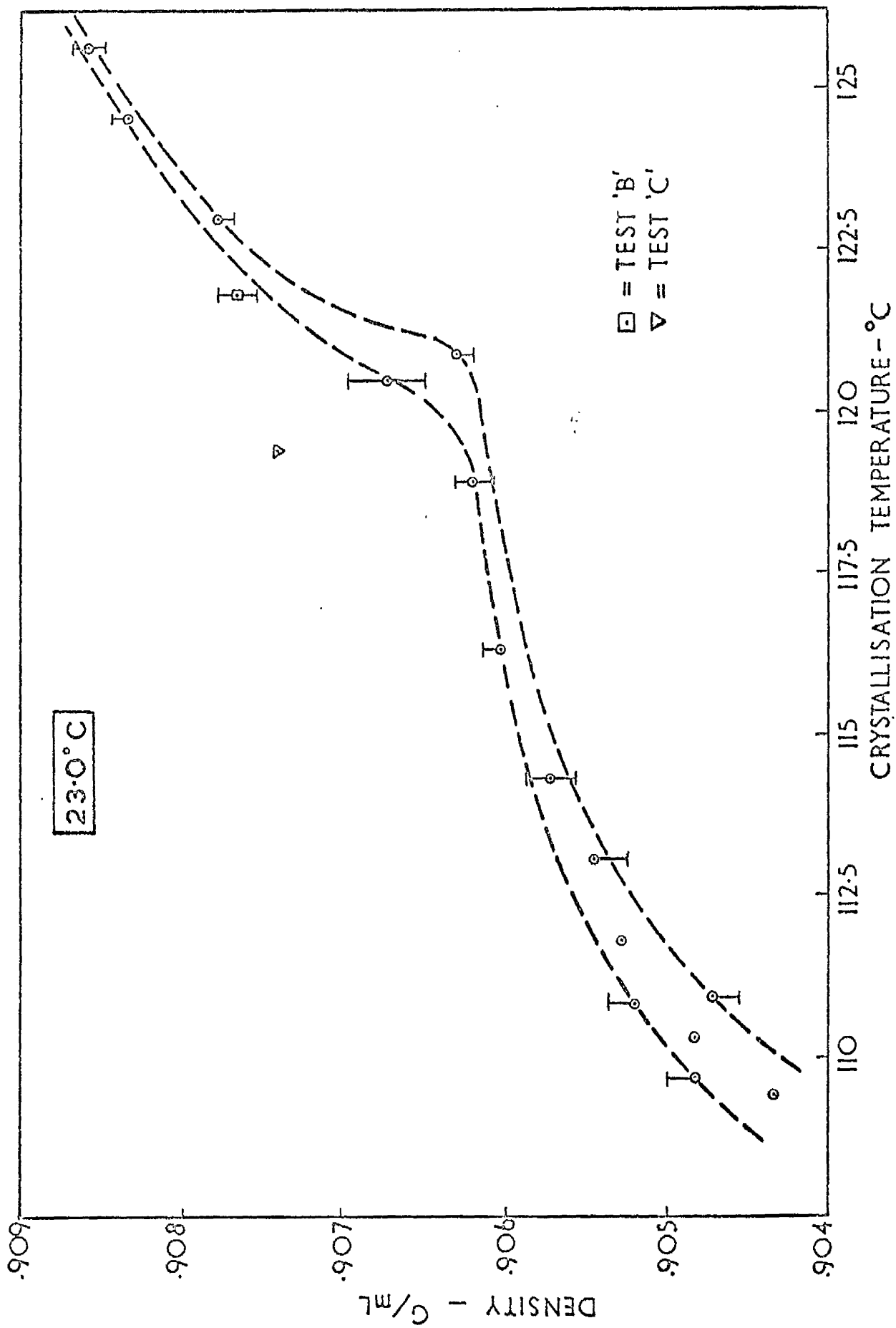


FIG. 3.7 DENSITY AT 14.40 HRS. VERSUS T_c .

4. TENSILE TESTING OF SAMPLES WITH VARIED THERMAL HISTORY.

Constant strain rate tests on tensile ^{pieces} machined from the sheets prepared in the moulding programme were chosen as exploratory mechanical tests of the effects of cooling rate, age and annealing on the stress-strain behaviour of PP.

4.1 Thermal History of Samples Tested.

Samples having various cooling rates covered a range of ages, as shown in table 4.1a, but two tests were completed on samples of different age having the same preparation, as shown in table 4.1b, to elucidate the effect of age. Annealing treatments given to samples are shown in table 4.1c.

Ageing was carried out in a controlled temperature room held at $23 \pm 2^{\circ}\text{C}$.

Annealing was carried out in air, in an oven, and cooling from the annealing temperature was at the natural rate of the oven, which required approximately 3 hours to cool ^{to} 40°C .

4.2 Tensile Test Piece.

The tensile test piece used throughout mechanical testing was based on that recommended in ASTM D 638 - 58T, but with a modified length overall and radius of fillet, which gave a gauge length of 6.0 cm., and a test cross-sectional area of about 0.48 cm^2 , see Fig. 4.1.

Jigs were made to support the plastic rigidly during machining. The first step was to mill off .025 ins. from both faces of a strip of the plastic using a jig which held the strip clamped under blocks at either side. A .025 ins. backing strip was inserted for machining the reverse face. The second step was to machine out the tensile test shape for which a rigid fully supporting jig was used, see Fig. 4.2. This comprised two metal profiles, the free one of which was located on pins passing through the plastic strip in the grip area, and was clamped down to sandwich the plastic.

Throughout machining a jet of compressed air was played onto the cutting edge to prevent a form of annealing due to work heat at the surfaces. Machining off the moulded sheet faces was felt to be desirable in order to prevent spurious results ⁽⁴⁰⁾ from the non typical columnar growth structure which is normally found against moulded sheet faces.

Inevitably, as discussed in section 2.24, there was a change in cooling rate, and hence structure, through the thickness direction of moulded sheets. However, it was found that there was only a relatively small change in structure after about .015 ins. from the sheet faces. After machining down to the tensile test thickness (=0.15 ins.) by removing .025 ins. from both faces, the overall change in thermal history in the thickness directions as inferred by a comparison of the mean spherulite diameter

at the face with that at the centre was found to be typically of the order of a 2°C . change in T_c for fast and slow cooled sheets alike. These results showed that thermal history variations in the thickness direction were of a slightly greater order than might be expected along the gauge length due to lateral changes in cooling rate during moulding as discussed in section 2.24. 51/

An overall tolerance in thermal history of about $T_c \pm 1^{\circ}\text{C}$. has, therefore, to be allowed in all as-moulded tensile test pieces.

By comparing the stress-strain results from an as-machined tensile piece with the results from a tensile piece which had its faces polished smooth with diamond paste, it was found that the machine marks, which had a depth of about .001 ins., had no measurable effect on mechanical properties. A light transmittance test, (see section 5.52) which was done simultaneously, also confirmed that machine marks had no influence on the internal rupture properties of samples.

4.3. Apparatus and Test Procedure.

All mechanical tests were carried out on an Instron tensile tester for which a constant temperature test cabinet was made.

4.3.1. Constant Temperature Test Cabinet.

A temperature-controlled cabinet was designed and built to fit into the test frame of the Instron. A description of the working features of the cabinet is given in Appendix III. Fig. 4.4 shows how the cabinet on its trolley fitted into the Instron.

The only adaptation required of the Instron was to make up extension pieces to take the grips into the cabinet, these had compression springs inserted at all joints to hold them tight against their pins to minimise movement when loading specimens. * The grip extension pieces utilised the universal joint which was already coupled to the load cell during use. A spacing ring was also required to lift the high capacity load cell, when this was used, to bring the top grip to a working position inside the cabinet; this can be seen on top of the Instron in Fig. 4.4.

The level of temperature fluctuations attained within the test area of the cabinet was of the order $\pm 0.1^{\circ}\text{C}$. A standard test temperature of 24.0°C . was used throughout mechanical testing. This temperature was monitored from three calibrated thermocouples along the gauge length on the same Kent recorder that was used in the sheet moulding programme.

Since the temperature control did not incorporate a cooling element, cooling being by conduction through the cabinet walls, some care was found necessary

* see Fig. 4.11

in maintaining this temperature on very hot days.

The above noted temperature fluctuation (δT) within the cabinet is related to the tolerance on the measured load (δF_t) at any time t by equation (1)

$$\delta F_t = E_t (\psi \cdot \delta T \cdot L_0) \frac{1}{L_0} A \quad \text{-----(1)}$$

where E_t = modulus at time t

ψ = coefficient of linear expansion of the plastic

L_0 = gauge length

A = cross sectional area

Substituting the value for ψ ($=11 \times 10^{-5} \frac{1}{^\circ C}$) for the PP used in this research and a typical short time value for E_t as obtained in the relaxation tests described in Chapter 6 ($=1.20 \times 10^4 \frac{Kgm}{cm^2}$), to give the most pessimistic tolerance in load measurement.

$$= \pm 0.63 \times 10^{-1} \text{ Kgm.}$$

Errors from this can be added to the reading error on a 0 - 100 Kgm span ($\pm 0.1 \text{ Kgm}$), to make the total error in load measurement = $\pm 0.16 \text{ Kgm}$.

The temperature fluctuation cycle was regarded as sufficiently frequent as not to affect the ^{overall} relaxation rate of the specimen.

4.32. Strain Measurement.

An optical observation system was used to follow the movement of gauge marks through the double glazed door of the cabinet. This comprised a Swift Utilix Vernier Measuring Microscope which was specially adapted by the manufacturers to have two microscopes mounted on separate sliding carriages, see Fig. 4.5. Each microscope was fitted with a 100 m.m. objective and a X10 Filar micrometer

eyepiece. The microscope carriages slide freely over a central steel rod which is spring-loaded, via a thrust bearing, against a Moore and Wright micrometer screw, fitted with a drum reading to 0.0001 ins., which is mounted on one end of the casting. When both sliding carriages are locked to this central rod their movement can be activated through a distance of 1.0 ins. and measured by the micrometer drum. Their positions on the central rod can be measured to the nearest 0.001 ins. by using a less accurate Vernier Scale set into the casting.

Several methods of applying gauge marks to the specimen were tried and the best found to be the use of a thin strip of opaque cellotape which had a razor score along its centre. Since the strain of the underlying material is homogeneous in the direction of extension the central score mark should represent the true displacement of the material. The gauge marks were illuminated by two 4.5 V bulbs supplied by a Farnell stabilised power pack. A stabilised source of light close to the specimen was necessary for the accurate measurement of transmitted light through specimens during ^{relaxation} testing as described in Chapter 6.

To obtain sufficient stability in operation the Utilex was slotted and bolted into a removable frame which was itself bolted onto the Instron, as can be seen in Figs. 4.4 and 4.5. The Utilex with its frame was made easily removable for ease of access to the cabinet.

In operation the gauge length (l_0) was measured on the Vernier Scale by the movement required of a single microscope carriage to make the hair line of the eyepiece meet the gauge marks. This was done with the tensile test piece held at the no-load condition between the grips, and gave a reading error of ± 0.002 ins. for l_0 . Extensions were then measured by first locking both microscope carriages to the central rod and arranging for the adjustable hair lines of each eyepiece to meet their

respective gauge marks in the no-load condition. After extension the movement of the micrometer drum required to make each hair line meet its respective mark measures the change in length of the gauge (δl) with a maximum reading error of ± 0.0004 ins.

It is to be noted that strict parallel alignment of the axis of the measuring system with the tensile axis of the test piece is not a prerequisite for the correct measurement of the ratio $\delta l/l_0$ where both l_0 and δl are measured with a consistent axis.

The greatest error in the measurement of strain with this equipment was for the smallest strain of 0.25% used in stress relaxation tests, see Chapter 6. and equals $(0.25 \pm 0.017)\%$. The measurement error in 5.0% strain is $(5.0 \pm 0.0022)\%$.

Advantages of an optical observation system for strain Measurement.

The advantages of this system are chiefly dictated by the disadvantages of alternative strain measuring equipment. These briefly are:

1. No encumbrance on the test piece.
2. Speed of setting up for a test.
3. No reinforcement of the relatively low modulus plastic by the attachment of linear transducers.
4. No stress concentration or contact problems between knife edges and sample or pin holes through the specimen.
5. Measurement of gauge length and extension with one set up, no alignment problems.
6. Could be used at any test temperature on the sample.

Disadvantages.

1. Low accuracy at small strains.
2. Long time (about 2 mins.) to take an accurate reading of strain.
3. No averaging out of bending strains.
4. No possibility of automatic feed back to regulate cross-head displacement.

These disadvantages are minimised where relaxation tests are involved and the strains used are greater than 0.0025, at which the percentage error is $\pm 7\%$.

The advantages are greatest where many relaxation tests are envisaged.

4.33 Experimental Errors.

The accuracy of the Instron cross-head speeds in their slowest range was tested using the Swift Utilix Vernier Measuring Microscope and was found to have the following tolerances.

Nominal c/H speed ($\frac{\text{cm}}{\text{min}}$)	Tolerance \pm (%)
<u>0.1</u>	<u>0.2</u>
<u>0.05</u>	<u>2</u>

The strain rate ($\dot{\epsilon}$) resulting from a cross-head speed of 0.1 cm/min. was measured over the gauge length using three 'dummy' specimens machined from the as received plastic sheets and the strain measuring equipment already described. A small but continuous increase in $\dot{\epsilon}$ over the gauge length was noted, see Fig 4.6. The increase in $\dot{\epsilon}$ was attributed to load cell, coupling and

and machine deflections and some early embedding of the plastic into the grip faces. Since the $\dot{\epsilon}$ shows an increase during testing, the progress of extended material to areas outside the radius fillet can be reasonably discounted. The manufacturer's claim for deflections of their high capacity load cell, the couplings and machine is about 0.0015 ins / 100 Kgm. The 100 Kgm. point is marked on Fig. 4.6 and shows that the deflections due to the grip extension pieces and embedding in the grips is of the order 0.055 ins/100 Kgm.

A relaxation test carried out on another 'dummy' specimen showed that elastic machine deflections were of the order 0.0025 ins/100 Kgm., and it was concluded that a relatively large amount of cross-head displacement was used in embedding of the plastic into the grip faces.

Using a standard cross-head speed of 0.1 cm/min., the change in $\dot{\epsilon}$ from the beginning of a test to the point of specimen yielding was repeatedly found to be $0.975 \pm 0.15^{\circ}/\text{o}/\text{min.}$, as shown in Fig. 4.6. Tests at $x \frac{1}{2}$ and $x 2$ of this cross-head speed, see Fig. 5.13 showed that the greatest o/o error in the load reading resulting from the strain-rate sensitivity of the material and the above deviations from constant $\dot{\epsilon}$ was $\pm 1.7^{\circ}/\text{o}$. Added to this there was a load measuring error of ± 0.16 Kgm, as detailed in section 4.31. In plotting all results the true $\dot{\epsilon}$, as given by Fig. 4.6. was used.

Strictly speaking, it was not possible to measure the initial $\dot{\epsilon}$ of the test piece with the Utilex measuring microscope. Errors arising from initial large variations in $\dot{\epsilon}$ were expected owing to a) the embedding of the relatively soft plastic into the grip faces; b) the very slight curvature of some tensile test pieces resulting from the quench cooling, as detailed in section 2.24; and c) any

slackness in the links between the cross-head drive screws. and the tensile test piece on the one hand and the load cell and links on the other hand.

The scatter in thermal history within the tested length of material, as estimated in section 4.2, will further serve to produce a scatter in results.*

4.34. Test Procedure.

After inserting a tensile test piece into the Instron jaws, the cabinet was closed and the heating circuit switched on. During heating of the cabinet the cross-head height was adjusted to take up expansion of the test piece. Once the temperature within the test area of the cabinet had reached 24.0°C., about 10 mins. were allowed for equilibration of the sample. This could be tracked on the most accurate load scale of the Instron as a small expansion load which diminished to negligible proportions after about 5 minutes.

* e.g. the scatter in density found in section 3.41 varies between $\pm .00015$ and $\pm .00025$ g/mL for slow to fast cooled sheets

4.4 Results.

Stresses throughout this work are defined as the measured load over the initial cross-sectional area of the test piece.

The results of stress versus strain for the constant test conditions of 24.0°C and $\dot{\epsilon} = 0.975^{\circ}/\text{o}/\text{min.}$ are shown in Fig. 4.8 as far as the yield point of each specimen.

The stress to reach a predetermined strain is a measure of the secant modulus of the material. Values for this modulus derived from the curves in Fig. 4.8 are given in Figs. 4.8c and 4.8d for strains of 5^o/o and 10^o/o respectively.

Many more additional results were available at smaller strains from the ramp part of the strain function imposed during the stress relaxation tests described in Chapter 6. Since the same standard $\dot{\epsilon}$ and test temperature were used, results from this ramp/strain region were used together with those obtained in this Chapter to obtain a more complete picture of the effects of cooling rate and age on modulus.

The data from which the effects of cooling rate on modulus was compiled are given in tables 4.2 and 4.3, for two different age bands of samples. The effect of age induced density changes on the material modulus was found to be quite large, especially at higher strains. It was therefore found necessary to plot the results for samples differing by a fairly small age band, in order to correlate modulus changes against the effects of cooling rate.

The effects of cooling rate on modulus are shown in Figs. 4.9 and 4.10, as a solid line and a chain dotted line for the data of tables 4.2 and 4.3 respectively. More results were available at the lowest strains plotted in

Fig. 4.9. This alone could account for the greater scatter in results, but early discrepancies in ϵ from one sample to another as outlined in section 4.33 might also contribute to a larger scatter. Results for specimens taken from test B of Chapter 2 which has shown signs of thermal degradation, are shown as sample 8A.

Table 4.4 gives the data from which the effect of sample age was determined. Results for this data are shown in Figs. 4.9 and 4.10 as a chain line.

The data for annealed samples 19 from Chapter 6 is given in table 6.1c. Results for this data are shown in Fig. 4.10 joined with a dotted line.

4.5 Discussion.

To aid in interpretation, the $\sigma - \epsilon$ curves of 'as moulded' samples and annealed/are presented separately in Figs. 4.8a and 4.8b respectively.

4.51. Strain to Yield.

The strain to yield shown in Fig. 4.8a has a tendency to decrease as the moulding cooling rate is reduced or age of specimen increases. This trend agrees with the normal trend in mechanical properties with increase in crystalline content, as outlined in the introduction, section 1.3.

Its cause may be due to either

- a) the effect of crystalline content on the microscopic $\dot{\epsilon}$ in amorphous regions
- b) a weakening of bonding between spherulites or between crystalline regions.

Prior to testing no voiding was visible between spherulites in any 'as moulded' sheets although spherulite boundaries became more well-defined towards the slow cooling rates.

The first cause (a) may be tested by assuming the worst condition in which all deformation is concentrated into the amorphous phase, see Appendix IV . The total change in the strain rate in amorphous regions $\dot{\epsilon}_a$ found for the overall change in sample density in table 4.1a varies from $2.17 \times \dot{\epsilon}$ to $2.28 \times \dot{\epsilon}$.

Results obtained for $\dot{\epsilon}$ sensitivity on samples of identical thermal history, see Fig 5.13, show that a change in $\dot{\epsilon}$ from $0.48^\circ/\text{o}/\text{min.}$ to $1.89^\circ/\text{o}/\text{min.}$ produced a total change in strain to yield from $12.0^\circ/\text{o}$ to $11.2^\circ/\text{o}$.

This relatively low susceptibility of yield strain to imposed $\dot{\epsilon}$ agrees with a more thorough investigation by Hall (80)

who varied the $\dot{\epsilon}$ applied to orientated PP filaments in the range 1.98°/o/min. to 29.4×10^5 °/o/min. and found a change in yield strain of approximately 25°/o to 18°/o.

Cause (b) seems, therefore the more likely mechanism and is discussed further following microscopy of the extended structure as detailed in Chapter 5.

The increased strain to ^{yield} following annealing treatments shown in Fig. 4.8b may result from an increase in the state of relaxation in amorphous regions following gross melting and reorganisation of the structure as proposed by Wyckoff (45) and Miller (50). The ability for an annealing treatment to melt and reorganise structure depends on the ratio T_A/T_C where T_A and T_C are the annealing temperature and crystallisation temperature of the structure respectively, such that at $T_A/T_C > 1$, a melt and reordering is possible. Since the recorded T_C is representative of the majority of the material the increase in strain to ^{yield} going from sample 1B to 5A to 1A would follow from the increase in the ratio of T_A/T_C in the same order, and agrees with the above authors' interpretation.

These interpretations of the cause for slower cooling rates or age reducing ductility whilst annealing treatments improve ductility are consistent if the former treatments selectively weaken one part of the structure compared with another part, (e.g. spherulite boundaries compared with spherulite interiors), such that during testing the weaker regions fail prematurely due to strain concentration. Annealing might then be considered to weaken the whole structure so that no one region prematurely fails and ductility is improved.

4.52. Modulus.

The stress to reach a prescribed strain is a measure of the secant modulus of the material. These moduli at strains of 0.5^o/o, 1.5^o/o, 5^o/o and 10^o/o, are plotted in Figs. 4.9, 4.10, 4.8c and 4.8d respectively.

More readings were available at the lowest strain of 0.5^o/o (Fig. 4.9). These show the degree of scatter obtained in results for modulus, following from errors as outlined in section 4.33. A fairly well-defined trend in modulus was nevertheless found for the mean values indicated in Figs. 4.9 and 4.10. The increased scatter in slow cooled sample 15 is of interest in the light of the results of Beck and Ledbetter ⁽⁶⁸⁾ reproduced in Fig. 4.7. These show an increased scatter for samples having $T_C \gtrsim 118^{\circ}\text{C}$ and a peak in the lower modulus limit (added as a dashed line) at this point. This may indicate a tendency to embrittlement where T_C is in the range $T_C \gtrsim 120.5^{\circ}\text{C}$ in this research where the abrupt increase in density was noted to occur in Chapter 3. The rate of modulus increase with density (the slope of the lines in Figs. 4.9, 4.10) following changes in cooling rate or annealing was found to be essentially the same at low strains (0.5^o/o) but at slightly higher strains (1.5^o/o) ageing appeared to be much more efficient in its ability to increase modulus.

These observations may be interpreted structurally as indicating that ageing produces relatively little change in crystalline content, but has a tendency to make the bonding between crystalline regions less flexible. Slower cooling rates, however, increase the crystalline content by a relatively larger amount and may produce a tendency to more flexible bonding between crystalline regions.

The near coincidence of the lines for modulus changes depending on cooling rate for two age groups up to 905 hours in Figs. 4.9 and 4.10, and the general agreement in trend for samples varying in age from 6 to 695 hours in Figs. 4.8c and d suggest that the beneficial effects of ageing may not be found until sample age exceeds at least 1000 hours, see for example, sample 4 in Figs. 4.8c and d.

The lower modulus of sample 8A in both Figs. 4.9 and 4.10 is probably due to its thermal degradation (loss in molecular weight) during moulding.

Following annealing treatments occasional voids between spherulites were observed in sample 5A and explain the anomalous post-anneal density found in this sample. In the faster cooled samples which were annealed, sample 1 of this chapter and sample 19 of Chapter 6, voiding may have been present but could not be identified in the optical microscope owing to the small size of the structure.

Sample 5A shows a particularly low modulus value in Figs. 4.10, 4.8c and d which is probably due to this voiding and the comparative ease of separation of spherulites. The lower moduli found for all the annealed samples at the $\dot{\epsilon}$ used in these tests would follow from the overall structural weakening already discussed in section 4.51. In the case of sample 19, annealed as in table 6.1c, greater control of the ratio T_A/T_C was possible, and the time of annealing t_A was varied. The results in Fig. 4.10 for $T_A/T_C < 1$, joined with a dotted line, show the progress of the modulus toward a limit or maximum with increase in the annealing time. For $T_A/T_C > 1$ the modulus was lower. Oxidation attack can be ruled out for the results on samples 19a - d all of which were annealed in an inert atmosphere.

The small range of densities capable of being covered with these results and their scatter did not permit a

critical examination of the applicability of existing empirical equations⁽¹²⁹⁾⁽¹³⁰⁾ relating modulus to sample density in PE regardless of thermal history or crystallisable fraction, see equation (2)

$$\log (\text{modulus}) = A + B \rho \text{ ————— } \text{---(2)}$$

where A and B are constants , ρ = density

Reding⁽¹³¹⁾ has pointed out some limitations to this simple relationship where segmental mobility of molecular chains is changed independently of density.

The above results confirm quite clearly that density alone is not a sound basis on which to compare mechanical properties particularly at strains greater than about 1%. At this level of strain the mobility of large segments of molecular chains is unlikely to be the same for differently cooled, annealed, or aged samples as has been demonstrated.

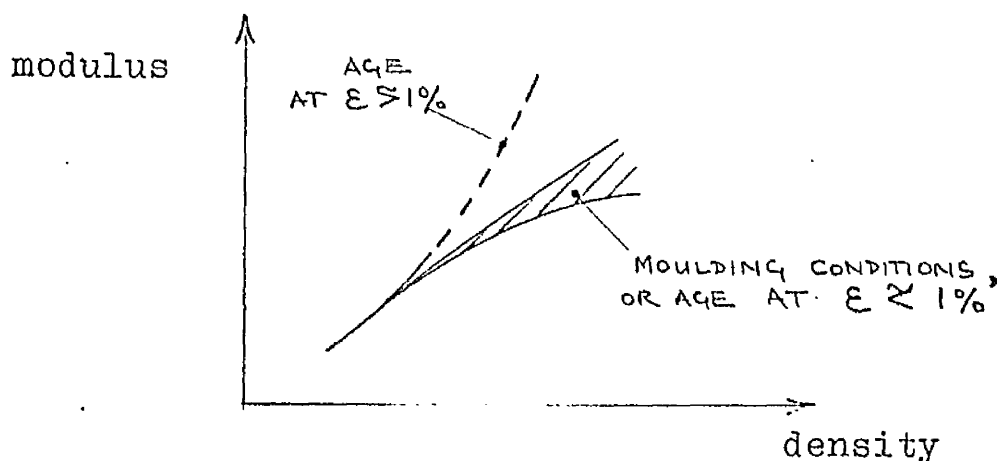


FIG. 4.12

Equation (2) predicts a tendency in the modulus - density relationship of the type shown in Fig. 4.12 to be due to ageing at strains above approximately 1%. Moulding cooling rates and annealing treatments* appear more inclined to produce a different modulus - density relationship as shown in Fig. 4.12 and might be better described by an equation of the type proposed by Becker⁽⁹⁷⁾ equation (3)

* and ageing at $\epsilon \gtrsim 1\%$ —————

$$\sigma = \frac{E_{\alpha}(t,x)}{2} \left\{ 1 - \frac{1}{[1 + \epsilon \cdot g(x)]^2} \right\} \text{-----}(3)$$

where $E_{\alpha}(t,x)$ is the modulus of the amorphous phase at time t and for crystalline fraction x

Further discussion of the morphological implications of these stress-strain tests is deferred until after the results of microscopy on the extended tensile test pieces, see Chapter 5.

4.6 Conclusions.

- 1) The rate of modulus increase following from either slower moulding cooling rates or ageing was found to be essentially the same at small strains ($\approx 1^{\circ}/o$). At slightly higher strains ageing appears to have a more beneficial effect on modulus than reducing the cooling rate. For the test conditions applied here ($T = 24.0^{\circ}C$, $\dot{\epsilon} = 0.975^{\circ}/o/min$) all the annealing treatments produced samples having a lower modulus, particularly where voiding occurred following annealing. The fall in the ability of these various thermal history treatments to increase modulus going from ageing, to slower moulding cooling rates, to annealing, strongly suggests that the state of relaxation in the non-crystalline phase is as important a factor as the degree of crystallinity in the absence of inter-spherulitic voiding.
- 2) The small changes in strain to yield may also be related to the state of relaxation in the non-crystalline regions and probably also the comparative moduli of spherulite boundaries and spherulite interiors. At slower cooling rates a condition of imbalance may be produced which so stiffens the spherulite interiors compared with spherulite boundaries that earlier cracking between spherulites occurs as a result of strain concentration in these regions.
- 3) The effects of annealing treatments can be related to the amount of polymer melted and reordered i.e. related to the ratio of annealing to crystallisation temperature T_A/T_C , and the duration of annealing. The improvement in modulus obtainable by annealing is limited by the progressive state of relaxation of the non-crystalline phase and the eventual voiding of spherulite boundaries.

TABLE 4.1a

Sample	C (°C/min)	T _c (°C)	Age Prior to Test (Hrs.)	ρ (g/ml)
1	155	110.4	23	.9029
2	106	111.8	192	.9048
3	51	114.3	575	.9055
4	9.3	121.0	2610	.9066
5	1.4	124.8	695	.9082

TABLE 4.1b

Sample	C (°C/min)	T _c (°C)	Age Prior to Test (Hrs.)	ρ (g/ml)
6A	96	112.8	6	.9035
6B	96	112.8	192	.9047

TABLE 4.1c

Sample	C (°C/min)	T _c (°C)	ρ ₁ (g/ml)	T _A (°C)	T _A /T _c	t _A (Hrs.)	ρ ₂ (g/ml)
1A	164	110.0	.9038	125	1.135	3	.9089
1B	155	110.4	.9042	100	.905	19	.9060
5A	1.4	125.0	.9084	118	.945	5	.9082

C=cooling^{rate}, ρ=density at time of test, ρ₁=preanneal density,
ρ₂=post anneal density.

TABLE 4.2.

The effect of cooling rate — (Age 274 — 575 hours.)

Sample	Cooling Rate (°C/min)	T _c °C	Age Hrs.	Density (g/ml)	Average Stress at ($\frac{KGM}{CM^2}$) Strains	
					0.5°/o	1.5°/o
9	127	109.6	322	.9042	61.1	133.5
10	119	110.9	274	.9040	58.9	130.9
12	73	113.1	524	.9052	62.8	139.1
3	51	114.3	575	.9055	64.6	138.0
14	8.3	120.5	521	.9065	68.3	144.8
8A*	10.5	121.5	274	.9071	67.6	141.8

TABLE 4.3

The effect of cooling rate — (Age 695 — 905 hours.)

Sample	Cooling Rate (°C/min)	T _c °C	Age Hrs.	Density (g/ml)	Average Stress at ($\frac{KGM}{CM^2}$) Strains	
					0.5°/o	1.5°/o
13	24	116.3	905	.9060	65.6	142.3
7	15	118.9	768	.9060	64.8	141.7
5	1.4	124.8	695	.9082	72.4	150.0
15	1.3	125.7	875	.9085	72.2	153.3

TABLE 4.4

The effect of age — (Cooling rate 96 — 106°C/min.)

Sample	Cooling Rate (°C/min)	T _c °C	Age Hrs.	Density (g/ml)	Average Stress at ($\frac{KGM}{CM^2}$) Strains	
					0.5°/o	1.5°/o
6A	96	112.8	6	.9035	54.9	118.0
6B	96	112.8	192	.9047	59.7	131.5
2	106	111.8	192	.9048	63.0	134.2
16	102	111.5	4450	.9052	64.1	148.0

* Thermally degraded sample B, from Chap. 2, see page 46.

TABLE 6.1c

Sample	C (°C/min)	T _c (°C)	ρ ₁ (g/ml)	T _A (°C)	T _A /T _c	t _A (Hrs.)	ρ ₂ (g/ml)
19A	116	109.4	.9035	106.0	.968	0.5	.9049
19B	116	109.4	.9035	105.9	.968	2	.9055
19C	116	109.4	.9035	105.9	.968	10	.9058
19D	116	109.4	.9035	112.0	1.022	2	.9059

C = cooling rate

ρ₁ = preanneal density

ρ₂ = post anneal density

T_A and T_C = annealing and crystallisation temperature

t_a = the duration of annealing

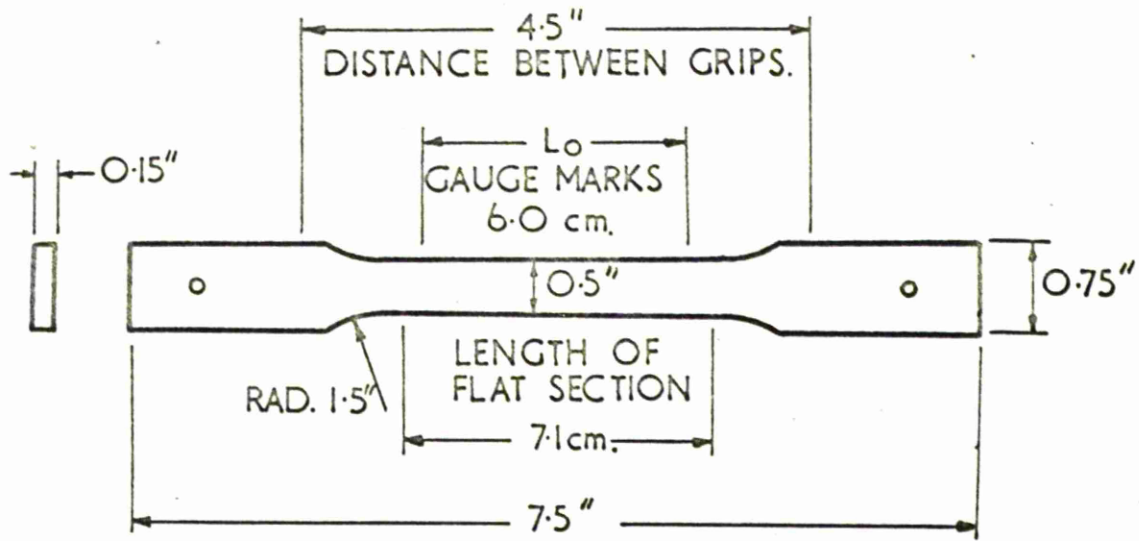


FIG. 4.1

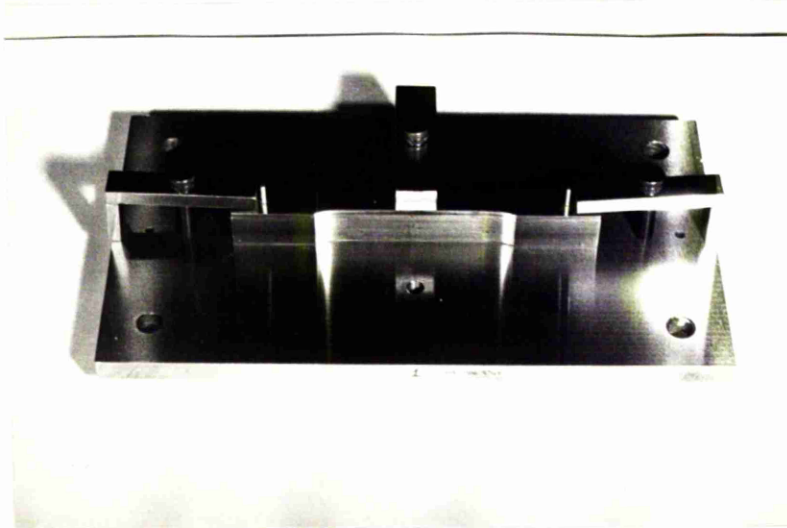
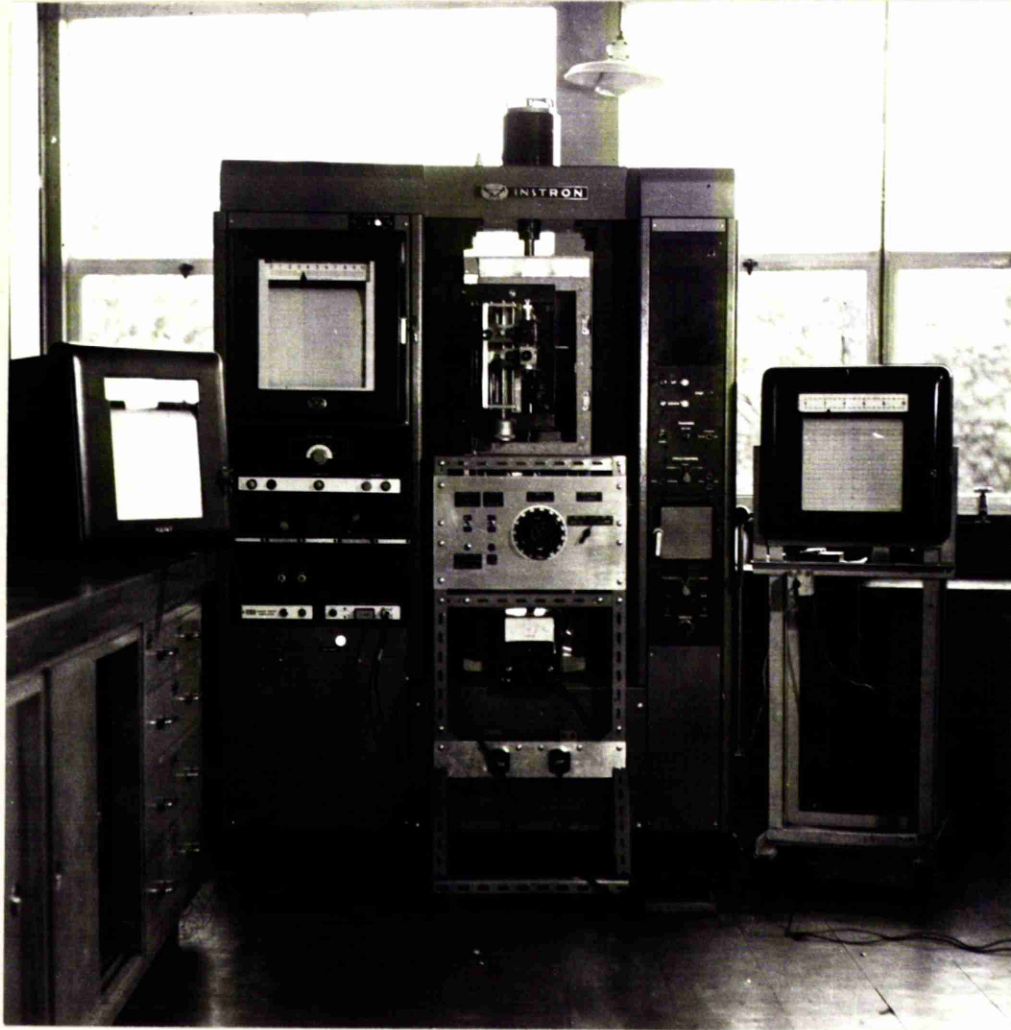


FIG. 4.2

FIG. 4.4



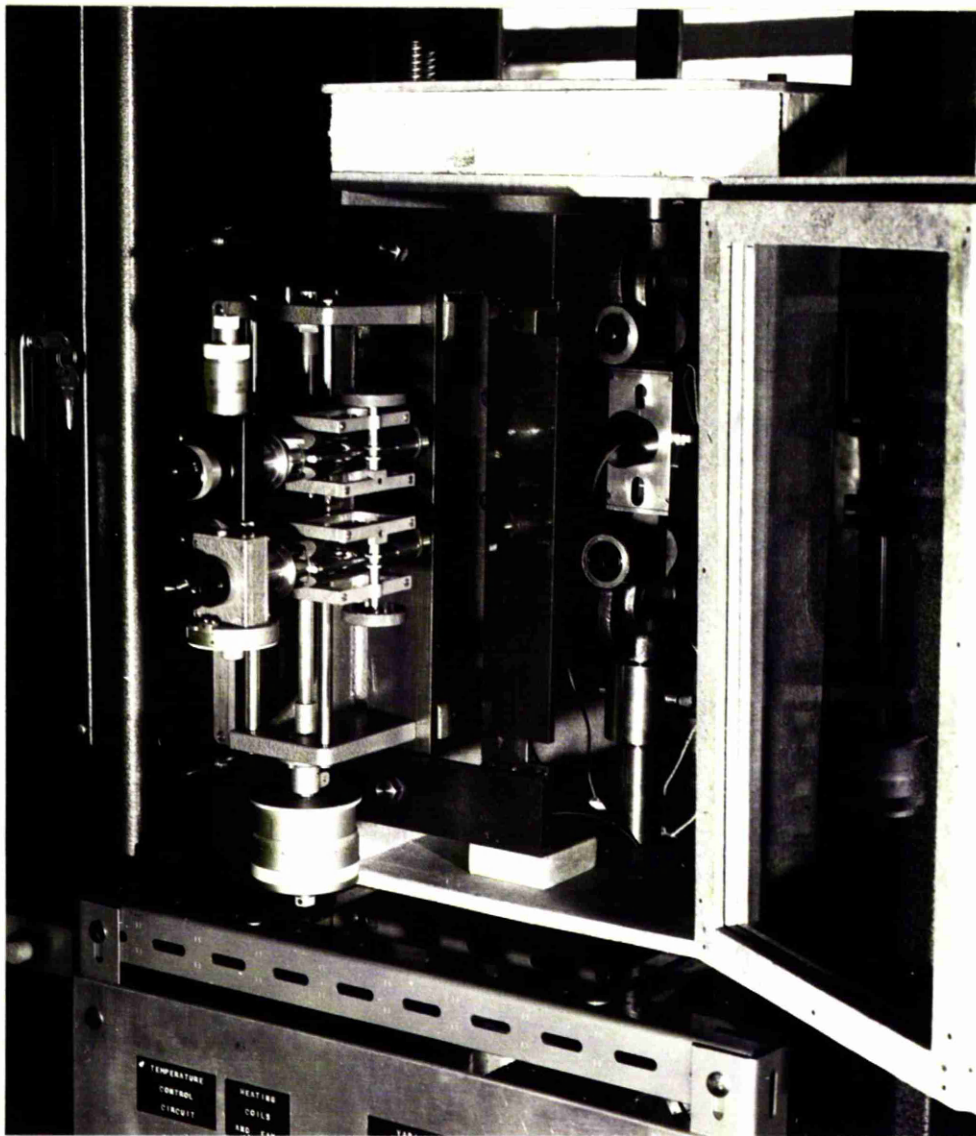


FIG. 4.5

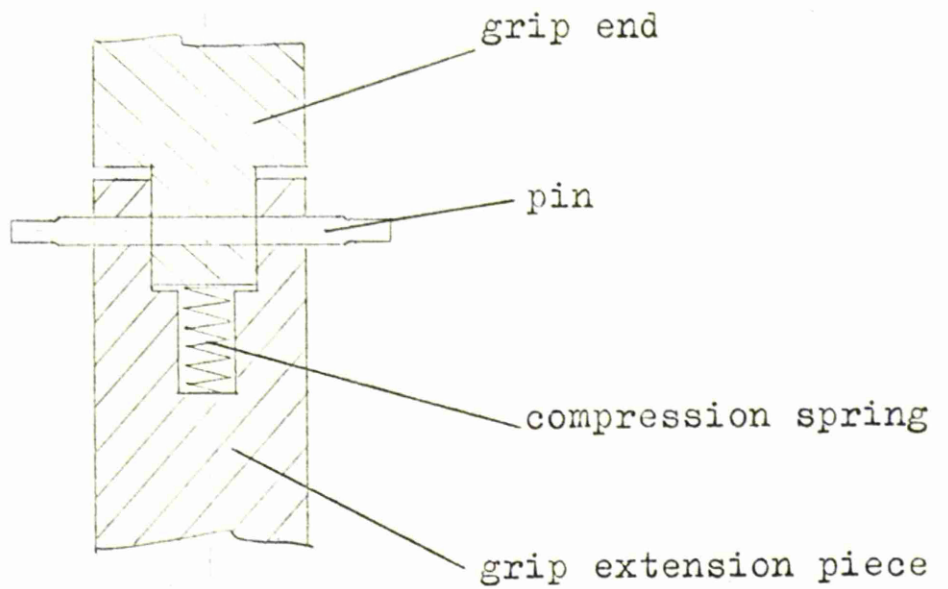


FIG. 4.11

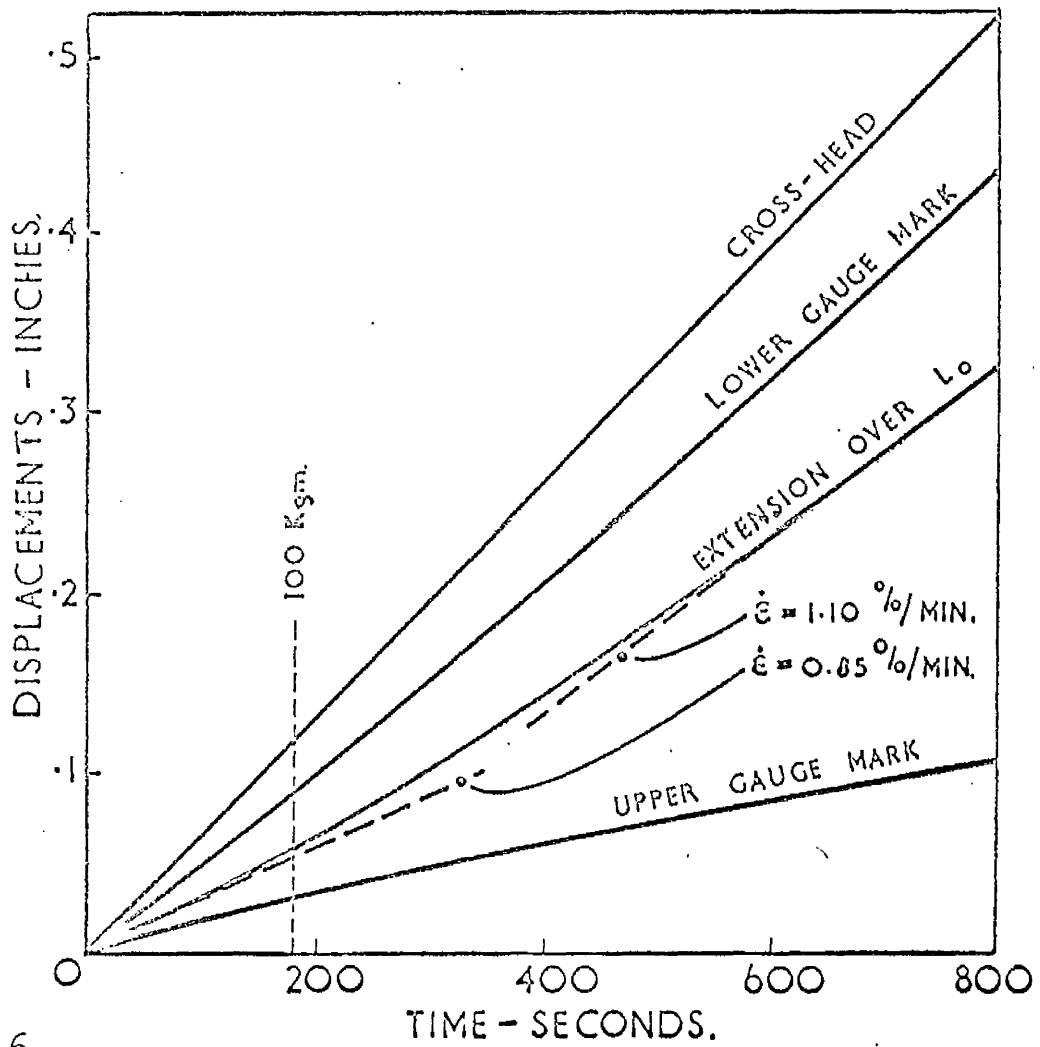


FIG. 4.6

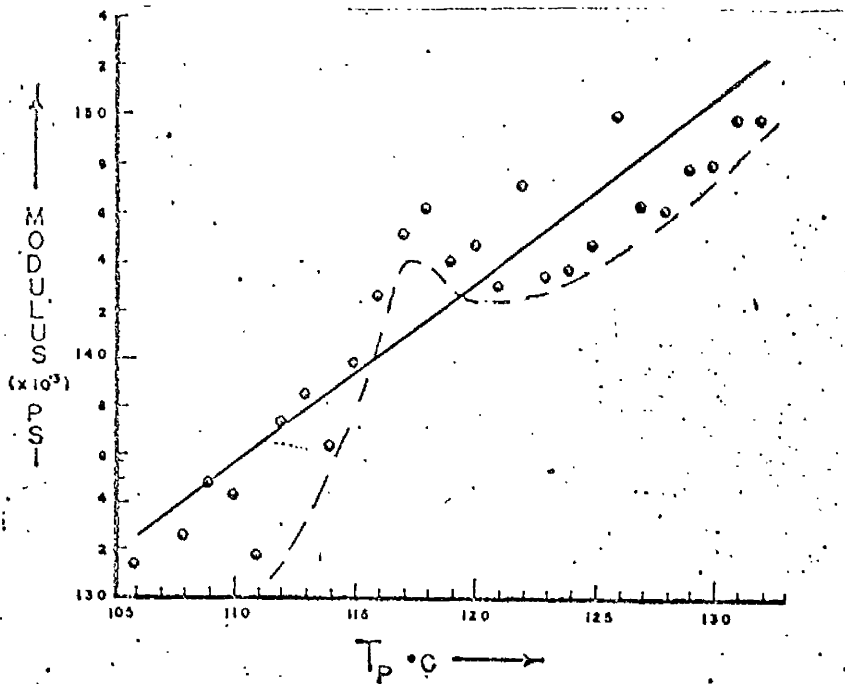


FIG. 4.7

Reproduced results of Beck and Ledbetter.⁽⁶⁸⁾
 T_p is equivalent to T_c in this research.

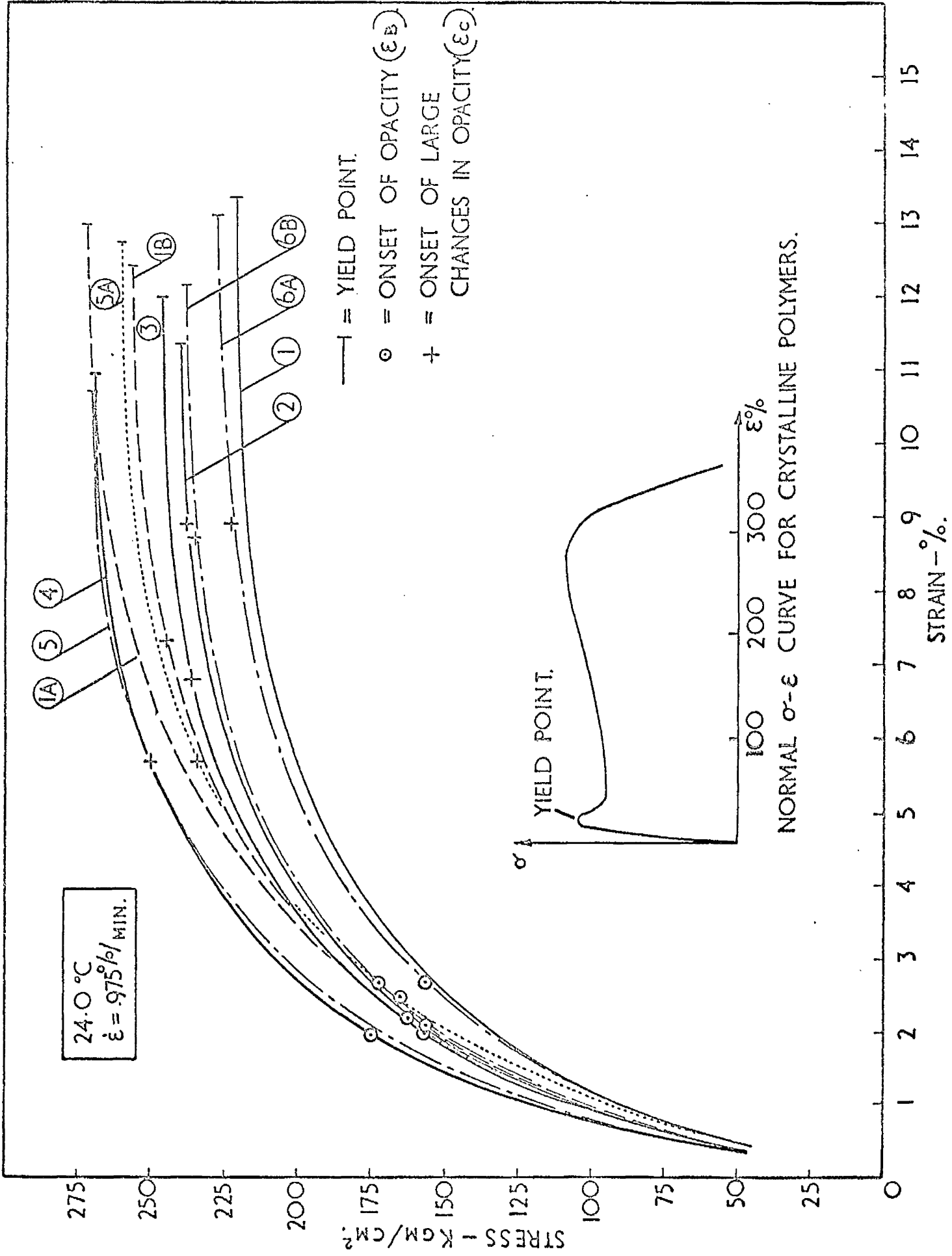


FIG. 4.8. THE EFFECT OF THERMAL HISTORY ON THE STRESS-STRAIN CURVE.

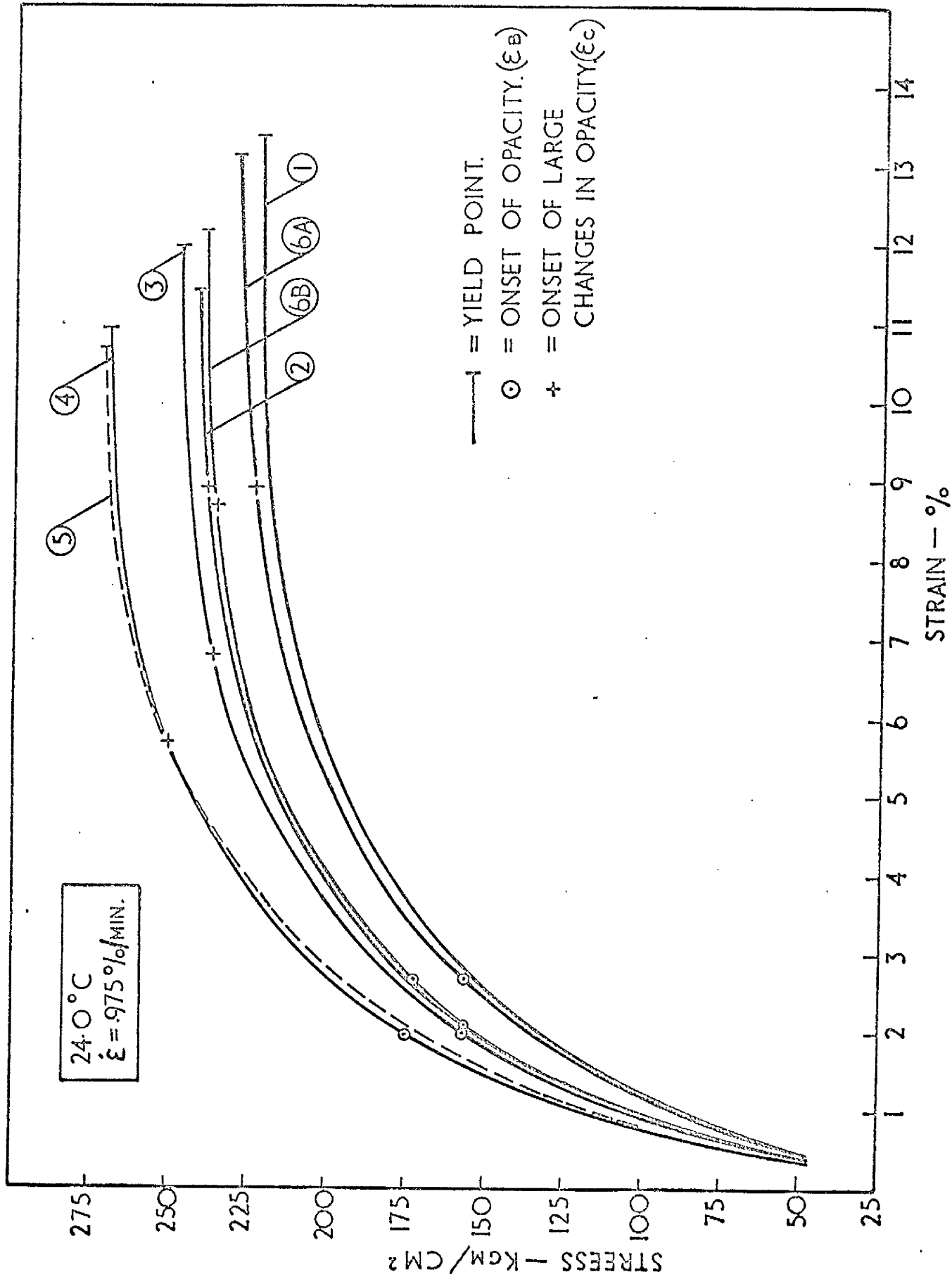


FIG. 4.8c.

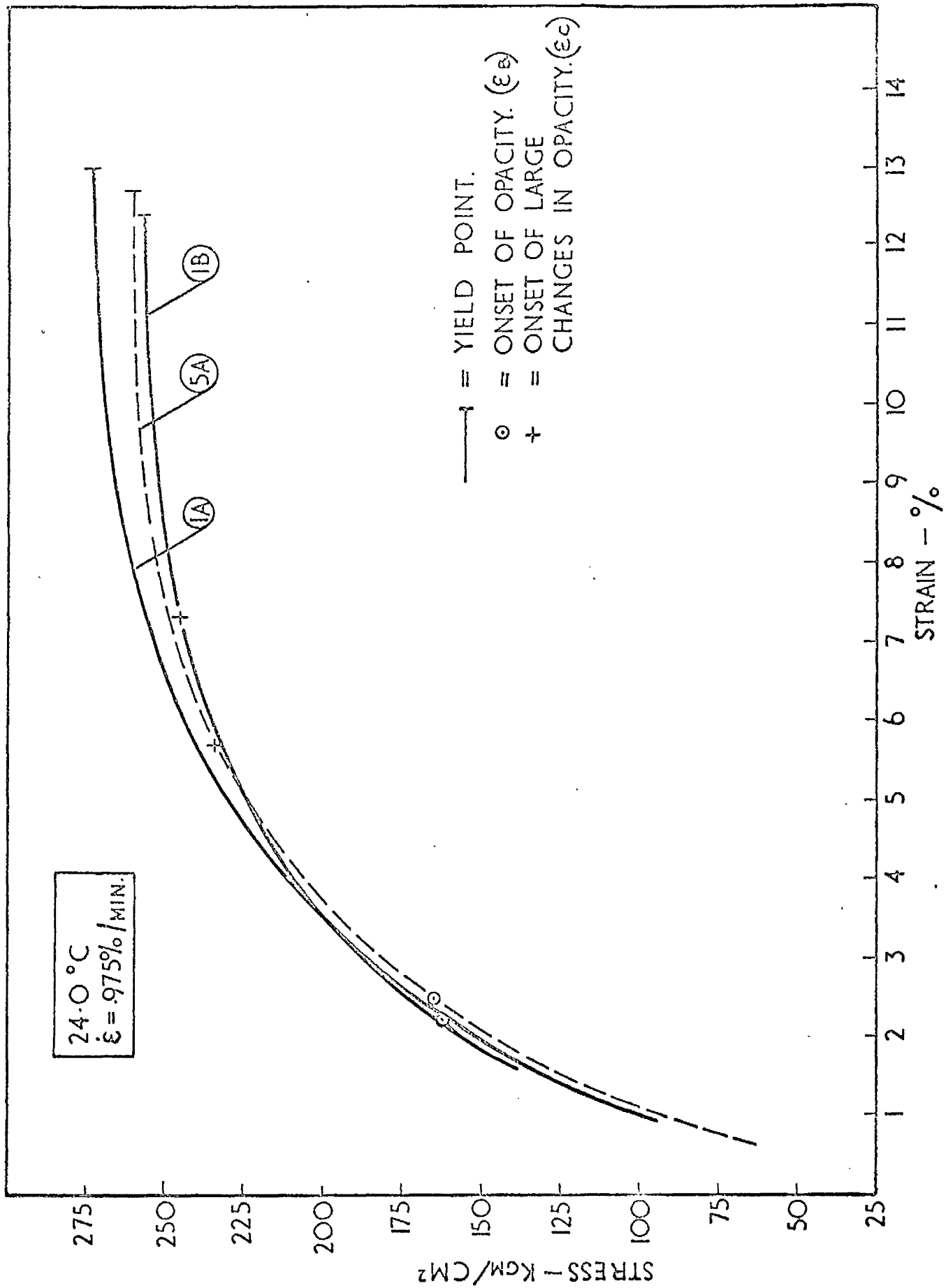
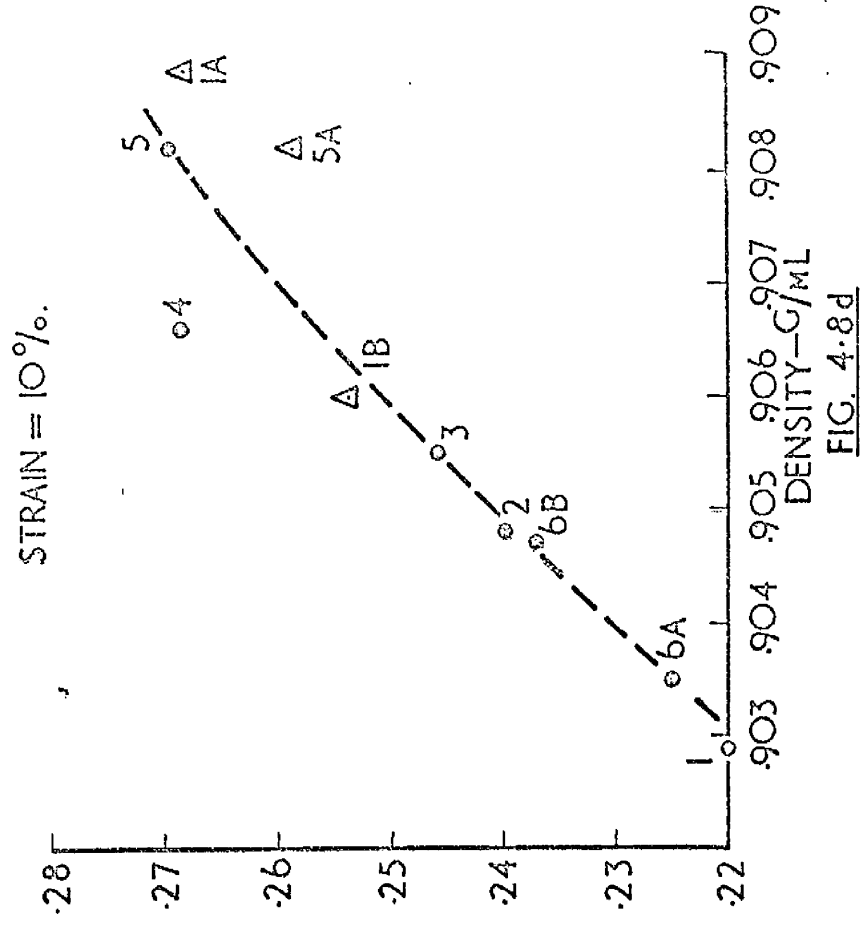
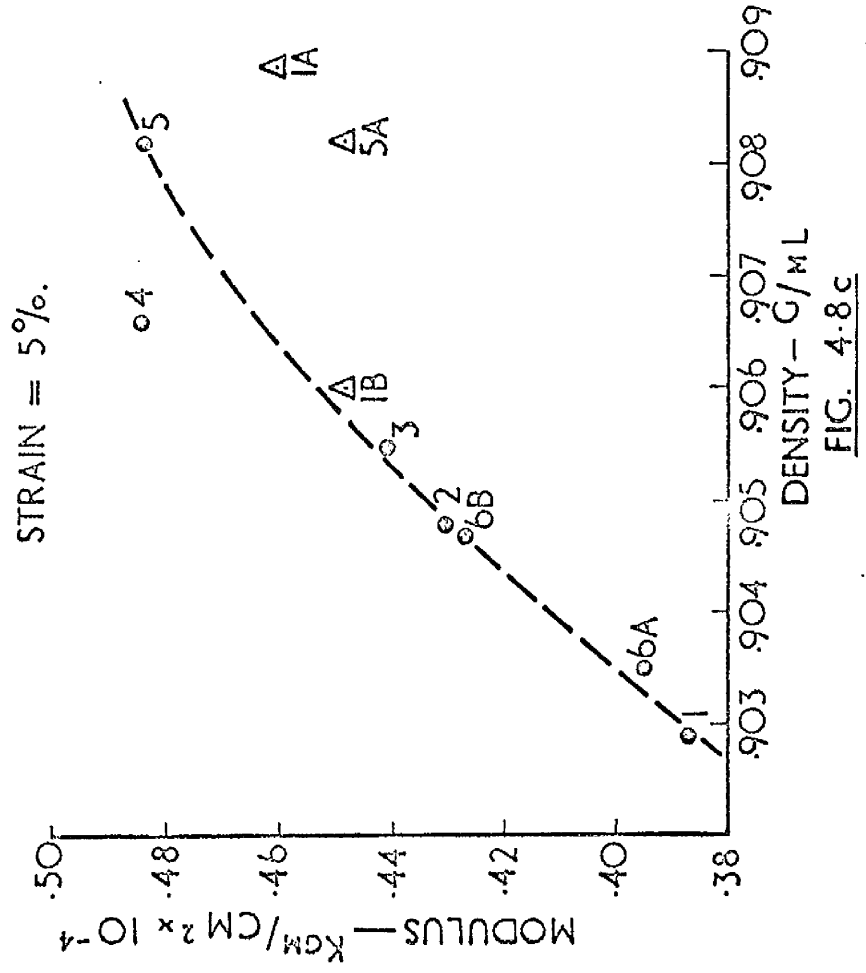


FIG 4.8b.



FIGS. 4.8c,d. THE EFFECT OF THERMAL HISTORY ON SECANT MODULUS.

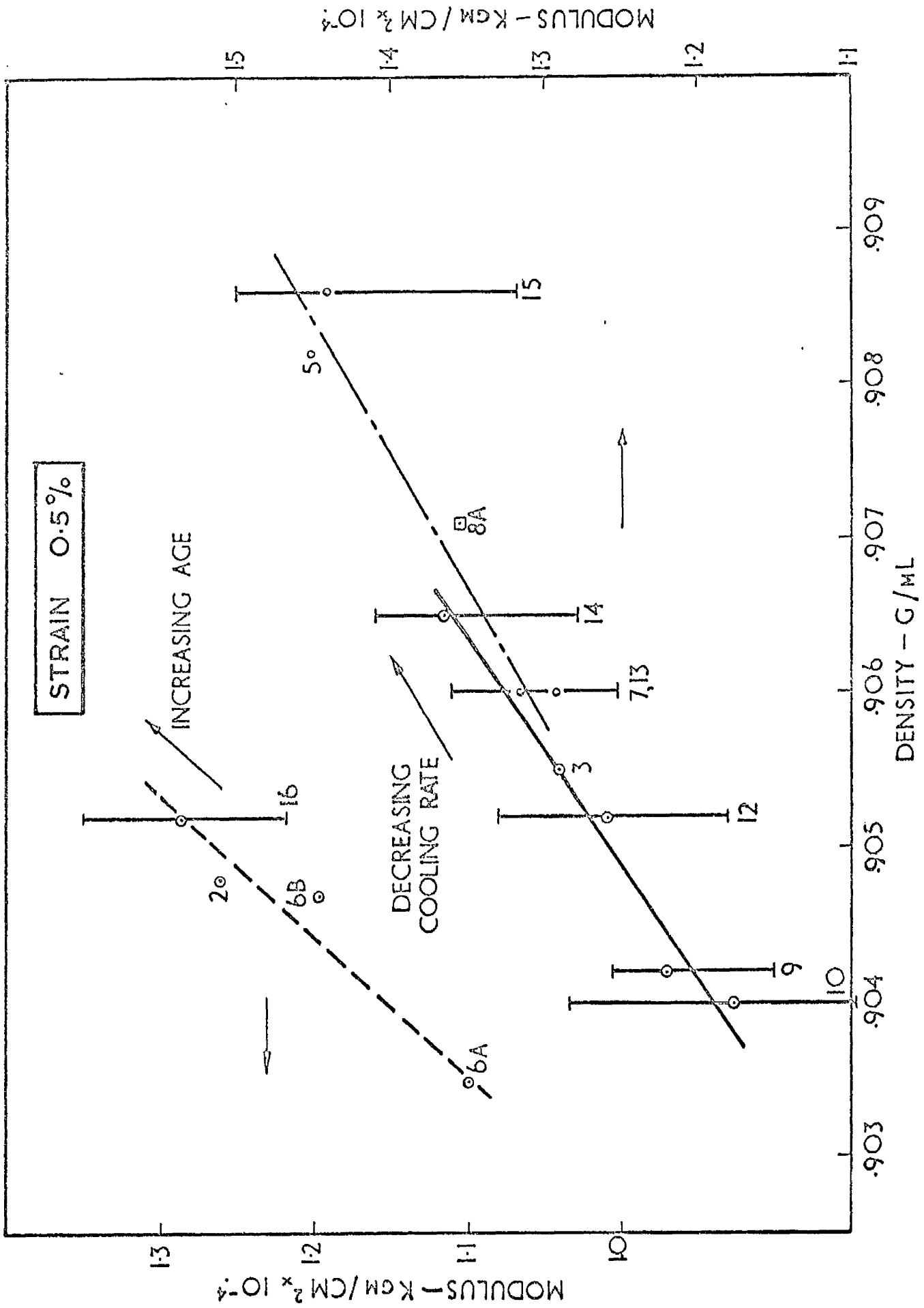


FIG. 4.9 THE EFFECT OF THERMAL HISTORY ON SECANT MODULUS.

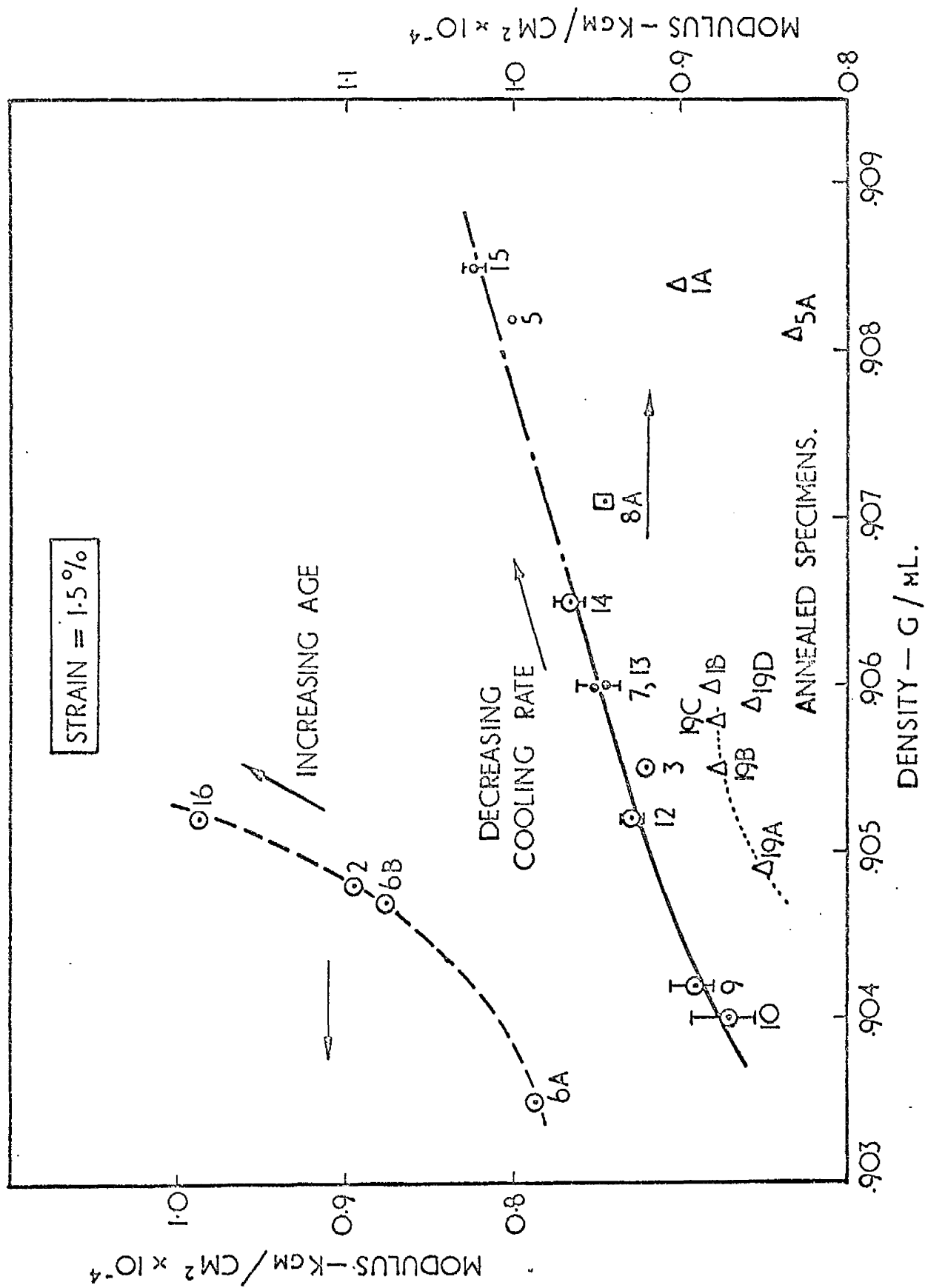


FIG 4.10. THE EFFECT OF THERMAL HISTORY ON SECANT MODULUS.

5. OBSERVATIONS ON THE COURSE OF DEFORMATION OF POLYPROPYLENE UNDER VARIOUS STRESS SYSTEMS.

5.1. Microscopy of tensile test pieces from Chapter 4

5.11. Strain Whitening.

Tensile test pieces from the tests described in Chapter 4 having all been subjected to the same strain of 15⁰/o showed clear signs of strain whitening. A measure of the overall change in whiteness or opacity from samples 2,4,5,1A, and 5A is shown in transmitted light negatives of the actual test pieces in Fig. 5.1. There is a marked tendency for decreased whitening as the specimen's cooling rate is increased, whilst the annealed specimens 1A and 5A showed very pronounced whitening. Annealed specimen 1B had a degree of whiteness between that of samples 4 and 5. For convenience the table of relevant thermal histories is reproduced at the end of this chapter.

5.12. Microscopy of Tensile Test Pieces.

After several stress-strain tests had been completed on samples which covered a range of thermal histories, pieces were microtomed from near the centre of the gauge length and the middle of the test piece to observe the deformed structure. In order that the effect of tensile testing on the microstructure was not confused with possible microtome damage all samples were microtomed in a direction at 45⁰ to the tensile axis of prior extension and liquid nitrogen was used as a coolant to minimise orientation of the structure. Since microtomed films would reveal a relaxed structure they were mounted under light tension along their tensile axis to simulate their condition in the tensile

test piece.

Cracking between spherulites was observed in relaxed films, but under this light tensioning many more cracks were revealed within spherulites. It therefore became necessary to ensure that this cracking did not occur as a direct result of the mounting procedure. This was ascertained using two films, one from an unstrained sample, the other from a prestrained tensile test piece, which were mounted side by side and tensioned by the same amount. The former showed no cracking whatsoever, whilst the latter showed a typical cracking pattern. This was later confirmed by extending microtomed films uniaxially up to high strains which still produced no tendency to cracking, see section 5.2.

A degree of cracking was noted to occur in all the tensile samples tested, but the amount of cracks varied, becoming most dominant in slow cooled and annealed samples, and barely traceable in the fastest cooled samples. Examples of the type of cracking found ^{within spherulites} are shown in Figs. 5.2 a - d.

In type I, II spherulites cracks were always perpendicular to the spherulite radius and positioned along the polar axis of the spherulite as defined by the extension direction see Figs. 5.2a, b, and c respectively.

In type III spherulites cracking was nearly always radial and positioned in the equatorial plane of the spherulite, as shown arrowed in Fig. 5.2d and c.

A count of the number of interspherulite 'cracks' per cm. in the stretched direction for samples covering the range of cooling rates and annealing treatments gave the results shown in table 5.1 over. Results for the rapidly cooled samples must be regarded as very approximate due to the small

size of the structure and the difficulty of clearly resolving the difference between a crack and a well defined spherulite boundary.

TABLE 5.1.

Sample		Number of inter-spherulite cracks per cm. in the extended direction.
1	C = 155°C/min	~ 0
2	" 106 "	6
4	" 9.3 "	15
5	" 1.4 "	80
5A	$T_A/T_C = .945$	20
1A	" 1.135	~ 35
1B	" .905	~ 20

Occasionally a drawing out of the structure was seen as a shadow within spherulites in the same position as cracks would have occurred, shown arrowed in Fig. 5.2e, or between spherulites, shown arrowed in Fig. 5.2f. The latter figure also shows how voiding can develop during drawing out, appearing as dark spots of unpolarised light. This is probably the cause of the dark spots which dominate the polar axis in many spherulites, see for example Figs. 5.2f and d. Fig. 5.2e also shows a void between spherulites.

5.13 Discussion.

The above observations of the deformed spherulite matrix for samples of varying moulded cooling rates and annealing treatments as detailed in tables 4.1a and c show that

- a) Strain whitening varies according to the cooling rate used in sample preparation becoming more severe as cooling rates are reduced. A large increase in whitening appears between samples 4 and 5.

and

- b) The degree of strain whitening varies in the same order as the number of inter-spherulitic cracks in 'as moulded' test pieces and sample 1B. In annealed samples 1A and 5A however, a larger degree of strain whitening occurs in the presence of a lesser degree of inter-spherulitic cracking. This greater whiteness is attributed to an additional amount of cracking within spherulites. In sample 1B. the value of $T_A/T_C = 0.905$ would appear to have been too low to produce a gross tendency to cracking within the spherulite.

It is not expected that the crystallisation conditions which prevail during the moulding programme produce voids between PP spherulites in the 'as moulded' condition. These were neither observed prior to testing nor does the continued upward trend in increase in density with increased T_C in Figs. 3.6 and 3.7 indicate their presence.

The above results for 'as moulded' samples, therefore, suggest that either

- i) spherulite boundaries may be weakened compared with spherulite interiors by an internal stress on the boundary following from an increase in

crystallinity of the spherulite interior during secondary crystallisation,

ii) the bonding between spherulites becomes inferior as T_C is raised,

or/and

iii) increased spherulite size induces larger compatibility forces between spherulites which are in themselves unable to relax faster than the applied strain-rate.

Electron microscopy on PE has shown for example, ⁽³¹⁾ that the number of inter-spherulite links may be considerably reduced at higher crystallisation temperatures which tends to support postulate (ii). However, samples 4 and 5 having T_C 's of 121.0 and 124.8°C respectively, have moulding conditions which place them either side of the discontinuity for both sample density and changed crystallisation kinetics found in Chapter 3. Sample 4 is in fact the sample having the highest T_C but still lying on the low density part of the curve to the left of the discontinuity in Figs. 3.6 or 3.7. The difference in average spherulite diameter between samples 4 and 5 is about 0.9×10^{-2} cm. to 1.15×10^{-2} cm. (see Fig. 3.3 for spherulite dia. versus T_C) and it is felt that this change in itself has very little effect on inter-spherulite compatibility forces during extension. The sudden increase in density in sample 5 would affect the internal stress on spherulite boundaries, and as concluded in Chapter 3, the accompanying change in crystallisation kinetics may involve a loss of intermediately ordered material which may well comprise the sort of tie molecule bundles found by Keith, Padden and Vadimsky ⁽³¹⁾ to link crystalline areas and spherulites with one another. It is concluded, therefore, that postulates (i) and (ii) are more important and contribute to the large increase in the degree of cracking going from sample 4 to sample 5.

The effect of moulding cooling rate would therefore appear to primarily affect the readiness of spherulite

boundaries to crack. Weakening within the spherulite, whilst it probably occurs also, especially at $T_C > 121^\circ\text{C}$, does not appear to be on the same scale as that found following the annealing treatments where there is evidence to suggest that some inter-spherulitic cracking gives way to cracking within the spherulite.

In the case of annealed samples 1A and 5A the observations made confirm the idea put forward in Chapter 4 that these weaken both spherulite boundaries and spherulite interiors. The fact that their ability to embrittle the spherulite interior follows where $T_A/T_C \approx 0.91$, (the annealing treatment given to 1B, $T_A/T_C = 0.905$) suggests that the cause is associated with a gross reordering of the fine structure which may involve conversion of partially ordered regions into more ordered regions and melting and recrystallisation of smaller crystalline regions. It has been previously suggested ⁽⁴⁵⁾⁽⁵⁰⁾ that such structural changes leave the inter-crystalline regions in a more relaxed state, and thereby improve ductility. This mechanism would, however, primarily affect the β stress propagation route, see Figs. 1.7a, b and c reproduced below.

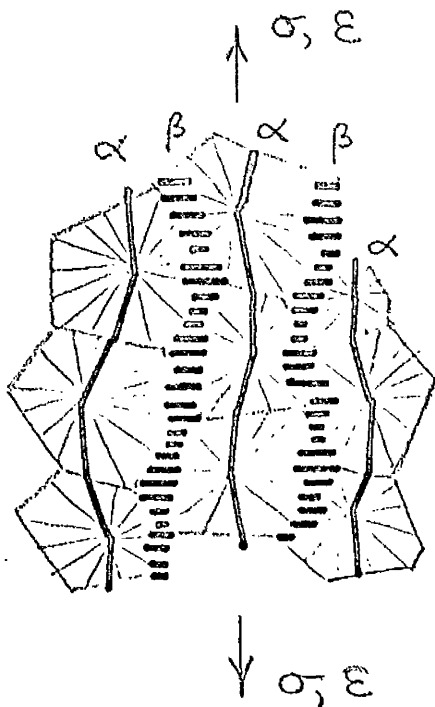


FIG. 1.7a

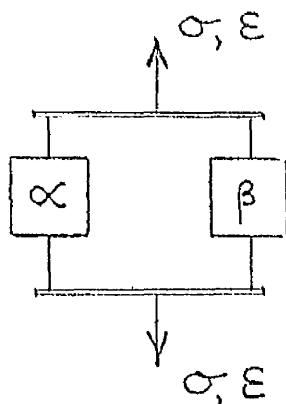


FIG. 1.7b

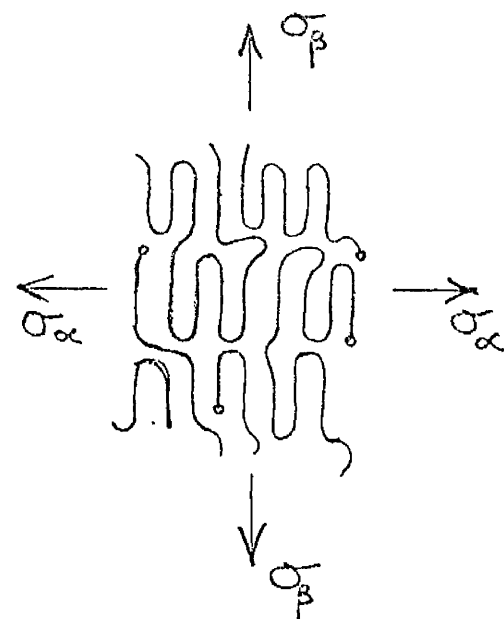


FIG. 1.7c

Microscopy has shown here that the cracking is largely concentrated into the polar regions of the spherulite which comprise the α stress propagation route. It is therefore suggested that since the α and β stress routes are connected in parallel, see Fig. 1.7b, the weakening in one such route which will throw greater stress onto the other is sufficient under the present test conditions to produce an increased tendency to crack in the other route. The overall ductility of the material may thus be increased whilst at the same time producing an earlier tendency to microscopic cracking within the spherulite. The fact that cracking still occurs within spherulites of annealed specimens shows that predominantly the spherulite boundaries must still be bonded at least as well as their interiors. In this context it might be concluded that cracking between spherulites may be chiefly the cause of the slightly decreasing strain to yield in 'as moulded' test pieces, but that cracking of the kind found within spherulites does not lead to this slightly premature yielding.

It is important to note that in crystalline polymers cracking which involves a drawing out of molecules into an aligned state at the crack root ⁽¹⁰⁴⁾⁽⁶⁶⁾ may be part of their normal visco-elastic response at strains greater than about 2⁰%. Relaxed microtomed films showed that the cracking which was within the spherulites was recoverable to the extent that these cracks collapsed, but that cracking (or separation) between spherulites was substantially non recoverable. It appears likely, therefore, that cracking within spherulites involves a process of localised drawing of the above type which may help reseal the crack during recovery but that rupture between spherulites may start earlier and proceed beyond this to a stage of complete separation.

A study of strain whitening in PE by Bettelheim and Stein⁽¹³²⁾ has shown that it is the direct result of a process of voiding which accompanies drawing out of the structure. Submicroscopic holes created in this way have a different refractive index to the parent polymer and cause turbidity and light scattering. The same authors also showed that the density of the matrix outwith the holes is very slightly reduced, probably due to a change in the unit cell, following extension. Similar results for both strain whitening and the production of a change in the ordering of the crystalline phase have been previously found⁽⁴⁵⁾ in PP. In this respect it is interesting to note that a low-angle light scattering study⁽⁸⁵⁾ on PE has shown that long after the spherulite has recovered its shape during recovery, considerable macroscopic strains remain in the overall specimen.

Biaxial tension has been shown by Geil⁽⁷⁾ (Chapter VII, part 3) to produce voiding between drawn out fibers as was found in the centre of the tensile test pieces in this work, see Fig. 5.2f. Others⁽¹³³⁾ have shown how imposing a biaxial stress can produce premature failure in lower M.W. samples of PE. Since a biaxial stress was not imposed during tensile testing as in Chapter 4, the voiding and cracking observed might develop as the result of more complex stresses induced at the microscopic level, or possibly because of lack of bonding between structural units. This factor is examined further by testing thin films in which complex stressing of this kind does not develop, see section 5.2.

5.2. Uniaxial extension of microtomed films.

5.21. Introduction.

In order to follow the deformation behaviour of the spherulitic matrix it was proposed to extend thin microtomed films taken from the sheets of moulded plastic.

Microtomed films have an advantage over films grown between glass slides for the purpose of extension because they do not have the natural constrictions of film thickness at spherulite boundaries which have been found (63)(134) in grown films. The presence of stress concentration between spherulites would lead to spurious results in assessing the response of a bulk spherulitic matrix to extension. Moreover, microtomed films can be taken from a block of material for which measurements of crystallisation temperature can be made at fast cooling rates. Up to the present most examinations of the extended spherulitic matrix have been on samples crystallised under artificial conditions comprising high crystallisation temperature and the constraint of two parallel surfaces to produce two dimensional spherulites. Spherulitic structures grown under such constraining conditions appear liable to abnormal nucleation (112)(21) and may even have a morphology different from the bulk grown structure, as evidenced by the variation of spherulitic growth rate with film thickness. (135)

Any study of the deformation behaviour of thin films must, however, be regarded as an approximation to the process of deformation in a three dimensional matrix since morphological connections out of the film's plane are eliminated.

Microtoming does, however, have the disadvantage of producing surface damage and orientation of the film.

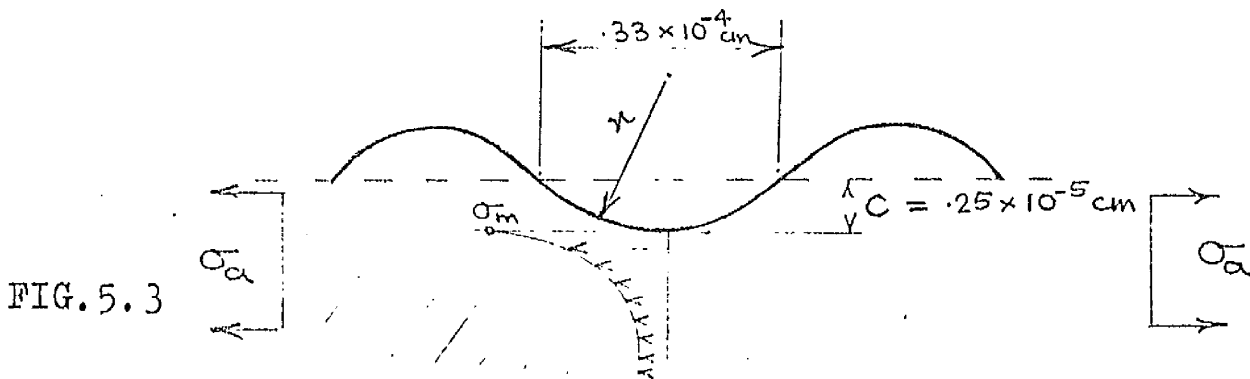
A measure of the typical size of surface indentation was assessed from an electron micrograph of a replica of the film surface. Both types of microtome damage could be identified as:

- a) broad parallel scores of regular undulations about 0.25×10^{-5} cm. deep and occurring with a frequency of about 0.66×10^{-4} cm.
- and b) a drawn out structure parallel with the microtoming direction. The depth of material orientated in this way has been found⁽¹³⁶⁾ by birefringence measurements to be of the order of several hundred Å.

The effect of surface 'notches' on the maximum stress σ_m of an elastic isotropic material is related to the applied stress σ_a , the depth of the notch c and its root radius r by the equation,⁽¹³⁷⁾

$$\sigma_m = \sigma_a \left[1 + 2 \left(\frac{c}{r} \right)^{1/2} \right] \quad \text{---(1)}$$

The geometry of the notch on the microtomed film surface is shown in Fig. 5.3. The ratio $c/r \cong .05$.



The fact that $r \gg c$ for the type of damage (a), makes stress concentration negligible.

The greatest fraction of orientated material from the source of damage (b) would be about 2% of the thickness of a 10μ thick film, as was used in this work, and this type of microtome damage was also neglected.

The effects of both types of damage were minimised by microtoming at 45° to the direction of subsequent extension and by using liquid nitrogen as a coolant during microtoming.

5.22. Apparatus and Procedure.

A jig for extending microtomed films was made which would bolt onto the observation stage of the Vickers Projection Microscope. This jig, which is shown in Fig. 5.4, comprised a fixed anvil and a sliding anvil both of which engaged via tongue and groove into a brass frame. The fixed anvil was held by a pin whilst the sliding anvil could be actuated against a compression spring by turning a wing nut, outside the frame, which engaged on a screw threaded rod joining the sliding anvil.

The microtomed film was made up into a small tensile test specimen by reinforcing with cellotape a length of the film at either end outside the extended length. The film width was trimmed to make the overall dimensions of tested material $\sim 0.6 \times 0.15 \times 10^{-3}$ cm. The film ends thus reinforced with cellotape were held in grips which were rotated through 90° and slotted into each anvil. Crude gauge marks of thin opaque cellotape strips were used, enabling identification against a hair line of two points on the film the separation of which could be measured on the microtometer which racked the microscope observation stage parallel with the direction of extension.

It was ascertained that overall strains measured for the film in this manner tended to underestimate the microscopic strain of the centre of the film and overestimate strains near the ends of the film due to the effects of lateral reinforcement/^{at film ends} on local strains.

Another method was used for assessing the macroscopic strain by noting the change in orientation of the surface score marks ($\frac{\tan\gamma'}{\tan\gamma}$) which can be related to the strain (see appendix V) by equation (2)

$$\epsilon_x = \sqrt{\frac{\tan\gamma'}{\tan\gamma}} - 1 \quad \text{-----(2)}$$

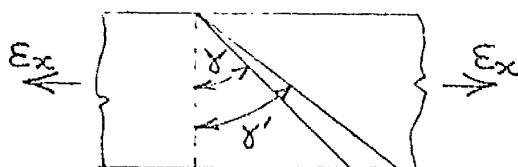


FIG. 5.5

The derivation of equation 2 requires the assumption that there is no change in volume or thinning of the film during extension, and consequently this method was found to break down at moderate strains of the order 10⁰/o.

An average strain from these two methods was used in measuring the development of drawing out of the structure at $\epsilon > 10^0/o$.

5.23. Results.

A drawing out of the structure in lines perpendicular to the direction of extension, of the kind frequently described in the literature, (see, for example, Geil⁽⁷⁾ chapter VII. part 3) was seen to occur for the whole range of moulding preparations and annealing treatments used in this work. A single exception was found in a sample which had been moulded incorrectly from granules; this is described in section 5.24. Line drawing of this kind became detectable at strains of the order 8⁰/o and took routes regardless of the spherulite matrix; an example of this is shown at a strain of 30⁰/o in Fig. 5.6a. With increased extension the lines of drawing moved to meet each other as can be seen in the RHS of Fig. 5.6a. until the whole structure was drawn out as in Fig. 5.6b.

which is at about 250^o/o strain. At these high strains, the spherulitic form could still be seen faintly.

At no time was the process of drawing seen to develop into cracking of the kind found in tensile test pieces. Weakness between spherulites in very slow cooled samples appeared only at high strains, and then took the form of a separation parallel with the strain as shown in Fig. 5.6b.

The fact that the drawn lines appearing in Fig. 5.6a spread in the direction of extension to meet one another is taken as clear proof that they are in fact drawn out structure and not cracks which could propagate at right angles to the extension direction. In annealed samples showing voids prior to extension these were found not to become catastrophic cracks but appeared to be held by drawn out material at the crack route.

Voiding, appearing as many small spots across the film, often accompanied the process of drawing out, but became very pronounced where drawing took place locally via a neck in the film. This can be seen clearly in the RHS of Fig. 5.6c which covers the region of drawn and undrawn material. Such films continued to draw out and were left with many ellipse shaped holes having their major axis parallel with the extension direction.

It should be noted that focusing in these photographs was made difficult by the different depth of features, such as drawn material and the edges of cracks.

5.24. Note on Failure in Improperly Moulded Material.

In a sample which had been moulded into a plug from granules, a type of columnar growth appeared between the interfaces of granules as the result of using an inadequate melting procedure (210^oC held for 30 secs.). This growth

could not be referred to as 'line' nucleated since it appeared to cross whole faces of granules. A microtomed film including such a structure was extended in the usual way and showed signs of early failure between the faces of columnar growth as shown in Fig. 5.6d which is at an overall strain of 40⁰/o.

This type of flaw, resulting from improper moulding, has been found (138) to provide the foci for a series of fracture initiation points, and it is interesting to note in this respect the alternation of poorly bonded regions with well bonded regions seemingly resulting from a point nucleus rather than a surface nucleation along the boundary between uncoalesced granules.

5.3. Extension under imposed non-axial conditions

5.31. Biaxial Tension on Microtomed Films.

Microtomed films, prepared as in the last section, were extended under biaxial tension simply by restraining part of the film edges by cello-taping them to a glass slide, whilst the film was extended in its axial direction. Under the assumptions of an elastic, isotropic material, and constant volume, in zone A of Fig. 5.7, $\sigma_y = \frac{1}{2}\sigma_x$. In this zone a large amount of cracking occurred of the type shown in Fig. 5.9. The area of most severe cracking within spherulites appeared dominantly in the radial direction, and was orientated at approximately 45° to the axis of the film as illustrated in Fig. 5.7. The stresses on this plane, which is the plane of maximum shear stress, are shown in Fig. 5.8.

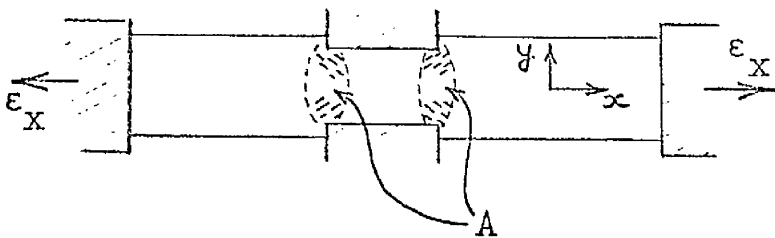


FIG. 5.7

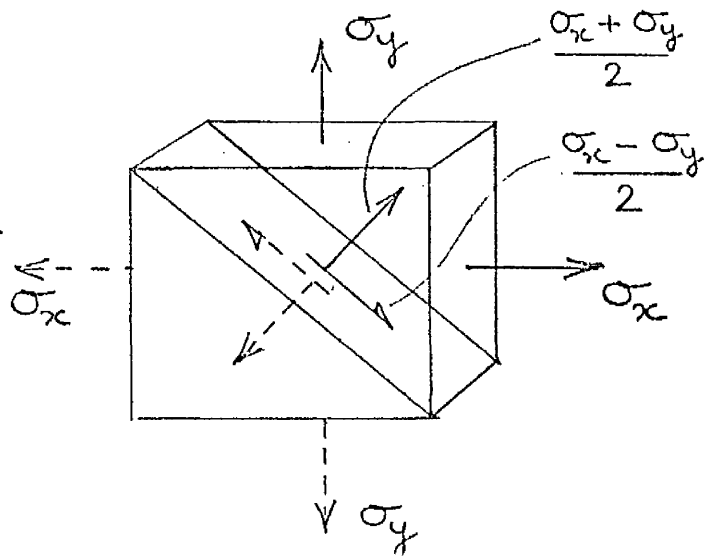


FIG. 5.8

As would be expected from the results of uniaxial extension of microtomed films cracking was not normally observed outside zone A. Cracking was, however, observed outside zone A in those cases where the film width in this reduced length of 'uniaxially' tested material was of the

same order as its length, and might be attributed to a similar development of biaxial stressing due to restriction across the film width. This effect could be checked quite independently by subjecting a tensile piece having a width/length ratio $\cong 1$ to a 'uniaxial' extension. Cracking under these circumstances was dominantly in the polar regions.

These results show that the occurrence of cracking is related to more complex stressing.

5.32. Testing Notched Specimens.

It is possible to increase the state of normal stressing compared with shear stressing on an element of material by utilising the stress field around the root of a notch.

The relationship for the maximum stress in the axial direction σ_m at the tip of an elliptic notch was given in equation (1).

$$\sigma_m = \sigma_a \left[1 + 2 \left(\frac{c}{r} \right)^k \right] \quad \text{—————(1)}$$

Whilst the shape of the stress σ_t in the transverse direction from the notch tip is known⁽¹³⁷⁾ to be of the form shown over in Fig. 5.10. its precise dependence on the notch geometry is very complicated and no explicit expression was found by the author for its dependence on $\frac{c}{r}$ although it is known that its peak value of σ_n increases as $\frac{c}{r}$ increases. The net result of this stress field is to produce a higher mean stress component = $\frac{\sigma_m + \sigma_n}{3}$ as $\frac{c}{r}$ is increased, somewhere very close to the notch root.

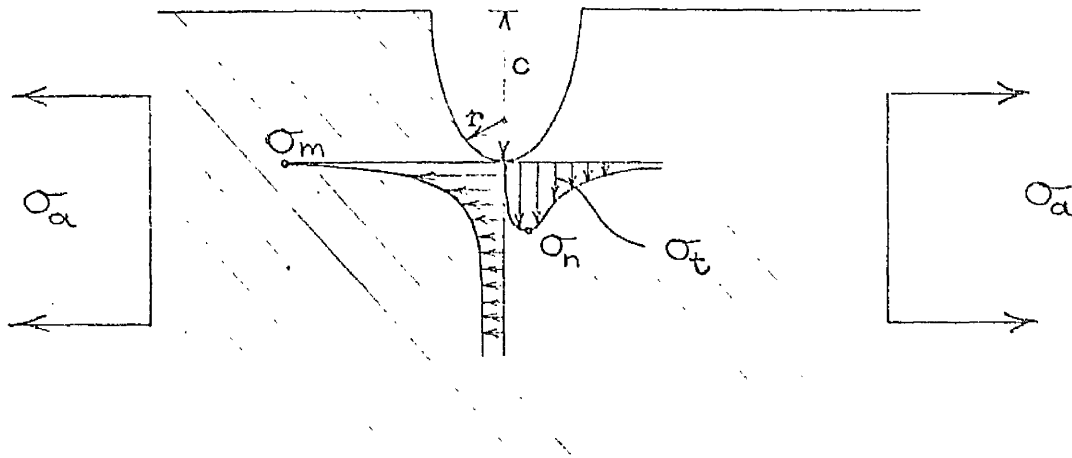


FIG. 5.10

Three pairs of notches of varying root radius r ($\frac{1}{8}$ " , $\frac{3}{32}$ " , $\frac{1}{16}$ "), were machined into a standard tensile test piece so as to leave the same cross sectional area of material under test between each notch pair, c being kept constant throughout ($=\frac{1}{8}$ "). The ratio of the maximum stress to applied stress at the notch root, σ_m/σ_a for each of these notch pairs is 3, 3.31, 3.83 respectively.

A tensile test of this sample showed that opacity occurred at the notch roots in the order of decreasing $\frac{c}{r}$. This shows that the level of stress σ_m and probably also the level of mean stress component $\frac{\sigma_m + \sigma_n}{3}$ influences the stress cracking behaviour of PP.

It was not possible to specify a / strain at which opacity started because it is not possible to define a gauge length within the area of the notch root.

5.4 Discussion on sections 5.2 and 5.3.

The most interesting aspects of the studies in sections 5.2 and 5.3 were

- a) the fact that no cracking developed during the line drawing process in microtomed films subjected to uniaxial extension,
- b) that voiding in these films became very pronounced where they necked down during extension,
- c) that severe cracking or opacity can be induced in biaxially tensioned microtomed films and notched tensile specimens,
- d) that the dominant site of cracking in biaxially tensioned thin films is along spherulite radii and not perpendicular to these radii as found in thick sectioned tensile test pieces.

Electron microscopy has shown (see Geil⁽⁷⁾, chapter VII part 3) that in a distinctly lamellate morphology the lamellae respond to an applied stress by a process of slipping over one another and also by drawing out into a fibrillar material. Furthermore it has been noted ⁽¹³³⁾ that the mode of orientation of the molecular axis in thin extended films can be different from that in thicker films. This can be attributed to the blocking of slip along preferred crystallographic planes in thicker films due to the fact that thicker films must develop complex stressing and have a variety of slip systems due to the inhomogenous nature of molecular packing.

The results of thin film extension in this research when compared with the cracking mode in thicker tensile test pieces would appear to substantiate this idea. The evidence of items (b) and (c) above shows further how

imposed complex stressing (quite apart from the kind of self induced structural complex stressing in thicker test pieces) can bring about the development of gross voiding and cracking.

It is also considered that where the strain-rate applied to a crystalline polymer exceeds the maximum rate at which the structural units can reorientate themselves to relieve the applied stresses the response of the structure will degenerate into a fracture mode. In thicker sections of material the relaxation rate for the various mechanisms of reorientation are probably much slower owing to the material restraint in the thickness direction and the multiplicity of slip systems which will interfere with one another. The cracking along the polar axis of spherulites in the middle of thick tensile specimens would then suggest that the applied strain-rate ($\sim 1^{\circ}/\text{o}/\text{min}$) in these tests exceeds the maximum natural relaxation rate in the α stress propagation route but not the β route in thick sections of plastic. By this argument it should still be possible to produce cracking in thin films if the strain-rates applied are sufficiently high, noting that these may have to be higher than those required in thick sectioned material. Cracking under these conditions has been shown most effectively by Burns. (139)

Extending this argument to tensile testing of normal sections of material it might be expected that testing across a band of strain-rates followed by microscopy of the extended matrix might show a progression from (i) no cracking at all (at $\dot{\epsilon} < 1^{\circ}/\text{o}/\text{min}$), (ii) to cracking along the polar axis of the kind observed here, (iii) to more catastrophic cracking across the spherulite equators or between spherulites.* These ideas were not followed up directly here but it is interesting to note that the broad coverage of strain-rates

* Burns (139) has demonstrated that the crack positions may be changed from (ii) to (iii) by increasing the strain-rate.

used by Hall⁽⁸⁰⁾ on PP shows an abrupt change from ductile behaviour (strain to rupture $\approx 50^{\circ}/o$), to brittle failure (strain to rupture $\approx 20^{\circ}/o$) at a strain-rate = $180^{\circ}/o/min.$ which might coincide with the transition from failure mode (ii) to failure mode (iii). The results of this research show that cracking in the α stress route is probably present in Hall's results up to strain rates = $180^{\circ}/o/min.$, and that if so, it does not contribute to premature failure. A slight tendency to improved crack resistance was also noted in a single test carried out at a slower strain rate, see section 5.5. Observations of this kind might lead to an understanding of the maximum permissible relaxation rates in various positions in the spherulite in normal sections of plastic and it is expected that these results will also differ from those of thin films in which the maximum relaxation rates of various sites within the spherulite are probably higher.

It must be concluded from this that thin extended films, of a thickness probably less than that of their constituent spherulites, do not give results comparable with the typical deformation mode of more normal sections of plastic material, in the respects that morphological connections out of the plane of the film are eliminated causing loss of structural complex stressing and a probable change in the natural relaxation rates of the structure.

A fairly distinct difference in the cracking site was also observed, as itemised in (d) under imposed complex stressing. Extending the above argument, this result might be interpreted as arising from the failure mode (iii) at the much lower strain-rates applied in extending thin films and could be precisely the effect of complex stress in slowing the typical relaxation rates of the structure as already suggested, such that a cracking mode is produced at a lower imposed strain-rate.

An indication of this mechanism's effect on the overall modulus is seen in some results given by Slonimskii and Pavlov⁽⁷³⁾. These authors have shown that as the ratio of film thickness to spherulite diameter increases up to a value approximately equal to unity there is an increase in relaxation modulus. Beyond this where the film is thicker than its constituent spherulites, they have shown that a fall in the overall relaxation modulus occurs. The suggestion made here is that this might follow from a slowing of the relaxation rate to a minimum value where the film thickness approaches that of its constituent spherulites, following from the reasons outlined above, but that beyond this (i) the number of spherulite boundaries, and (ii) the tendency to a cracking mode probably reduce the overall modulus.

(i) Slonimskii and Pavlov used cooling rates in the range of 12°C/min to 0.3°C/min in which this research has shown inter-spherulite bonding is affected.

(ii) They use a prescribed strain of 12.5% for their relaxation tests which is more than likely to cause cracking of the type found in this research.

The postulates made in the course of this discussion are consistent with these pieces of fragmentary evidence, and it is felt that they hold the key to the relationship between structure and strain-rate which was commented on in the introduction, pages 17 - 19, and furthermore, explain how differences may arise in experimental results where these are obtained with films of a thickness comparable with their constituent spherulites' diameter.

The difference in crack site in type III spherulites may be due to the weakness of inter-fibrillar regions in this morphological type, since as outlined in section 3.1, they appear to be of a simplified morphology possessing radiating lamellae alone, rather than lamellae of mixed orientation which may well serve to bind radiating fibrils together more strongly.

5.5 Transmitted Light Measurements during Tensile Testing

In order to measure the point on the stress-strain curve at which cracking starts, a technique was developed for continuously measuring the amount of light transmitted through the tensile test piece during a constant strain-rate test.

5.51 Apparatus.

The light source for light transmittance tests was a 4.5V bulb supplied by a stabilised power pack from the mains. Fig. 5.11 shows the experimental arrangement which comprised a light bench (j) holding the light source, two convex lenses, and an adjustable slit arranged as shown to produce a columnated light beam. A mirror at the far end of the light bench threw the beam of light into a long tube (k) which entered the constant temperature cabinet. Despite the use of a stabilised power pack fluctuations in the mains voltage produced a measurable change in light output from the source and tests were more often carried out during the evenings, to obtain more accurate results.

Within the cabinet a 0.3 in. sharp edged hole in the aluminium box (l) ^{which surrounds the specimen} admitted a narrow beam of light onto the specimen, the transmitted amount of which was measured by a Vickers CdS cell photometer (m) and displayed on a Second Kent Mk. III recorder. The inner surfaces of the aluminium box were carbon blacked to minimise reflected light reaching the light cell. The light cell was also hooded up to within a short distance of the plastic surface to further reduce the reading of stray light.

Preliminary tests showed that this equipment was very sensitive only to the amount of light transmitted through the specimen and was hardly affected by considerable changes in lighting outside the cabinet. During tensile testing where it was not necessary to measure the strain on the specimen the cabinet could be blacked out altogether, but during relaxation tests where strains were measured this was not possible. Where strains were measured using the optical

observation technique described in section 4.32 a constant source of illumination was provided close to the gauge marks of the specimen. This comprised two 4.5V bulbs supplied by a Farnell constant power pack.

Tests on the temperature stability within the test area of the cabinet showed that this did not suffer from introducing the open ended tube into the cabinet. At higher test temperatures a window in this tube might have been necessary.

A photograph showing the disc of light from the columnated beam source on the centre of the tensile test piece gauge length prior to testing, is shown in Fig. 5.11b.

5.52. Results.

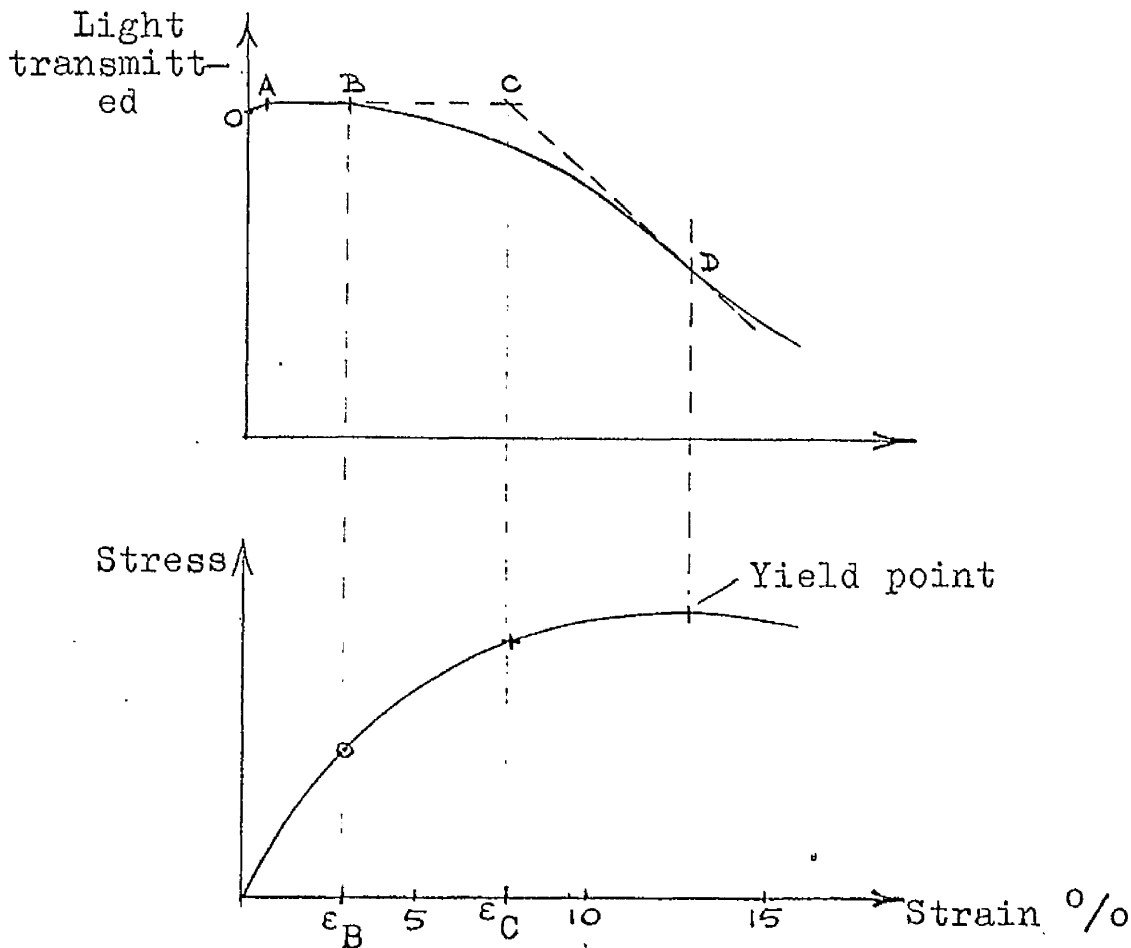


FIG 5.12.

A typical trace for the output from the light cell and its response with respect to the stress-strain curve is shown in Fig. 5.12. Between the points marked as oA a slight change in light reaching the light cell was often recorded due to the initial slight curvature of some tensile specimens. Under these circumstances the first few seconds of extension change the distance which separates the axis of the tensile test piece and the light cell. This, for example, if it comes closer to the light cell will increase the light reaching the cell by virtue of the increased angle subtended from the centre of the source of scattered light to the plane at which this is measured. Between the points marked as AB no change in transmitted light was measured but at B a well defined decline in the transmitted light occurred. The amount of transmitted light falls increasingly beyond this point, passing through a maximum rate of fall at a point D which corresponds to the yield point of the material. It should be noted that any thinning of the specimen section during extension would, if anything, increase the amount of light transmission during testing and that these results indicate the much larger changes which occur in the opacity of the material.

Two points^{are} of interest in elucidating the deformation process within the tensile test piece. They are point B, at which opacity or light scattering starts, and point C which is constructed from the light transmittance response as shown in Fig. 5.12 and is treated as a measure of the onset of large changes in opacity or light scattering which may be related to the beginning of cracking. Values of the strains ϵ_B and ϵ_C at which points B and C occurred for all the samples tested in this way, are listed in table 5.2a and shown in Fig. 4.8. and 5.14.

Duplicate tests were performed on test pieces from sample 2 which showed that on this sample the values of ϵ_B and ϵ_C , being 2.1% and 9.0% respectively, were reproducible to within $(2.1 \pm .025)\%$ and $(9.0 \pm .1)\%$.

Two further tests were completed on test pieces taken from the same sheet as sample 3 to find the effect of strain rate. The results are given in table 5.2b and are shown in Fig. 5.13.

To aid in the interpretation of the morphological meaning of points B and C, the following tests were carried out.

- i) Two samples from each of two sheets 7 and 8A, having the moulding conditions given in table 5.2c, were strained beyond point B to 2.5% and 3.0% respectively. They were left for 36 days to recover at room temperature prior to retesting. All again showed the same characteristic region AB in which no change in light transmittance occurs i.e. a recoverable behaviour. The results are given in table 5.2c from which it appears that ϵ_B may be slightly increased by a prior straining of the type given in these tests.
- ii) A fast cooled sample (sample 1) which had already been extended to beyond point D and which had been allowed to recover for 60 days at room temperature was retested and showed further decreases in the light it transmitted from the moment the cross-head was started i.e. non recoverable behaviour.
- iii) Two tests were also carried out on samples having the same thermal history, one of which had the standard machining finish, the other of which had all machine marks removed by polishing with emery cloth and diamond pastes until no machine marks were visible to the eye. These gave an identical response for

both stress-strain, and light transmittance tests, thereby showing that any stress raising from the machine marks had an insignificant effect on stress rupture properties within the test piece.

5.53 Discussion.

As mentioned earlier in section 5.13, it is expected that the start of drawing out of molecules from the crystalline phase is associated with voiding and a change to a state of semi-order in the drawn out material. Either of these could be responsible for the early changes in light transmittance in the tensile test piece.

In the early stages of this interaction between amorphous and crystalline regions, deformation of the structure and overall strain would still be recoverable. Long term recovery tests on PP after creep⁽¹⁴⁰⁾ show that the degree of recovery depends not only on the prior final creep strain, but on the time spent in the creep period, recovery becoming less complete the longer the creep period and the higher the final creep strain. The experiments carried out at different strain-rates (Fig. 5.13) confirm that the onset of opacity ϵ_B is a time and strain dependent point, the reasons for the trend indicated at the highest $\dot{\epsilon}$ used in Fig. 5.13 may be the result of an increased experimental scatter at higher strain rates in the measurement of the point ϵ_B .

In the region of C, however, it is likely that local deformations of the above kind become incapable of relieving the stresses induced by the rate of strain during extension such that a more severe cracking occurs either within or between spherulites. This mode of cracking is also time-dependent since it depends on the time-dependent orientation of smaller units within the spherulite, but owing to the co-operative nature of relaxation required to relieve stresses

at the macroscopic level, relaxation times for this mode of cracking will be longer.

The effect of thermal history on ϵ_B and ϵ_C is summarised in Fig. 5.14. The small changes found in ϵ_B probably represent no more than an experimental scatter and it would appear that this condition in the material is unaltered by the range of thermal histories applied in this research. There is, however, a general trend to improved resistance to gross stress cracking with faster cooling rates, as is generally appreciated⁽¹⁴¹⁾. The light transmittance technique used in this research has shown that the improvement is most pronounced for samples cooled faster than about $100^\circ\text{C}/\text{min}$ and having $T_C \approx 112^\circ\text{C}$ (samples 2, 6A, 6B). This crude boundary of cooling rate and T_C beyond which crack resistance is improved tallies with the fall in density at fast cooling rates shown in Figs. 3.6 and 3.7. The position of sample 1B in Fig. 5.14 again shows how a discrete annealing, say $T_A/T_C < 0.91$, may increase the strain to micro-cracking, a result which may be attributed to the more relaxed state of the spherulite interior such that strains are not so heavily concentrated into spherulite boundaries. Sample 5A appears more brittle in this respect at ϵ_C in Fig. 5.14, no doubt due to the inter-spherulitic voiding observed in 5A prior to testing which has resulted from a more thorough annealing treatment.

If this interpretation is correct then spherulite boundaries would appear to have little effect on cracking or disruption of the crystalline phase in its early stages such as at ϵ_B .

The position on Fig. 5.14 of sample 8A which had been thermally degraded, see table 4.2., shows that the melt condition may be more important than moulding cooling rates in its effect on the onset of opacity. It is concluded

that the range of cooling rates applied to samples in this programme produced very little change in the strain/time condition at which crystalline regions become deformed, but changed the strain/time conditions for more permanent cracking more markedly. In this respect, cooling rates faster than about $100^{\circ}\text{C}/\text{min}$ and $T_c \approx 112^{\circ}\text{C}$ are recommended as giving an improvement in resistance to gross cracking.

Sufficient material was not available to survey these points more fully, since a large number of tensile specimens were utilised in testing the effects on stress relaxation of strains which cover this zone of changing opacity.

An indication, however, of the generality of the findings obtained with this new technique when compared with other polymers may be indicated by some environmental stress rupture results obtained by Tung⁽¹⁴²⁾ on PE. He has shown that despite the extreme susceptibility of PE to the detergent environment of "Igepal", no rupturing was obtained for prolonged periods where the test strain in either creep or relaxation experiments was below about $2.0^{\circ}/\text{o}$. The results of this research would then suggest that the environmental stress rupture behaviour which is puzzling in its origin, see for example ref(143), is in some way associated with the condition which pertains when the crystalline phase begins to be disrupted.

5.6 Conclusions.

1) It has been found that the cooling rate from the melt affects the strain whitening characteristics of extended PP quite markedly. Strain whitening becomes very pronounced where moulding conditions are such that $T_C \gtrsim 120^\circ\text{C}$ (cooling rates $\lesssim 10^\circ\text{C}/\text{min.}$) These effects may be related to the abrupt increase in sample density and changed crystallisation kinetics which were found in the slow cooling rate range in Chapter 3.

Annealing treatments where $T_A/T_C \gtrsim 0.91$ also produce a severe increase in strain whitening.

2) The degree of strain whitening follows the same order as the degree of cracking within the tensile test piece. There are indications that more cracking might occur within spherulites rather than between spherulites in annealed samples compared with 'as moulded' samples.

3) Imposed complex stress conditions induce both voiding and cracking. Cracking within thick sectioned uniaxial tensile test pieces may be due to complex stressing induced at the microscopic level due to the anisotropic and inhomogeneous structure of the spherulitic matrix; it might also be due to the testing strain-rate exceeding the maximum rate of relaxation of one or other of the deformation modes within or between spherulites.

Since cracking within the tensile test specimens was very markedly distributed along the polar axis of the spherulite, as defined by the extension direction, it is concluded that the relaxation rate in these regions is the slowest of the possible relaxation modes within the matrix, and that the applied strain-rate has exceeded its fastest rate of reorientation. The conclusion 2) would then show that the structural changes following annealing make this relaxation mode even slower compared with the relaxation

behaviour of other regions within or between spherulites.

4) Uniaxial thin film extensions at comparable strain-rates show no tendency to cracking but instead a typical line-drawing behaviour from all regions in the spherulitic matrix. It is concluded that in the absence of both material restraint in the film's thickness direction and a multiplicity of slip systems through the thickness

- a) no serious complex stressing develops,
- b) the relaxation rates for deformation in the various parts of the spherulite might be faster.

Either conclusion suggests that some care should be exercised in comparing the deformation mode of thin films directly with that in the bulk matrix in crystalline polymers or any other crystalline material.

5) A technique has been developed for following the course of opacity within a tensile test piece whilst it was being extended. This technique made it possible to distinguish the difference between the onset of opacity and large changes in opacity, the former of which was found to be recoverable and was attributed to the early stages of disruption of the crystalline phase, the latter of which was non-recoverable and was attributed to gross cracking. Both of these stages of deformation were found to be strain and time dependent.

6) Using this technique, it was found that the range of cooling rates applied to samples in this programme produced very little change in the strain/time condition at which crystalline regions become deformed*, but changed the strain/time condition for more permanent cracking more markedly. In this respect, cooling rates faster than about $100^{\circ}\text{C}/\text{min}$. and $T_c \approx 112^{\circ}\text{C}$ are recommended as producing the greatest improvement in resistance to non-recoverable cracking.

* this being at a strain $\approx 2\%$

A low temperature annealing treatment appears capable of improving the resistance to gross cracking, where comparison is made on a density basis with 'as moulded' material. At low annealing temperatures Wyckoff⁽⁴⁵⁾ has suggested that material of intermediate order may be removed. The results of this research would suggest that a limited transformation of this kind probably incorporates a relaxation of the non-crystalline phase to an extent which improves crack resistance slightly without affecting the relaxation mode in polar regions as concluded in note 3).

7) A condition where no gross cracking occurs or where it is delayed until higher strains/longer times may occur at low strain rates, lower than about 0.5°/o/min.

TABLE 4.1a

Sample	C (°C/min)	T _c (°C)	Age Prior to Test (Hrs.)	ρ (g/ml)
1	155	110.4	23	.9029
2	106	111.8	192	.9048
3	51	114.3	575	.9055
4	9.3	121.0	2610	.9066
5	1.4	124.8	695	.9082

TABLE 4.1b

Sample	C (°C/min)	T _c (°C)	Age Prior to Test (Hrs.)	ρ (g/ml)
6A	96	112.8	6	.9035
6B	96	112.8	192	.9047

TABLE 4.1c

Sample	C (°C/min)	T _c (°C)	ρ ₁ (g/ml)	T _A (°C)	T _A /T _c	t _A (Hrs.)	ρ ₂ (g/ml)
1A	164	110.0	.9038	125	1.135	3	.9089
1B	155	110.4	.9042	100	.905	19	.9060
5A	1.4	125.0	.9084	118	.945	5	.9082

C=cooling^{rate}, ρ=density at time of test, ρ₁=preanneal density,
ρ₂=post anneal density.

TABLE 5.2a

Sample	ϵ_B ($^{\circ}/o$)	ϵ_C ($^{\circ}/o$)	Density g/mL
6A	2.7	8.9	.9035
6B	2.7	8.7	.9047
2	2.1	9.0	.9048
3	2.0	6.8	.9055
4	2.0	5.7	.9066
1B	2.2	7.3	.9060
5A	2.5	5.7	.9082

TABLE 5.2b

Sample	ϵ ($^{\circ}/o/min$)	ϵ_B ($^{\circ}/o$)	ϵ_C ($^{\circ}/o$)
3	.47	4.0	8.4
"	1.89	3.6	6.8

TABLE 5.2c

Sample	$^{\circ}C/min$	$^{\circ}C^T$	ρ g/mL	ϵ_B^1 / $^{\circ}/o$	$\hat{\epsilon}$ / $^{\circ}/o$	ϵ_B^2 / $^{\circ}/o$
7	15	118.9	.9060	2.0	2.5	2.5
"	"	"	"	2.1	3.0	2.7
8A*	10.5	121.5	.9071	1.4	2.5	2.1
"	"	"	"	"	3.0	2.5

* Thermally degraded sample B; from Chap. 2, see p. 46.

ϵ_B^1 = initial strain to point B

$\hat{\epsilon}$ = maximum strain during experiment

ϵ_B^2 = strain to point B after 36 days of recovery

FIG. 5.1

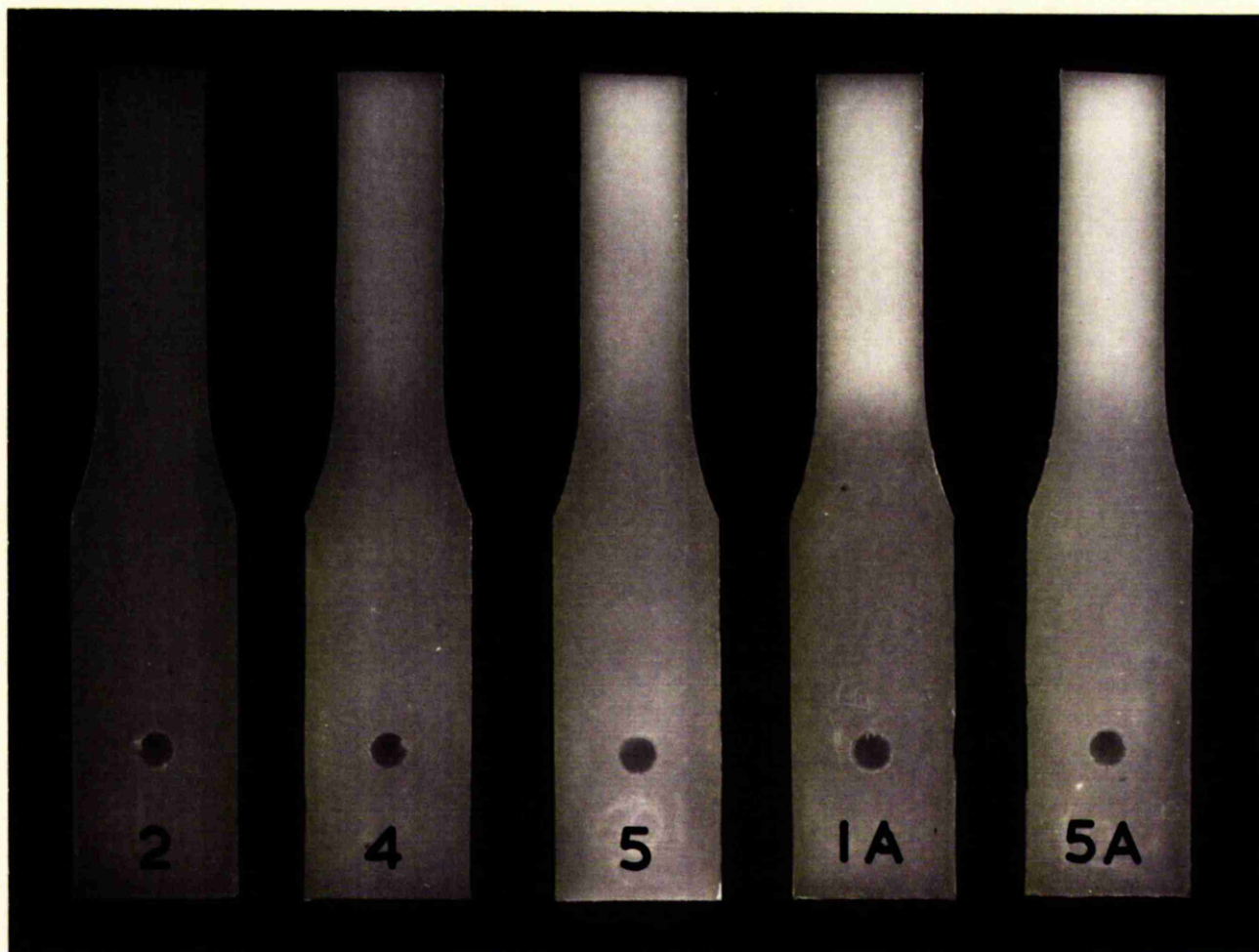




FIG. 5.2a SAMPLE 5
x 200



FIG. 5.2b SAMPLE 4
x 200



FIG. 5.2c SAMPLE 2
x 650



FIG. 5.2d SAMPLE 5A
x 350

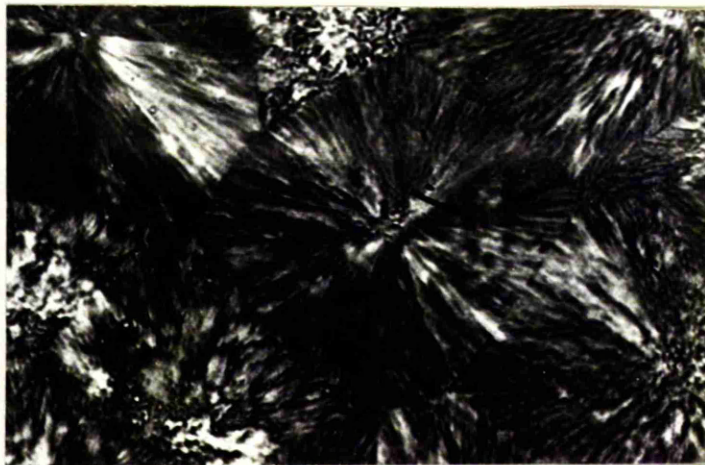


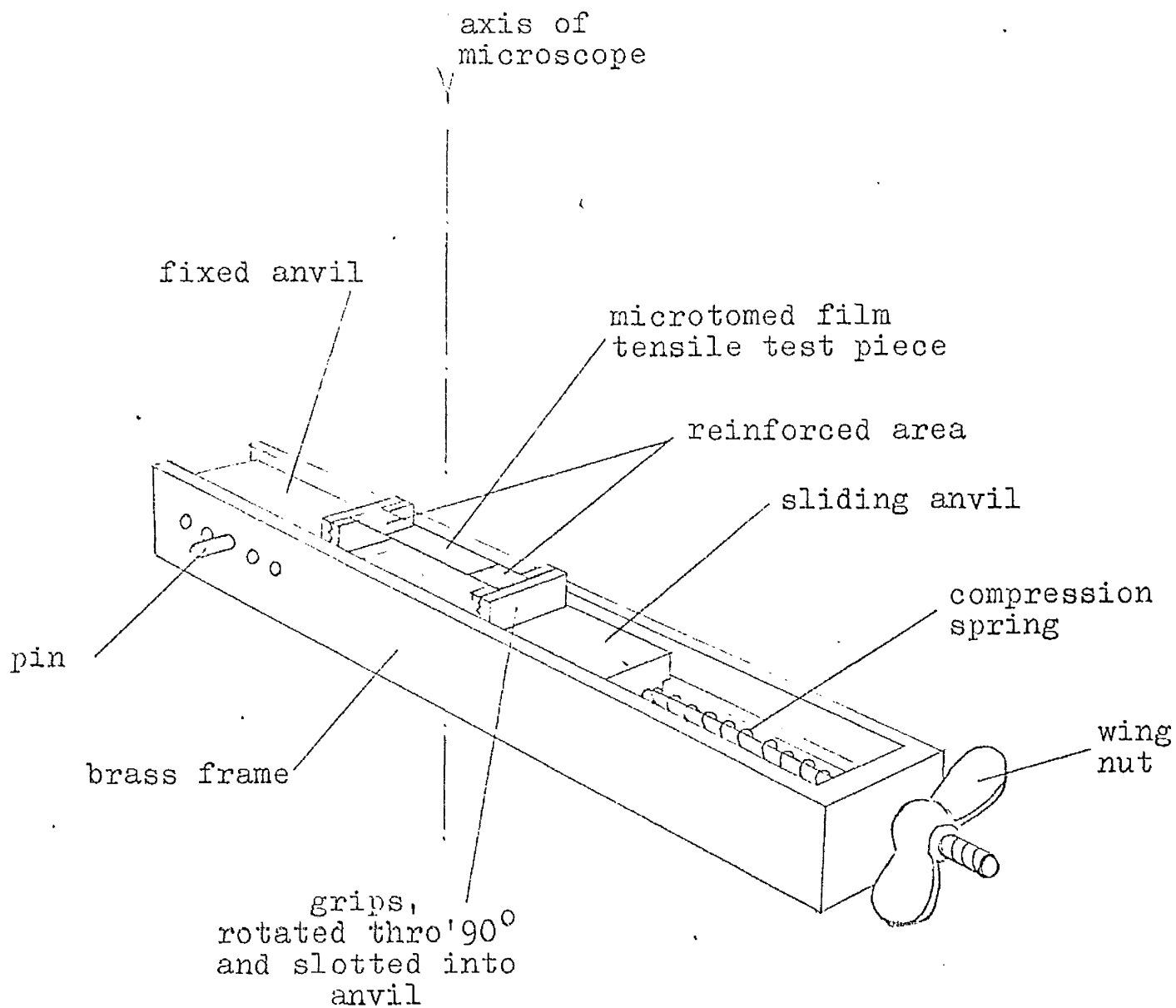
FIG. 5.2e SAMPLE 5A
x 350



FIG. 5.2f SAMPLE 5A
x 350

EXTENSION DIRECTION HORIZONTAL

FIG. 5.4



In operation this jig was turned over so that the tensile test film was next to the objective lens of the Vickers Projection Microscope. The jig was bolted down in this position by two yokes. Transmitted light illumination passed through a hole in the brass frame.



FIG. 5.6a SAMPLE 4
x 350

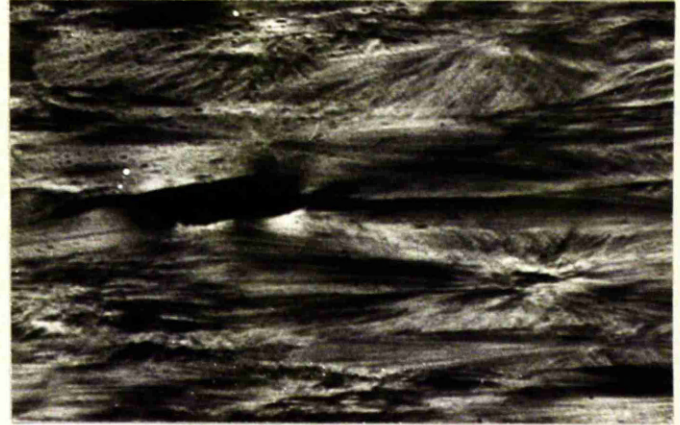


FIG. 5.6b SLOW COOLED SAMPLE
x 350



FIG. 5.6c SAMPLE 5
x 200



FIG. 5.6d IMPROPERLY MOULDED
SAMPLE x 200



FIG. 5.9 SAMPLE 4
x 200

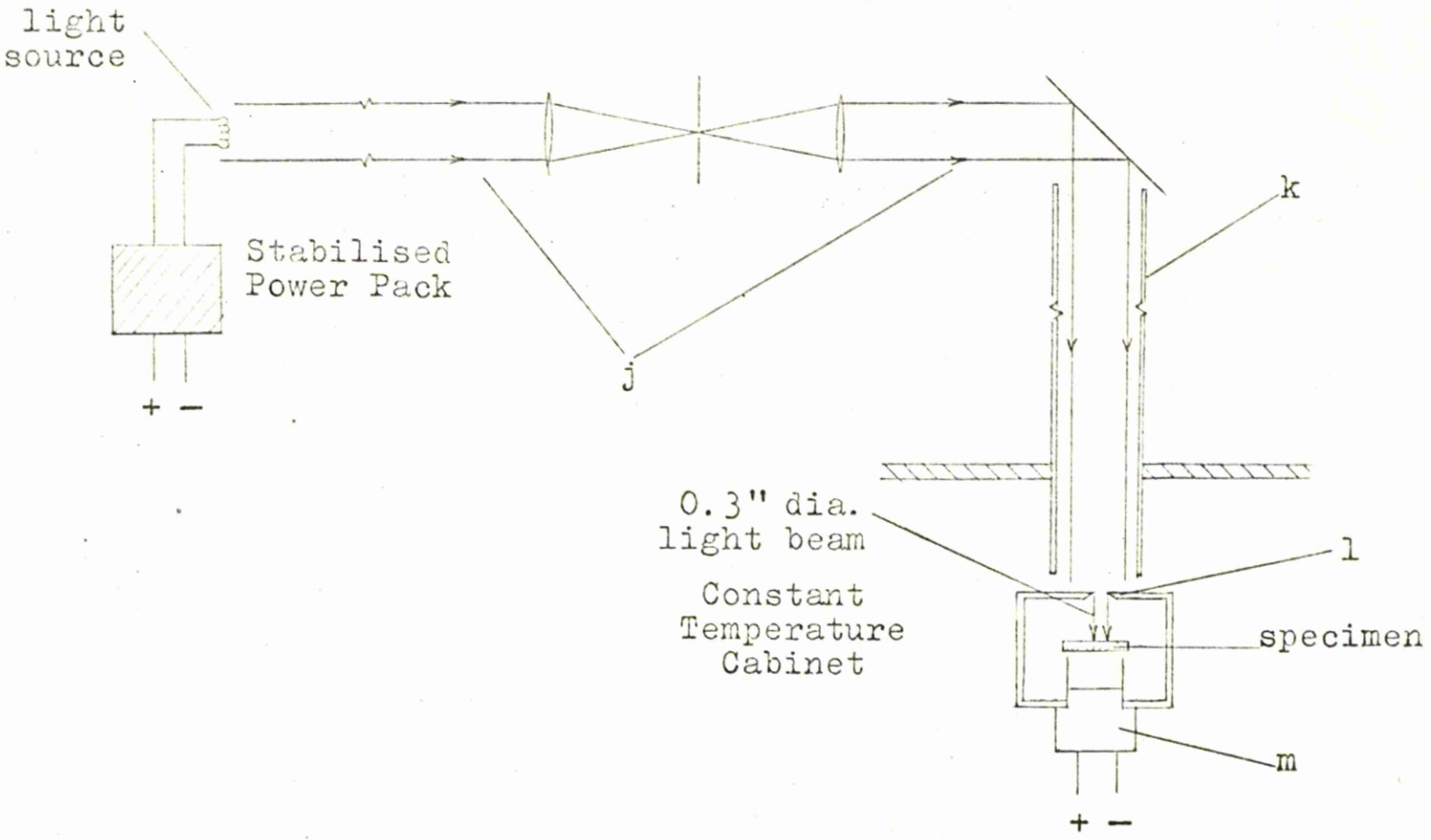


FIG. 5.11a

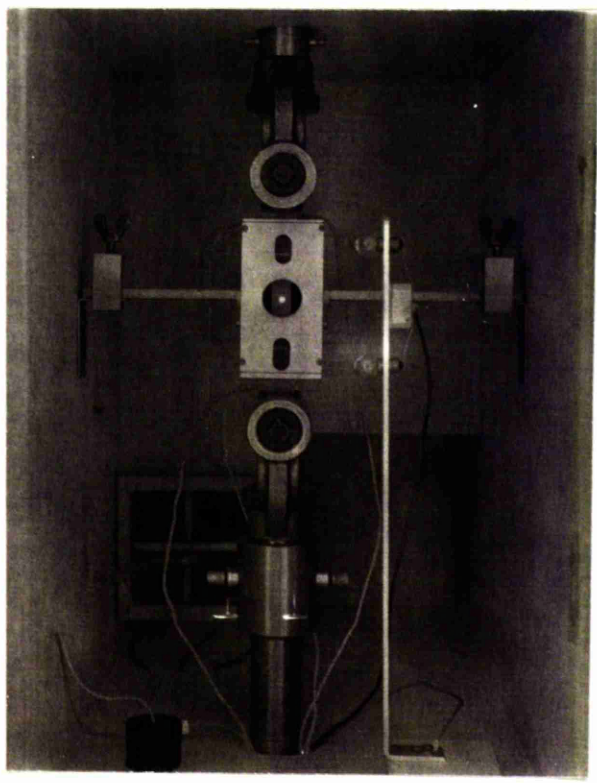


FIG. 5.11b

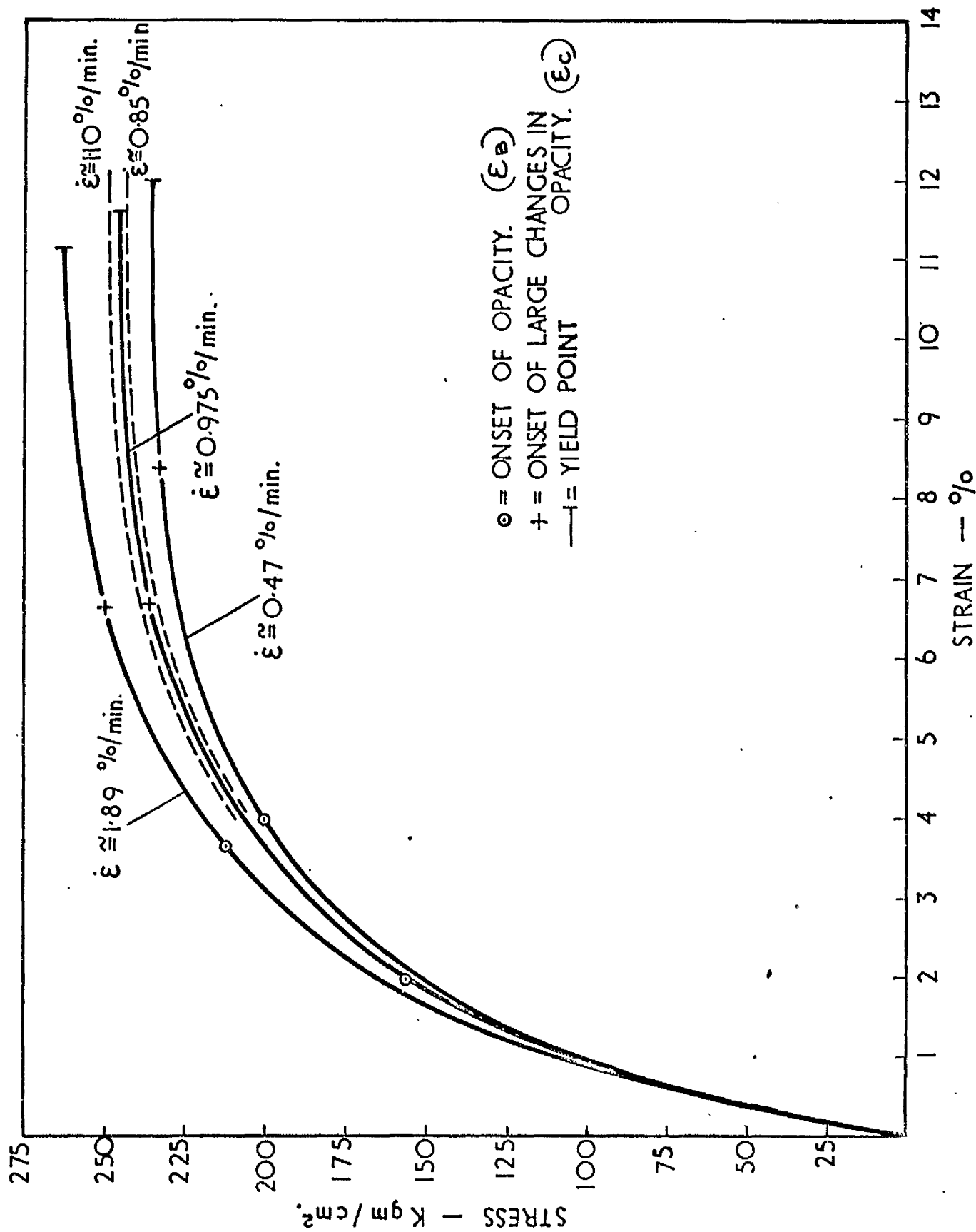


FIG. 5.13. THE EFFECT OF STRAIN RATE ON THE STRESS - STRAIN CURVE.

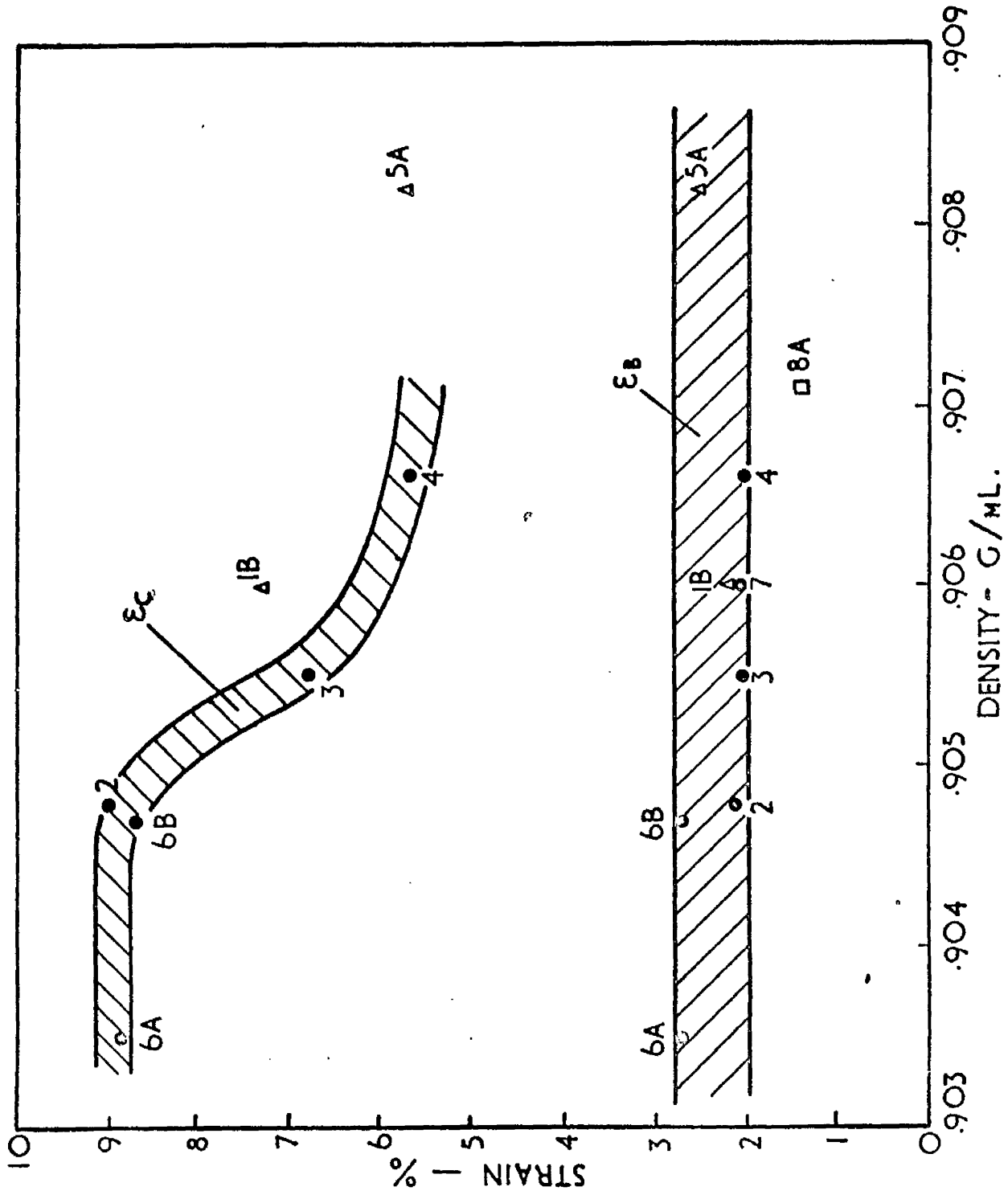


FIG. 5.14. THE EFFECT OF DENSITY ON THE PROGRESS OF CRACKING.

6. RELAXATION TESTS.

6.1. Introduction.

6.11. Scope of Tests.

The purpose of these tests was to ascertain the strain dependence of stress relaxation for samples of varying thermal history. To this end, tensile test pieces having the same thermal history were subjected to a range of prescribed strains from 0.25% to 5.0%. Occasionally the same tensile test piece was used for first testing at 0.25% or 0.5% and then at a higher strain, after allowing about 2 days for recovery.

The number of relaxation tests undertaken and the availability of only one test rig limited the relaxation experiments to 3 hours each to give a time span of 4 decades in seconds from 10^0 to 10^4 secs.

Throughout the relaxation tests a constant test temperature of $24.0 \pm 0.1^\circ\text{C}$. was used.

6.12. Choice of Strain Rate to Attain the Prescribed Strain. strain rate

The constant/ $\dot{\epsilon}$ tests described in section 5.5. showed that the point at which opacity starts (attributed to drawing out of molecules from crystallites) is a time dependent phenomenon. It was, therefore, decided to use the same $\dot{\epsilon}$ to extend tensile test pieces to the prescribed strain of each relaxation test, so that the state of extension of the structural matrix at the start of relaxation could be related to the results of the last chapter.

6.13. Material Samples Tested.

a) Moulding Conditions. A selection of sheets of plastic moulded as in Chapter 2 was chosen to cover the available range of moulding cooling rates. Most sheets yielded either 2, 3 or 4 tensile test pieces according to how much of the sheet was detached for density, microscopy or thin film extension work. For the purposes of correlation, an average moulding condition was taken for all the test pieces from each sheet from the recorded cooling rates and crystallisation temperatures at each thermocouple. Likewise, by using the graphs of density versus age, Fig. 3.4, and density versus T_c , Figs. 3.6 and 3.7, it was possible to estimate a fairly accurate average density for each sheet and its corresponding test pieces to cover the period of time during which relaxation tests on any one sheet were carried out. The sheets tested, listed as samples, are shown together with their relevant moulding conditions, average age and density at the time of testing in Table 6.1a.

b) Ageing. The samples listed in the above category had approximately two age groups, of about 410 hours (samples 9, 10, 12, 14) and about 984^{1010} hours (samples 11, 13, 15). These two sets of samples were treated as different age groups. A further age group for prolonged ageing is detailed in table 6.1b. Ageing was carried out in a controlled temperature room held at $23 \pm 2^\circ\text{C}$.

c) Annealing. A single fast cooled sheet, yielding four tensile test pieces, was used to examine the effects of annealing above and below the sample's T_c . Details of the annealing temperatures T_A and times t_A are given in

Table 6.1c. The procedure used for annealing is given in section 6.14.

6.14. Annealing Procedure.

Individual test pieces were annealed at accurately controlled temperatures in an inert Argon atmosphere. The test piece was contained in a boiling test tube which was fitted with a stopper through which passed an inlet tube from a cylinder of Argon and an outlet tube to an air lock. Argon was passed through the test tube at a very slow rate whilst the test ^{tube} being supported beneath a lid, was immersed in a Grant thermostatted oil bath held at the desired annealing temperature. A mercury thermometer reading to 0.2°C . and a calibrated iron/constantan thermocouple connected to a potentiometer were held close to the test tube and measured the annealing temperature, fluctuations of which did not exceed $\pm 0.1^{\circ}\text{C}$. Cooling after annealing was by leaving the test piece in the test tube in air for 5 mins. before removing it. This represented a cooling rate of approximately $15^{\circ}\text{C}/\text{min}$.

6.2. Apparatus, Procedure, and Errors

6.2.1. Apparatus and Experimental Errors.

The Instron tensile tester was used for stress relaxation tests together with the constant temperature cabinet already described in Appendix III.

Two load cells giving load spans of 0 - 50 Kgm. and 0 - 100 Kgm. together with a zero suppression unit enabled the entire range of strains to be covered with load measuring errors of ± 0.05 Kgm. and ± 0.1 Kgm. respectively on each span, plus the error of ± 0.06 Kgm. due to temperature fluctuations within the cabinet.

The experimental arrangement for measuring the loads continuously in a relaxing material is shown in Fig. 6.1.

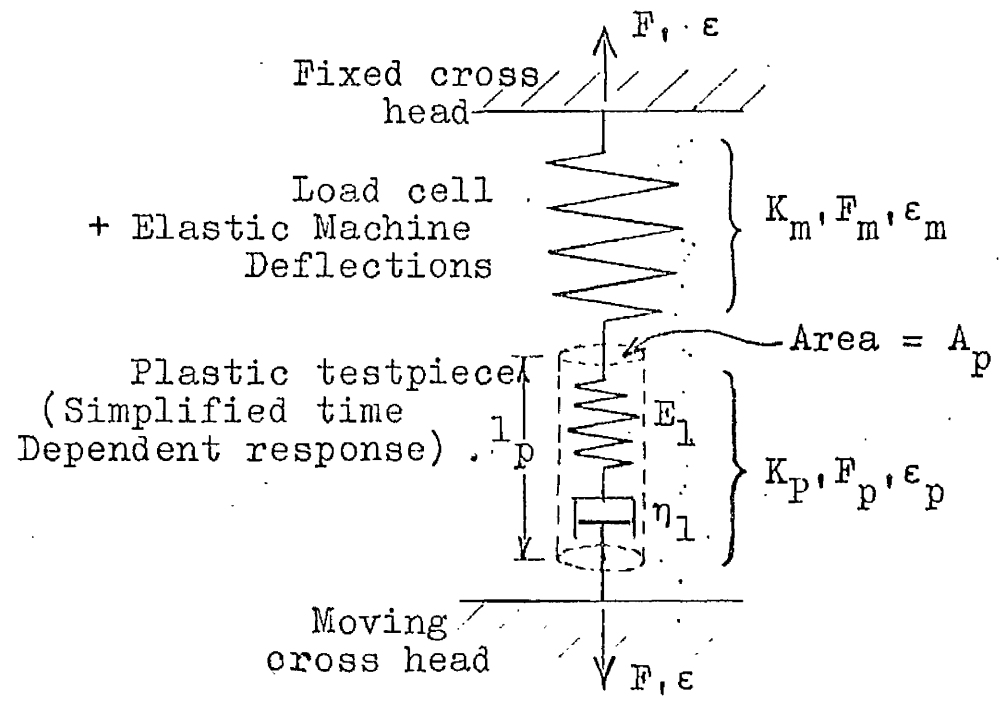


FIG. 6.1

where K , F and ϵ refer to the spring constant, the force, and the strain in either the machine or the plastic. A_p and l_p refer to the cross section and the length of the plastic under test.

Assuming that the plastic is a linear visco-elastic material (not the case at strains $\gtrsim 0.2\%$ in the case of highly crystalline PP), its spring constant K_p can be represented simply by,

$$K_p = \frac{A_p}{l_p} \times E_1 \exp\left(-\frac{E_1}{\eta_1} t\right) \quad \text{-----(1)}$$

since $F_m = F_p$

$$K_m \cdot \epsilon_m = K_p \cdot \epsilon_p$$

and $\epsilon_m = \frac{K_p}{K_m} \cdot \epsilon_p$

In a relaxation test which is approximated to by holding the lower cross-head fixed,

$$\epsilon_m + \epsilon_p = \epsilon = \text{constant} = \epsilon_0 \quad \text{-----(2)}$$

$$\therefore \frac{K_p}{K_m} \cdot \epsilon_p + \epsilon_p = \epsilon_0$$

$$\epsilon_p = \frac{\epsilon_0}{\left(1 + \frac{K_p}{K_m}\right)}$$

$$\text{i.e. } \epsilon_p = \frac{\epsilon_0}{1 + \frac{A_p E_1}{l_p K_m} \exp\left(-\frac{E_1}{\eta_1} t\right)} \quad \text{-----(3)}$$

Equation (3) describes the time dependent strain on the plastic $\epsilon_p(t)$ due to its own relaxation.

The most pessimistic change in ϵ_p from the start to finish of a pseudo-relaxation test is obtained when the plastic has completely relaxed i.e. $t \gg \frac{E_1}{\eta_1}$.

Feeding into equation (3) the largest value for the expression $\frac{A_p}{l_p} \cdot \frac{E_1}{K_m}$; for the plastic, at short times and

small strains $E_1 \cong 1.20 \times 10^4 \frac{\text{Kgm}}{\text{cm}^2}$; for the weakest load

cell, $K_m \cong 1.0 \times 10^4 \frac{\text{Kgm}}{\text{cm}}$; $A_p = 0.480 \text{ cm}^2$, $l_p = 7.0 \text{ cm}$;

$$\frac{A_p}{l_p} E_1 / K_m = .08.$$

A realistic estimate of the amount of relaxation during the time duration of these tests puts the value of the expression $\exp(-\frac{E_1 t}{\eta_1}) = 0.6$, making the total change in ϵ_p from equation (3),

$$\epsilon_p \text{ (at } t = 0) = \frac{\epsilon_o}{1.08}$$

$$\epsilon_p \text{ (at } t = 10^4 \text{ secs.)} = \frac{\epsilon_o}{1.04}$$

making a total change in ϵ_p of about 4%.

Strains were measured three times during relaxation tests and an average value taken for ϵ_p . The maximum error found in this way throughout stress relaxation testing was for small strains where $\epsilon_o = (0.24 \pm 0.005)\%$, which represents an error of $\pm 2.0\%$, as predicted above. The maximum error at high strains was of the order $\pm 0.5\%$, the improvement resulting from a fall in the value of $\frac{A_p}{l_p} E_1 / K_m$

due to (a) the effect of non-linearity in reducing E_1 , with increased strains, and (b) an increase in the value of K_m with the use of a higher capacity load cell.

6.22. Experimental Procedure.

The equilibration procedure prior to testing at 24.0°C was the same as was used in Chapter 4. Gauge length and strain measurement was again carried out using the 'Utilex' measuring microscope.

To produce the prescribed strain ϵ_0 for a stress relaxation test the cross-head movement, producing the $\epsilon(t)$ path shown in Fig. 4.6, was timed with a stop watch.

A light transmittance measurement was taken continuously during the relaxation test, and in order that strains could be measured without interrupting these tests, a constant source of light was arranged within the cabinet using two 4.5 V bulbs supplied by a Farnell stabilised power pack. These can be seen in Fig. 5.11b.

6.3 Results.

Duplicate tests on two fast cooled samples 9, 10 were completed at 0.5^o/o strain to test the reproducibility of results. These samples were considered to have as near as possible the same thermal history. The greatest difference in stress measured in the course of relaxation represented a scatter of $\pm 6^{\circ}/o$. In a determination of relaxation modulus based on these stress relaxation results, the additional error in the measurement of strain brings the maximum total scatter in modulus measurement to the order $\pm 10^{\circ}/o$.

The effects of strain on modulus were sufficiently large despite this scatter to justify plotting results as modulus versus log (time). Results for samples having a reasonable coverage of strain are shown for samples (9,10), 12, 14 and 15 in Figs. 6.4, 6.5, 6.6 and 6.7 respectively. Values are not shown for 0.25^o/o strain because of the increased size of errors in modulus at this strain owing to larger errors of strain measurement and the initial slight curvature of the tensile test pieces from fast cooled sheets.

The greatest change produced in modulus with extremes of cooling rate during moulding was of the order 14^o/o, where values are compared at 1000 seconds after the start of the relaxation test. This meant that a critical interpretation of the results was not possible. The stress relaxation of samples of varying moulding conditions at strains of 0.5^o/o and 1.5^o/o is given in Figs. 6.8 to 6.11.

The stress relaxation of annealed samples at strains of 0.5^o/o and 1.5^o/o is given in Figs. 6.12 and 6.13 respectively.

The greater number of tests completed on samples 9 and 10 having practically the same thermal history were used to find the basic variation in the relaxation response with strain. The limited number of tests which could be completed with the amount of material available from one batch could then hopefully be related in their tendency to the form of the results obtained for samples 9 and 10.

In order to correlate the effects of both thermal history and strain in a way which might show up any small differences a measure of relaxation rate was chosen. It is important to realise that no absolute value exists for the measurement of relaxation rate since stress relaxation changes constantly and apparently never reaches an equilibrium value within practical time limits.

Kubat⁽¹⁰²⁾ has suggested the criterion for relaxation rate shown below.

$$\frac{[\frac{d\sigma}{d \log t}]_{\max}}{[\sigma_0 - \sigma_\infty]} \quad \text{---} \quad (4)$$

where $[\sigma_0 - \sigma_\infty]$ is the total dissipation of stress during a stress relaxation experiment.

For the purposes of comparison in this research this expression was modified to

$$\frac{[\frac{d\sigma}{d \log t}]_{\max}}{[\sigma_{10^0} - \sigma_{10^4}]} \quad \text{---} \quad (4A) *$$

The value of this expression versus strain for all the samples tested is given in Table 6.2, and the values for samples 9 to 15 are plotted in Fig. 6.14.

* where σ_{10^0} = the stress at 1 sec.

σ_{10^4} = the stress at 10^4 secs.

6.4 Discussion

The effects of strain on the stress relaxation response in Figs. 6.4 to 5.7 show the very pronounced effects of non-linearity. It is obvious from the results obtained that despite the experimental scatter expected on these curves, they all predict that non-linearity is present at strains above at least about 0.5°/o to 0.9°/o. This means that the relaxation modulus is a function simultaneously of both time and strain.

The form of the relaxation curves obtained show a tendency toward an equilibrium zone in the strain range above approximately 2°/o. This behaviour may well be related to the stiffening role of the crystalline regions, as has been interpreted by Turner⁽⁷⁴⁾⁽⁷⁵⁾ to explain a tendency to equilibrium behaviour in creep experiments on PP and PE. On this basis it would be expected that a similar behaviour should occur in samples strained to below 2°/o but taking place at progressively longer times outwith the duration of these relaxation experiments as the strain is reduced.

A slight form of strain dependence for stress relaxation is shown by the curve for samples 9, 10 in Fig. 6.14, which may result from this pseudo-equilibrium zone effect. The points obtained for the other samples would appear to share in their prediction of this strain dependent phenomenon and estimated curves for their response are drawn in based on the more complete curve obtained for samples 9, 10. In the range of strains below approximately 2°/o.

the relaxation behaviour of the samples of varying thermal history appears to be slightly different. With one or two inconsistencies which are probably due to experimental scatter the general trend found was toward an increased relaxation rate (as measured by expression 4A) for slower cooled specimens, lower age, or more thoroughly annealed specimens. This trend is what might be expected on the basis of the earlier conclusions made in Chapter 4 on the importance of the state of relaxation in the non-crystalline phase. Since the degree of crystallinity is increased with any of the thermal history changes stated above, and yet relaxation rates still increase marginally, it is concluded that the state of relaxation in non-crystalline regions up to strains of about 2^o/o under the present test condition is probably more important than either the degree of crystallinity or the perfection of the crystalline state. The similarity in relaxation behaviour at strains greater than 2^o/o may, by reference to the previous discussion in Chapter 5, be related to deformation of the crystalline phase. Under these circumstances it would appear that no gross difference in relaxation behaviour is detectable once crystalline areas are deformed. This is another indication that within the sensitivity of these experiments no difference in the strength of crystalline phase is detected for fast and slow cooled test pieces alike.

If this interpretation is correct, then some differences in relaxation behaviour would be expected to reappear at strains beyond the threshold for gross cracking (say greater than 5^o/o), as found in Chapter 5. Whilst there are some slight indications of this at strains greater than 3^o/o, results were again not entirely consistent, probably due to experimental scatter.

Too detailed an interpretation of these results apart from the above comments, was felt to be unwarranted by the

expected experimental scatter. However, one major conclusion that can be made from an observation of the results in Figs. 6.8 to 6.11 and Fig. 6.14, is that the differences in relaxation behaviour where they exist are quite small and that these differences are more likely to be observed at smaller strains and times which do not disrupt the crystalline phase.

Passaglia and Martin⁽⁴⁷⁾ have reported finding difference in the relaxation response of PP at room temperature following various extremes of thermal history by a torsional oscillation technique, which complies with the recommendation made above. Their results show a slightly larger difference in relaxation rates for samples of varying thermal history and in view of the results of this research it would appear that as strains are increased, differences in the relaxation behaviour as varied by thermal history, progressively decrease until no differences are detectable in the strain (and time) zone where the crystalline phase is deformed. In the presence of stress-cracking however, differences may again reappear owing to the different susceptibility to cracking for various thermal histories as found in Chapter 5.

The same authors⁽⁴⁷⁾ however, report a more substantial difference in the relaxation of annealed PP specimens at temperatures in the range of the high temperature relaxation ($\sim 363^{\circ}\text{K}$). This observation would naturally suggest the involvement of the crystalline phase in some way with this difference which these authors attribute to movement of the lamellar surfaces or inter-lamellar regions. This interpretation cannot be tested for comparing fast cooled specimens with slow cooled ones because tensile testing in the region of the high temperature relaxation would produce an annealing treatment which would vary from sample to sample in its effect according to the ratio T_A/T_C .

It, therefore, appears impossible to compare directly the relaxation response of variously cooled samples in the temperature range of this high temperature relaxation. In the absence of annealing treatments which have stabilised the structure to a higher temperature than the test temperature, it is to be expected that the mechanical properties of variously cooled samples would become considerably different at test temperatures approaching the crystallisation temperature band ($108^{\circ}\text{C} - 125^{\circ}\text{C}$) owing to this variable ratio of T_A/T_C and its effect on melting and reordering structure. Since in Chapter 5 it was concluded that a ratio of $T_A/T_C \gtrsim 0.91$ is required to significantly alter the fine structure, it might be concluded from the values of T_C obtained for the fastest cooled sheets of this research that differences in the mechanical behaviour of unannealed PP may show^{up} at test temperatures above about 95°C .

In the region of ambient temperatures the small differences obtained in the relaxation rates within the strain range .25% to 3% also means that at a chosen strain within this range a fairly accurate description of the relaxation behaviour following any thermal history treatment can be obtained from a single relaxation curve at the same strain and a knowledge of the effect of thermal history on the material's isochronous stress-strain curve. The latter curve would enable an assessment of the vertical shift to be applied to the relaxation curve as shown in Fig. 6.16 over, to bring it into line with the thermal history change. This method would break down beyond those conditions which produce crading and a significant change in the relaxation response at the same strain of materials with varying extremes of thermal history.

An isochronous stress-strain curve, derived from the results of the relaxation experiments where they covered an adequate range of strains is given in Fig. 6.15.

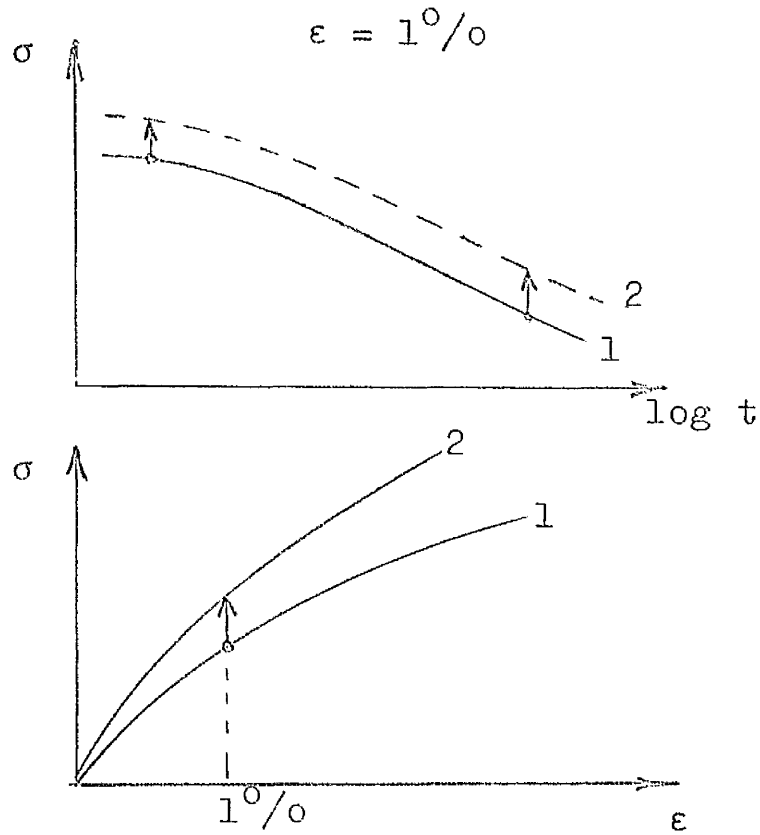


FIG. 6.16

6.5 Conclusions

1) A slight strain dependent relaxation process has been found which may be related to the strain and time at which the crystalline phase is probably deformed.

2) At strains below which the crystalline phase is not deformed to a large extent within the time duration (~ 3 hours) of these relaxation tests a small difference in relaxation behaviour is detected for samples of varying thermal history. The general trend in relaxation rate is such as to suggest that the state of relaxation in the non-crystalline phase is more important than either the degree of crystallinity or the state of perfection of the crystalline phase.

At strains beyond which the crystalline phase is probably deformed no difference is detected in the relaxation behaviour of samples of varying thermal history. However, beyond strains which cause cracking of the material small differences again reappear according to the various crack resistant properties of each sample.

3) The small differences in the relaxation rate of PP samples of varying thermal history found in this research at strains in the range $.25^{\circ}/o$ to $8^{\circ}/o$ extends the findings at smaller strains of other workers⁽⁴⁷⁾ in this field. The results show that up to these strains the differences in relaxation behaviour become progressively smaller until no detectable difference occurs in the region where there is probably interference from the crystalline phase, and prior to the process of cracking mentioned above.

4) Transmitted light tests show no detectable level of recovery of the state of opacity (disruption of the crystalline phase or cracking) during these stress relaxation tests.

TABLE 6.1a

Sample	C ($^{\circ}C/min$)	T ($^{\circ}C$)	Age Prior to Test (Hrs.)	ρ (g/ml)	No. of Relaxation Tests
9	127	109.6	322	.9042	5
10	119	110.9	274	.9040	5
11	116	110.6	1270	.9051	2
12	73	113.1	524	.9052	5
13	24	116.3	905	.9060	3
14	8.3	120.5	521	.9065	4
15	1.3	125.7	875	.9085	4

TABLE 6.1b

Sample	C ($^{\circ}C/min$)	T ($^{\circ}C$)	Age Prior to Test (Hrs.)	ρ (g/ml)	No. of Relaxation Tests
16	102	111.5	4450	.9052	2
17	66	116.0	2950	.9066	2
18	5.0	122.8	4800	.9081	3

C =cooling rate, ρ =density at time of test

TABLE 6.1c

Sample	C (°C/min)	T _c (°C)	ρ ₁ (g/ml)	T _A (°C)	T _A /T _c	t _A (Hrs.)	ρ ₂ (g/ml)
19A	116	109.4	.9035	106.0	.968	0.5	.9049
19B	116	109.4	.9035	105.9	.968	2	.9055
19C	116	109.4	.9035	105.9	.968	10	.9058
19D	116	109.4	.9035	112.0	1.022	2	.9059

C = cooling rate

ρ₁ = preanneal density

ρ₂ = post anneal density

T_A and T_c = annealing and crystallisation temperature

t_a = the duration of annealing

TABLE 6.2

Sample	Strain(°/o)	$\frac{KGM}{CM^2}$ (A) $\sigma_{10^0} - \sigma_{10^4}$	$\frac{KGM}{CM^2} / (SEC)$ (B) $[\frac{d\sigma}{d \log t}]_{max}$	$\frac{(B)}{(A)}$
9	.25	5.19	1.85	.357
	.50	10.05	3.74	.372
	1.5	28.10	9.95	.354
	2.7	32.9	11.5	.350
	4.6	35.7	12.9	.361
10	.25	5.85	1.98	.339
	.50	10.70	4.35	.406
	0.9	18.95	7.25	.383
	2.0	29.95	10.90	.364
	3.6	34.3	12.2	.356
11	.50	10.65	4.15	.390
	8.0	43.6	15.3	.351
12	.25	5.26	1.91	.363
	.50	11.28	4.41	.391
	1.5	29.25	10.30	.352
	2.7	32.7	11.4	.349
	4.7	37.8	13.6	.360
13	.50	10.53	4.0	.380
	1.5	26.32	9.36	.356
	2.6	32.5	11.2	.345
14	.25	5.08	1.91	.376
	.50	9.65	4.05	.420
	1.5	27.1	9.9	.366
	3.2	34.0	12.2	.359

continued/

TABLE 6.2 (continued)

Sample	Strain(°/o)	$\frac{K_{GM}}{CM^2}$	$\frac{K_{GM}}{CM^2}/(SEC)$	$\frac{(B)}{(A)}$
		(A) $\sigma_{10^0}-\sigma_{10^4}$	(B) $[\frac{d\sigma}{d \log t}]_{max}$	
15	.50	9.00	3.73	.413
	1.5	26.9	9.6	.357
	2.6	32.0	11.2	.350
	3.5	34.5	12.9	.374
16	.50	10.10	4.03	.399
	1.5	27.9	9.6	.345
17	.50	10.75	4.04	.375
	2.6	32.3	11.4	.353
18	.25	5.61	2.23	.393
	.50	11.08	4.50	.406
	2.3	33.6	11.6	.290
19A	.50	10.25	3.70	.361
	1.5	24.4	9.0	.370
19B	.50	11.20	4.3	.384
	1.5	25.9	9.2	.355
19C	.50	9.70	3.88	.400
	1.5	25.2	9.1	.363
19D	.50	11.1	4.1	.370
	1.5	24.5	8.6	.351

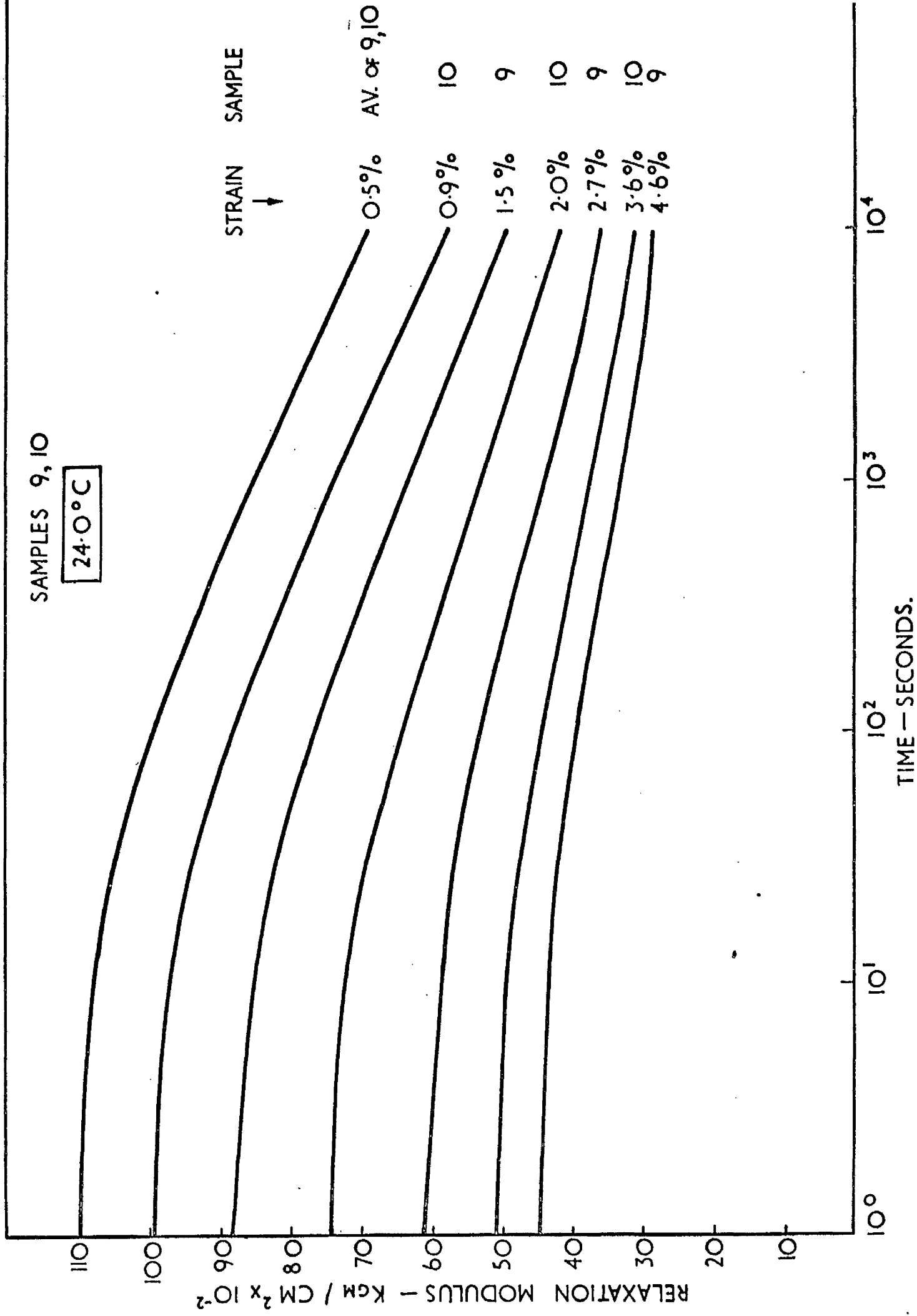


FIG. 6.4. THE EFFECT OF STRAIN ON RELAXATION MODULUS.

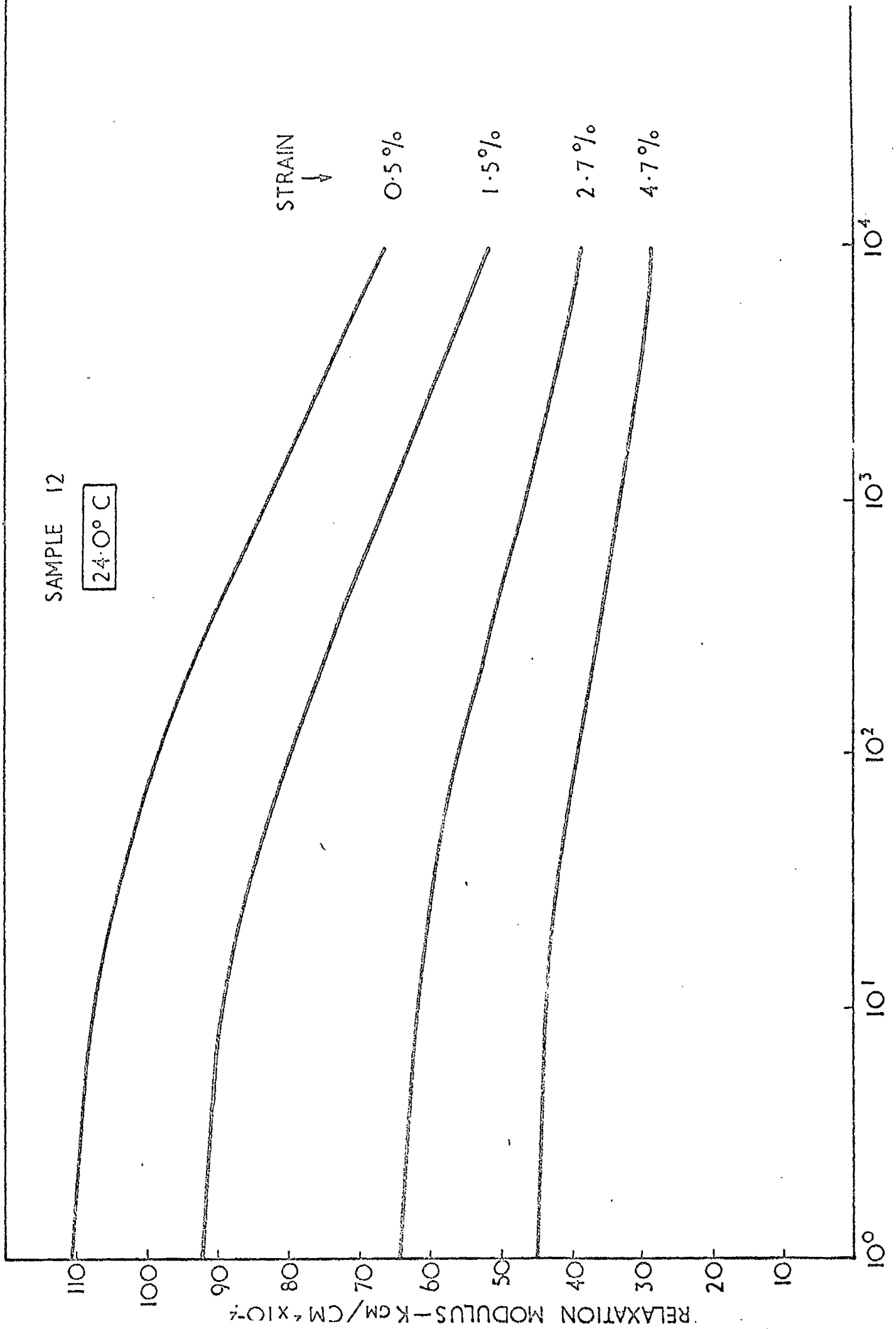


FIG 6.5. THE EFFECT OF STRAIN ON RELAXATION MODULUS.

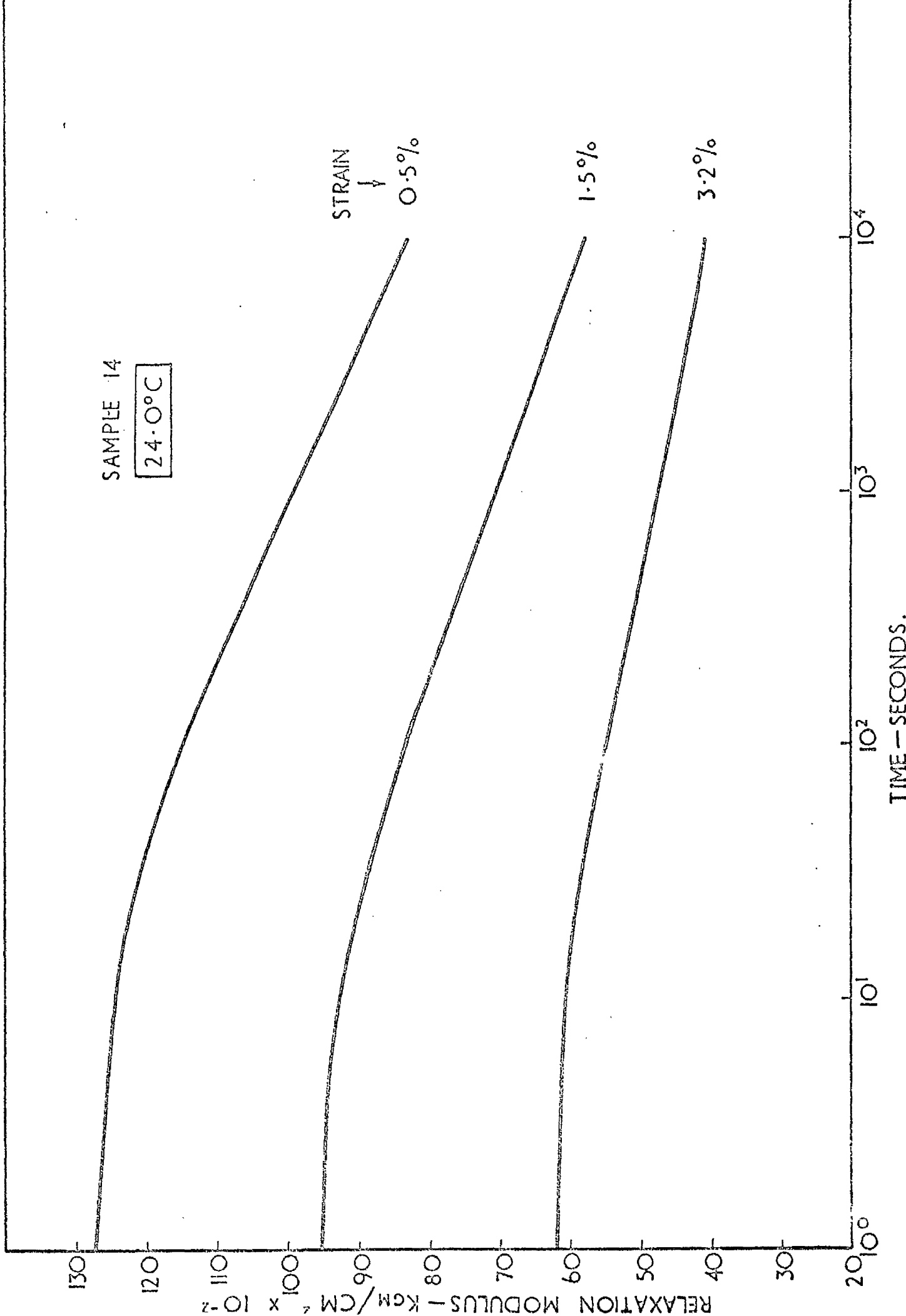


FIG. 6.6. THE EFFECT OF STRAIN ON RELAXATION MODULUS.

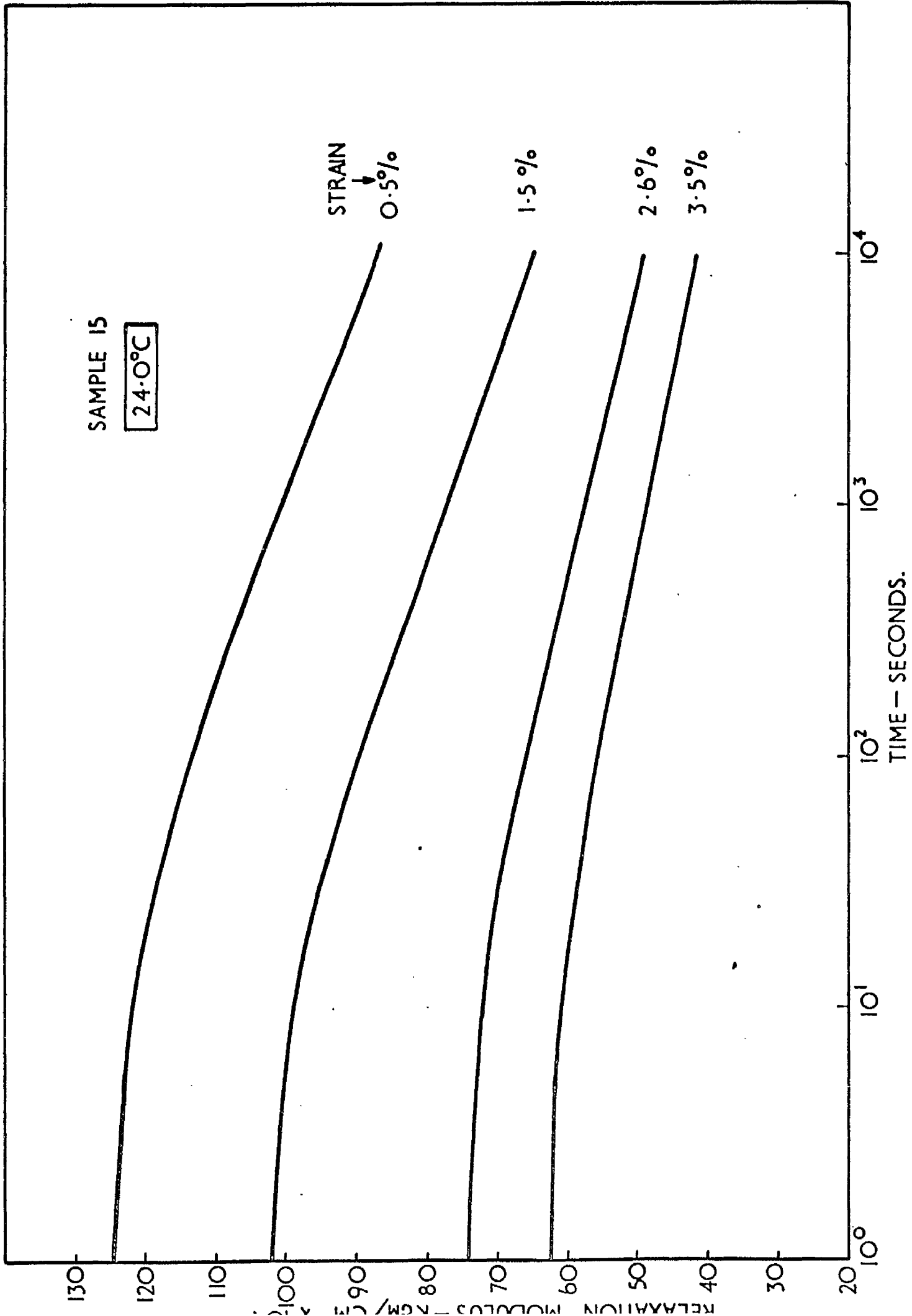


FIG. 6.7. THE EFFECT OF STRAIN ON RELAXATION MODULUS.

AGE = 274 - 524 HRS.
STRAIN = 0.5%
TEMP. = 24.0°C.

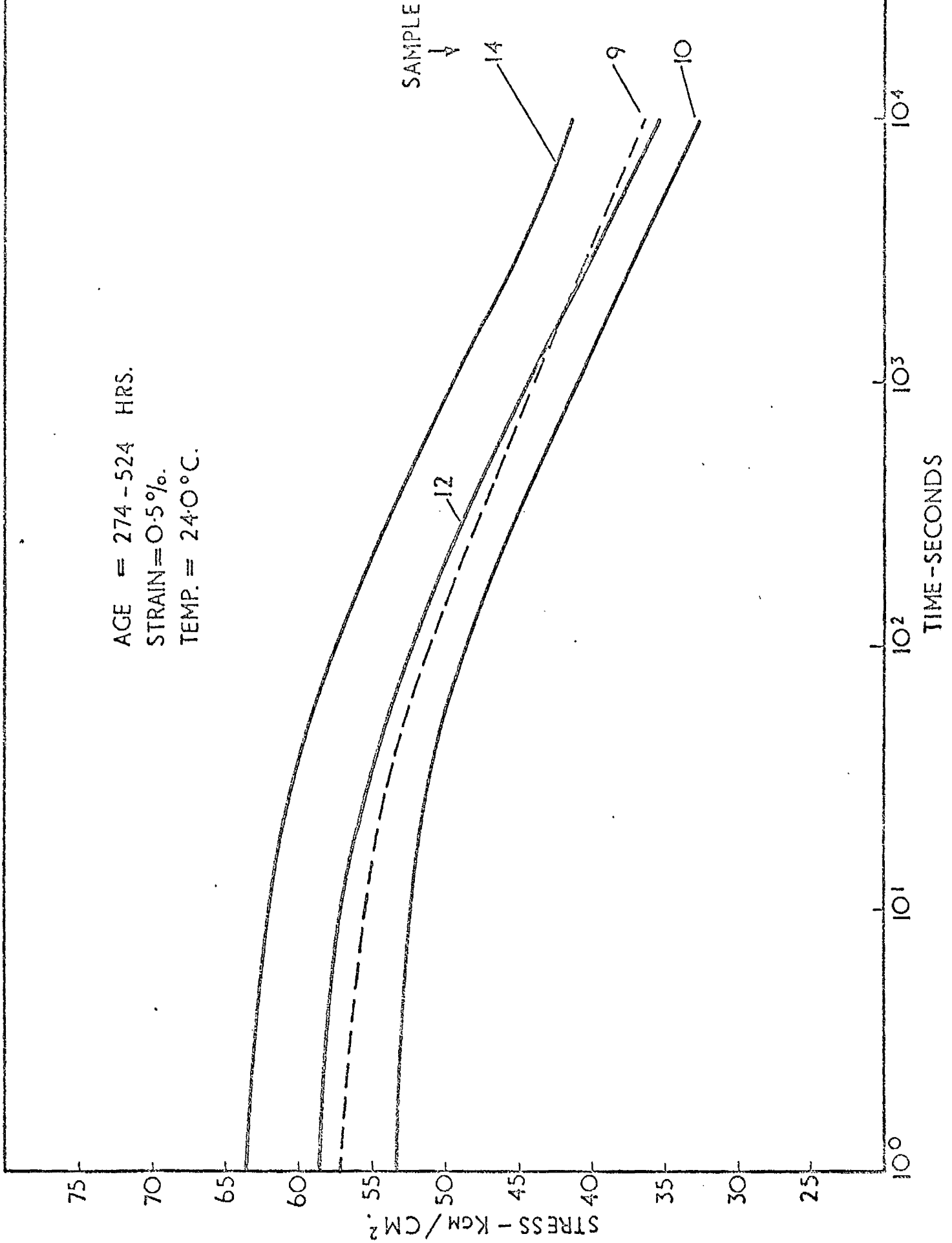


FIG. 6.8. THE EFFECT OF COOLING RATE ON STRESS RELAXATION.

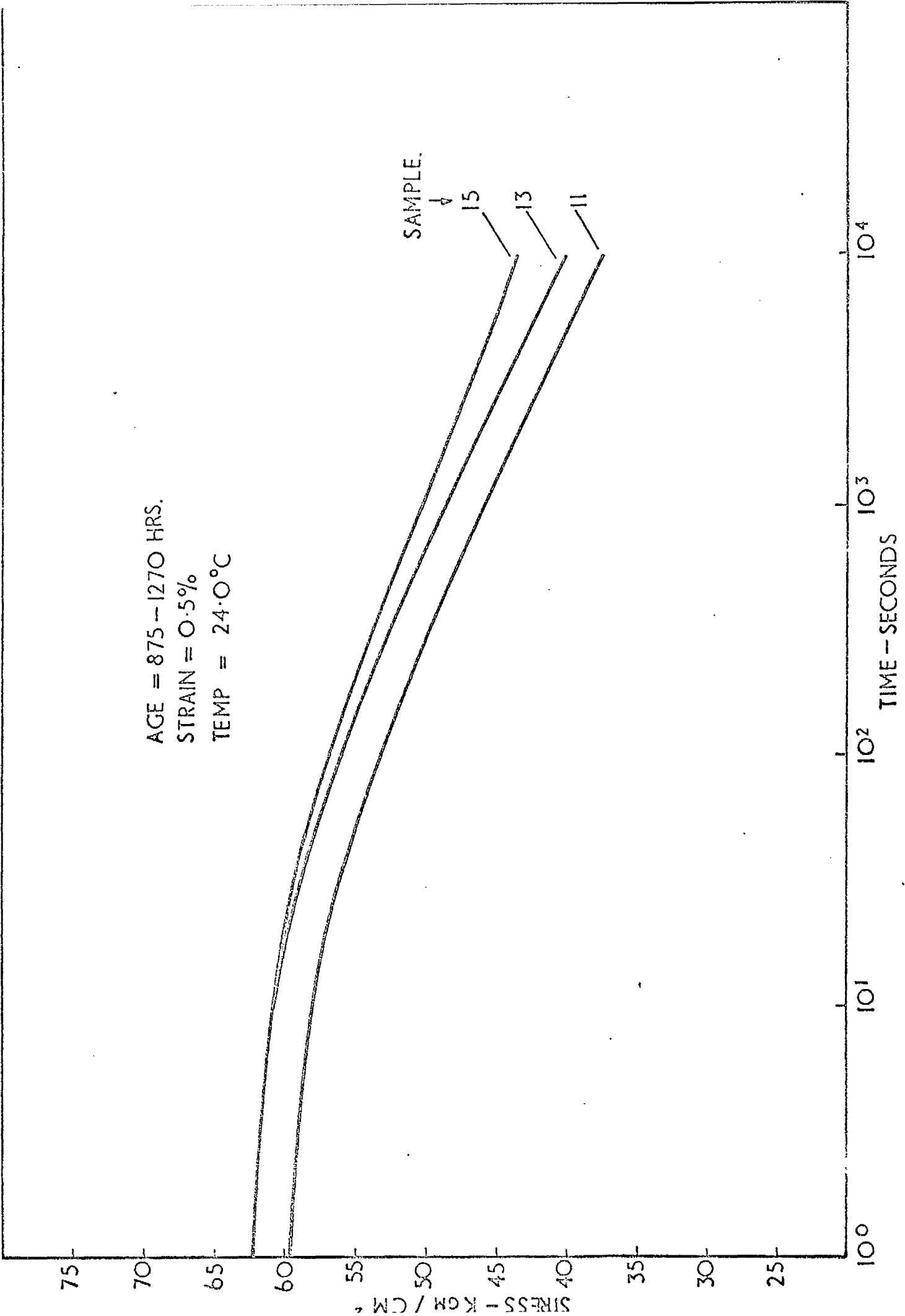


FIG. 6.9. THE EFFECT OF COOLING RATE ON STRESS RELAXATION.

AGE = 274 - 524 HRS.
STRAIN = 1.5%
TEMP. = 24.0°C.

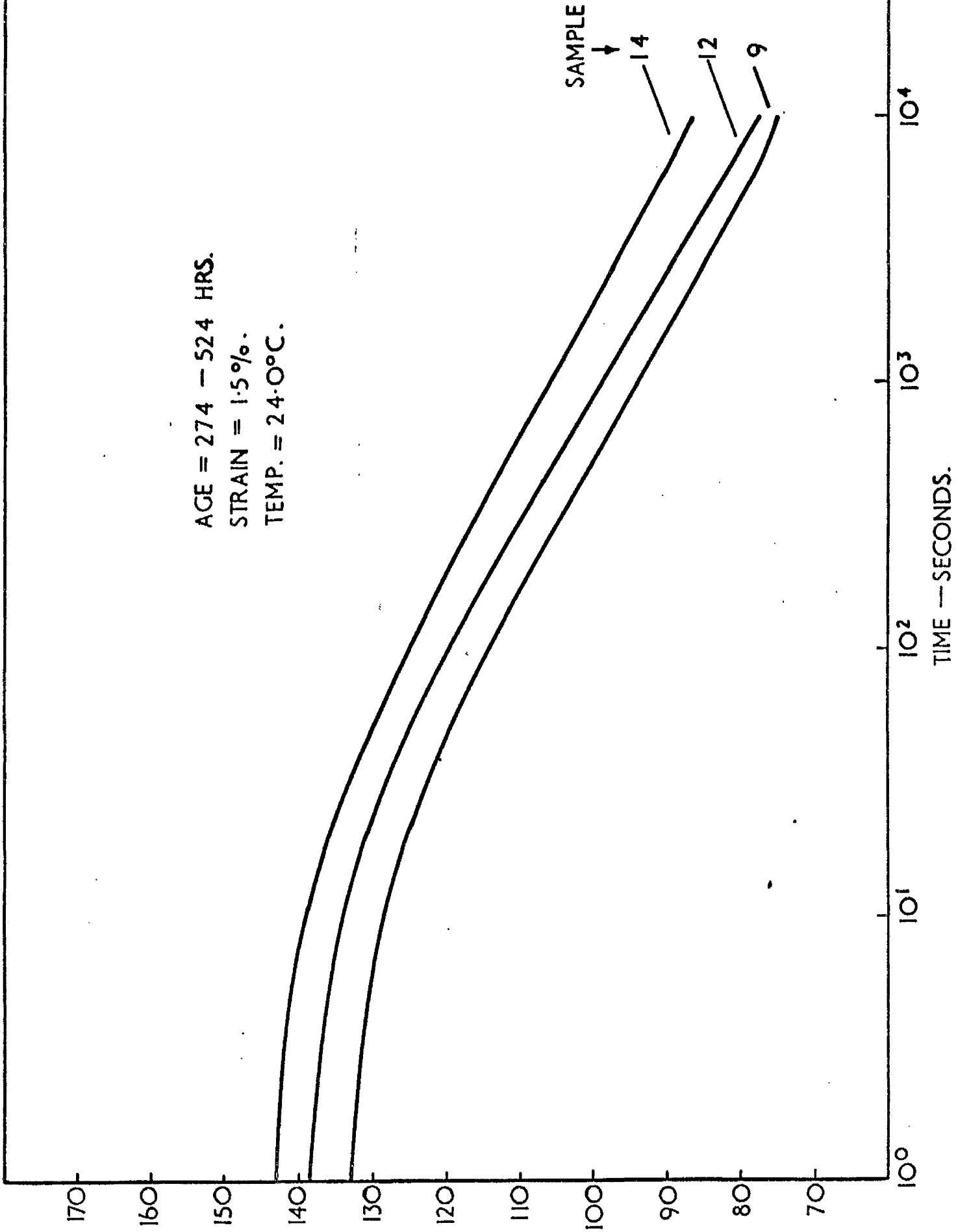


FIG. 6.10. THE EFFECT OF COOLING RATE ON STRESS RELAXATION.

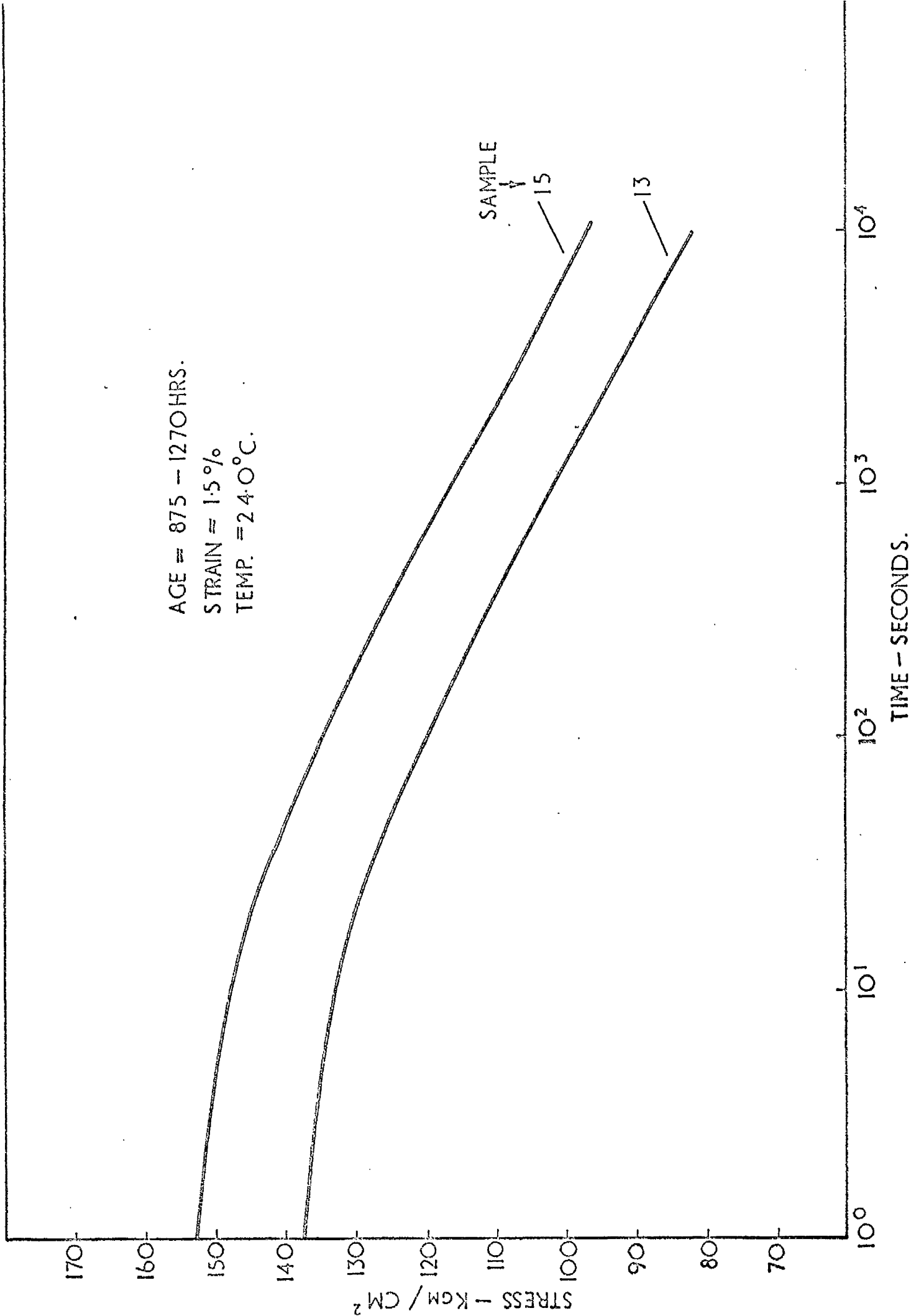


FIG. 6.11. THE EFFECT OF COOLING RATE ON STRESS RELAXATION.

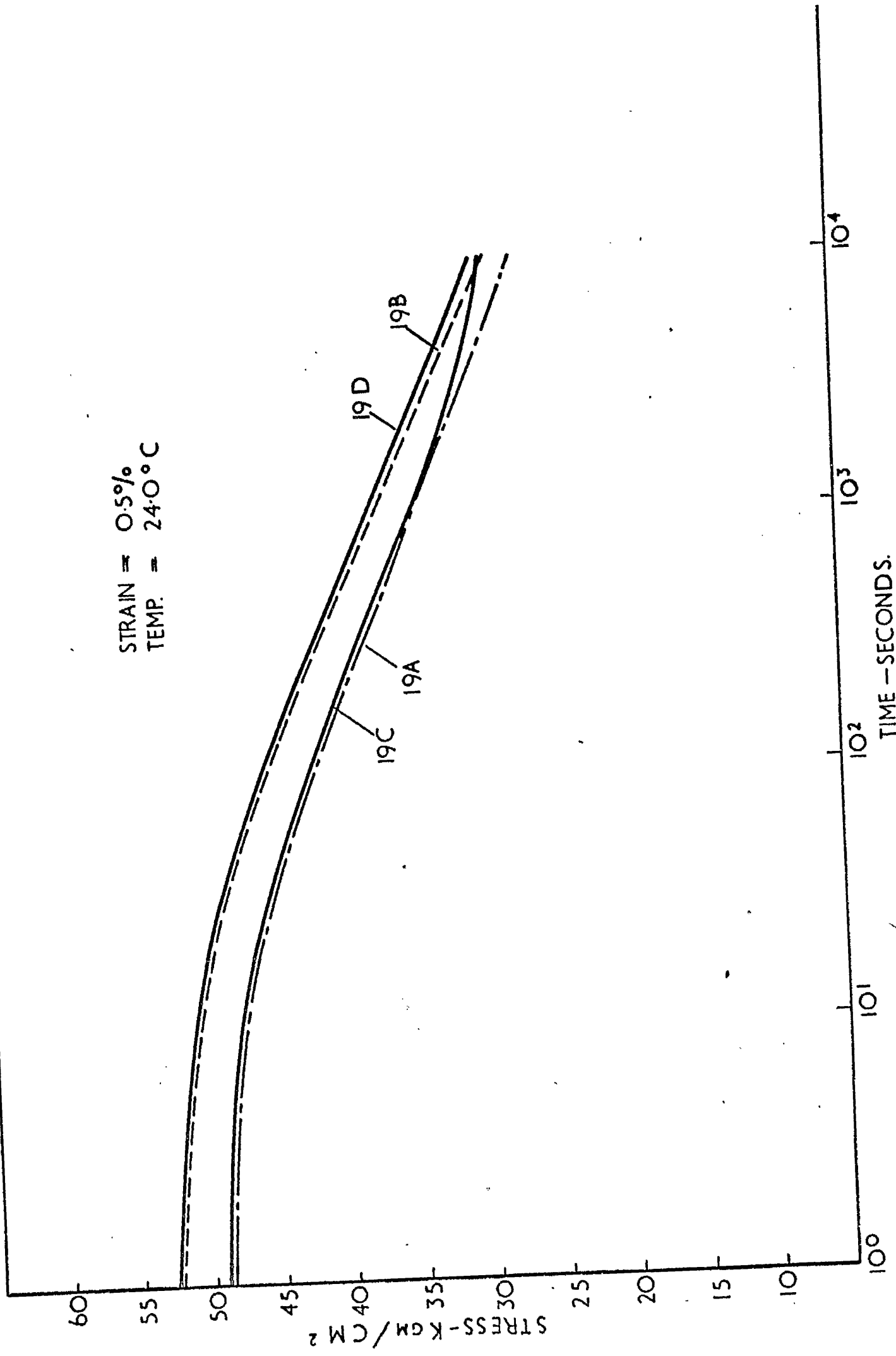


FIG. 6.12. THE EFFECT OF ANNEALING ON STRESS RELAXATION.

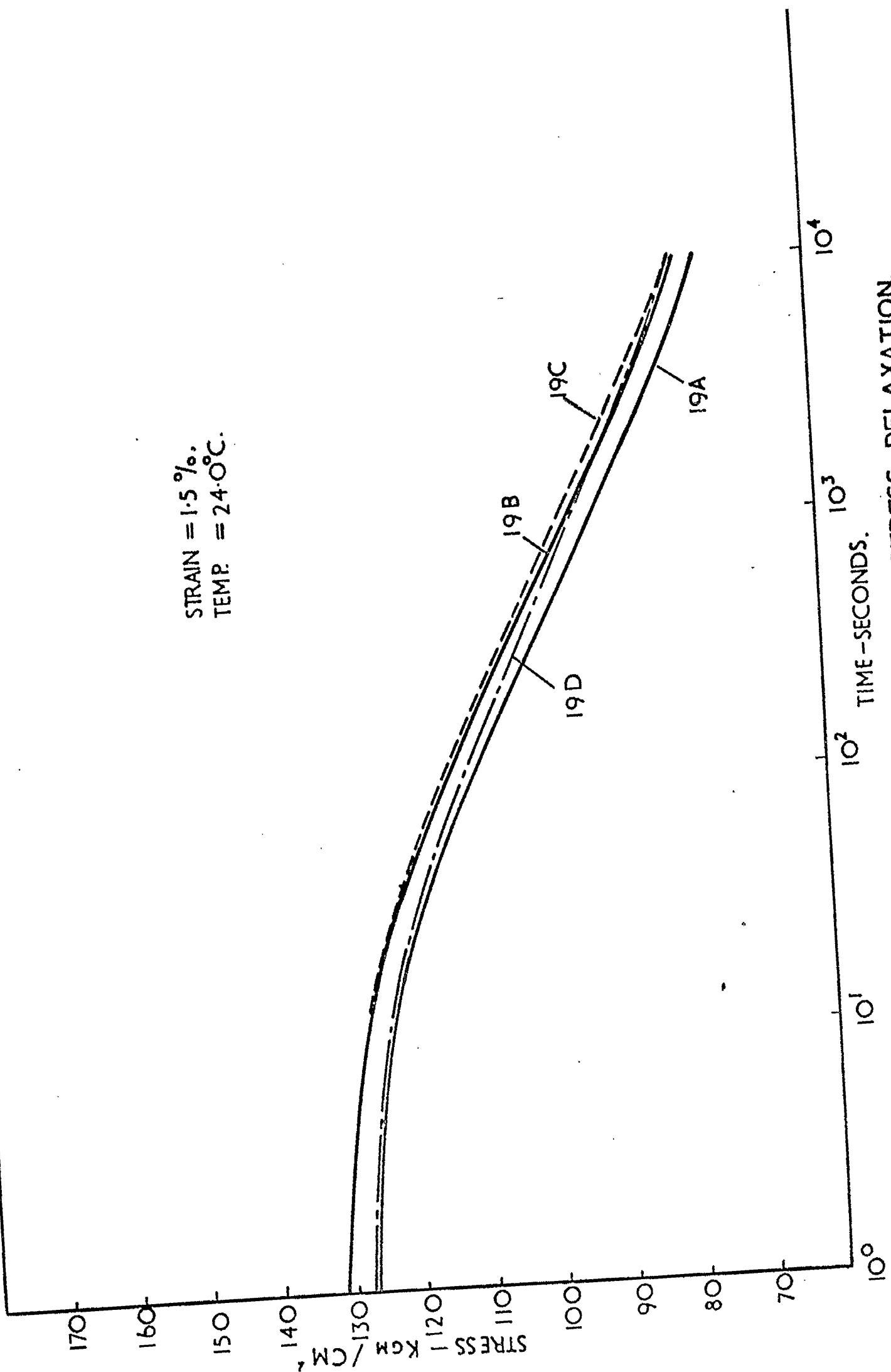


FIG 6.13. THE EFFECT OF ANNEALING ON STRESS RELAXATION.

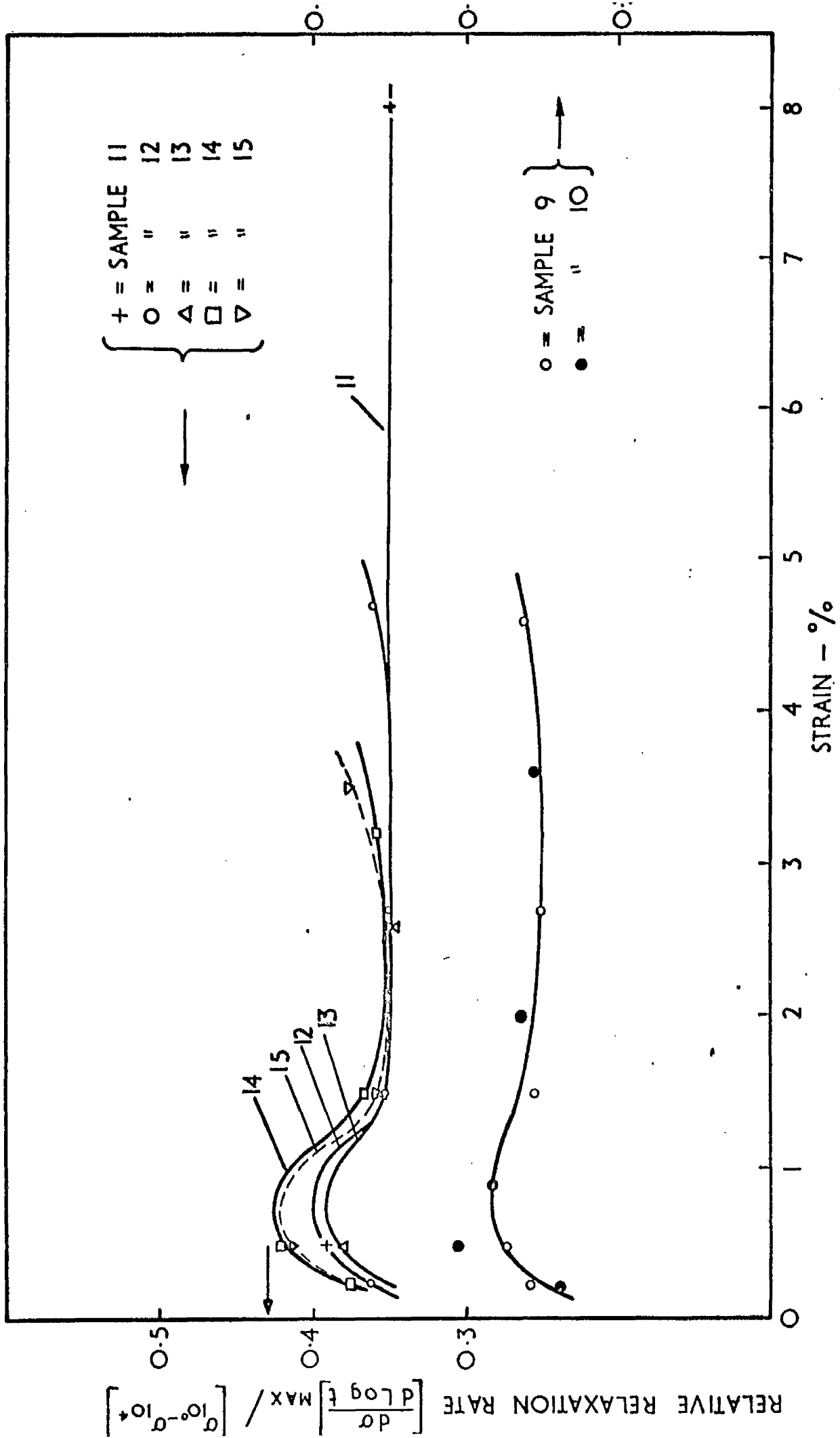


FIG. 6.14. THE EFFECT OF STRAIN AND THERMAL HISTORY ON THE RELAXATION RATE.

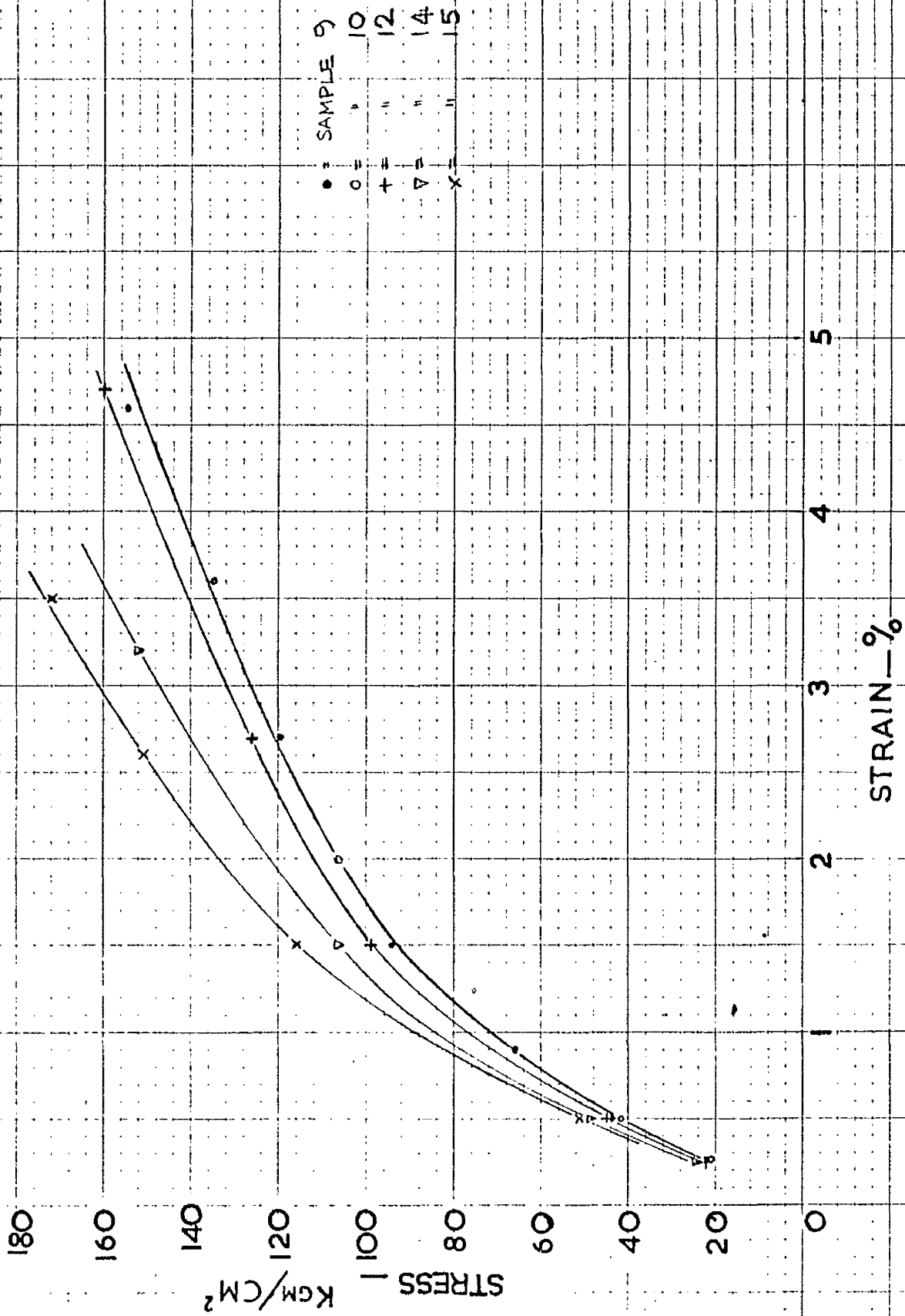


FIG 6.15 1000 SEC. ISOCHRONOUS STRESS _ STRAIN CURVE

7. CONCLUSIONS.

Using a moulding technique which was developed as part of this research, it has been possible to measure the cooling rate and crystallisation temperature within compression moulded sheets of polypropylene.

Some fairly simple techniques of density measurement, optical microscopy and a measure of the rate of crystallisation have confirmed the previous report by Magill (116) that a change in crystallisation kinetics in polypropylene occurs in the temperature range 115 - 120°C. This research places this change as occurring at about 120.5°C. The change manifested itself at crystallisation temperatures greater than this by an abrupt increase in density and spherulite size, and the beginning of a tendency to much slower crystallisation rates. In the polypropylene used in this research, a T_c of 120.5°C followed from cooling at approximately 10°C/min.

This change in crystallisation kinetics was found to coincide with the onset of a large amount of strain whitening following tensile testing up to 15% strain. This is seen as a fairly clear indication that the crystallisation behaviour in the range of $T_c \gtrsim 120.5^\circ\text{C}$ may involve a significant loss of tie molecules which link crystalline units and spherulites to each other. It is concluded that a loss of bonding between spherulites together with the effect of secondary crystallisation in producing an internal stress on spherulite boundaries, is the cause of a very pronounced increase in the rate of inter-spherulitic cracking following moulding in the crystallisation temperature range above $\sim 120.5^\circ\text{C}$.

Despite these pronounced changes in the strain whitening which follows from the internal cracking very little discontinuity could be found in the secant modulus of samples

with moulding conditions which covered this zone. It is concluded that the change in mechanical properties which would be expected to follow from this is probably masked by the degree of scatter of thermal history through the thickness direction of the tensile specimens, such that less embrittled layers of material serve to reinforce those regions which have seriously cracked. This effect would not however, disguise the tendency to change the optical properties through the thickness direction. In this respect somewhat thinner test sheets would be expected to show a fairly dramatic change in modulus and ductility in this zone. It is considered that some more work could be done using thin sections of plastic to obtain a more detailed correlation between structure and mechanical properties, especially in this zone of slow cooling rates. Elsewhere in this research it has been shown that the thickness of the tensile test piece is not an independent parameter in determining the relationship between structure and mechanical properties. This factor is in agreement with the results of Slinimskii and Pavlov⁽⁷³⁾, and should be taken into account in the choice of film thickness under investigation. It is considered that this might form the grounds for an independent examination of the effects of film thickness and spherulite size on the deformation mode.

In view of the opposing effects following raising the crystallisation temperature in stiffening the matrix by the addition of more crystalline material, and simultaneously removing tie molecules joining these crystalline regions, it is to be expected that a turning point in the overall modulus might result. This research has shown that this occurs well outside the normal range of moulding cooling rates.

In addition to inter-spherulitic cracking, a type of cracking situated along the polar axis of the deformed

spherulite was found. This cracking mode in polypropylene has not been reported previously, to the knowledge of the author. Its occurrence is attributed to either the development of structural complex stressing or/and an interplay of the applied strain-rate and the maximum rate of relaxation of the different visco-elastic mechanisms within the matrix proposed by Matsuoka⁽⁸⁹⁾⁽⁸²⁾. Either conclusion suggests that some care should be exercised in comparing the deformation mode of thin films directly with that in the bulk matrix, since

a) little complex stressing can develop in such films and
b) it is conjectured that the typical reorientation rates of the structure in thin films may be an order of magnitude faster than their rates within the bulk matrix. The results of thin film extension under uniaxial and an imposed complex stress system have confirmed that a considerable difference in the deformation mode can be induced, such that a very ductile line drawing behaviour in thin films subjected to uniaxial tension can be transformed into a mode of severe cracking under a more complex stress system.

It is recommended therefore, that future work on the relationship between film thickness and deformation mode should include the related factor of strain-rate up to the range of impact testing.

These results have also shown that the response of crystalline polymers to complex stressing might be different from that in normal uniaxial tensile testing. In this respect, a comparison of their behaviour under more complex stress states on the basis of an effective stress-effective strain response should make interesting additional research.

A new technique has also been developed which enables an accurate measurement of the strain/time point at which gross cracking starts within tensile test pieces. This

technique, which measures the amount of light transmitted by the plastic during a stress-strain test, has shown that at rapid cooling rates during moulding there is a significant improvement in the crack resistance of the material. The preparation which produces this improvement does not coincide with the change in crystallisation kinetics, ^{already outlined,} but occurs following cooling rates which exceed about $100^{\circ}\text{C}/\text{min}$. This observation must suggest that beyond the onset of cracking there probably still exists some significant differences in the progress of cracking. For example, it could well be that following the start of cracking there is still the ability for cracks to heal rather than propagate due to the aligned state of the molecules at the crack root. This would explain why, following the same crack initiation point in samples cooled at a rate ^{between} $100^{\circ}\text{C}/\text{min} \rightarrow 10^{\circ}\text{C}/\text{min}$, there is still only a slight tendency to strain whitening. Samples having a slower cooling rate than $10^{\circ}\text{C}/\text{min}$ would then appear not to have the same ability to draw out at the crack root in this manner, but rather in the manner of the observation made of an improperly moulded sample which could fracture 'cleanly' without drawing out between uncoalesced granules. This line of conjecture would certainly agree with the earlier conclusion that the tie molecule population may be considerably lowered (the more so probably between spherulites) at $T_c \gtrsim 120.5^{\circ}\text{C}$, with the change in crystallisation kinetics. It is concluded that these links are probably removed primarily from inter-spherulite regions rather than from between crystallites within the spherulite following the evidence that the cracking within spherulites was recoverable to the extent that these cracks collapsed compared with the permanent state of cracking between spherulites.

Any observation of a deformation between spherulites would immediately vitiate the sort of models proposed by Matsuoka (89)(82) and Takayanagi et al (93) since such a behaviour would eliminate the continuous connection between the crystalline phase incorporated in these models to explain the polymer's mechanical properties at smaller strains.

The light transmittance technique has also traced a point at which opacity starts which assumes some significance because (a) the strain/time point at which it occurs (2°/o strain at a strain-rate of 0.975°/o/min), is practically unaltered by the changes in thermal history of the samples, and (b) because relaxation tests show a discontinuity in behaviour at the same point. A group of tests on the permanence of the state of opacity beyond this zone suggests that this point coincides with the disruption or re-orientation of the crystalline phase.

The relaxation experiments carried out have shown that whilst some small differences in the relaxation rate exist between samples of varying thermal history in the strain range below 2°/o, these differences diminish and become negligible in the strain range above 2°/o and prior to the commencement of gross cracking.

With the above interpretation of the cause for the onset of opacity these results would indicate that no significant difference exists in the deformability of crystalline regions following varying thermal histories. If this were true, then a simplified approach to relating the mechanical properties to structure at small strains might be possible. This could follow along the lines of those developed by Beuche (96), Becker (97), Krigbaum et al (98), and Nielson and Stockton (111), which effectively analyse the modulus of the β stress route alone, since the added modulus of the α stress route comprising the deformation of

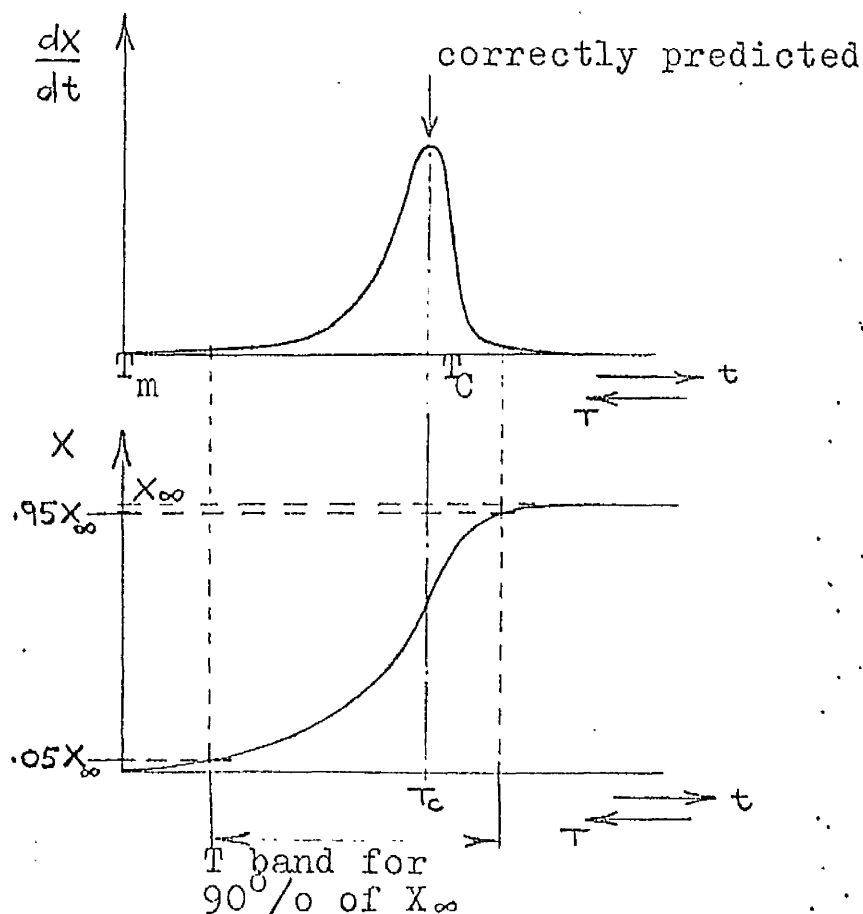
the crystalline phase might be substantially unaltered by thermal history.

The occurrence of voiding during the disruption of the crystalline phase and of cracking at higher strains suggests that the compressive mechanical behaviour of crystalline polymers may become quite different to their tensile behaviour in the strain range beyond about 2%, if not earlier. An apparatus has recently been described (144) which greatly increases the sensitivity of compressive testing by using long, slender specimens suitably restricted to prevent buckling. This may be of considerable use for comparing compressive and tensile creep behaviour and possibly also correlating results against the effect of thermal history.

The stress-strain tests have shown that slower moulding cooling rates produce a relatively smaller increase in secant modulus than ageing, and that annealing treatments where $T_A/T_C > 0.905$ produce an even smaller modulus increase, where comparisons are made on a density basis. The order in which these various thermal histories affect the overall modulus is such as to suggest that the state of relaxation in the non-crystalline phase has relatively more effect than the quantity or perfection of the crystalline phase. Relaxation tests, whilst they were not entirely consistent in trend, would also suggest that in general the relaxation rates are increased as samples are moulded at slower cooling rates. Again it is felt that the degree of scatter of thermal history through the thickness direction of samples had a hand in moderating the size of the effect of thermal history on the relaxation rate of samples.

Some success has been achieved in adapting the Avrami equation to predict the temperature at which there is a maximum in the crystallisation rate during constant cooling. The agreement in trend that was obtained in predicting the

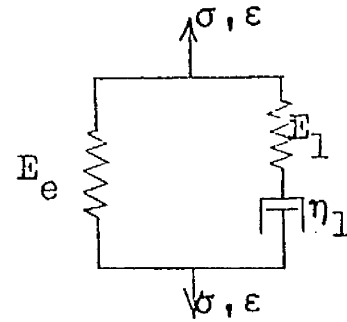
dependence of crystallisation temperature (the point of maximum crystallisation rate) on the cooling rate at least up to $150^{\circ}\text{C}/\text{min}$, leads the author to suggest that this method might be extended to give a measure of the temperature band over which crystallisation proceeds at any chosen significant level. For example, the figure below shows the temperature band during which 90% of the final crystallinity takes place. This information may then be used as a parameter to describe the spread in the type and agglomeration of structure present, and also the temperature zone at which this becomes unstable and liable to reordering during annealing or high temperature testing.



The annealing treatments given during this research were related to the point of maximum crystallisation rate T_C in the above figure. The limited results available show that the lowest temperature at which the structure is significantly reordered following rapid cooling, is at least $0.9 \times T_C^{\circ}\text{C}$.

As the annealing temperature T_A approaches T_C , the quantity of structure which is reordered becomes much greater. Some experiments on rapidly cooled samples have shown that where $\frac{T_A}{T_C} < 1$, the secant modulus may be increased up to a limiting or maximum value provided the structure does not become voided. The ability of annealing treatments to improve modulus will depend on the increased content of crystalline phase, the state of relaxation of the non-crystalline phase, the number of tie molecules which link crystalline areas and the spherulites together, and the state of internal stress on spherulite boundaries. All these factors will depend on the prior thermal history of the sample and it is not possible to give an annealing treatment which will continue to give increased modulus. With the moulding technique developed in this research and the theoretical approach outlined above, it should be possible, however, to obtain a fuller understanding of the effects of heat treatments on structure and mechanical properties.

FIG. 1.9



This model's stress-strain behaviour is related through the equations (1), (2), (3),

$$\dot{\sigma}_1 + \frac{E_1}{\eta_1} \sigma_1 = E_1 \dot{\epsilon}_1 \quad \text{---(1)}$$

$$\sigma_e = E_e \epsilon \quad \text{---(2)}$$

$$\sigma_1 + \sigma_e = \sigma \quad \text{---(3)}$$

For an instantaneously applied strain ϵ_0 which is held constant, the solution to equation (1) at a time T is,

$$\sigma_1(T) = E_1 \epsilon_0 \exp\left(\frac{-E_1 T}{\eta_1}\right) \quad \text{---(4)}$$

combining equations (2), (3) and (4) gives,

$$\sigma(T) = E_e \epsilon_0 + E_1 \epsilon_0 \exp\left(\frac{-E_1 T}{\eta_1}\right)$$

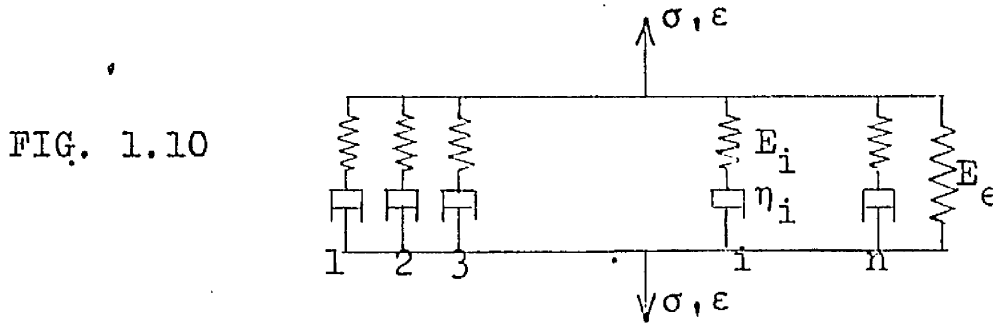
$$\text{i.e. } \frac{\sigma(T)}{\epsilon_0} = E(T) = E_e + E_1 \exp\left(-\frac{T}{\tau_1}\right) \quad \text{---(5A)}$$

$$\text{where } \tau_1 = \frac{\eta_1}{E_1}$$

Equation (5A) describes the stress relaxation response to a prescribed strain ϵ_0 . Similar response equations involving time dependent terms of the form $e^{-t/\tau}$ may be derived for any imposed stress or strain function.

continued/

τ is called either a relaxation time or a retardation time, depending on whether the strain or stress is prescribed. Although the behaviour of polymeric materials can be loosely approximated by a differential equation involving only a few terms a close approximation requires that the number of elements becomes large.



e.g. in the model shown in Fig. 1.10 having n spring and dashpot series elements (Maxwell elements) connected in parallel, the overall stress σ is related to the stress in each element by,

$$\sigma = \sigma_e + \sum_{i=1}^n \sigma_i$$

and for the stress relaxation case as derived above,

$$\sigma(T) = \epsilon_0 E_e + \epsilon_0 \sum_{i=1}^n E_i \exp\left(\frac{-T}{\tau_i}\right)$$

$$\text{where } \tau_i = \frac{\eta_i}{E_i}$$

$$\text{and } \frac{\sigma(T)}{\epsilon_0} = E(T) = E_e + \sum_{i=1}^n E_i \exp\left(\frac{-T}{\tau_i}\right) \quad \text{----- (5B)}$$

In the limit the summation has to be replaced by integration over an infinite distribution of relaxation times, so that

$$E(T) = E_e + \int_0^{\infty} E(\tau) \exp\left(\frac{-t}{\tau}\right) d\tau \quad \text{----- (5C)}$$

in which τ is now a continuous function, and $E(\tau)$ is called the relaxation spectrum.

APPENDIX II

The dependence of $\log k_s$ on temperature, as found by fitting a 'least squares' straight line by a curve fitting computer programme to the data published by a number of authors, is given overleaf. The constants A and m respectively refer to the value of $\log k_s$ at 110°C and the slope of the line on a plot of $\log k_s$ (mins) against temperature ($^\circ\text{C}$).

TABLE 2.3

AUTHORS	CURVE	n	A	M	MOLECULAR WT.	MELT CONDITION
GRIFFITH, RANBY REF. 109	1A	3.0	6.322	.362	$M_n = 5.05 \times 10^4$	T = 190°C FOR ~20 MIN.
	1B	"	9.307	.544	= 9.70×10^4	
	1C	"	5.614	.354	= 3.08×10^5	
MARKER, HAY, TILLEY, EARLY, SWEETING. REF. 107	4	3.0	1.824	.305	MI = 1.05 (a)	T = 220°C FOR ~30 MIN.
FALKAI REF. 33	3A	3.0	2.030	.276	$M_n = 5.1 \times 10^4$	INCOMPLETE MELTING AT T = 180°C, FOR 15 MIN. MORE THOROUGH MELTING AT T = 200°C, FOR 15 MIN.
	3B	GRAPHICAL FIT TO TWO DATA POINTS (d)				
MAGILL REF. 116	5	3.0	4.1(b)	.36	$M_w = 1.96 \times 10^5$	T = 270°C FOR 30 MIN.
GORDON, HILLIER REF. 117	2	2.5	2.665	.271 (c)	$M_n \approx 4.13 \times 10^5$	NOT SPECIFIED

a) other single values of k_s at T=136.0°C show very little variation with molecular weight as measured by MI. (melt index).

MI	1.05	0.45	0.11
Log k_s	-6.14	-5.56	-6.10

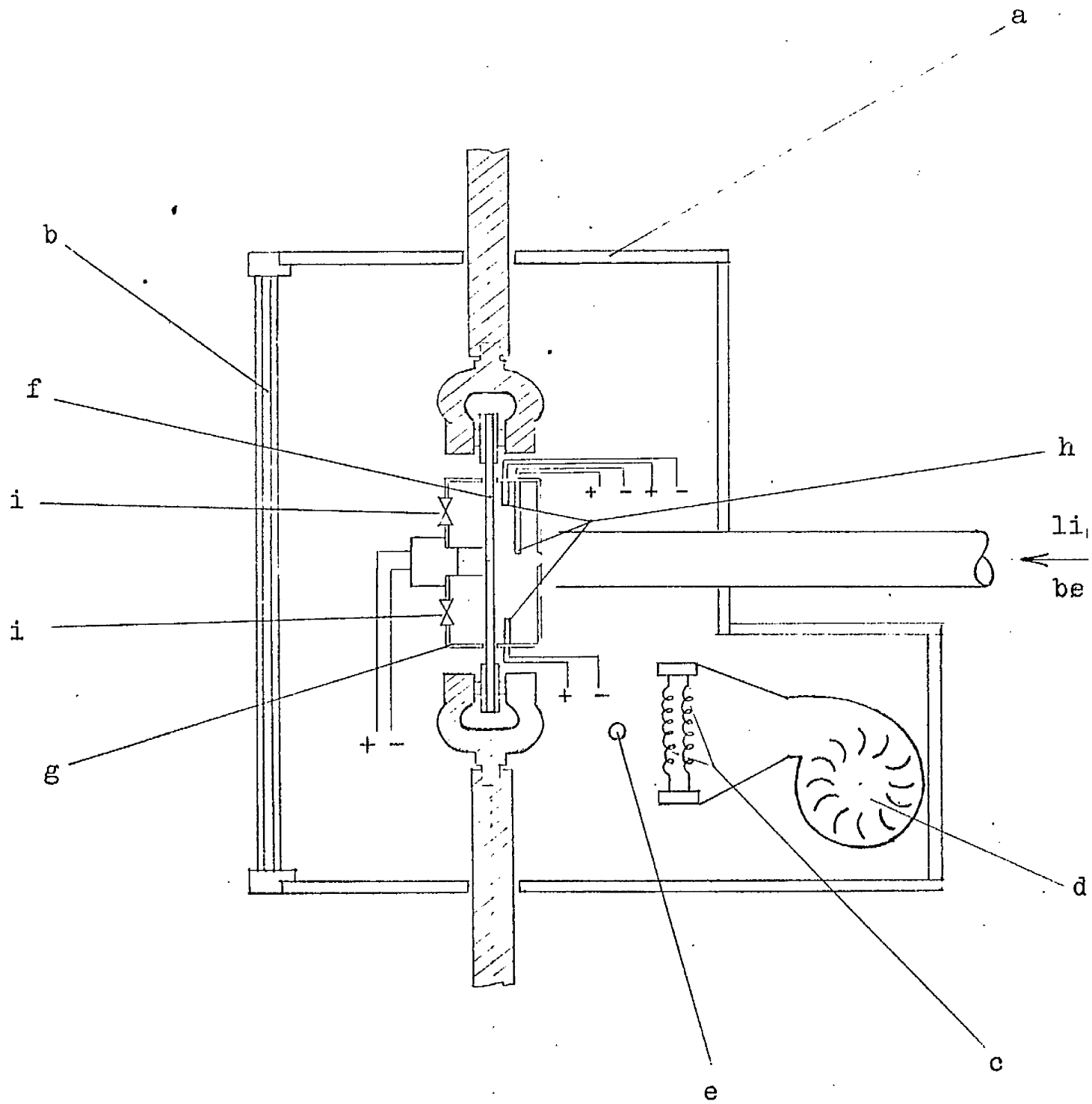
b) from graphical data

c) fitted to data in the temperature range 134.1 to 140.2°C.

d) single values of $\log k_s$ are given following this more thorough melt condition

T	130	140
Log k_s	-4.20	-6.96

FIG. 4.3



Temperature Controlled Cabinet.

The cabinet shown in Fig. 4.3. consisted of a sindanyo box (a) having a double glazed glass door (b). Heating was by two 20- Ω resistance coils (c) which could be switched either into series or into 'individual' control from a dual variac. Air within the cabinet was circulated about 3 times a minute by a Planair blower (d) which was ducted to pass the air through both sets of heating coils. Temperature control was via an Electro Methods contact thermometer (e) mounted close to the heat source, which operated a relay switch on the heating circuit. With the heating coils switched into series they were both switched on/off by the contact thermometer, when switched into 'individual' one heating coil by-passed the relay to become a constant 'background' heater. The cabinet was capable of being heated up to about 140°C if necessary.

The tensile specimen (f) was surrounded by an aluminium box (g) within which the temperature was measured at three points covering the specimen's gauge length by calibrated thermocouples (h) the output of which was measured on the Kent Mk. III recorder. Extensions were measured using an optical observation method, via two windows (i) in the aluminium box.

Preliminary tests showed that temperature fluctuations within the aluminium box were no greater than $\pm 0.1^\circ\text{C}$. The apparatus was, however sited near large windows and since the temperature control did not incorporate a cooling element, cooling being by conduction through the cabinet walls, some care was found to be necessary in maintaining the standard test temperature of 24.0°C on very hot days.

APPENDIX IV

Assuming that the overall strain ϵ is due to strain in the amorphous phase ϵ_a alone, these ^{strains} are related by equation (1)

$$\epsilon_a = \epsilon \left(1 + \frac{l_c}{l_a}\right) \text{-----(1)}$$

where l_c and l_a are the lengths of the crystalline and amorphous paths respectively in the direction of applied stress.

$$\frac{l_c}{l_a} \cong \left(\frac{V_c}{V_a}\right)^{1/3} = \left(\frac{V_c}{1 - V_c}\right)^{1/3} \text{-----(2)}$$

where V_c is the volume fraction of the crystalline phase.

Using the density method to determine the approximate crystalline fraction V_c

$$V_c = \frac{\rho_o - \rho_a}{\rho_c - \rho_a} \text{-----(3)}$$

where $\rho_a = .85$, $\rho_c = .936$ and ρ_o is the observed density, the maximum and minimum values for X from the data in table 4.1a are respectively

$$\rho_o = .9082, \quad X = .677$$

$$\rho_o = .9029, \quad X = .615$$

Substituting these values into (2) and (1) gives the overall change in ϵ_a as,

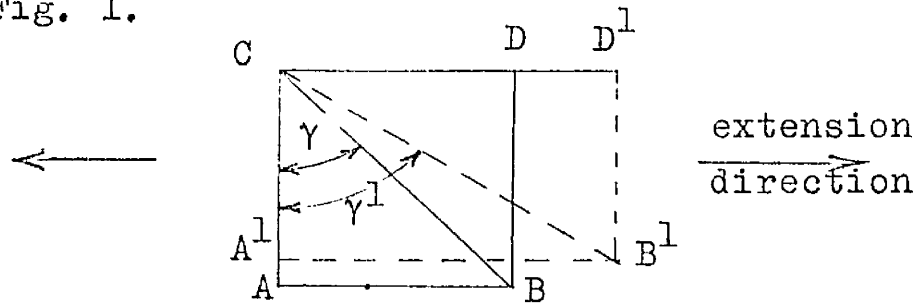
$$\epsilon_a = \epsilon \left[1 + \left(\frac{.677}{.323}\right)^{1/3}\right] = \epsilon \times 2.28$$

$$\epsilon_a = \epsilon \left[1 + \left(\frac{.615}{.385}\right)^{1/3}\right] = \epsilon \times 2.17$$

APPENDIX V

Using the score marks on microtomed films as a measure of strain.

The changes in orientation of the score marks is given in Fig. 1.



The strain along the axis ϵ_x is given by,

$$\begin{aligned} \epsilon_x &= \frac{A^1B^1 - AB}{AB} \\ &= \frac{A^1B^1}{AB} - 1 \quad \text{---(1)} \end{aligned}$$

Substituting $AB = CA \tan \gamma$

$$A^1B^1 = CA^1 \tan \gamma^1$$

gives, $\epsilon_x = \frac{CA^1}{CA} \frac{\tan \gamma^1}{\tan \gamma} - 1 \quad \text{---(2)}$

Assuming constant volume and no thinning in the thickness direction of the film then,

$$CA \cdot AB = CA^1 \cdot A^1B^1 \quad \text{---(3)}$$

$$\therefore \frac{CA^1}{CA} = \frac{AB}{A^1B^1} = \frac{1}{\epsilon_x + 1} \quad \text{(from (1))}$$

substituting into (2) gives,

$$\epsilon_x = \frac{1}{\epsilon_x + 1} \frac{\tan \gamma^1}{\tan \gamma} - 1$$

$$\therefore \epsilon_x^2 + 2\epsilon_x + \left(1 - \frac{\tan \gamma^1}{\tan \gamma}\right) = 0 \quad \text{---(4)}$$

The roots of equation (4) are given by,

$$\begin{aligned}\epsilon_x &= \frac{-2 \pm \sqrt{4 \frac{\tan \gamma^1}{\tan \gamma}}}{2} \\ &= -1 \pm \sqrt{\frac{\tan \gamma^1}{\tan \gamma}}\end{aligned}$$

Taking the negative value would lead to the impossible condition that ϵ_x is negative \therefore conclude that ϵ_x is given by,

$$\epsilon_x = \sqrt{\frac{\tan \gamma^1}{\tan \gamma}} - 1 \text{ ————— (5)}$$

REFERENCES.

1. Kresser, 'Polypropylene', Reinhold Plastics Application Series, (1960).
2. Van Schooten, Van Hoorn, Boerma, "Polymer" 2, 161, (1961).
3. Raspopov, Pirogov, Pol. Sci. USSR., 5, 881, (1964).
4. Huff, Bushman, Cavender, J. Appl. Pol. Sci., 8, 825, (1964).
5. Ross, J. Pol. Sci., 9, 2729, (1965).
6. Keller, Phil. Mag., 2 (1171) (1957)
7. Geil, "Polymer Single Crystals", Interscience Pub. (1963).
8. Natta, Corradini, "Nuovo Cimento" Suppl. to Vol. 15, 1, 40, (1960).
9. Keith, Padden, Walter, Wyckoff, J. Appl. Phys., 30, 1485, (1959).
10. Price, SPE Trans., 4, 151, (1964).
11. Lindenmeyer, SPE Trans., 4, 157, (1964).
12. Keller, Waring, J. Pol. Sci., 17, 447, (1955).
13. Bunn, Alcock, Trans. Faraday Soc., 41, 317, (1945).
14. Keith, Padden, J. Appl. Phys., 34, 2409, (1963).
15. Keller, J. Pol. Sci., 17, 291, (1955).
16. Keller, J. Pol. Sci., 39, 151, (1955)
17. Padden, Keith, J. Appl. Phys., 30, 1479, (1959).
18. Padden, Keith, J. Appl. Phys., 37, 4013, (1966).
19. Selikhova, Markova, Kargin, "Vysokomolekul Soedin" 6, 1136, (1964). Chem. Abstr. 61, 8426a.
20. Keller, J. Pol. Sci., 39, 151, (1959).
21. Palmer, Cobbold, "Makromol Chem.", 74, 174, (1964).
22. Keith, Padden, J. Appl. Phys., 35, 1886, (1964).
23. Basset, Frank, Keller, Phil. Mag. 8, 1739, (1963).
24. Hock, J. Pol. Sci. A5, 471, (1967).
25. Hock, J. Pol. Sci. A2, 4, 227, (1966).
26. Rånby, Morehead, Walter, J. Pol. Sci., 44, 349, (1960).
27. Kojima, J. Pol. Sci., A5, 597, (1967).

28. Keith, Padden, J. Appl. Phys., 35, 1270, (1964).
29. Richards, J. Appl. Chem. (London), 1, 370, (1951).
30. Bunn, paper summarised in Brit. J. Appl. Phys.,
12, 261, (1961).
31. Keith, Padden, Vadimsky, J. Pol. Sci. A2, 267, (1966).
32. Davis, J. Pol. Sci., 4A, 1009 (1966).
33. Falkai, Makromol Chem., 41, 86, (1960).
34. Beck, J. Pol. Sci., A2 (4), 631, (1966).
35. Banks, Gordon, Sharples, "Polymer" 4, 289, (1963).
36. Sharples, Appl. Mats. Res., April 1965.
37. Dole, Wunderlich, Makromol. Chem., 34, 29 (1959).
38. Baer, Kardos, J. Pol. Sci., A3, 2837, (1965).
39. Natta, J. Pol. Sci., 16, 147, (1955).
40. Farrow, "Polymer" 2, 409, (1961)
41. Beck, Hiltz, SPE Trans , 5, 15, (1965).
42. Mandelkern, Posner, Diorio, Roberts, J. Appl. Phys., 32,
1509 (1961).
43. Peterlin, J. Appl. Phys., 15, (1964).
44. Keith, J. Appl. Phys., 35, (1964).
45. Wyckoff, J. Pol. Sci., 62, 83, (1962).
46. Turley, Keskkula, J. Appl. Pol. Sci., 9, 2693, (1965).
47. Passaglia, Martin, J. Res. Natl. Bur. Stds., (A), 68,
519, (1964)
48. Natta, Peraldo, Gorradini, Atti. accad. nazl. Lincei,
Rend., 26, 14, (1959).
49. Boye, Watson, Patton, J. Pol. Sci., 39, 534, (1959).
50. Miller, "Polymer", 1, 135, (1960).
51. Ross, J. Appl. Pol. Sci. 9, 2729, (1965).
52. Farrow, "Polymer" 2, 409, (1961)
53. Farrow, J. Appl. Pol. Sci., 9, 1227, (1965).
54. Sasaguri, Hoshino, Stein, J. Appl. Phys., 35, 47 - 54,
(1964)
55. Inoue, J. Pol. Sci., 55, 443, (1961).

56. Van Schooten, J. Appl. Pol. Sci., 4, 122, (1960).
57. Kavafian, J. Pol. Sci., 24, 499, (1957).
58. Hoshino, Meinecke, Powers, Stein, Newman, J. Pol. Sci. A3, 3041, (1965).
59. Barish, J. Appl. Pol. Sci., 6, 617, (1962).
60. Matsuoka, J. Appl. Phys. 32, 2334, (1961).
61. Matsuoka, J. Pol. Sci., 57, 569, (1962).
62. Keith, Padden, J. Pol. Sci., 41, 525, (1959).
63. Yung-Fang Yu, Ullman, J. Pol. Sci., 60, 55, (1962).
64. Harris, Magill, J. Pol. Sci., 54, 547, (1961).
65. Reding, Brown, Ind. Eng. Chem., 46, 1962, (1954).
66. Isaksen, Newman, Clark, J. Appl. Pol. Sci., 7, 515, (1963).
67. McCrum, Morris, Proc. Roy Soc., A292, 506, (1966).
68. Beck, Ledbetter, J. Appl. Pol. Sci., 9, 2131, (1965).
69. Turner, Appl. Mats. Res., p.10, January, 1965.
70. Gul, Kovriga, Vasserman, Dokl. Akad. Nauk. SSR.; Chem. Abstr. 58, 2512 h (1963).
71. Oda, Nomura, Kawai, J. Pol. Sci. A 3, 1993 (1965).
72. "Inside Polypropylene - Its Crystallisation and Fabrication", Plastics Dept., Dow Chemical Co., Midland, Michigan.
73. Slonimskii, Pavlov, Pol. Sci. USSR., 7², 1419, (1965).
74. Turner, "British Plastics", August, 1964.
75. " " " September, 1964.
76. " " " December, 1964.
77. " " " January, 1965.
78. Flocke, Kolloid Z, 180, 118, (1962)
79. Sauer, Woodward, Rev. Modern Phys., 32, 88, (1960).
80. Hall, J. Pol. Sci., 54, 505, (1961).
81. Stein, SPE Trans., 4, 178 (1964).
82. Matsuoka, Winslow, Mats. Res. and Standards, 134 March (1965).
83. May, Appl. Mats. Res., 81, April (1966).
84. Samuels, J. Pol. Sci., A3, 1741, (1965).

85. Erehardt, Sasaguri, Stein, J. Pol. Sci. c no 5, 179, (1964).
86. Treloar, "Physics of Rubber Elasticity" (1949), 2nd. Edition, (1958).
87. Holland, J. Appl. Phys., 35, 11, (1964).
88. Renecker, J. Pol. Sci. A,3, 1069 (1965).
89. Moore, Matsuoko, J. Pol. Sci. C,5, 163, (1964).
90. Payne, "Rheology of Elastomers" ed Mason and Wookey, Pergamon Press (1958).
91. Nagamatsu, Kolloid Z, 172, 141, (1960).
92. Sasaguri, Yamada, Stein, J. Appl. Phys., 35, 3188, (1964).
93. Takayanagi, Uemura, Minami, J. Pol. Sci., c 113 - 122 (1964).
94. Treloar, 'Polymer', (1), 95, (1960).
95. Sakurada, Ito, Nakamal, "Makromol Chem." 75, 1, (1964).
96. Bueche, J. Pol. Sci., 22, 113, (1956).
97. Von Becker, Kolloid Z, 175, 99, (1961).
98. Krigbaum, Roe, Smith, "Polymer ", 5, 533, (1964).
99. Rouse, J. Chem. Phys., 1272, 21, (1953).
100. Faucher, Trans. Soc. Rheology, III, 81, (1959).
101. Turner, " Polymer Eng. and Science", 6, 306, (1966).
102. Kubat, Laible, "Arkiv für Fysik", 25, 285, (1964); 26, 439, (1964).
103. Findley, SPE Journal, 16, 57, (1960).
104. Halpin, J. Appl. Phys. 35, Nov. (1964).
105. Mandelkern, " Growth and Perfection of Crystals" (1958).
106. Chiu, " Anal. Chem. ", 36, 2058, (1964).
107. Marker, Hay, Tilley, Early, Sweeting, J. Pol. Sci., 38, 33, (1959).
108. Majer, "Kunststoffe", 50, 565, (1960), Chem. Abstr. 55, 4035e (1961).
109. Griffith, Rånby, J. Pol. Sci., A1, 3317, (1963).
110. Parrini, Corrieri, "Makromol Chem." 62, 83, (1963).
111. Nielson, Stockton, J. Pol. Sci. A 1, 1995, (1963).
112. Banks, Hay, Sharples, Thomson, 'Polymer', 5, 163, (1964).

113. Keller, J. Pol. Sci., 15, 31, (1955).
114. Private Communication, Banks, Sharples, Thomson,
A.D. Little Research Institute, Musselburgh, Scotland.
115. Avrami, J. Chem. Phys., 7, 1103, (1939); 8, 212, (1940).
116. Magill, 'Polymer', 3, 35, (1962).
117. Gordon, Hillier, 'Polymer', 6, 213, (1965).
118. Donald, Humes, White, J. Pol. Sci. C 6, 93, (1964).
119. Lambert, Baer, J. Pol. Sci. A 1, 3317, (1963).
120. "Statistical Methods and Research and Production"
edited by O.L. Davis, (1949), p. 136.
121. Private Communication, Dr. Burnett, I.C.I. Welwyn Garden.
122. Stratton, J. Am. Chem. Soc., Div. Pol. Chem., Preprints,
3, 50, (1962).
123. Collins, J. Pol. Sci., 27, 75, (1958).
124. Krigbaum, Uematsu, J. Pol. Sci., A3, 2915, (1965).
125. Sobiczewski, Wajnryb, 'Polimery', 8, 69, (1963); Chem.
Abstr. 59, 11675a.
126. Golik, Rindich, Kuchinka, Sokolovska, Ukr. Fiz. Zh., 9,
783, (1964); Chem. Abstr. 61, 14833 e.
127. Putti, Sabbioni, 'Materie Plastiche', 25, 729, (1959).
128. Kuribayashi, Tanaka, Nakai, 'Sen - i Gakkaishi' 17,
1088, (1961); 18, 64, (1962); 19, 386) (1963).
129. Sperati, Franta, Starkweather, J. Am. Chem. Soc., 75,
6127, (1953)
130. Nielsen, J. Appl. Phys., 25, 1209, (1954).
131. Reding, J. Pol. Sci., 32, 487, (1958).
132. Bettelheim, Stein, J. Pol. Sci., 31, 123, (1958)
133. Hopkins, Baker, Howard, J. Appl. Phys., 21, 206, (1950).
134. Ohlberg, Roth, Raff, J. Appl. Pol. Sci., 1, 114, (1959).
135. Inoue, J. Pol. Sci., 60, 81, (1962).
136. Private Communication, R.P. Palmer, ICI, Welwyn Garden City.
137. Inglis, "Trans. Inst. Nav. Architects(London)", 55, 219,
(1913).

138. "Fracture", proceedings of an international Conference, ed. Averbach, Felbeck, Hahn, Thomas, (1959) Chap. 13.
139. Burns, MSc Thesis, Glasgow University, Dept. of Mechanics and Mechanisms, Autumn 1967.
140. Private Communication, P. Powell, ICI, Welwyn Garden City
141. Howard, SPE Trans., 4, 217, (1964).
142. Tung, J. Pol. Sci. A 3, 1045, (1965).
143. Howard, "Stress Cracking", Chap. 2 of "Crystalline Olefin Polymers", Part II, Interscience Publication 1964.
144. Jones, Koo, O'Toole, "Mats. Res. and Stats." 6, 241 (1966).

